Effects of shallow cover depth, corrosion and soil erosion on the mechanical performance of corrugated steel culverts

by

Elham Nakhostin

A thesis submitted to the Faculty of Graduate and Postdoctoral Affairs in partial fulfillment of the requirements for the degree of

Doctor of Philosophy

in

Civil Engineering

Department of Civil and Environmental Engineering
Carleton University
Ottawa, Ontario

The Doctor of Philosophy in Civil Engineering Program is a joint program with University of Ottawa, administrated by the Ottawa-Carleton Institute of Civil Engineering

Abstract

Corrugated steel culverts (CSC) are key components of infrastructure to support water management and foundation integrity. Some installed culverts in North America are buried at shallow cover depths based on the engineering practices and exposed to deterioration effects, such as corrosion and soil erosion, during their service life.

The primary goal of this research is to investigate the CSC (e.g., force, moment, deflection, strain) at shallow cover depths subject to surface loads. The secondary goal of this research is to study effect of corrosion and soil erosion on the CSC mechanical response. The mechanical response and load transfer mechanisms are investigated using analytical models and finite element method (FEM).

For shallow cover depths, the numerical results illustrate the localization of internal forces and bending moments, in the CSC at the crest and trough of the CSC profile, is influenced by the corrugated geometry profile and load transfer mechanisms. The analysis demonstrates current practice using the average strain response cannot account for the local peak stress and strain response and cannot account for the onset of local effects (e.g., deformation mechanism, load concentration).

Based on the CSA S6-19 requirements for wall strength in bending and compression, a global sensitivity analysis was conducted. The Sobol and Morris methods is used to quantify uncertainty in the model output with respect to the governing design parameters and their interaction. A thrust magnification factor was proposed for intact corrugated culverts buried in shallow cover depths to estimate the maximum local force in the CSC cross section.

A comprehensive numerical analysis is undertaken to study the impact of wall section loss due to corrosion, and soil voids, typically caused by erosion, at the soil/culvert contact interface on the CSC mechanical response with respect to deformations and internal forces.

The impact of wall section loss due to corrosion is investigated with respect to percentage of corroded area (i.e., length and angle of corrosion), thickness of wall section loss, and corrosion rate. The global sensitivity analysis identifies that independent variables related to corrosion model have strong interaction and culvert/soil models deteriorated by corrosion is as a nonlinear model. The probability analysis predicts the safety index and probability of failure of the corroded culvert buried in a shallow cover depth during the service life.

The effect of soil void size, position relative to the culvert and combined effects with corrosion deterioration on the CSC mechanical response is investigated using FEM. The sensitivity study evaluates soil damage state, as defined by the location and volume of soil erosion voids adjacent to the CSC perimeter, for specific cohesionless soil conditions and design parameters. The loss of surface contact, along the soil/culvert contact interface, is a key parameter affecting culvert mechanical performance and integrity. The most significant effect is observed when the loss of contact and support occurs in the upper half of the CSC had culvert/soil structure. The results indicate an erosion void is more influential on the CSC mechanical response than corrosion deterioration. Combined erosion void and corrosion in lower half of the structure can cause undesirable deformation, stress concentration and eventually failure of load-carrying system for CSC at shallow cover depth.

Acknowledgements

First and foremost, I would like to thank my supervisor Professor Shawn Kenny, who has been a tremendous teacher and mentor throughout my graduate studies at Carleton University. I would like to express my sincere thanks to my co-supervisor Professor Siva Sivathayalan for his support, encouragement, and guidance.

My sincere thanks to Prof. David Lau, Prof. Mohammad Rayhani, Prof. Abhijit Sarkar, Prof. Paul Simms, Prof. Ning Guo, and Prof. Beatriz Martin-Perez for their useful inputs during my course of study and comprehensive exam.

I would like to thank Prof. Neil Hoult, Prof. Mamadou Fall, Prof. Abhijit Sarkar, and Prof. Heng Khoo, members of the examination board, on providing valuable feedback that has improved the manuscript.

I would like to thank Compute Canada for providing access to the computing platform and research software used in this study. I would like to thank NSERC for supporting my research through the Discovery Grant Program and Carleton for additional support through internal awards and scholarships.

Finally, I would like to extend a heartfelt thanks to my family and friends for their support and encouragement throughout this work. Specifically, my husband Soheil, my parents Matanat and Bahman, my sister Parnaz, and my brother Amin.

Table of Contents

List of Tables

List of Figures

List of Abbreviations

CDF	Cumulative Distribution Function
CHBDC	Canadian Highway Bridge Design Code
CL-W	Idealized five-axle truck
CL-625	Truck with 625 kN weight
COV	Coefficient Of Variations
CP	Control Pipe
CPE4	Four node bilinear plane strain quadrilateral elements
CSC	Corrugated Steel Culverts
C3D8	Fully integrated 3-dimentional solid continuum elements with linear 8-node
EE	Elementary Effects sensitivity analysis method
DLA	Dynamic load allowance
FEM	Finite Element Model
FEA	Finite Element Analysis
FOSM	First-Order Second-Moment method
GP-SP	Poorly graded granular soil
LE	Logarithmic Strain
OAT	One-At-a-Time sensitivity analysis method
S4	Shell elements with 4 nodes
S4R	Reduced integrated Shell elements with 4 nodes

TANA	Two-point Adaptive Nonlinear Approximation
U1	Horizontal displacement of culvert
U3	Vertical displacement of culvert
2D	Two Dimensional
2D-EQEt	Smooth Ring with Equivalent Elastic Modulus and Thickness
3D	Three Dimensional
3D-Corr	Three-Dimensional Corrugated Culvert
3D-EQEt	Smooth Cylinder with Equivalent Elastic Modulus and Thickness

List of Symbols

A	Area of the rectangular footprint
A_p	Culvert cross-sectional area per unit length
B_d	Effective trench width
C_d	Load factor
C_t	Wheel load coefficient
C_1	Thrust multiplying constant
C_2	Thrust power constant
c_v	Erosion void chord
D	Culvert or pipe diameter
D	The best r combination of M with the highest value in EE method
De	Depth of corrugated culvert profile
D_h	Horizontal diameter
D_v	Vertical diameter
d_{ml}	Distance between a pair of trajectories, m and l
d_v	Erosion void depth
E	Young's modulus of steel
EE_i	Elementary effect associated with factor i
$\bar{E}$	Equivalent elastic modulus of culvert
E_p	Culvert elastic modulus

E_s	Elastic modulus of soil
E(Y)	Mean or expected value of Y
F	Shallow cover depth local force
F_y	Yield tensile stress
f	Square integrable function in Sobol method
$g(U)$	Limit state function in U-space
$g(X)$	Limit state function in X-space
H	Cover depth
h	Radial distance between the strain gauges ε_1 and ε_2
I	Second moment of area per unit length
I_p	Culvert second moment of area per unit length
k	Number of independent variables in EE method
k	Number of variables in Sobol method
k	Iteration step in probability analysis
k	Multiplying constant in corrosion model
L	Culvert length
L_c	Culvert Length
LL	Wheel load
L_v	Erosion void length
M	Section bending moment per unit length in culvert internal forces
M	Number of trajectories in EE method
M_D	Moment in the wall of a soil-metal structure due to a dead load

M_f	Maximum moment in the culvert due to applied fill and truck loads per unit length
M_L	Moment in the wall of a soil-metal structure due to live load
M_{pf}	Moment capacity of a corrugated metal section
M_1	Moment in a soil-metal structure resulting from fill to the crown level
m_f	Modification factor for multi lane loading
N_{m_f}	Number of lanes in roadway
n	Exponential constant in corrosion model
P	Loss of wall thickness in corrosion model
Pi	Pitch of corrugated culvert profile
P_{pf}	Compressive strength of a corrugated metal section
p_f	Probability of failure
R	Resistance in probability analysis
Ra	Radius of corrugated culvert profile
r	Number of best selected trajectories in EE method
r	Nonlinear index in probability analysis
r_v	Erosion void distance from the CSC wall edge
S_C	Culvert span
S	Load effect in probability analysis
S_i	First-order sensitivity index in Sobol method
S_{ij}	Second-order sensitivity index in Sobol method

S_{Ti}	Total effect index in Sobol method
T	Exposure time in corrosion model
T_D	Dead load thrust
T_f	Conduit wall due to live loads and dead loads
T_L	Live load thrust
TL	Tangent length of corrugated culvert profile
$V_{Crn.}$	Erosion void located at the crown of culvert
$V_{Hnch.}$	Erosion void located at the haunch of culvert
$V_{Inv.}$	Erosion void located at the invert of culvert
$V_{Loc.}$	Erosion void location
$V_{Shldr.}$	Erosion void located at the shoulder of culvert
$V_{Spr.}$	Erosion void located at the springline of culvert
V(Y)	Variance of Y
W	Wheel load on a rectangular footprint
W_{fill}	Total weight on pipe per unit of length
W_{wheel}	Wheel load
X	Variables in Sobol method and probability analysis
$X_{\sim i}$	Vector of all factors but X_i in Sobol method
$x^*_{(1 \times k \times M)}$	Start point matrix in EE method
Y	Output vector in Sobol method
Z	Safety margin in probability analysis

α	Ramberg-Osgood coefficient in steel material model (chapter 3)
β	Erosion void angle (chapter 5)
γ	Unit weight of soil
Δ	Step of variation in EE method
ε	Total strain of steel
ε_{avg}	Average strain
ε_{EF}	Extreme fiber strain
ε_1	Surface membrane strains at the trough location
ε_2	Surface membrane strains at the crest location
ϵ	Error in probability analysis
θ	Angle of corrosion
κ	Curvature
μ_i	Mean value of measures for evaluation of the EE
μ_i^*	Absolute mean value of measures for evaluation of the EE
μ_Z	Mean of Z in probability analysis
ν	Poisson's ratio of soil
σ	Steel stress
σ_i	Standard deviation of measures for evaluation of the EE
σ_u	Ultimate tensile stress
σ_y	Yield tensile stress
σ_Z	Standard deviation of Z in probability analysis
σ_o	Minimum yield stress of steel

Φ	Standard Normal distribution function in probability analysis
φ	Friction angle of soil
ψ	Dilation angle of soil
Ω^k	Unit hypercube in Sobol method

Chapter 1: Introduction

1.1 Motivation

Culverts are components of core municipal infrastructure that control the water flow rate and direction, typically under linear infrastructure (e.g., bridge, railbed, roadway, runway) or built-up areas (e.g., residential, industrial infrastructure). Culvert may also connect bisected drainage pathways (e.g., natural elevation contours, drainage ditches), or water bodies (e.g., ponds, lakes, streams, rivers). There are different types of culverts (e.g., arch, box, bridge, pipe, pipe-arch) that have inherent technical advantages, constraints, and limitations with respect to several factors including geotechnical and hydraulic considerations, long term performance, cost, and risk (i.e., technical, project, societal). This research study is focused on the numerical performance, characterized by the CSC deformation and internal forces for specific load events and boundary conditions, of corrugated steel culverts (CSC) that are widely used in civil engineering practice.

Across North America, most existing culverts were installed in 1950s and 1960s, particularly in the United States through the expansion of the US Interstate highway system. Corrugated steel culverts are a significant proportion of the buried infrastructure in these highways. Most of these buried culverts are nearing the end of their service life due to ageing related deterioration processes including corrosion mechanisms and geotechnical processes such as long-term ground movement, erosion and void creation, and thaw/heave cycling. Flexible culverts are composite systems that integrate the geometric stiffness of the culvert profile with the stiffness of the surrounding soil. The

deterioration mechanisms may degrade the culvert performance and depending on the extent of the deterioration, the culvert may fail to meet serviceability requirements, or may even cause failure of the soil-culvert system; this may result in adverse effects on the public (e.g., service disruption to transportation networks) and, in the most severe cases, potentially fatalities. The significance of culvert failure on infrastructure instability has been observed, including the 2005 Finch Avenue failure[1]. The frequency of such extreme events may increase in the future due to climate change effects.

The replacement of all culverts beyond their initially anticipated service life is not practical due to limited funding and many of these metal culverts may still be usable and may not pose a safety risk for transportation systems and public. It is important to understand how culverts behave throughout their service life and assess how much deterioration would cause yield and finally failure in the soil-culvert structure.

Steel corrosion and voids created in surrounding soil due to erosion are two main environmental deteriorations in buried culvert systems. These deterioration mechanisms happen for buried cases in shallow cover depths due to the complex interaction between the soil and corrugated culvert. A clear understanding of complex soil-culvert interaction and its mechanisms is required to study the effects of these deteriorations. Detailed numerical models are required to investigate load transfer mechanisms and their effects on the internal forces within the culvert. Finally, the detailed numerical model of corrugated

[1] https://pievc.ca/wp-content/uploads/2021/01/City-of-Toronto-Study-of-Three-Road-Culverts-Final-Report-with-Executive-Summary.pdf; Jane-Finch.com - Pictures - Finch Flood - August 19, 2005; Sinkhole on Trans-Canada Highway won't be fixed until weekend | CBC News; Road Collapse- Maine 2008 – (YouTube)

culverts would be trusted to apply the environmental deteriorations (e.g., erosion voids and steel corrosion) to study their influence on the responses.

1.2 Research objectives

The goal of this research study is to assess the mechanical performance of CSC buried in shallow cover depth for intact conditions and assess the effects of CSC wall loss due to corrosion and surrounding soil support due to erosion voids.

Specific objectives of this study are to investigate:

- The relative bias of different modelling approaches to assess the mechanical response (i.e., deflection, internal forces) of CSC for shallow cover depth. The approaches include closed-form analytical expressions, simplified numerical models (e.g., equivalent thickness approach) and comprehensive numerical models accounting for the corrugation profile.
- The load transfer, soil/culvert interaction and mechanical response for intact CSC at shallow cover depth,
- importance of considering bending moment in internal forces of culverts with shallow corrugations,
- the effective internal force in performance of the shallow corrugated culvert buried with a shallow cover depth, thrust or bending moment,
- the effects of CSC wall loss due to corrosion on the CSC mechanical response, for shallow cover depth, through a numerical parameter study

- the key influential parameters and interactions, through a global sensitivity analysis, for CSC with wall thickness loss due to corrosion at shallow cover depth
- the effects of CSC wall loss due to corrosion on the CSC mechanical service life through probabilistic analysis
- the loss of circumferential contact at the soil/culvert interface, due to soil voids, on the CSC mechanical response, and
- the combined effects of corrosion and soil voids on the CSC mechanical response.

1.3 Scope of research

The boundaries of this research study include:

- the CSC is buried at shallow cover depth with backfill soil classified as poorly graded, granular soil (GP-SP),
- the surface loading conditions are defined by CSA S6-14 (2014) for the single wheel pair and single axle load (Axle #4 for CL-625 truck),
- the closed-form equations are based on Canadian Highway Bridge Design Code (CSA S6-14, 2014) and current engineering practice,
- the numerical simulations are based on three-dimensional finite element methods verified using third-party physical modeling studies conducted at Queen's University,
- the constitutive models for the CSC (i.e., von Mises) and soil (i.e., Mohr-Coulomb) are conventional plasticity models,

- the effects of CSC wall loss and soil voids on the CSC mechanical response are investigated through a numerical parameters study, however, the underlying mechanisms causing corrosion and soil erosion are not modelled.

In this research project, continuum finite element modeling procedures, using Abaqus/Standard 6.13 finite element software, are developed to examine the mechanical response of a buried steel culvert. Different approaches were used to model the culvert profile. For the intact numerical models, the experimental full-scale test data are used to verify the validity of analytical model results which were compared with closed-form equations and engineering design code from the Canadian Highway Bridge Design Code (CHBDC). Two different sensitivity analysis (i.e., Sobol and Morris) methods were used to conduct the quantitative approaches that recognized the influential variables for the intact culvert. Finite Element simulations and Global Sensitivity Analysis results were used to propose a correction factor for the recommended closed-form equations (i.e., CSA S6-14, 2014) to calculate local force in the section which is different noticeably from net force (thrust) considered in the current engineering practices for corrugated culverts buried in shallow cover depths.

The analytical model deteriorated with corrosion and erosion voids due to aging is verified using the experimental full-scale test conducted by third party. A series of soil-culvert analytical models were established to investigate the effects of different environmental deteriorations (i.e., corrosion on the culvert wall, erosion voids in the backfill soil) on the soil-culvert structure. Sensitivity analyses were used to identify the important variables in the model that affects the bearing capacity of the culvert-soil

structure. Different sensitivity and probabilistic analysis approaches are used for each type of deteriorations considering the background information which were available from field observations, experimental/laboratory, or full-scale tests. These findings can improve the condition assessment and decision-making capabilities of utilities reduce the chance of high-risk culvert failure.

1.4 Contributions to research and practical applications

This research program investigates numerical modeling procedures, using Abaqus/Standard 6.13 finite element software to examine the mechanical response (i.e., thrust, bending moment, vertical deflection, and membrane strain) of a buried steel culvert. The numerical parametric study investigated the effects of key modelling considerations, including the culvert cover depth (i.e., soil surface to crown), circular and elliptical culvert cross sectional shape with vertical and horizontal orientation, and smooth surface versus annular and spiral ridge depth and pitch profile. Two different approaches were used to model the intact culvert profile including an idealized smooth-surface cylinder with equivalent thickness, and a more detailed and accurate corrugated steel culvert profile with depth and pitch. The analysis included assessment of the culvert strength with respect to the sectional moment, local force, net force, and deformation mechanisms. The results for intact culvert-soil structure were compared with closed-form equations and engineering guidance from the Canadian Highway Bridge Design Code (CHBDC). This investigation can be differentiated from other studies with respect to the more detailed numerical modelling considerations of the corrugated culvert geometry that highlight the

corresponding influence on nonlinear behaviour, soil-structure load transfer processes and deformation mechanisms.

Surrounding soil compaction is another parameter which can affects a culvert's internal stresses and strains in two ways, first the value of transformed truck load, and second the value of the overlying soil loads on the buried culvert. The effect of soil compaction and consolidation has been applied in the numerical simulation using the data from third-party physical modeling study. The soil material behaviour in the numerical analysis was defined using elasto-plastic hardening/softening soil constitutive model with a Mohr-Coulomb yield criterion.

The membrane strain at the crest and trough of the corrugated culvert profile using FE modelling procedures is investigated in this numerical analysis. The FEM strains and thrusts are compared with the measured strains in the experimental tests and calculated thrusts using common closed-form equation in the lab tests. The thrust (i.e., used in the lab tests) does not account for local variations in the corrugated culvert response, consequently, can underestimate the peak local force in the section.

Thrust and failure mechanism which comes from this internal load have been considered as an important aspect of failure of culverts. The value of internal thrust for buried culverts with shallow cover depth and the effect of local bending moments and development of plastic hinges are key factors that govern the failure modes. This mechanism depends on the level of support which surrounding soil provides to the culverts. This research studied both failure mechanisms in buried culverts due to applied conditions which are mentioned in the previous paragraph.

The causes of deterioration are not considered in this study; the focus is limited to the reduction in load carrying capacity because of existing deteriorations. The amount of wall section loss due to corrosion, uniform distribution or general corrosion in longitudinal direction, and corrosion angle in different locations of the culvert and their relation to the carrying capacity are assessed. Determining a safety index for deteriorated culverts is another goal of this research since it facilitates practical assessment of the need for repair or replacement.

The deterministic and probabilistic sensitivity analyses identify variables which have the most impact on the culvert-soil performance. The sensitivity analyses determine how the model output responds to different input conditions and they also determine which variables are the most critical. The sensitivity analyses are completed in two parts. Based on the type of deteriorations and the available information (field, experimental, and analytical) different sensitivity approaches have been used. A deterministic sensitivity analysis was conducted to investigate the input variables of erosion voids in the backfill soil. To study the effects of corrosion deterioration on culverts, probabilistic sensitivity analysis was conducted to investigate the interaction of the input parameters and their effects on output responses. The analyses examine the effect of variation in each variable on the yield stress and the probability of failure over time.

The impact of deterioration of steel culverts and surrounding soil on the culverts' performance is investigated for a more detailed and accurate corrugated culvert-soil structure. Environmental deterioration happens during the service life of the steel culverts. Changes in the volume of the water flow and culverts' exposure to air circulation causes these pipelines' deterioration; corrosion is one of the important environmental deterioration

that affects culverts strength. Erosion of surrounding soil is another deterioration which happens in the buried culverts during their service life due to a variety of different reasons. The performance of the buried deteriorated culverts under overlying soil and traffic loads is considered in this research. The deterioration of surrounding soil changes the load carrying and transferring mechanism which are of interest in this research. Erosion voids have been created around the buried culverts in distinct sizes and positions. In the case of load carrying capacity, these erosion voids can affect pipe-soil interaction mechanisms which lead to changes in culverts internal stresses and their serviceability condition. Studying erosion voids under different conditions (i.e., with and without corrosion deteriorations) and assessing their effect on the performance of the culverts in their service life is another goal of this research.

1.5 Outline of thesis

1.5.1 Integration overview

This manuscript is presented as an integrated thesis comprising the introduction and objective of this research presented in Chapter 1, a review of available literature and background information presented in Chapter 2, integrated research papers presented in Chapters 3 through 6 and finally, the summary, conclusions and recommendations presented in the Chapter 7.

The development and verification of the numerical models is presented in Chapter 3 Research Methods and highlighted in the conference publications (#6) and journal publications (#1) as listed in Section 1.5.2. Chapter 3 discusses the numerical performance assessment of intact buried corrugated steel culvert-soil structure subjected to the service

load conditions. It includes different numerical modeling and detailed verification procedures. The soil/culvert interaction mechanisms and load transfer processes and internal forces of the culvert for each numerical modelling approaches are discussed in this chapter.

The key learning outcomes that shape this chapter is presented as follows:

1. Intact model verification with vertical diameter changes of CSC
2. Importance of 3D modeling with Abaqus
3. The difference of smooth and corrugated surfaces of culvert and observed local variation in the strain magnitude at the crest and trough locations in the corrugated model
4. Importance of culvert cross-section shape, round and horizontal/vertical elliptical culvert
5. Importance of shallow vs deep cover depth of buried culvert
6. Observed good agreements in analytical, experimental and FE prediction measures for bending moment
7. Observed differences in analytical, experimental and FE prediction measures for net and local force.

Because of the observed difference in FE predicted measures with experimental and closed-form equation responses, a multiplying factor for recommended closed-form equations for calculating the local force of CSC buried in shallow cover depth is proposed in Chapter 4. A global sensitivity analysis is conducted to explore the influence of the culvert profile, cover depth, steel and soil material properties, and service load magnitude on the predicted culvert internal forces (i.e., section force and section moment response).

The effects of all influential variables have been studied using Finite Element simulations and closed-form equations to develop a factor for calculating local force response of corrugated culverts buried in shallow cover depths. The results achieved in this chapter presented in journal publications (#2) as listed in Section 1.5.2.

The key learning outcomes that shape this chapter is presented as follows:

1. Intact model verification with circumferential bending moment of CSC
2. The averaging method for calculating strain and thrust in laboratories does not reflect the maximum local force in the corrugated culvert
3. Identified the influential variables for intact CSC and linear/additive features of these variables
4. Proposed thrust multiplying factor for calculating local force for buried corrugated culverts in shallow cover depths

Chapter 5 and 6 include the applied environmental deteriorations, corrosion of steel culvert and creation of erosion voids in the backfill soil, on the culvert-soil structure. In chapter 5, the local and global sensitivity analyses are conducted to measure sensitivity through the entire input space and variable interactions for intact and corroded steel culvert. FE simulations generated to investigate corrosion features (e.g., angle and location) that are not considered in corrosion formulations. Closed-form equations are used to investigate the corrosion deterioration at the location with maximum internal forces (i.e., crown). Variance-based sensitivity analysis used to identify the influential variables and their interactions to conduct the probability analysis to calculate safety index for the corroded culverts. The results achieved in this chapter presented in journal publications (#3) and the conference publications (#5) as listed in Section 1.5.2.

The key learning outcomes that shape this chapter is presented as follows:

1. Observed vulnerability of culvert to corrosion deterioration located at shoulders and crown
2. Observed sensitivity of responses to corrosion angle
3. Additive and linear features of the intact and lightly corroded culvert systems
4. Highly nonlinear feature of influential variables in heavily corroded culverts
5. Generated safety index of corroded culverts based on time-dependent probability study

In chapter 6, the erosion void effects on buried corrugated steel culvert performance is studied. The sensitivity study evaluated soil damage state, as defined by the location and volume of soil erosion voids adjacent to the CSC perimeter for specific non-cohesive soil conditions and design parameters. The combined effects of corrosion and erosion void are investigated for the critical cases. The results achieved in this chapter presented in journal publications (#4) and the conference publications (#5) as listed in Section 1.5.2.

The key learning outcomes that shape this chapter is presented as follows:

1. Introduced voids with different volume (e.g., angle depth, and length) and position (e.g., distance and location in comparison with culvert)
2. Observed sensitivity of the upper half of the culvert to void creation and its effects on internal force responses
3. Observed structural interactions and effect of introduced voids in the backfill soil with high pressure
4. Importance of surface contact loss between soil and culvert due to void creation

5. Destructive effect of combined erosion void and corrosion at lower half of culvert/soil structures

The summery of the conducted research and final conclusions are presented in chapter 7.

1.5.2 List of publications

As part of my research activities, the following manuscripts have been published, submitted for review or in preparation for submission as part of a referred contribution.

Journal Publications (published)

1. Nakhostin, E., Kenny, S. and Sivathayalan, S., 2021. Numerical performance assessment of buried corrugated metal culvert subject to service load conditions. Canadian Journal of Civil Engineering, 48(2), pp.99-114. doi: 1139/cjce-2019-0316.

Journal Publications (under review)

2. Nakhostin, E., Kenny, S. and Sivathayalan, S. (2021). "Thrust Modification Factor for Corrugated Steel Culvert (CSC) Buried in Shallow Cover Depth", Journal of Bridge Engineering (Under Review).
3. Nakhostin, E., Kenny, S. and Sivathayalan, S. (2021). "Buried corrugated steel culverts subjected to corrosion deterioration." (in preparation).
4. Nakhostin, E., Kenny, S. and Sivathayalan, S. (2021). "Erosion Void and Corrosion Effects on Performance of Buried Corrugated Steel Culverts", Engineering Structures Journal, (Under Review).

Conference Proceedings (published)

5. Nakhostin, E., Kenny, S. and Sivathayalan (2019). “Buried corrugated steel culvert failure mechanisms due to environmental deteriorations.” Proc., Int. Conf. Sustainable Infrastructure (ICSI), Leading Resilient Communities through the 21st Century, Los Angeles, CA USA, ISBN 9780784482650, 12p.
6. Nakhostin, E., Kenny, S. and Sivathayalan, S. (2017). “Examination of buried corrugated metal culvert failure mechanisms using finite elements methods.” Proc., GeoOttawa-447:8p.

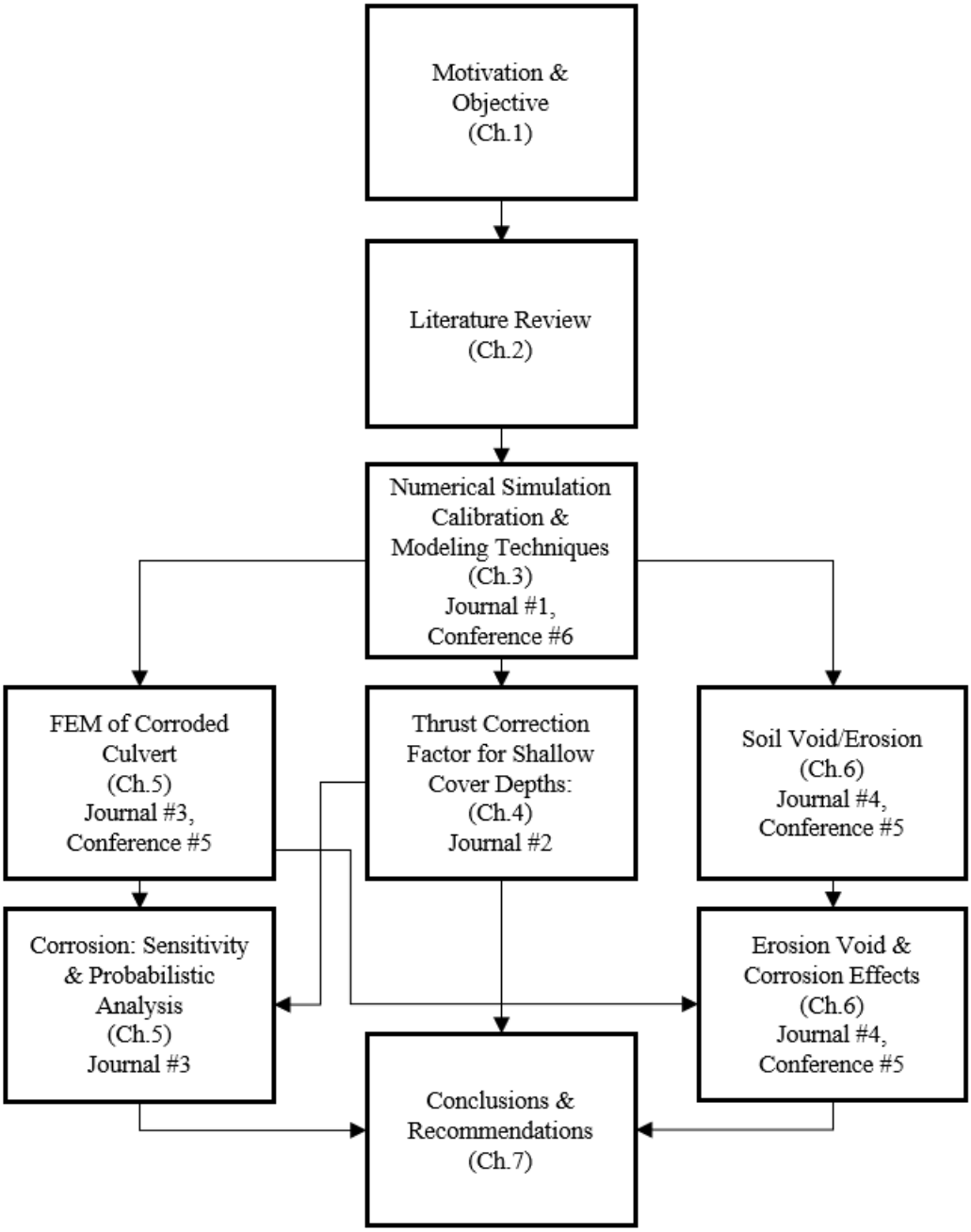
Motivation & Objective (Ch.1)
Literature Review (Ch.2)
Numerical Simulation Calibration & Modeling Techniques (Ch.3) Journal #1, Conference #6
FEM of Corroded Culvert (Ch.5) Journal #3, Conference #5
Thrust Correction Factor for Shallow Cover Depths: (Ch.4) Journal #2
Soil Void/Erosion (Ch.6) Journal #4, Conference #5
Corrosion: Sensitivity & Probabilistic Analysis (Ch.5) Journal #3
Erosion Void & Corrosion Effects (Ch.6) Journal #4, Conference #5
Conclusions & Recommendations (Ch.7)

Chapter 2: Background and Literature Review

2.1 Overview of in-service buried pipes

Steel is a common material used in a wide range of structures such as pipelines because of its strength and affordability. Corrugated Steel Culverts (CSC) are civil structures used for water drainage and watercourse management. These thin-walled structures have been installed since the 1960's due to their beneficial characteristics. Depending on the geographic location and environmental conditions, the estimated service life of this type of culvert has been predicted to be from 10 to 100 years (Beaton and Stratfull, 1962).

Different pipe materials installed in North America were presented by percent of length in Folkman (2012). These materials include cast-iron (CI), ductile iron (DI), Polyvinyl Chloride (PVC), concrete pressure pipe (CPP), steel, and asbestos cement (AC). Based on this study, about 3% of pipes are made of steel that is a low percent in comparison with other materials. Despite the low number of installed steel pipes for this purpose, the failure rate of these pipes per 100 km per year showed that steel pipes had the second-highest breakage rate of all pipe materials after cast-iron pipes, at almost 8.5 failures per 100 km of pipe per year (Folkman, 2012; Wilson, 2014).

The frequently encountered concepts in this research are introduced in this section. Two different corrugated shape of culverts are studied, annular and spiral corrugated profiles as shown in Figure 2.1 a and b.

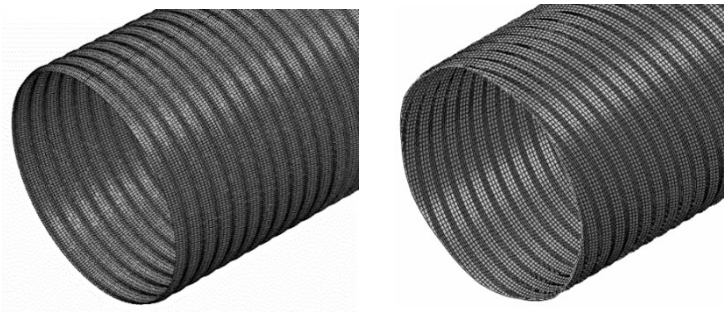

(a) (b)

Figure 2.1. Steel culvert a) annular and b) spiral corrugated profiles

A two-dimensional view of culvert is shown in Figure 2.2 that presents the location of Crown (12:00 clock position), Shoulder (1:30 and 10:30 clock positions), Springline (3:00 and 9:00 clock positions), Haunch (4:30 and 7:30 clock positions), and Invert (6:00 clock position).

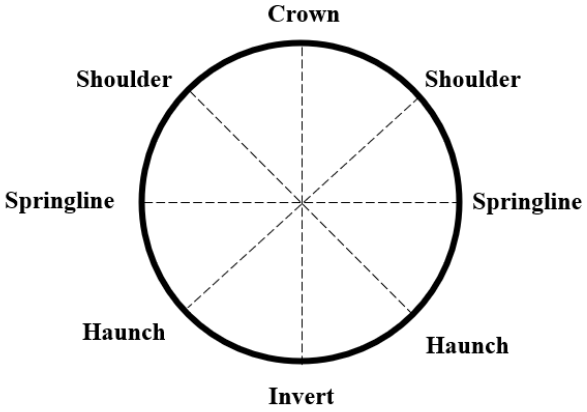

Figure 2.2. A two-dimensional view of culvert

The key geometric features, including crest, trough, pitch, depth and radius, of the corrugated culvert section profile is shown in Figure **2.3**.

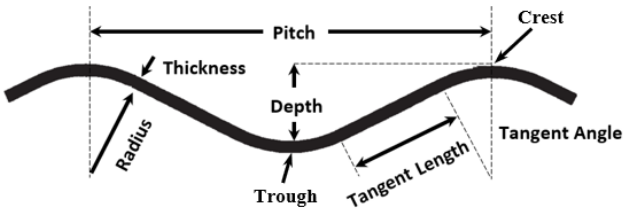

Figure 2.3**. Corrugated section of steel culvert profile**

2.2 Analysis methods

There are three main analysis methods for corrugated steel pipes buried in soil, Laboratory tests and Field measurements, Numerical simulations, or analytical solutions. Field measurements conducted on full-scale corrugated culverts provide the most reliable means of performance assessment. Numerical simulations using the finite element method enable a systematic, cost-effective evaluation of the effects of different variables, and can yield accurate and trusted results, if verified against actual field data. The closed-form analytical equations are based on basic assumptions and simplifications and may be guided by experimental studies. This performance established from experimental, or field studies are discussed first in this chapter followed by a review of the numerical studies and analytical closed-form solutions.

The conducted studies in this field focus on the culvert responses and internal forces (i.e., thrust, moment, strain). The thrust internal force presented in this study is equal to net section force for experimental tests and analytical equations. This thrust value is different from local force values presented at crest and trough of the corrugated profile in the numerical simulation of the corrugated culvert.

2.2.1 Full-scale field and experimental tests

The origins of buried flexible pipe design subject to the effects of backfill surcharge and surface loads can be traced back to the research conducted at the Iowa State University more than 100 years ago (Marston and Anderson, 1913; Spangler and Shafer, 1938). Semi-empirical expressions were developed to predict the stress and ovality of buried flexible pipe (Spangler et al.,1947; Spangler 1964).

Marston et al. (1913) studied the effect of different backfill materials, compaction, and water content on buried flexible pipes; they calculated the loads on pipes buried in trench from actual measurements of the weights of the backfill soil. An equation was proposed based on these measurements and tests to determine the vertical earth load on rigid pipe.

The transferred surface load to the buried pipes was computed based on the results of the experiments conducted at the Iowa engineering experiment station. A truck wheel load was applied as a point load at the roadway surface and the transmitted load through the semi-infinite elastic solid was computed using the Boussinesq formulation and the Newmark table (Spangler et al., 1947).

Various researchers have expressed concerns that the Marston formula is conceptually conservative (Scarino, 2003; Tian et al., 2015). They considered the Marston formula to provide an approximate simulation of earth loads on rigid pipes buried in trenches based on the limited original test data and considering the lack of accuracy of the testing and some modifications that were made. The Marston formula was modified for different soil classifications by Scarino (2003) and the accuracy of the stress and

deformation calculations were improved by Tian et al. (2015) with the main assumption that the vertical earth pressure is not distributed uniformly.

Bakht (1981) investigated the influence of live loads on internal thrust for corrugated steel plate shells used for bridges and culverts in soil/steel structures and buried in soil. Three structures were tested to measure thrusts and moments in the metal shell due to live loads. Uniaxial strain gages installed on the inside of the pipes, one at the top of the crest, one at the bottom of the trough, and the third at the geometric neutral axis of the corrugated plate and the live load was applied by two testing vehicles. The thrust and moments were calculated using measured strains. It was observed that the maximum thrust is induced when the two axles are symmetrically placed above the cross-section center line.

Full-scale field tests were conducted to collect data on the stresses, strains, and deformations in pipe and the surrounding soil embedment as the pipe/soil system is being constructed (McGrath et al., 1999). A total of 14 tests were conducted including a reinforced concrete, corrugated or profile wall polyethylene, and a corrugated steel pipe. It was not possible to test every possible combination of parameters because of the number of variables, but the specific combinations were selected based on the judgement of the research team. Narrow (0.6 m) and wide (>1.8 m) trench widths, different back-fill materials (silty sand and stone with different degree of compactions) and pipe diameter (900 and 1500 mm) were the main variables of the tests. Strain gages and interface pressure cells installed on the metal pipe, and earth pressure cells used to monitor horizontal soil stresses at the trench wall-backfill interface and vertical soil stresses in a plane over the top of the pipe. The inductance strain gages were installed to monitor horizontal soil displacements between the springline of the pipe and the trench wall. Based on the test

results, the left and right sides of the pipes showed approximately the same trend, and reasonable symmetry was achieved in the tests. The strains had opposite signs measured inside and outside of metal pipe at springline and invert.

Large-scale experiments on two deteriorated metal culverts were conducted to study the response of the culverts at different burial depths (Mai 2013). The responses of deteriorated metal culverts were measured during backfilling and during the application of surface live loading. A single axle and a single wheel pair loading were used in the study. The culverts were backfilled to 900 mm cover and loaded under CL-625 design truck loads based on CHBDC, then the cover was reduced to 600 mm and the loading regime was repeated. The vehicle loads and deflections on the culverts became more critical at shallow burial depths and the deflections, thrust forces and bending moments increased due to the reduction in cover from 900 mm to 600 mm. The critical case for surface loading was at shallow burial depth with 600 mm cover. The results indicated that both specimens did not fully recover after the initial load tests with burial depth equal to 900 mm and the one of the specimens had residual bending moments of -696 N.mm/mm during the single wheel pair load tests (Mai 2013; Mai et al., 2013).

Full-scale tests were conducted to study different failure mechanisms on circular corrugated steel culverts buried in a shallow cover depth by Regier (2015). Two different cover depths for intact and corroded corrugated culverts have been studied in these experimental tests and behaviour of the deteriorated culverts were compared to the behaviour of the intact (uncorroded) culverts. Single wheel loading was applied by an actuator to a steel plate on the ground surface representing a single wheel pair positioned over the crown of the corrugated steel culvert at both 0.9 m and 0.45 m of cover depth.

Fiber optic cables were installed in the trough and crest of each culvert specimen tested. The original loading sequence for the control pipe (Intact pipe) was to only apply the maximum service load of 115 kN, rather than the fully factored load of 195 kN. However, during testing at 0.45 m of cover, the control pipe experienced strains above the strain threshold and the maximum service load was not reached (CSA/S6-14, 2014; Regier, 2015). The thrust forces and bending moments at the crown and shoulders were higher than those at and below the springlines.

2.2.2 Numerical simulations

Equivalent thickness and orthotropic shell theory are two common approximate methods used in simulation of corrugated profiles. In the equivalent thickness approach, equivalent Young's modulus is calculated for a isotropic steel structure and corrugated profile is simulated as smooth cylinder with equivalent thickness. This modeling approach is not able to simulate the wall stiffness of the corrugated culvert. Orthotropic shell is the other simplified modeling approach. The equivalent thickness in orthotropic shell theory is an order of corrugation depth and the modulus of elasticity should be reduced to provide the correct EI value. This approach recommends two different values for elastic modulus in circumferential and longitudinal directions (El-Taher, 2009; Elshimi, 2011; Moore et al., 2014).

The behaviour of corrugated metal buried pipes and surrounding soil was studied by Haggag (1989). Finite element analysis was used to model soil/pipe systems. A design approach for pipe wall thrust was developed which considers the effects of pipe shape, width of structural backfill envelope, fill height, pipe size, and compression and bending stiffnesses. These values are considered in calculating the thrust induced in the pipe due to

the backfill load. This simulation results showed that the buckling strength of buried pipe is a function of relative stiffness between the structure and the backfill soil, the height of fill, and the width of structural backfill envelope.

Using finite element methods, Duncan (1978) simulated both the culvert structure and surrounding soil and used soil/culvert interaction design procedure and the results of these analyses verified with the field measurements. This provided a rational method for designing culverts with deep or shallow cover depth. The design was based on consideration of ring compression forces for deep cover depth and for shallow cover it was based on consideration of both ring compression forces and bending moments. The results of these FEM analyses used to derive coefficients for ring compression forces and bending moments for design.

Elshimi (2011) studied the explicit and orthotropic modelling of the geometry of the specific deep-corrugated long-span metal box culvert having a 10 m span and 2.4 m rise using 3D numerical FEM and compared the results of the numerical analysis with the full-scale experimental tests conducted in the laboratory (Mak et al., 2009). The results of the numerical modeling studies indicate the corrugated model provided the best estimate of the section moment, whereas the simplified models such as employing orthotropic shell theory underestimated the bending moment.

The corrugated analysis provided strain values much closer to those that were measured. Moment and thrust values from the corrugated analysis were within 3 and 2% of the experimental values, respectively, whereas the orthotropic analysis cannot model local effects (Brachman et al. 2012). The corrugated model successfully calculated the strains at different locations and provided values closest to the measured values in the

experimental tests, but the orthotropic model had 40% difference in the calculated strains compared to the measured values.

Similar trends were noted for the internal forces (i.e., thrust and bending moment) of the box culvert; the calculated maximum moment using FEM with orthotropic modelling had a difference of 40% and this model was unable to calculate reasonable values of thrusts. The corrugated model successfully calculated the bending moments within 3% of the maximum experimental values of positive and negative moment and provided the best agreement with experimental values at other points across the structure. While the calculated thrust by the corrugated model showed a noteworthy difference with the experimental values in locations with high thrust values (Elshimi 2011).

The behaviour of the box culvert during backfilling was successfully predicted using the 3D FEM simulations. Modelling the increase in lateral stresses due to soil compaction has a minor effect on the response of long-span deep-corrugated metal box culvert during backfilling and the crown displacement due to compaction was less than 4% of the calculated displacement without modelling compaction (Elshimi et al., 2011).

Two finite element analysis (i.e., CANDE and Abaqus) programs were used to study corrugated culverts that were modeled by two-dimensional simulations. All the finite element models were unable to capture the non-linear behaviour of the deteriorated culvert with poor backfill as well as both culverts at high surface loading due to the use of linear elastic models. CANDE provided very poor estimates of culvert diameter change and ABAQUS predicted culvert diameter change and thrust force with good accuracy in the linear elastic region but not beyond (Moore et al., 2014).

2.2.3 Closed-form equations of buried pipe internal forces

According to the Marston theory the vertical earth load on rigid pipes (sewer pipe) can be determined from the following equation:

Equation 2.1 $$W_{fill} = C_d \gamma B_d^2$$

where W_{fill} is total weight on pipe per unit of length, γ is the unit weight of the backfill, B_d is the effective trench width, C_d is the load factor . The backfill unit weight, the outside diameter of pipe, the cover depth of pipe, the lateral earth pressure, the internal friction, and the interface friction between the native and backfill soil conditions are integrated in the C_d coefficient (Marston et al., 1913).

Based on this formulation, the frictional resistance relieves part of the vertical pressure near the sides of the trench, so at the top level of the pipe the vertical pressure of the filling material is much heavier in the middle of the trench than at the sides. In trenches with common width, the trench filling above the top of the pipe receives a negligible support from the filling at the sides of the trenches. Hence the pipe must be strong enough to carry safely the entire weight of the trench filling materials above the top of the pipe and for deeper cases the value of C_d is magnifying the backfill load effects (Marston et al., 1913).

Spangler computed the load transmitted to the buried pipe due to the wheel load as follows:

Equation 2.2 $$W_{wheel} = 4 C_t \left(\frac{W*D}{A}\right)$$

where C_t is a wheel load coefficient, W is the wheel load on a rectangular footprint, D is the pipe diameter and A is the area of the rectangular footprint. The value of

rectangular load coefficient C_t was determined considering different trench geometries and rectangular footprints (Spangler, 1964).

Spangler (1947) proposed the Spangler stress formula which estimates the circumferential stress at the bottom of the pipe cross section due to fill and surface live loads. In this formula the bending moment was considered in the calculation based on theory of elasticity solutions for elastic ring bending.

Duncan (1978) used FEM to derive equations for bending moment for design. This study mentioned that the bending moment need to be calculated for the cases that the cover depth is less than one-quarter of the span and should be calculated as follows:

Equation 2.3 $$\boldsymbol{M = R_B\, K_{M1}\, \gamma\, {S_c}^3 - R_B\, K_{M2}\, \gamma\, {S_c}^2\, H + R_L\, K_{M3}\, S_c\, LL}$$

where M is bending moment due to backfill and live load with cover depth H, $K_{M1}, K_{M2}\ and\ K_{M3}$ are moment coefficients, $R_B\ and\ R_L$ are moment reduction factors, γ is unit weight of backfill, S_c is culvert span, and LL is the live load. The values of moment coefficients depend on the flexibility of the culvert section relative to the backfill.

For laboratory tests and field studies, to estimate the thrust and moment, the CSC wall strain should be sampled at the extreme fiber locations on the crest and trough at paired locations distributed along the CSC perimeter. The thrust and bending moment can be calculated using the linear elastic mechanics. The strains for each culvert were measured on the corrugation trough and the corrugation crest. Each test specimen was instrumented with uniaxial strain gauges or fiber optic strain sensing along a corrugation. Gauges were installed in both the trough and the crest of the corrugation to permit post-test calculations of both the average axial strain and the curvature. Fiber optic strain sensing provides a distributed strain profile around the full circumference or along the full length of the

culvert, eliminating the issue of optimizing the circumferential sensor location required with conventional strain gauges, and creating a better understanding of the culvert's total structural behaviour.

The FEM strains at trough (ε_1) and crest (ε_2) locations on the outside culvert surface (at the culvert/soil interface) of the corrugated profile were used to estimate (extrapolate) the extreme fiber strain (ε_{EF}) at the trough location on the inside surface of the culvert corrugated profile using the linear interpolation (Equation 2.4),

Equation 2.4 $$\boldsymbol{\varepsilon_{EF} = \frac{(\varepsilon_1 - \varepsilon_2)}{h} t + \varepsilon_1}$$

where h is radial distance between the strain gauges ε_1 and ε_2, and t is intact wall thickness of the corrugated pipe.

The average strain (ε_{avg}) can be estimated using Equation 2.5 (Simpson et al., 2015, Simpson et al., 2016, Regier, 2015).

Equation 2.5 $$\boldsymbol{\varepsilon_{avg} = \frac{\varepsilon_2 + \varepsilon_{EF}}{2}}$$

The thrust calculated using average strain.

Equation 2.6 $$\boldsymbol{N = \varepsilon_{avg} EA}$$

where N is thrust per unit length along the CSC circumference, E is young modulus, and A is cross section area per unit length.

In the various lab-test studies and field measurements of strain, the reported results indicate that the measured strains at crest and trough of corrugated steel pipe have opposite signs with small differences in their values (Elshimi, 2011;, Mai, 2013; Simpson et al., 2016; Regier, 2015; Sargand et al., 2018; Liu et al., 2020; Khoury et al., 2020; Tehrani et

al., 2021). These references used the presented approximate method to calculate thrust in the corrugated steel culverts.

2.3 Design methodology

Semi-empirical approaches were developed to predict the stress and ovality of buried flexible pipe. The structural performance of flexible culverts studied in the laboratory at the Iowa State University by Spangler et al. (1938) to develop a design theory. Although the laboratory results showed relatively large radius of curvature and deflections, the conclusion indicated that the elastic theory was applicable to corrugated metal pipes within a tolerance that is not greater than the induced tolerance by variation in material and geometrical properties of the corrugated culvert.

The transmission of surface wheel loads to the buried pipe was based on Boussinesq theory. This theory based on elasticity calculates the vertical stress under a point load in a homogeneous, semi-infinite half space and ignores soil/culvert interactions.

Subdividing the cover of the pipe into smaller sub-layers was a common method to calculate the live load in each sub-layer and then compute the live load on the structure by summation of loads on all the sub-layers. Later, the Boussinesq formula was integrated to obtain the pressure over a finite rectangular area in the undersoil in native soil. Newmark integrated the Boussinesq formula to evaluate the pressure at a point in the undersoil due to a uniformly distributed load applied over a rectangular area at the soil surface. The transferred surface load to the buried pipes computed based on the results of experiments conducted in the Iowa engineering experiment station (Spangler et al., 1947).

The primary accepted design practice for buried corrugated pipes was based on hoop compression capacity with the thrust limit state governing structural performance. Because the interaction between soil and corrugated shell was very complex, various approximate methods were developed for calculating load effects in the shell.

Bakht (1981) investigated the influence of live loads on internal thrust for corrugated steel plate shells used for bridges and culverts in soil/steel structures and buried in soil. The influence of live loads on internal thrust for shallow cover depths was experimentally investigated for round ($D_h/D_v = 1$) and horizontally elliptical ($D_h/D_v > 1$) culverts. The need for simplistic design procedures led to the development of approximate methods of calculating load effects with a large depth of cover about 2.5 m and a modification to existing simplified methods for predicting thrust due to live loads was proposed.

The distributed live load was calculated using Boussinesq theory and the importance of an impact factor on the section thrust due to live loading was identified by Bakht (1981).

The FE simulation by Haggag (1989) presented the arching factor changes relative to the cover depth, and pipe span; updated results of this study are presented in the design standards and codes. The buckling design chart was developed by considering the width of structural backfill envelope, relative stiffness between the pipe and the backfill soil, relative stiffness between the surrounding soil and the backfill soil, and the cover depth.

Duncan (1978) simulated culvert/soil system using finite element method. The soil/culvert interaction was considered in the design procedure and the results of these analyses verified with the field measurements. The results of these FE analyses used to derive coefficients for bending moments. The value of minimum cover depth calculated

using the soil/culvert interaction method considering the bending moment due to backfill load and surface live load (Duncan, 1978).

Based on the study conducted by Duncan (1978), the factor of safety against yield and creation of plastic hinge under live load is low for the culvert buried in the shallow cover depth. The factor of safety was calculated for different cover depths and the minimum acceptable cover depth determined based on these results (Duncan, 1978). The conducted finite element studies to estimate the sectional moment response in the buried pipeline are applied in the current practice design approach (CSA S6-14, 2014).

Choi et al. (2004) evaluated the moment equation proposed by Duncan (1978) for soil/metal arch structures. The FEM simulation was used in the study and the results indicated that the location of maximum moment in the pipe is changing for different cases where are located at crown or the shoulder based on the arc spans.

The results of truck position and multiple truck loading study using FEM indicates that the maximum moment and displacements were obtained when the applied loads were centered over the culvert crown for box and arc culverts (Elshimi et al., 2014).

The explicit and orthotropic model of corrugation geometry for the specific deep-corrugated long-span metal box culvert showed a noteworthy difference between the calculated thrust by FEM and the experimental values in locations with high thrust values. Based on the results of the study, it is mentioned that the Canadian Highway Bridge Design Code (CSA S6, 2006) thrust equations underestimate the earth and live load thrust values for arch culverts (Elshimi, 2011). Calculated thrust of corrugated culvert modeled by two-dimensional simulations using finite element method software (i.e., CANDE and Abaqus) compared with the estimated thrust using the design equations given in the Canadian

Highway Bridge Design Code. Based on this study the design code equations underestimated the thrust in the culverts, suggesting that these approaches could be unconservative (Moore et al., 2014).

Full-scale tests conducted to study different failure mechanisms on corrugated steel culverts buried in a shallow cover depth (Regier, 2015). The structure ultimately failed due to the formation of plastic hinges collapse mechanism developing at the shoulders and crown. This failure mechanism is recognized as a mechanism which is different to that addressed in the design standards and codes and it occurred at loads lower than the required load capacity (Regier, 2015; Moore et al., 2017).

It is mentioned that the load carrying mechanism changes from thrust at 0.9 m of cover to bending at 0.45 m of cover due to the live loading of the culvert (Regier, 2015). Based on the results, it is concluded that the current design procedures consider the wrong failure mode for new pipes in some instances, as the intact control pipe tested at shallow cover in the study had strength limited by local bending in the top half of the pipe, which does not match the expectation of failure controlled by thrust at the springlines (Regier et al., 2018).

2.4 Environmental deteriorations on culverts and backfill soil

Corrosion and erosion voids are the two environmental deteriorations that can affect stability and factor of safety of the culvert structures and can change the load distribution. Deterioration may occur in the buried culverts due to corrosion on the inside of CSC and erosion voids in the surrounding soil. The CSC/soil structure deterioration is thus related to the culvert material and the surrounding soil.

The deterioration of the culvert system can result in life-threatening and expensive damage to the culverts and the related systems (Perrin Jr and Jhaveri, 2004; Meegoda et al., 2009). The collapse of a CSC occurred in Northern Sardinia, Italy, after an extreme rainfall event in 2013. The possible causes of collapse are related to the conditions before and during the rainfall (Giresini et al., 2016).

The condition of buried steel pipes in Ontario and their deterioration mechanisms was reviewed by Cichocki et al. (2021). The deteriorations were due to both void formation around the buried structures in contact with the backfill soil due to piping or infiltration, and loss of wall thickness due to corrosion or abrasion. The age, condition, and rehabilitation of steel buried pipes with span greater than 3m which were installed as bridges in Ontario were investigated to understand the structural deterioration and rehabilitation opportunities for structures nearing the end of their service lives. The condition of the steel corrugated culverts was rated using bridge condition index metric (BCI) which was calculated based on the original and remaining value of a structure after deterioration (MTO 2009). For steel bridges with a BCI < 60, rehabilitations should be undertaken within the year, for 60 < BCI < 70, the steel bridges need rehabilitation within the next 5 years, and steel bridges with BCI > 70 do not need any rehabilitations. For corrugated steel structures, out of the 194 bridges in-service with known construction dates, 18% of the bridges are known to be over 50 years old and 70% are known to be over 30 years old. Comparing the corrugated steel bridges with other installed pipes (i.e., reinforced precast concrete, prestressed precast concrete, steel, weathering steel), corrugated steel bridges have the highest proportion of bridges with the lowest BCI as 23% of the

investigated corrugated steel bridges has a BCI between 60 and 70, and 17% has a BCI of 60 or lower (Cichocki et al. 2021).

2.4.1 Steel pipe corrosion

The corrosion rate of metal culverts is influenced by the hydrogen ion concentration (pH), and the electrical resistivity of the soil and water (Beaton and Stratfull, 1962). Some long-term corrosion models developed based on the environmental parameters on the corrosion rate of steel that predicts the corrosion based on the given exposure time of material to the atmosphere. A large database based on the reported information from different countries was used to establish a universal equation (Feliu et al., 1993).

Long-term atmospheric corrosion model of steel was proposed based on different atmospheric sites (i.e., rural, urban, industrial, and marine). The effect of corrosion was quantified in term of mass loss and the effect of environmental parameters considered on the corrosion rate (De la Fuente et al., 2011).

The corrosion effect of environment on steel was investigated by field observations, full-scale and laboratory tests and the steel corrosivity was classified based on data obtained in Europe and North America climate conditions (Mikhailov et al., 2004, Cichocki et al. 2021).

El-Taher (2009) studied the effects of metal corrosion on culvert stability using two-dimensional Finite element modeling to explain how stability could be endangered by these forms of deterioration. The material failure and yield in the steel was considered. Corrosion in the lower half of the structure (at the water line) was introduced including a range of losses in wall thickness and it was found that the factor of safety against yield decreased in proportion to the wall thickness (El-Taher and Moore, 2008).

Large-scale experiments on two deteriorated metal culverts were conducted to evaluate and study the response of the culverts under surface live loads at different burial depths (Mai 2013). The responses of deteriorated metal culverts were measured during backfilling and during the application of surface live loading. A single axle and a single wheel pair loading were used in the study. The culvert named CSP1 was a heavily corroded steel culvert and its remaining wall thicknesses on either side of the invert were 70% (West haunch) and 48% (East haunch) of the original values. The second case, CSP2, had light corrosion on both sides of the invert (e.g., remaining wall thicknesses of 83% at the West haunch and 90% at the East haunch). The side fill used for each specimen was different and CSP1 was backfilled with uncompacted side fill, whereas the side fill was compacted for CSP2 (e.g., loose for CSP1 and dense for CSP2) in order to simulate poorly compacted soil surrounding CSP1 and well compacted soil surrounding CSP2. The standard Proctor values for the backfill material beside specimens CSP1 and CSP2 were 86.12% and 92.56% respectively. Both culverts were backfilled to 900 mm cover and loaded under CL-625 design truck loads based on CHBDC, then the cover was reduced to 600 mm and the loading regime was repeated. Specimen CSP1 started to contract significantly in the vertical direction and expand in the horizontal direction while specimen CSP2 experienced very little change in diameter. This difference in behaviour was likely due to the substantially different stiffness of the fill supporting the sides of each specimen. Although CSP1 was a heavily deteriorated metal culvert (with 48% and 70% remaining wall thickness on either side of the invert), it was able to carry the single axle working load and did not fail until reaching 340 kN, which was equal to 90% of the fully factored single axle load based on both the Canadian and AASHTO design trucks. The results from the analyses

were compared to design method (i.e., CHBDC). Incremental thrusts obtained using the CHBDC design equations were unconservative for most of the tests (Mai 2013; Mai, Hoult, Moore, 2013).

The effects of cover depth and culvert deterioration (i.e., wall loss due to corrosion) were examined through full-scaled physical models of annular culverts subjected to surface loading. Two different covers with 450 mm and 900 mm depths for intact and corroded corrugated culverts have been studied in these experimental tests. Single truck wheel used in loading and positioned over the crown of the corrugated steel culvert. Uniaxial strain gauges and fiber optic strain sensing used to measure the strains in culvert and thrust and bending moments were calculated by approximate closed-form equations. Gauges were installed in both the trough and the crest of the corrugation to permit post-test calculations of both the average axial strain and the curvature. The corrosion is applied at the invert of the culvert with angle equal to 100 degrees and different remaining thicknesses at the water line (Regier 2015, Regier et al., 2018). The full-scale test results showed that the surrounding soil compaction has a greater impact on the overall behaviour of corrugated metal culverts. Consequentially, density and soil stiffness of surrounding soil had a greater effect on the overall behaviour than the level of steel corrosion. The experimental observations indicated that the level of deterioration influenced the failure mode with local buckling in the corroded region (34% remaining wall thickness at the water line), and plastic hinges in the top half of the culvert (47% remaining wall thickness).

A metal culvert with 600 mm (24 in) diameter under Coopermill Road near Zanesville in Muskingum County, Ohio, was tested because of its advanced level of invert metal loss. The load was applied statically, and a truck parked over the crown of the culvert.

The culvert was tested under an external load of up to 267 kN placed over the crown. The culvert was instrumented with strain gauges and string potentiometers. The strains and deflections were measured from the sensors, and the corresponding stresses, thrusts, and bending moments were computed. The measured strains at crest and trough of the corrugation in untreated section of corroded culvert were found to have almost equal magnitudes but opposite signs. Despite the highly deteriorated conditions in the invert and shallow cover (600 mm), there was a significant load-carrying capacity remaining in the culvert which supported a load considerably larger than the legal limit of 80 kN (Sargand et al., 2018).

2.4.2 Soil erosion voids

Erosion voids can develop in the backfill due to environmental conditions. The deterioration mechanisms are influenced by the presence of moisture, and soil characteristics including type, homogeneity, density, clay content and mineralogy (Bradford 2000; Hepfner 2002). The deterioration of the culvert system can result in life-threatening and expensive damage to the culvert and its related system (Perrin Jr and Jhaveri 2004; Meegoda et al. 2009).

The soil voids may be created due to water leakage through corrosion features at the base of the CSC. Hydraulic pressure and flow may washout and transport fines within the backfill that results in the creation of soil voids. Field observations have indicated that the concentration of solid particles transported with the sewage causes the formation of a groove around the pipe (Rubin et al. 2013; Cichocki et al. 2021).

The creation of voids within the backfill, particularly adjacent to the structure/soil interface, can influence the structure-soil interaction and load transfer processes (i.e.,

amplitude, distribution) and failure mechanisms that may affect the stability and integrity of buried structures. Operational experience with buried structures, such as pipelines and tunnels, has observed the creation of local soil voids distributed around the structure, which can affect the structural load carrying capacity.

The erosion void creates a separation or region of non-contact between the structure and surrounding soil backfill, which may result in undesirable deformation and stress being developed within the buried structure (Yasuda et al. 2017). The simulation of erosion voids can be achieved through considerations of the contact region and interaction mechanics between the structure and surrounding soil. In the numerical simulations, erosion voids can be modeled with removing the contact and partial interaction between the soil and culvert (Giresini et al., 2016; Xu and Cheng, 2013). Local, discrete voids (i.e., separation between the structure and soil) may be introduced at different locations on the interface. Due to these changes in the contact interface, changes in the normal contact pressure were measured and the simulations indicated noticeable changes in the magnitude and distribution of earth pressure within the region experiencing loss of contact (Leung and Meguid 2011, Wang et al. 2014).

Simplified modeling techniques have been used to study the stability of the buried culverts using Abaqus finite element software. The most popular methods have idealized the corrugated steel section as a simple cylinder, orthotropic shell theory and explicit model of corrugated geometry by considering hoop stress and the development of yield. Stability and the factor of safety against yield were found to decrease in proportion to deterioration owing to the fact that the presence of deterioration changes the distribution of thrust and moment (El-Taher and Moore, 2009).

The presence of soil voids may reduce structural load carrying capacity, induce local soil deformation mechanisms, cause eccentric loading on the structure that can lead to unexpected stresses and may cause progressive structure deterioration and failure (Meguid and Dang 2009, Meguid and Kamel 2014).

A corroded corrugated steel pipe was buried with an erosion void simulated from the haunch to the springline on one side (Peter and Moore, 2019). Testing under simulated service loads revealed that the void appeared to compromise the stability of the structure at a load of 87% of the full-service load. Changes in curvature under load in the springline adjacent to the simulated erosion void were about 3 times higher than those at the springline with soil support. Bending moments were also substantially higher on the side adjacent to the erosion void.

2.5 Sensitivity analysis

Sensitivity analysis can assess the uncertainty in model input parameters and corresponding influence on the predicted model outcomes across an analysis or design space (Saltelli et al., 2004). Sensitivity analysis can be classified as local or global methods. Local sensitivity analysis assesses the local impact of the input variables by concentrating on the sensitivity in vicinity of a set of factor values. Global sensitivity analysis provides an overall view of input variables influences on output responses. This method quantifies the importance of the input variables and their interactions. The importance of factor interactions in the results and variance based methods are well known methods for global sensitivity analysis which investigate the entire factors distribution (Saltelli et al., 2010). In this study, the Morris and Sobol methods are examined because these methods measure

sensitivity across the whole input space and deal with nonlinear responses and measure the effect of interactions in non-additive systems. The Morris method is a variance-based sensitivity analysis method with low computational costs in comparison with well-known methods such as Sobol method.

2.5.1 Morris method

The uncertainty in the output of a model is allocated to different sources of uncertainty in input factors. Sensitivity analysis orders the importance of the input factors in determining the variation in the output (Saltelli et al., 2008). One-at-a-time (OAT) is the most common screening method to identify main important input factors between all input factors. OAT is a common method because of practical reasons such as low computational costs and comparable results that one variable is changing at a time and all other variables are fixed to the baseline value. OAT method dose not explore the input space; that is the disadvantage of this method and interactions between input factors are neglected in this approach (Czitrom, 1999). Elementary effects (EE) method is a sensitivity analysis to identify noninfluential input variables. The original concept of EE method is derived from the OAT screening method and introduced by Morris (1991). This method provides two sensitivity measures which are mean μ and standard deviation (σ) for each input factor to identify the influential factors. Campolongo et al. (2007) proposed a revised version of the EE method that solved the problem of the nonmonotonic model with the effect of responses with opposite signs. Campolongo et. al. (2007) improved this method and introduced a revised measure, the mean of the distribution of the absolute values of the elementary effects of the input factors (μ^*), to avoid the error that might occur when the output contains both positive and negative value and these opposite values would cancel out their effects

in mean calculations. EE is a screening method to determine which factors are negligible or which factors are linear and additive, nonlinear or involved in interaction with other factors (Saltelli et al., 2008).

2.5.1.1 Sampling and generating the trajectories

The EE sampling method is used in this study. This method introduces wider ranges for input variations and removes the dependence on a single sample point. In the EE sampling method, k independent variables vary in the k-dimensional unit cube across p selected level with the step of variation equal to Δ. The p-level should be selected to reflect the variation of input parameters inside the domain. The p is even and the Δ for all variables is chosen to be equal to $p/(2(p-1))$ (Saltelli et al. 2008; Morris 1991). The start point matrix, $x^*_{(1 \times k \times M)}$, is a random selection of the start point for all input variables and is used to generate the trajectory points. Using this start point will generate a randomized version of the sampling matrix. For detailed procedure, see Saltelli et al. (2008).

To maximize the spread of the selected points in the variable domain a method is proposed by Campolongo et al. (2007). The method is selecting the best r trajectories out of M trajectories with scanning the input domain to achieve the highest spread. The design starts by generating M trajectories and selects the subset of r with the highest spread to optimize the scanning of the input space (Saltelli et al. 2008). The best r combination of M with the highest value of D, the sum of the squared distances between all possible pairs of trajectories belonging to the combination, is equal to $\binom{\mathrm{M}}{\mathrm{r}}$.

The concept of spread is based on the following definition of distance, d_{ml}, between a pair of trajectories m and l:

Equation 2.7

$$\begin{cases} \boldsymbol{d_{ml} = \sum_{i=1}^{k+1} \sum_{j=1}^{k+1} \sqrt{\sum_{z=1}^{k} \left[X_z^{(i)}(m) - X_z^{(j)}(l) \right]^2}} & \boldsymbol{if\ m \neq l} \\ \boldsymbol{d_{ml} = 0} & \boldsymbol{if\ m = l} \end{cases}$$

For instance, for the combination 4, 6, 7, and 9 (i.e., $r = 4$) from the possible $M = \{1, 2, 3, 4, 5, 6, 7, 8, 9, 10)$, $D_{4,6,7,9}$ can be defined as:

Equation 2.8

$$\boldsymbol{D_{4,6,7,9} = \sqrt{d_{4,6}^2 + d_{4,7}^2 + d_{4,9}^2 + d_{6,7}^2 + d_{6,9}^2 + d_{7,9}^2}}$$

Developing M trajectory is repeated several times to select the best M trajectories with the highest spread because of the computing limitations.

The input points are not sampled directly for normally distributed variables. In a k-dimensional hypercube, each set of values varies in [0 1]. The actual input values are derived using the inverse of the normal cumulative distribution function (CDF).

2.5.1.2 First order Elementary Effect method

A global sensitivity analysis method examines the influence of uncertain parameters over the whole parameter range. The proposed screening method by Morris (1991) identify parameters that can be fixed in analysis without affecting the model outputs. The sampling and generating trajectories are discussed in detail. Each variable change one time in a trajectory. The Elementary Effect of each variable can be calculated by the magnitude of variation of that specific variable in the model output. The elementary effect associated with factor i is defined as follows:

Equation 2.9

$$\boldsymbol{EE_i^j\left(x^{(l)}\right) = \frac{[y(x^{(l+1)}) - y(x^{(l)})]}{\Delta}}$$

if the ith component of $x^{(l)}$ is increased by Δ, and

Equation 2.10

$$\boldsymbol{EE_i^j\left(x^{(l+1)}\right) = \frac{[y(x^{(l)}) - y(x^{(l+1)})]}{\Delta}}$$

if the ith component of $x^{(l)}$ is decreased by Δ (Saltelli et al., 2008).

While one trajectory allows the evaluation of one elementary effect for each parameter i, a set of r trajectories enable statistical evaluation of the finite distribution of the elementary effects. Once r elementary effects per input are available, the statistical measures for evaluation of the EE, the mean (μ_i), the absolute mean (μ_i^*), and the standard deviation (σ_i), relative to the distributions can be computed for each input factor.

Equation 2.11 $$\boldsymbol{\mu_i = \frac{1}{r}\sum_{j=1}^{r} EE_i^j}$$

Equation 2.12 $$\boldsymbol{\mu_i^* = \frac{1}{r}\sum_{j=1}^{r} \left|EE_i^j\right|}$$

Equation 2.13 $$\boldsymbol{\sigma_i = \sqrt{\frac{1}{r-1}\sum_{j=1}^{r}\left(EE_i^j - \mu\right)^2}}$$

where the index r is the number of trajectories.

The computation cost for calculating the first-order elementary effect indices for each exposure time is r × (k+1) runs. The calculations can be repeated x times to calculate the error bars for reported quantitative values.

The elementary effects (EE) method is one of approaches which is used to identify the influential variables. Morris (1991) introduced the concept of elementary effects which determines effective input factors in interaction with other factors for linear, additive, and nonlinear models using two sensitivity measure, the mean and the standard deviation of the distribution. The absolute values of the mean of the distribution is used in this study proposed by Campolongo et al. (2007) to solve the problem of type II errors in the elementary effect analysis (Saltelli et al., 2008).

2.5.2 Sobol method

Sensitivity analysis method is an effective method for identifying the important factors in the model. The Monte-Carlo based numerical procedure has been used for

computing the first- and total-order indices for the buried corrugated steel culvert with k variables. Random sequence of generated points has a high discrepancy with cluster and gaps in the domain. To avoid this problem, Quasi-random sampling technique which is a low discrepancy sequence is commonly used. These sampling techniques are not completely random and unpredictable, but they bias the selection of points to maintain a uniform distribution of points across the sampling domain. The Halton sequence is a well-known low-discrepancy sequence that is used in this study (Homma & Saltelli, 1996; Saltelli, 2002; Saltelli et al., 2008). N is called the base sample in order to have an evident low discrepancy considering independent variables.

2.5.2.1 Sensitivity indices

Monte Carlo-based implementation for computing sensitivity measures provided by Sobol (2005). Sobol considered f as a square integrable function and Ω^k as the k-dimensional unit hypercube. The expansion of f was considered into terms of increasing dimensions.

Equation 2.14 $$\boldsymbol{\Omega^k = (X|\ 0 \le x_i \le 1;\ i = 1, \dots, k)}$$

Equation 2.15 $$\boldsymbol{f = f_0 + \sum_i f_i + \sum_i \sum_{j>i} f_{ij} + \cdots + f_{12\dots k}}$$

Where X refers to the variables, and k is the number of variables.

This decomposition has a finite number of terms, f_0 is constant, $\binom{k}{1} = k$ are first-order functions $(f_i = f_i(X_i))$, $\binom{k}{2} = \frac{k!}{2!\,(k-2)!}$ are second-order functions $(f_{ij} = f_{ij}\,(x_i, x_j))$ and higher-order functions. To have a unique expansion of High Dimensional Model Representation (HDMR), each term in the expansion should has zero mean (Sobol,

2005). By applying this condition, each term of the decomposition can be calculated as follows:

Equation 2.16 $$f_0 = E(Y)$$

Equation 2.17 $$f_i = E(Y|X_i) - E(Y)$$

Equation 2.18 $$f_{ij} = E(Y|X_i, X_j) - f_i - f_j - E(Y)$$

where Y is the output vector, $E(Y)$ is mean or expected value of Y.

The variance of decompositions can be shown as:

Equation 2.19 $$V_i = V(f_i(X_i)) = V[E(Y|X_i)]$$

Equation 2.20 $$V_{ij} = V\left(f_{ij}(X_i, X_j)\right) = V[E(Y|X_i, X_j)] - V[E(Y|X_i)] - V[E(Y|X_j)]$$

By square integrating each term of the decomposition (Equation 2.14) over Ω^k, ANOVA-HDMR decomposition of total model variance can be written as:

Equation 2.21 $$V(Y) = \sum_i V(f_i) + \sum_i \sum_{j>i} V(f_{ij}) + \cdots + V(f_{12\ldots k})$$

By dividing both sides of the equation 13 by V(Y) which indicates the variance of Y, we obtain:

Equation 2.22 $$\sum_i S_i + \sum_i \sum_{j>i} S_{ij} + \cdots + S_{12\ldots k} = 1$$

where S_i is the first-order sensitivity index represents the main effect contribution of each input factor to the variance of the output (Fenton & Griffiths, 2008; Homma & Saltelli, 1996; Iman & Hora, 1990; Saltelli et al., 1993).

Equation 2.23 $$S_i = \frac{V[E(Y|X_i)]}{V(Y)}$$

S_{ij} is the second-order sensitivity index representing the joint effect of the pair (X_i, X_j) on Y minus the first-order effect for X_i and X_j. Higher-order sensitivity indices quantifies higher-order interactions. First-order effect plus all higher-order effects of factor X_i calls total effect index of factor X_i that is useful to investigate the all interactions

involving the parameter X_i. Homma and Saltelli (1996) proposed a technique to calculate total effect indices at the same cost of first-order indices.

Equation 2.24 $$\boldsymbol{S_{Ti} = 1 - \frac{V[E(Y|X_{\sim i})]}{V(Y)} = S_i + S_{ij} + \cdots + S_{ij\ldots k}}$$

Where $X_{\sim i}$ is the vector of all factors but X_i.

The first-and total-effect indices are calculated in this study. Two matrices ($N \times k$) are generated called matrix A and B. N is the base sample to cover the entire parameter space. These matrices are generated by applying quasi-random Holton sequence. Matrix C_i formed by all columns of matrix B except the ith column which is taken from matrix A. The model output for all input values in the matrices A, B, and C are calculated, $y_A = f(A)$, $y_B = f(B)$, and $y_{Ci} = f(C_i)$. The computation cost for this method is $N \times (k + 2)$ runs. The first-order and total-effect indices are estimated based on the following equations (Saltelli et al., 2008).

Equation 2.25 $$\boldsymbol{S_i = \frac{V[E(Y|X_i)]}{V(Y)} = \frac{y_A \times y_{Ci} - f_0^2}{y_A \times y_A - f_0^2}}$$

Equation 2.26 $$\boldsymbol{S_{Ti} = 1 - \frac{V[E(Y|X_{\sim i})]}{V(Y)} = 1 - \frac{y_B \times y_{Ci} - f_0^2}{y_A \times y_A - f_0^2}}$$

Equation 2.27 $$\boldsymbol{f_0^2 = \left(\frac{1}{N}\sum_{j=1}^{N} y_A^{(j)}\right)^2}$$

2.6 Probability analysis, First-Order Second Moment (FOSM) theory

The non-influential variables that do not significantly affect the response can remain constant in the probability analysis. The First-Order Second Moment (FOSM) method is a probabilistic method to determine the structural reliability index. The reliability index can be determined for the nonlinear limit state function and for calculating the reliability index, the Most Probable Point (MPP) which is the point of greatest probability density within the

space incorporated by the failure region needs to be found (Ahammed and Melchers, 1997, Melchers and Beck, 2018). For highly nonlinear problems, there is the convergence issue that the algorithm may converge very slowly. To solve this convergence issue, the Two-point Adaptive Nonlinear Approximation (TANA) is recommended. Based on TANA, the nonlinearity of approximation can be changed by using the information which is generated during the iteration process (Rackwitz and Flessler, 1978, Wang and Grandhi, 1996, Grandhi and Wang, 1999).

In probability theory, the FOSM is a probabilistic method to determine the stochastic moments of a function with random input variables. The name of this method is based on the derivation, which uses a first-order Taylor series and the first and second moments (i.e., mean and standard deviation) of the input variables. In the second moment concept, the limit state equation is the safety margin (Z), and the probability of failure p_f can be calculated as follows:

Equation 2.28 $$\boldsymbol{Z = R - S}$$

Equation 2.29 $$\boldsymbol{p_f = \Phi(-\beta)} \qquad \boldsymbol{\beta = \frac{\mu_Z}{\sigma_Z}}$$

where R is resistance, S is load effect, β is the safety index and Φ is the standard Normal distribution function. Equation 2.29 yields the exact probability of failure p_f when both R and S are Normally distributed.

β is the safety or reliability index and it is a measure (in standard deviation σ_Z units) of the distance that the mean, μ_Z is away from the origin Z = 0. This point marks the boundary of the failure region and β is a direct measure of the safety of the structural element where greater β represents greater safety, or lower failure probability.

The limit state function is a random function consisting of more than two basic random variables as follows:

Equation 2.30 $$g(X) = Z(X) = a_0 + a_1X_1 + a_2X_2 + \cdots + a_nX_n$$

where $g(X)$ is the linear approximate limit state function and X is the vector of all relevant basic variables and g is some function expressing the relationship between the limit state and the basic variables. The limit state equation $g(X) = 0$ defines the boundary between the satisfactory or safe domain $g > 0$ and the unsatisfactory or unsafe domain $g \leq 0$ in n-dimensional basic variable space.

In general, the limit state function $g(X) = 0$ is not linear and the first two moments of nonlinear $g(X)$ cannot be computed easily. The recommended approach is to linearize $g(X) = 0$ and this can be done by expanding $g(X) = 0$ as a first-order Taylor series expansion about point x^* which is the point of maximum likelihood or most probable point (MPP) on the limit state function (Melchers and Beck, 2018).

When the limit state function is non-linear, the first two moments of $g(X)$ in x space cannot be obtained exactly because nonlinear combination of implicit Normal distributions do not lead to a Normal distribution for $g(X)$. To solve this issue, instead of using fixed approximation models in generating the limit state functions, using adaptive approximations for different types of problems is recommended. The first-order Tylor series expansion in terms of adaptive intervening variables are used to construct the adaptive approximation. The known information, which is generated during the iteration process of problem-solving steps, should be used to change the nonlinearity of the adaptive approximations and update the used value for the next iteration. Two-point adaptive

nonlinear approximation (TANA) is a method to solve these types of problem with fast convergence.

First, the failure surface $g(X) = g(x_1, x_2, \dots, x_n)$ needs to be mapped from X-space to U-space and all variables should be transferred into their standardized forms:

Equation 2.31 $\boldsymbol{u_i = \frac{x_i - \mu_{x_i}}{\sigma_{x_i}}}$

where μ_{x_i} and σ_{x_i} represent the mean value and standard deviation of x_i respectively. The distributions of $U = \{u_1, u_2, \dots, u_n\}^T$ are rotationally symmetric with respect to the second-moment distribution. Based on the transformation, the mean value point in the original space (i.e., X-space) is mapped into the origin of the standard normal space (i.e., U-space) and the failure surface $g(X) = 0$ in X-space is mapped into the corresponding failure surface $g(U) = 0$ in U-space. The geometrical distance from the origin in U-space to any point on $g(U) = 0$ is simply the number of standard deviations from the mean value point in X-space to the corresponding point on $g(X) = 0$. distance to the failure surface can then be measured by the safety index function as follows:

Equation 2.32 $\boldsymbol{\beta(U) = (U^T U)^{\left(\frac{1}{2}\right)} \qquad U \in g(U) = 0}$

The β is the minimum value or shortest distance from the origin to the failure surface, $\tilde{g}(U) = 0$. $\tilde{g}(U)$ is the approximate U-space limit state surface and computed using $\tilde{g}(X)$ which is the adaptive approximate limit state surface in X-space can be calculated as follows:

Equation 2.33 $\boldsymbol{\tilde{g}(X) = g(X_k) + \frac{1}{r}\sum_{i=1}^{n} x_{i,k}^{1-r} \frac{\partial g(X_k)}{\partial x_i}(x_i^r - x_{i,k}^r)}$

Where r is nonlinear index and k is the iteration step.

$\tilde{g}(X)$ is mapped into $\tilde{g}(U)$ by using the standard normal or equivalent normal transformations,

Equation 2.34 $$\tilde{\boldsymbol{g}}(\boldsymbol{U}) = \tilde{\boldsymbol{g}}\left(\boldsymbol{\sigma}_{x_1}\boldsymbol{u}_1 + \boldsymbol{\mu}_{x_1}, \boldsymbol{\sigma}_{x_2}\boldsymbol{u}_2 + \boldsymbol{\mu}_{x_2}, \dots, \boldsymbol{\sigma}_{x_n}\boldsymbol{u}_n + \boldsymbol{\mu}_{x_n}\right)$$

The nonlinear index r can be any positive or negative real number and can be calculated from Equation 2.35

Equation 2.35 $$\boldsymbol{g}(\boldsymbol{X}_{\boldsymbol{k-1}}) - \left\{\boldsymbol{g}(\boldsymbol{X}_{\boldsymbol{k}}) + \frac{\mathbf{1}}{\boldsymbol{r}}\sum_{\boldsymbol{i=1}}^{\boldsymbol{n}} \boldsymbol{x}_{\boldsymbol{i,k}}^{\mathbf{1-r}} \frac{\boldsymbol{\partial g}(\boldsymbol{X}_{\boldsymbol{k}})}{\boldsymbol{\partial x_i}}\left(\boldsymbol{x}_{\boldsymbol{i,k-1}}^{\boldsymbol{r}} - \boldsymbol{x}_{\boldsymbol{i,k}}^{\boldsymbol{r}}\right)\right\} = \mathbf{0}$$

The iteration searching for r starts from r = 1. The difference ϵ between the exact and approximate function needs to be calculated and the final answer would be acceptable if the allowable error ($\epsilon = \left|\frac{\beta_{k+1}-\beta_k}{\beta_k}\right|$) is smaller than the initial error ($\epsilon = 0.001$) (Grandhi and Wang, 1999).

References

Ahammed, M. and Melchers, R. (1997). “Probabilistic analysis of underground pipelines subject to combined stresses and corrosion.” Engineering structures, 19(12), 988–994.

Bakht, B. (1981). “Soil-steel structure response to live loads.” Journal of the Geotechnical Engineering Division, 107(6), 779–798.

Beaton, J. and Stratfull, R. (1962). “Field test for estimating service life of corrugated metal pipe culverts.” Highway Research Board Proceedings, Vol. 41.

Brachman, R., 25 Elshimi, T., Mak, A., and Moore, I. (2012). “Testing and analysis of a deep corrugated large-span box culvert prior to burial.” Journal of Bridge Engineering, 17(1), 81–88.

Bradford, S. A. (2000). "The practical handbook of corrosion control in soils". CASTI Publishing Inc. Edmonton, Alberta, Canada.

Campolongo, F., Cariboni, J., and Saltelli, A. (2007). “An effective screening design for sensitivity analysis of large models.” Environmental modelling & software, 22(10), 1509–1518.

Choi, D.-H., Kim, G.-N., and Byrne, P. M. (2004). “Evaluation of moment equation in the 2000 canadian highway bridge design code for soil–metal arch structures.” Canadian journal of civil engineering, 31(2), 281–291.

Cichocki, R., Moore, I., and Williams, K. (2021). “Steel buried structures: condition of Ontario structures and review of deterioration mechanisms and rehabilitation approaches.” Canadian Journal of Civil Engineering, 48(2), 159–172.

CSA/S6-14. 2014. “Canadian Highway Bridge Design Code S6-14 CSA”. Canadian Standards Association, Canada.

Czitrom,V. (1999). “One-factor-at-a-time versus designed experiments.” The American Statistician, 53(2), 126–131.

Dhar, A. S., Moore, I. D., and McGrath, T. J. (2004). “Two-dimensional analyses of thermoplastic culvert deformations and strains.” Journal of geotechnical and geoenvironmental engineering, 130(2), 199–208.

Duncan, J. (1978). “Soil-culvert interaction method for design of metal culverts.” Transportation research record, (678).

El-Taher, M., & Moore, I. D. (2009). Stability of deteriorated metal culverts including the effect of soil erosion. Geo Engineering Centre at Queen’s – RMC, Queen’s University, Kingston, ON.

El-Taher, M. (2009). “The effect of wall and backfill soil deterioration on corrugated metal culvert stability.” Ph.D. thesis, Queen’s University.

El-Taher,M. andMoore, I. D. (2008). “Finite element study of stability of corroded metal culverts.” Transportation Research Record, 2050(1), 157–166.

Elshimi, T., Mak, A., Brachman, R., and Moore, I. (2011). “Behaviour of a deep-corrugated large span box culvert during backfilling.” Pan-American Conference on Teaching and Learning of Geotechnical Engineering, Toronto, Canada.

Elshimi, T. M. (2011). “Three-dimensional nonlinear analysis of deep-corrugated steel culverts.” Ph.D. thesis, Queen’s University.

Elshimi, T. 52 M., Brachman, R. W., and Moore, I. D. (2014). “Effect of truck position and multiple truck loading on response of long-span metal culverts.” Canadian Geotechnical Journal, 51(2), 196–207.

Feliu, S., Morcillo, M., and Feliu Jr, S. (1993). “The prediction of atmospheric corrosion from meteorological and pollution parameters—ii. long-term forecasts.” Corrosion Science, 34(3), 415–422.

Fenton, G. A., Griffiths, D. V., et al. (2008). Risk assessment in geotechnical engineering, Vol. 461. John Wiley & Sons New York.

Folkman, S. (2012). Water Main Break Rates in the USA and Canada: A Comprehensive Study. Utah State University.

Giresini, L., Puppio,M. L., and Sassu,M. (2016). “Collapse of corrugated metal culvert in northern sardinia: analysis and numerical simulations.” International Journal of Forensic Engineering, 3(1-2), 69–85.

Grandhi, R. V. and Wang, L. (1999). “Structural reliability analysis and optimization: Use of approximations.” Wright State University, Dayton.

Haggag, A. A. (1989). Structural backfill design for corrugated metal buried structures. University of Massachusetts Amherst.

Hepfner, J. J. et al. (2002). “Statewide corrosivity study on corrugated steel culvert pipe.” Report no., Montana. Department of Transportation. Research, Development and Technology.

Homma, T. and Saltelli, A. (1996). “Importance measures in global sensitivity analysis of nonlinear models.” Reliability Engineering & System Safety, 52(1), 1–17.

Iman, R. L. and Hora, S. C. (1990). “A robust measure of uncertainty importance for use in fault tree system analysis.” Risk analysis, 10(3), 401–406.

Khoury, I., Sargand, S.M., Hussein, H. H., and Al Rikabi, F. T. (2020). “Field investigation of metal multi-pipe culvert under shallow cover.” Pipelines 2020, American Society of Civil Engineers Reston, VA, 21–30.

Leung, C. and Meguid, M. (2011). “An experimental study of the effect of local contact loss on the earth pressure distribution on existing tunnel linings.” Tunnelling and underground space technology, 26(1), 139–145.

Liu, Y., Hoult, N. A., and Moore, I. D. (2020). “Structural performance of in-service corrugated steel culvert under vehicle loading.” Journal of Bridge Engineering, 25(3), 04019142.

Mai, V. T. (2013). “Assessment of deteriorated corrugated steel culverts.” Ph.D. thesis, Queen’s University, 233p.

Mai, V. T., Hoult, N. A., and Moore, I. D. (2014). “Effect of deterioration on the performance of corrugated steel culverts.” Journal of Geotechnical and Geoenvironmental Engineering, 140(2), 04013007.

Mak, A. C., Brachman, R. W., and Moore, I. D. (2009). “Measured response of a deeply corrugated box culvert to three dimensional surface loads.” Transportation Research Board Annual Conference, Washington DC, Paper, Citeseer, 09–3016.

Marston, A., & Anderson, A. O. (1913). The theory of loads on pipes in ditches: and tests of cement and clay drain tile and sewer pipe (Iowa State College of Agriculture and Mechanic Arts).

McGrath, T. J., Selig, E. T., Webb, M. C., Zoladz, G. V., et al. (1999). “Pipe interaction with the backfill envelope.” Report no., University of Massachusetts at Amherst. Transportation Center.

Meegoda, J. N., Juliano, T. M., and Tang, C. (2009). “Culvert information management system.” Transportation research record, 2108(1), 3–12.

Meguid, M. A. and Dang, H. (2009). “The effect of erosion voids on existing tunnel linings.” Tunnelling and Underground Space Technology, 24(3), 278–286.

Meguid, M. A. and Kamel, S. (2014). “A three-dimensional analysis of the effects of erosion voids on rigid pipes.” Tunnelling and underground space technology, 43, 276–289.

Moore, I. D., Hoult, N. A., et al. (2014). “Performance of two-dimensional analysis: Deteriorated metal culverts under surface live load.” Tunnelling and underground space technology, 42, 152–160.

Moore, I. D., Regier, C., and Hoult, N. A. (2017). “Surface load testing of new circular and elliptical metal culverts at shallow cover.” Archiwum Instytutu Inżynierii Lądowej.

Morris, M. D. (1991). “Factorial sampling plans for preliminary computational experiments.” Technometrics, 33(2), 161–174.

MTO (2009). Bridge condition index (BCI) an overall measure of bridge condition. Ministry of Transportation Engineering Standards Branch, St. Catharines, ON.

Perrin Jr, J., Jhaveri, C. S., and Perrin Jr, J. (2004). “The economic costs of culvert failures.” Prepared for TRB 2004 Annual Meeting, Washington DC.

Peter, J. M. and Moore, I. D. (2019). “Effects of erosion void on deteriorated metal culvert before and after repair with grouted slip liner.” Journal of Pipeline Systems Engineering and Practice, 10(4), 04019031.

Rackwitz, R. and Flessler, B. (1978). “Structural reliability under combined random load sequences.” Computers & Structures, 9(5), 489–494.

Regier, C. (2015). “Investigation of the failure mechanisms of intact and deteriorated culverts.” Ph.D. thesis, Queen’s University. 147p.

Regier, C., Moore, I. D., and Hoult, N. A. (2018). “Remaining strength of deteriorated corrugated steel culverts.” Journal of Pipeline Systems Engineering and Practice, 9(2), 04018002.

Rubin, H., Tokarev, D., Rubin, E., and Schuttrumpf, H. (2013). “Bed load erosion patterns and their effect on the structural strength of rigid pipes made of homogeneous materials.” The Open Civil Engineering Journal, 7(1), 32–49.

Saltelli,A. (2002). “Making best use of model evaluations to compute sensitivity indices.” Computer physics communications, 145(2), 280–297.

Saltelli, A., Andres, T., and Homma, T. (1993). “Sensitivity analysis of model output: an investigation of new techniques.” Computational statistics & data analysis, 15(2), 211–238.

Saltelli, A., Annoni, P., Azzini, I., Campolongo, F., Ratto, M., and Tarantola, S. (2010). “Variance based sensitivity analysis of model output. design and estimator for the total sensitivity index.” Computer physics communications, 181(2), 259–270.

Saltelli, A., Ratto, M., Andres, T., Campolongo, F., Cariboni, J., Gatelli, D., Saisana, M., and Tarantola, S. (2008). Global sensitivity analysis: the primer. John Wiley & Sons.

Saltelli, A., Tarantola, S., Campolongo, F., and Ratto, M. (2004). Sensitivity analysis in practice: a guide to assessing scientific models, Vol. 1. Wiley Online Library.

Sargand, S. M., Khoury, I., Hussein, H. H., and Masada, T. (2018). “Load capacity of corrugated steel pipe with extreme corrosion under shallow cover.” Journal of Performance of Constructed Facilities, 32(4), 04018050.

Scarino, J. H. (2003). “Reappraisal of marston’s formula.” Journal of transportation engineering, 129(6), 703–712.

Simpson, B., Moore, I. D., and Hoult, N. A. (2016). “Experimental investigation of rehabilitated steel culvert performance under static surface loading.” Journal of Geotechnical and Geoenvironmental Engineering, 142(2), 04015076.

Sobol’, I. M. (2005). “Global sensitivity indices for the investigation of nonlinear mathematical models.” Matematicheskoe modelirovanie, 17(9), 43–52.

Spangler, M., Hennessy, R., and Barber, E. (1947). “A method of computing live loads transmitted to underground conduits.” Highway Research Board Proceedings, Vol. 26.

Spangler, M. G. (1964). “Pipeline crossings under railroads and highways.” Journal-American Water Works Association, 56(8), 1029–1046.

Spangler, M. G. and Shafer, G. (1938). “The structural design of flexible pipe culverts.” Highway Research Board Proceedings, Vol. 17.

Tehrani, A., Kohankar Kouchesfehani, Z., Chimauriya, H. R., Raut, S., Najafi, M., and Yu, X. (2021). “Structural evaluation of invert-cut circular and arch shape corrugated steel pipes through laboratory testing.” Canadian Journal of Civil Engineering, 48(2), 187–201.

Tian, Y., Liu, H., Jiang, X., and Yu, R. (2015). “Analysis of stress and deformation of a positive buried pipe using the improved spangler model.” Soils and Foundations, 55(3), 485–492.

Wang, J., Huang, H., Xie, X., and Bobet, A. (2014). “Void-induced liner deformation and stress redistribution.” Tunnelling and Underground Space Technology, 40, 263–276.

Wang, L. and Grandhi, R. V. (1996). “Safety index calculation using intervening variables for structural reliability analysis.” Computers & structures, 59(6), 1139–1148.

Wilson, D. (2014). “Investigation of the failure of large-diameter cast-iron water mains using a stochastic, physical model.” Ph.D. thesis, Queen’s University.

Xu, L. and Cheng, Y. (2013). “Development of a finite element model for simulation and prediction of mechanoelectrochemical effect of pipeline corrosion.” Corrosion Science, 73, 150–160.

Yasuda, N., Tsukada, K., and Asakura, T. (2017). “Elastic solutions for circular tunnel with void behind lining.” Tunnelling and Underground Space Technology, 70, 274–285.

Chapter 3: Numerical Performance of Intact Buried Corrugated Steel Culvert

3.1 Methodology

In this chapter, two- and three-dimensional continuum finite element modeling procedures are used to examine the mechanical response (i.e., thrust, bending moment, vertical deflection, and membrane strain) of a buried metal culvert. The numerical parametric study investigated the effects of key modelling considerations, including the culvert cover depth (i.e., soil surface to crown), circular and elliptical culvert cross sectional shape with vertical and horizontal orientation, and smooth surface versus annular and spiral ridge depth and pitch profile. Surface load effects of a single wheel pair positioned over the culvert crown at the ground surface on the pipe mechanical response was examined with respect to a variation in the culvert cover depth. Two approaches were used to model the culvert profile including an idealized smooth-surface cylinder with equivalent thickness, and a more detailed and accurate corrugated metal culvert profile with depth and pitch. The soil material behaviour was defined using elastic-plastic hardening/softening soil constitutive model with a Mohr-Coulomb yield criterion. Confidence in the numerical modeling procedures was established through verification with data from third-party physical modeling studies (Regier, 2015).

The primary objective was to gain an improved understanding of the failure mechanisms for shallow and deep buried culverts through a systematic analysis on an equivalent basis. Secondary objectives were to develop modeling procedures to assess the

effects of culvert profile, orientation and shape on culvert mechanical response, and to compare with engineering practice for shallow cover depth. The selected analysis parameters were based on an assessment of the knowledge gap in current practice and expected nonlinear behaviour across the parameter range. The analysis included assessment of the culvert strength with respect to the sectional moment, thrust, and deformation mechanisms. The results were compared with closed-form equations and engineering guidance from the Canadian Highway Bridge Design Code (CHBDC). This investigation can be differentiated from other studies with respect to the more detailed numerical modelling considerations of the culvert geometry that highlight the corresponding influence on nonlinear behaviour, soil-structure load transfer processes and deformation mechanisms.

3.2 Modeling procedures

Continuum finite element methods, using Abaqus/Standard 6.13 finite element software, were used to examine the mechanical response of a buried metal culvert subject to service loads.

3.2.1 Steel culvert

A 900 mm diameter culvert was evaluated in 2D (i.e., plane strain) and 3D (i.e., continuum) space, using Abaqus/Standard 6.13 software, with two different approaches used to define the section mechanical response. As shown in Figure 3.1a, the first modeling approach idealized the corrugated culvert section geometry by transforming the nominal wall thickness and ridge profile of the culvert to an equivalent section for a right, circular

hollow cylinder with an equivalent wall thickness ($\bar{t} = 15.0\,mm$ wall thickness) using Equation 3.1and equivalent elastic modulus ($\bar{E} = 20.2\,GPa$) using Equation 3.2,

Equation 3.1 $$\bar{t} = \sqrt{\frac{12 * E_p * I_p}{E_p * A_p}}$$

Equation 3.2 $$\bar{E} = \frac{E_p * A_p}{\bar{t}}$$

where E_p is the culvert elastic modulus, A_p is the culvert cross-sectional area per unit length, and I_p is the culvert second moment of area per unit length. This approach is consistent with conventional analysis and modelling practices, and has been used in other studies (El-Taher and Moore, 2008, Mai, 2013, Mai et al., 2018). This modeling approach is unable to account for the orthotropic behaviour of a corrugated profile (i.e., difference in the extensional or membrane, and flexural or bending stiffness) and to capture local deformation mechanisms due to the corrugation profile response.

The second, more detailed modelling approach, explicitly accounts for the culvert section geometry as shown in Figure 3.1b. The nominal wall thickness (1.60 mm), depth (12.7 mm), pitch (67.7 mm), tangent length (19.58 mm), tangent angle (26.73 deg.), and radius (17.46 mm) of the corrugated culvert profile was modelled. These selected parameters were based on physical modelling studies (Corrugated Steel Pipe Institute, 2010) for a culvert with a cross-sectional area of 1.51 mm^2 per unit length, a moment of inertia of 28.4 mm^4 per unit length, and section modulus 4.02 mm^3 per unit length.

The elastic modulus (200 GPa) and yield strength (230 MPa) are based on Regier (2015) with the mechanical properties summarized in Table 3.1. As the steel stress-strain relationship was not presented by Regier (2015), the corresponding stress-strain amplitude

pairs were defined through piecewise approximation using a Ramberg-Osgood mathematical expression (Equation 3.3).

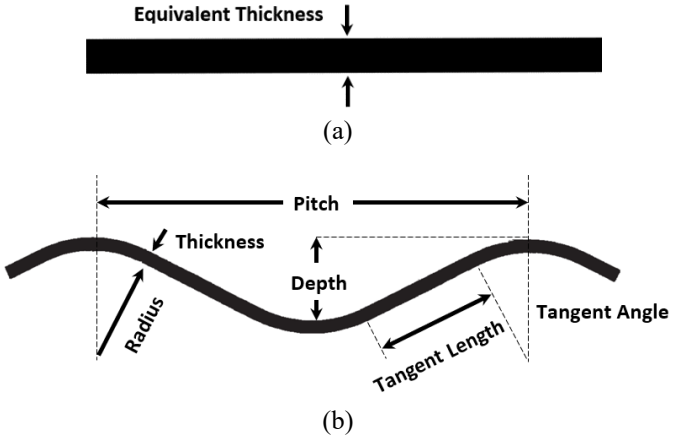

Figure 3.1. Steel culvert profile a) equivalent and b) corrugated sections

Equation 3.3 $\varepsilon = \frac{\sigma}{E} + \frac{\alpha\sigma_o}{E}(\frac{\sigma}{\sigma_o})^N$

where ε is total strain, σ is applied stress, E is the Young's modulus, α and N are constant values of equation and σ_o is equal to minimum yield stress. Grade A steel was considered representative of the culvert material with the physical constants summarized in Table 3.1 (Ramberg and Osgood, 1943, Walker and Williams, 1995). The constitutive behaviour was defined using J2 plasticity theory with the von Mises yield criterion and combined hardening model (Hibbitt et al., 2013). In steel material, the elastic part of the material is isotropic and the hardening behaviour in the plastic part is combined. This combined model uses stress versus plastic strain values of the first half cycle for calibrating the kinematic hardening parameters.

The culvert section was discretized using fully integrated linear 8-node (C3D8) solid continuum elements in Abaqus software for 2D model space with equivalent thickness. The C3D8 element is a fully integrated linear element with eight integration points.

Conventional stress/displacement shell elements with 4 nodes (S4) are used to model three-dimensional culvert structure which one dimension, the thickness, is significantly smaller than the other dimensions. Conventional shell elements use this condition to discretize a body by defining the geometry at a reference surface. This element has displacement and rotational degrees of freedom.

Table 3.1. Culvert mechanical properties

Parameters	Symbol	Magnitude	Units
Young's (elastic) modulus	E	200	GPa
Yield tensile stress	σ_y	230	MPa
Yield tensile strain	ε_o	0.50	%
Ultimate tensile stress	σ_u	331	MPa
Ramberg-Osgood coefficient	α	3.95	
Ramberg-Osgood exponent	N	9.36	

3.2.2 Soil domain and boundary conditions

For the 2D equivalent section model, the soil domain was 2000 mm deep and 2600 mm wide (Figure 3.2a). The 3D equivalent section and 3D annular corrugated profile FE models extended the domain 1500 mm along the length of the culvert segment (Figure 3.2b). As shown in Figure 3.2a & b, the boundary conditions replicated the experimental setup (Mai et al., 2018, Regier, 2015, CSA S6-14, 2014) where the soil domain base was fixed from motion (i.e., X = Y = Z = 0), and the sidewall vertical faces were constrained

from the transverse lateral motion (i.e., X = 0). Based on a sensitivity study, this soil domain, representing backfill conditions around the culvert was determined to sufficiently mitigate end boundary conditions effects for these FE models and reduce the wallclock time for running the FE model.

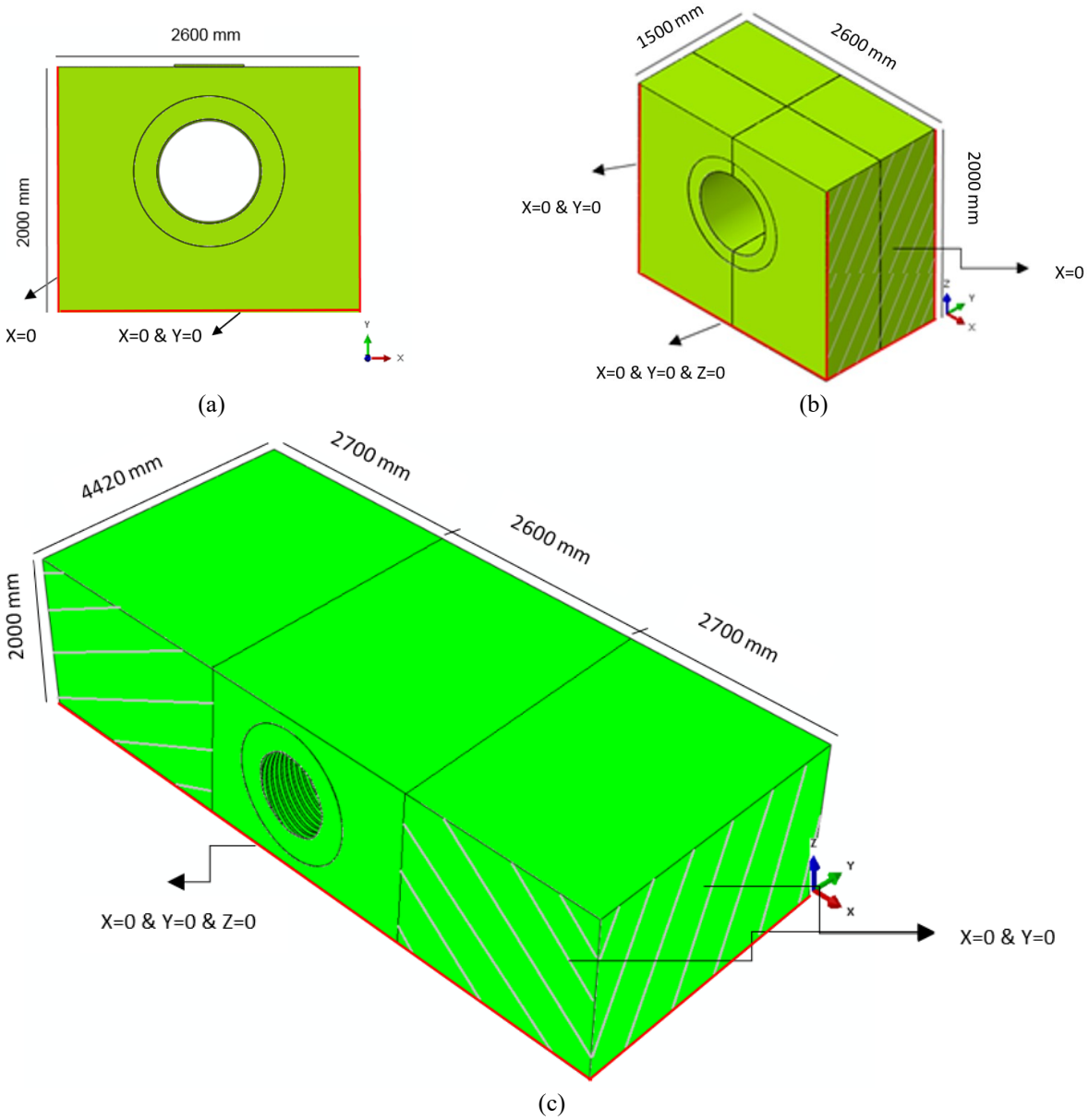

Figure 3.2. Finite element model dimensions and boundary conditions for the a) 2D equivalent smooth ring culvert model, b) 3D equivalent smooth cylinder and annular corrugated culvert models, and c) 3D spiral corrugated culvert model

For the 3D spiral corrugated profile FE model, the soil domain was extended to 8000 mm wide and 4420 mm long (Figure 3.2c) to have soil box dimensions consistent with the full-scale test parameters (Regier, 2015). The 3D spiral corrugated profile model had an additional boundary condition along the headwall blocks (2700 mm wide section) to simulate the transverse lateral constraint of the concrete reinforcement blocks used in the experimental setup (i.e., Y = 0). It is shown in this study that lateral boundary conditions only had minimal influence on the mechanical response of the culvert; the deflections, strains, section local force and thrusts and section moments were comparable in the 3D annular (Figure 3.2b) and spiral (Figure 3.2c) corrugated profile models. Differences in the numerical predictions were also attributed to the orientation of the corrugation (i.e., annular versus spiral).

The soil mechanical behaviour was defined as linear elastic, strain hardening/softening plastic with the Mohr-Coulomb yield criterion. The plastic flow potential is characterized by a hyperbolic function in the meridional stress plane and smooth elliptic function in the deviatoric stress plane (Menetrey and Willam, 1995). A non-associated flow rule, which requires an unsymmetrical matrix storage and solution scheme (Simulia, 2013) was used. The soil parameters, summarized in Table 3.2, were based on experimental studies (Elshimi and Moore, 2013, Elshimi et al., 2011, McGrath et al., 1999), and used to calibrate the numerical modeling procedures. For the experimental studies, the backfill could be characterized as poorly graded granular soil (GP-SP) using the unified classification system (ASTM, 2011). This soil is granular, and it has a drained condition and pore water can easily drain out from the soil and the extra pressure will be dissipated.

Consequentially, free water is not considered in the numerical simulation of backfill soil in this study.

The soil domain was discretized using four node, bilinear plane strain quadrilateral elements (CPE4) for the 2D models and eight node, linear brick elements (C3D8) for the 3D models with full integration.

Table 3.2. Soil material properties

Soil parameters	Symbol	Magnitude	Units
Young's (elastic) modulus	E	14.8	MPa
Poisson's ratio	ν	0.3	
Angle of friction	φ	43	deg.
Dilation angle	ψ	13	deg.
Cohesion	c	1	kPa
Unit weight	γ	21	kN/m^3

3.2.3 Culvert/soil interface modeling

The contact interface between the steel culvert and backfill soil was modeled as two deformable surfaces. Tangential interface behaviour was used to define friction contact through isotropic friction using the penalty formulation with finite sliding on the contact area which is the most general and allows any arbitrary motion (i.e., separation, sliding, and rotation) of the surfaces. Penalty is a stiffness method and permits some relative motion of the surfaces. The penalty contact algorithm for a balanced master-slave contact pair computes contact forces. One set of forces is calculated considering one surface as the master surface, and the other surface as the slave surface. Culvert and soil was defined as a contact pair with the culvert as the master and soil as a slave surfaces (Wriggers, 1995,

Hibbitt et al., 2013). Penalty contact introduces numerical softening to the contact enforcement by adding elastic springs to the contact interface. This algorithm stores the energy upon impact in the springs which is recoverable and does not dissipate it. In this modeling slave node is in contact along the master surface and it can slide along the surface. The position of slave nodes relative to the master surface have been tracked when the culvert-soil deforms, and the transfer paths and contact directions are been updated during the analysis. When the slave node penetrations in the current configuration contact forces are applied to the slave nodes to oppose the penetration.

3.2.4 Loading

The soil cover depths examined in this study are defined as a distance between the ground surface and the highest point of culvert which is crown. CL-W Truck load is applied on the surface at ground level. The CL-W Truck is an idealized five-axle truck. Figure 3.3 shows CL-W Truck wheel load in Ontario where CL-625 Truck with 625 kN weight is recommended to be used. The wheel load that has maximum effect is applied considering the culvert span which is equal to 900 mm. The wheel load of axle No. 4 is applied in the numerical simulations and one lane of loading is considered in this study. Based on CHBDC as shown in the Figure 3.3, the wheel pad, 250 mm x 600 mm in plan, was imposed on the ground surface and positioned over the culvert crown to get the maximum effects.

Two-dimensional view of applied wheel load based on CHBDC for Ontario is shown in Figure 3.4.

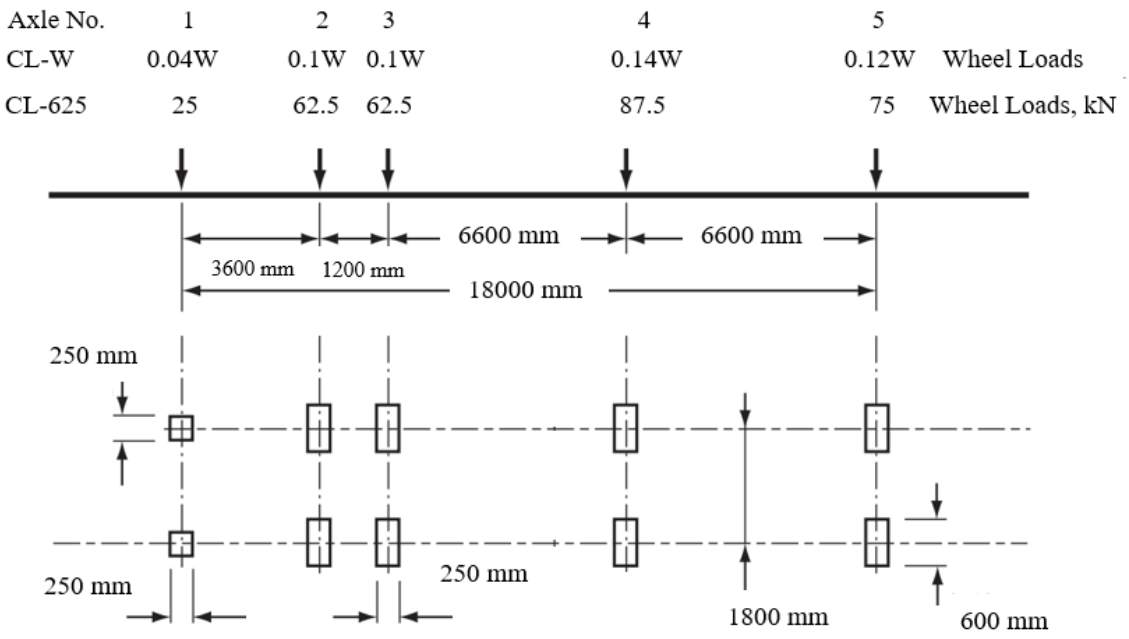

Figure 3.3. CL-W Truck wheel loads based on CHBDC (2014)

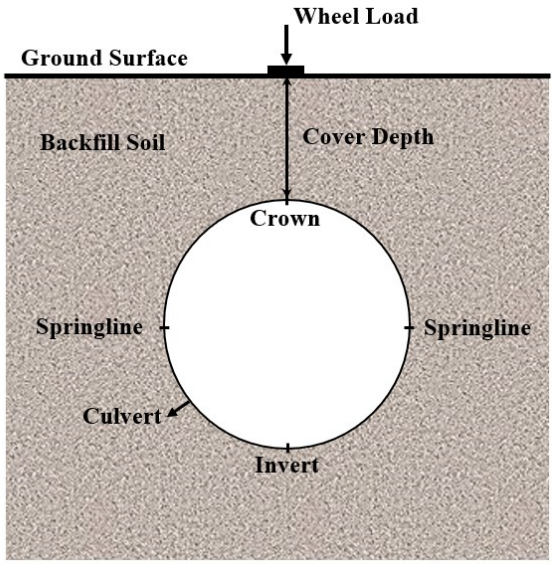

Figure 3.4. Two-dimensional view of applied wheel load

Based on the requirements of CHBDC (2014), a dynamic load allowance, which can be expressed as a fraction of surface load and accounts for the effects of moving vehicles travelling over the culvert, was applied to the service load used in the numerical simulations (Deng et al., 2011, Billing and Green, 1984, Regier, 2015). Dynamic load allowance for loads on buried structures can be calculated using

Equation 3.4. $$DLA = 0.4(1 - 0.5H) > 0.1$$

Where H is a cover depth in meters.

The service loads, summarized in Table 3.3, are based on the CHBDC design loads for the soil cover depths examined in this study. Five different burial depths are studied that are categorized into groups of shallow and deep cover depths. The final applied loads in the numerical models are given as the maximum service load in kN for each burial depth.

Table 3.3. CSA S6-14 (2014) single wheel pair loading for different cover depth

Cover Depth (mm)	Unfactored Design Vehicle Load (kN)	Multiple Lane Loading Factor	Dynamic Load Allowance	Maximum Service Load (kN)
450	87.5	1	0.31	115
900	87.5	1	0.22	107
1500	87.5	1	0.1	96
2000	87.5	1	0.1	96
3000	87.5	1	0.1	96

3.3 Evaluation of numerical modeling procedure

3.3.1 Model verification process

Confidence in the finite element modeling procedures developed and used in this study was established through verification with third party physical modelling

investigations. The control test, reported by Regier (2015), was used to calibrate the numerical modelling procedures with respect to the culvert deflection and deformation mechanisms. The control test (Control Pipe, CP) examined the response of an intact 900 mm diameter and 1500 mm long spiral, corrugated profile culvert subject to changes in the service load conditions. The corrugated profile of the control pipe had a depth of 12.7 mm, pitch of 67.7 mm, and nominal wall thickness of 1.6 mm with no deterioration effects (Figure 3.5). The culvert material was conventional steel grade with a Young's modulus of 200 GPa, yield strength of 230 MPa and ultimate strength of 310 MPa.

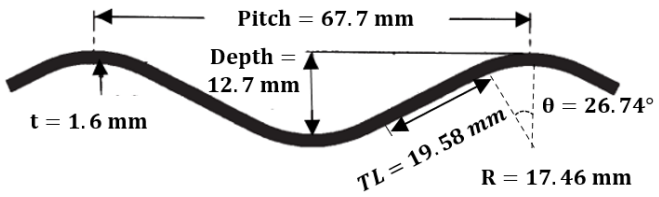

Figure 3.5. The profile of verified corrugated steel culvert

The culvert was backfilled with poorly graded sandy gravel conditions that was classified as "GP-SP" using the unified soil classification system. The bedding and the backfill soil from the invert to the crown was compacted to 95% and 90% standard proctor respectively using a vibrating plate tamper. The load configuration, simulated standard wheel pair, based on CHBDC with the wheel pad (250 mm x 600 mm in plan) was imposed on the ground surface and positioned over the culvert crown.

In the experimental program, culvert displacement and strain were measured, and these were used to estimate the bending moments and thrust using closed-form equations. However, the measured strains were not reported. Consequently, the verification process

focused on numerical predictions of culvert deflection for comparison with the experimental investigations. The predicted experimental section forces are also compared with the numerical simulations conducted in this study.

During the verification process, a mesh sensitivity study was conducted to assess numerical convergence and relative model inaccuracy with respect to successive simulations and the experimental data. The finite element models using the equivalent section approach (i.e., idealized smooth cylinder) did not exhibit any strong dependency on changes to the mesh topology. For numerical procedures explicitly modelling the culvert corrugated profile, the mesh density had a significant influence on the deformation mechanisms, section mechanical behaviour and modal response. Increasing the number of elements provided a refined discretization of the culvert corrugation profile (Figure 3.6) and improved prediction of the culvert mechanical response. Surface smoothing was used to enhance contact interactions between the culvert (S4) and soil elements. The element type and number, numerical prediction of culvert vertical displacement and relative numerical model difference with the experimental data, with a central vertical displacement of 11.7 mm, is summarized in Table 3.4.

The influence of full and reduced integration element formulations on the solution performance and predicted culvert mechanical response was also evaluated when using the shell element (S4 and S4R) to discretize the metal culvert. The artificial strain energy, which includes energy stored in hourglass resistance and transverse shear in shell and beam elements, was examined (Simulia, 2013). As shown in Figure 3.7, the large value of artificial strain energy, for model E3HG in Table 3.4, indicates that the use of reduced

integration elements reduced the amplitude of culvert deflection and increased the relative difference.

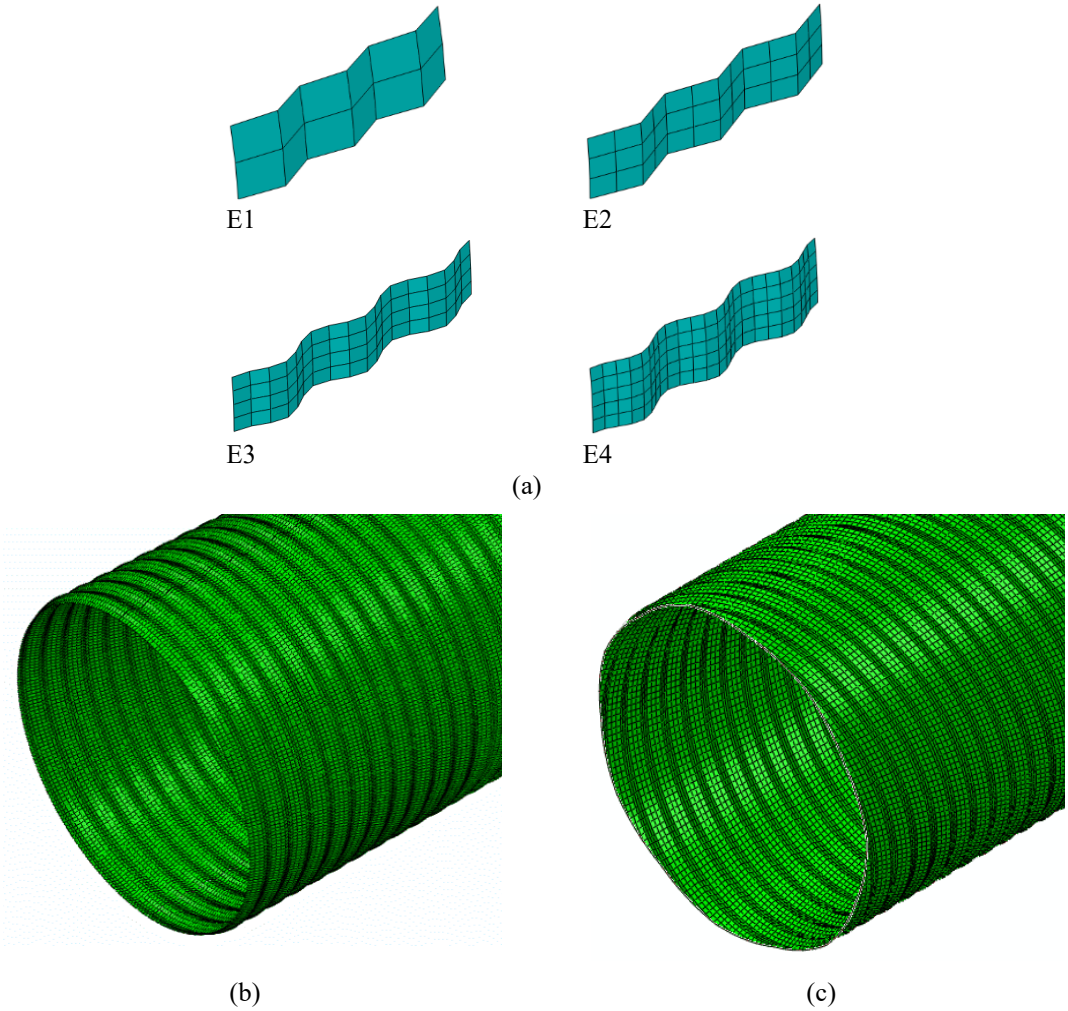

Figure 3.6. Modelling approaches for culverts with a corrugated profile including a) mesh topology study, and isometric view of the b) annular and c) spiral corrugated culvert models

Based on the relative (i.e., numerical prediction to experimental data) model differences (Table 3.4), artificial strain energy response (Figure 3.7) and solution run time (i.e., Abaqus wall clock time), the finite element model E3 was considered to be optimal and was used in subsequent parameter analysis in this study.

Table 3.4. Parameters for mesh convergence study for the annular corrugated culvert

Model	Culvert Element	Number of Elements	Vertical Diameter Change (mm)	Differences (%)
E1	S4	1056	9.2	21
E2	S4	4224	10.1	14
E3	S4	9504	10.5	10
E4	S4	12672	10.6	10
E3HG	S4R	9504	8.6	27

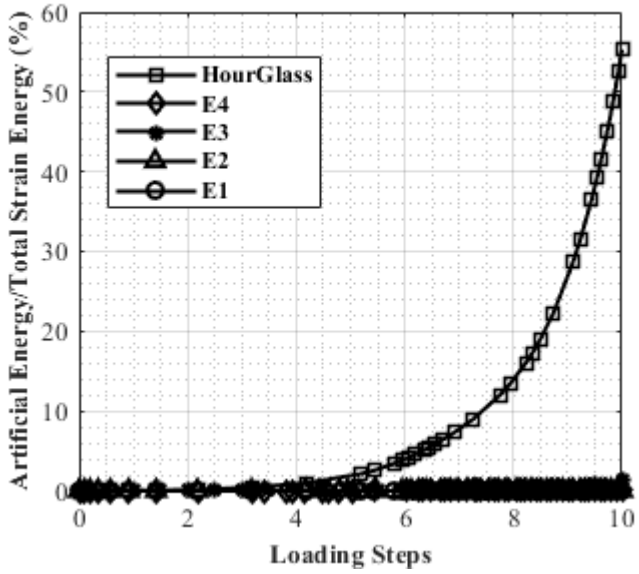

Figure 3.7. Normalized artificial strain energy to total strain energy for the sensitivity study and hourglass control effects models

3.3.2 Evaluation of modeling approach

The numerical analyst must assess the appropriateness of specific modeling strategies when predicting the mechanical response of the buried culvert to service loads.

The modeling considerations may include the dimensional space (i.e., 2D versus 3D), section discretization (i.e., idealized smooth cylinder versus annular and spiral corrugated profile) and constitutive behaviour (i.e., elastic versus elastic-plastic material response, total stress versus effective stress analysis).

For deeper cover depth analysis cases, the use of 2D models with an idealized equivalent section and elastic response may be more efficient and adequate to simulate the service load distribution with depth, culvert/soil load transfer mechanisms and culvert mechanical response. As the cover depth decreases, the influence of nonlinear behaviour may favour the use of more detailed modelling procedures that account for complex stress or strain states and deformation mechanisms.

The influence of modelling approaches on the predicted culvert mechanical response was examined through models using an equivalent section in 2D and 3D space, and 3D corrugated profile models. The numerical simulations were compared with the study by Regier (2015) for the CP test that examined a 900 mm diameter culvert with 1.6 mm wall thickness and 450 mm cover depth, subject to a 76.5 kN axle load over a pad area of 250 mm × 600 mm. The culvert was buried in a poorly graded granular soil (GP-SP).

In comparison with the experimental data, the 2D and 3D equivalent section models predicted a central culvert diameter change difference of 5% and 4 %, respectively. The more detailed 3D models, which accounted for the annular and spiral corrugated profiles, predicted a central diameter change difference of 10% and 7.7%, respectively. As shown in Figure 3.8, the longitudinal distribution of the change in culvert diameter was different for each modelling approach used in the study. The 2D equivalent section model only provides a single data point for the culvert deformation at the plane of symmetry at the

mid-length (Culvert Position = 0 mm). The 3D equivalent section model predicts a generally uniform culvert diameter change with position away from the plane of symmetry at mid-length with a relative difference (from the plane of symmetry to the culvert end) of only -13%. The corrugated culvert's displacement is undulated where the defined longitudinal path for sampling data goes through the corrugated profile and the vertical diameter change is reported for this path. The more detailed 3D annular and spiral corrugated pipe models exhibited a greater variation in the vertical diameter change (i.e., diameter change gradient) with no influence (i.e., 0 mm diameter change) on the vertical diameter change at the culvert ends. This verification study did not iteratively select parameters for convergence on a specified tolerance. In the verification process, the selected parameters were consistent with the full-scale tests to be able to compare FE predictions with the full-scale data.

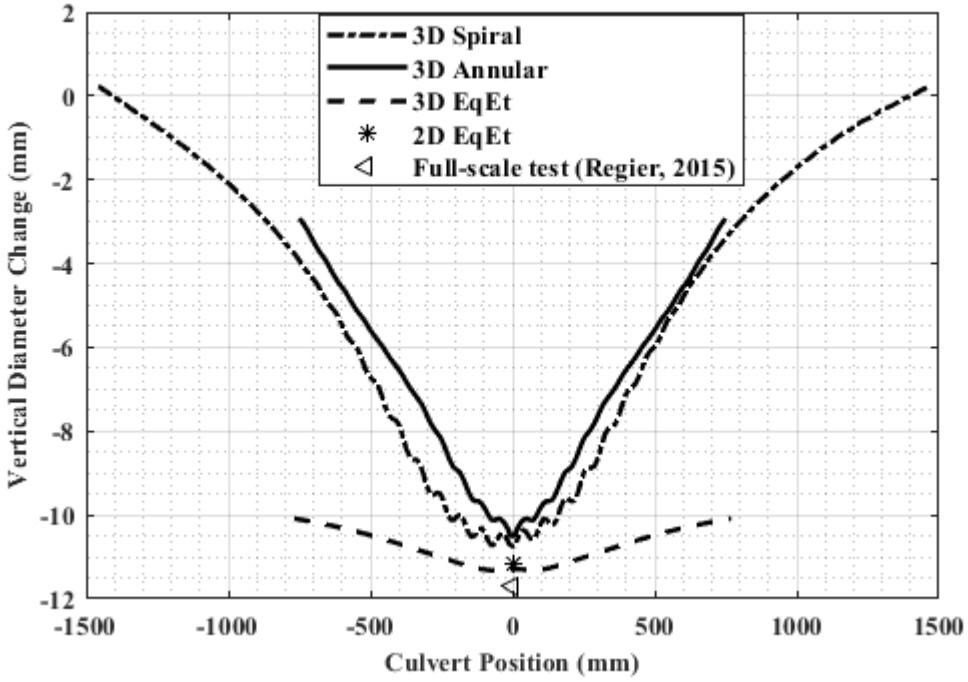

Figure 3.8. Variation in the culvert vertical diameter change with position along the culvert length

Further examination of the culvert deformation profile, as shown in Figure 3.9, highlights differences in the structural deformation modes and mechanisms for each modelling approach used in the study. The 2D equivalent section model (Figure 3.9a) suggest a dominant lateral ovalization mode with bedding support at the culvert invert, which is consistent with the mechanics for a 2D ring subject to non-uniformly distributed loading (Timoshenko and Gere, 1961). At the plane of symmetry, the 3D corrugated profile model suggests a similar deformation mechanism as the 3D idealized cylinder model at the cross-sectional deformed shape (Figure 3.9b &c). However, the changing mechanism of deformation away from the culvert mid-length towards to the far field (end) boundary conditions is significantly different for these two modeling approaches (Figure 3.8). The annular (Figure 3.9c) and spiral (Figure 3.9d) corrugated pipe models exhibit nominally similar deformation response. As the axle service loads are effectively point loads applied on the soil surface, the non-uniform variation of culvert displacement along the length (Figure 3.8) as predicted by the 3D annular and spiral corrugated culvert model appears to be more consistent with the redistribution of the point load with increasing soil depth; such as a Boussinesq type solution.

The culvert results for section bending moment obtained through numerical simulation is verified with the experimental full-scale test. More details about this verification are presented in Chapter 4.

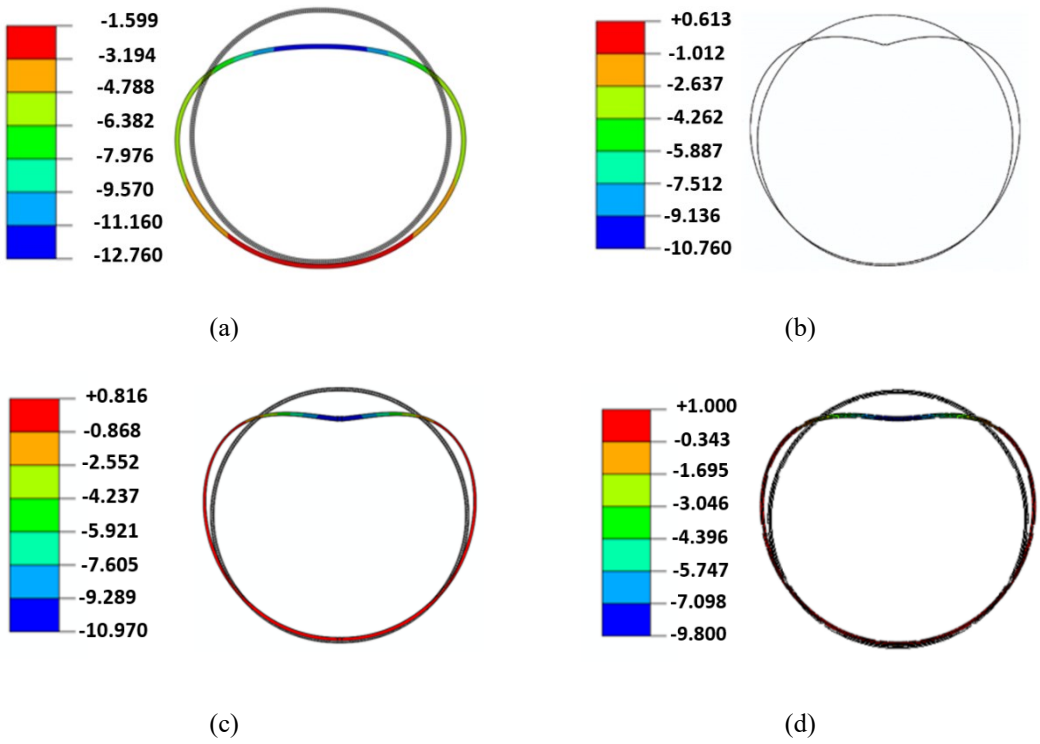

Figure 3.9. Culvert vertical displacement (mm) for the a) 2D equivalent smooth ring, b) 3D equivalent smooth cylinder profile, c) 3D annular corrugated profile and d) 3D spiral corrugated profile FE models (×10 magnification factor)

3.4 Parametric case study

The effects of a single wheel pair surface load (unfactored design vehicle load of 87.5 kN) on the mechanical response (i.e., thrust load, bending moment, vertical deflection, and membrane strain) of a buried metal culvert, across a range of design parameters, were investigated through verified numerical modelling procedures. The numerical sensitivity study evaluated the effects of culvert section shape (i.e., round, elliptical), orientation (i.e., vertical, horizontal), geometric length (radius, major and minor axis), cover depth (H), model dimensional space (i.e., 2D, 3D) and cross-section modelling approach (i.e.,

equivalent section, annular and spiral corrugated profile). The culvert geometric properties, section shape and orientation are presented in Table 3.5 and the culvert section shape and orientation are illustrated in Figure 3.10. The continuum finite element modeling procedures were developed using Abaqus/Standard 6.13 software and adopted the same approach as the verification procedures.

Table 3.5. Culvert geometric properties for the parameter study

Dimension	Horizontal Elliptical Culvert $\left(\frac{D_h}{D_v} = 1.4\right)$	Round Culvert $\left(\frac{D_h}{D_v} = 1\right)$	Vertical Elliptical Culvert $\left(\frac{D_h}{D_v} = 0.6\right)$
D_h (mm)	1300	900	900
D_v (mm)	900	900	1500

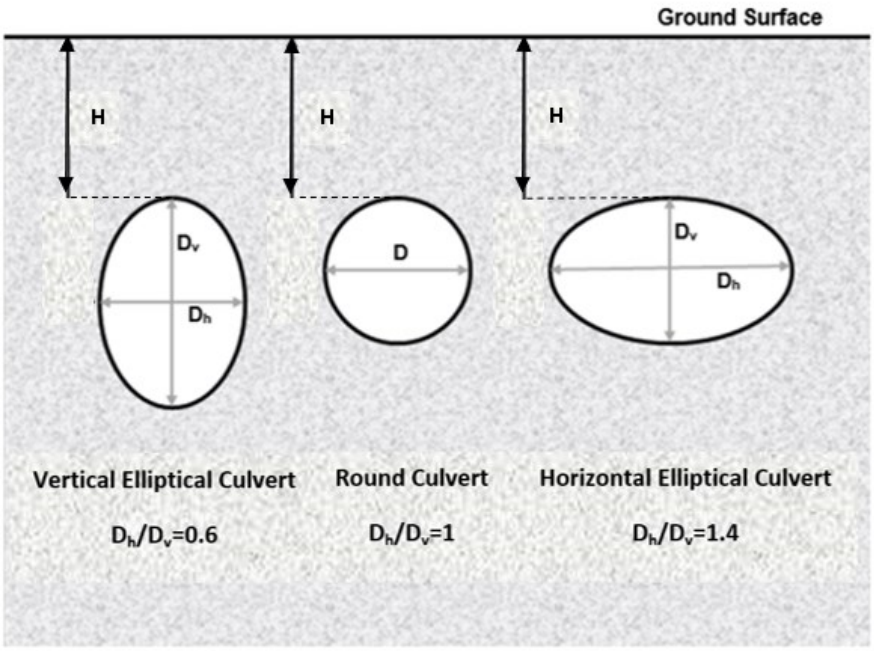

Figure 3.10. Burial depth (H) and section aspect ratio (D_h/D_v) for the buried culverts

For soil/structure interaction problems, including energy pipelines, lifelines and culverts, the cover depth has a significant influence on the soil stress, load transfer processes and failure mechanisms (Regier, 2015, Roy et al., 2015, Pike and Kenny, 2016,

Roy et al., 2018). In this study, the culvert was placed at different cover depths, 450 mm (H/D_v=0.5), 900 mm (H/D_v =1), 1500 mm (H/D_v =1.7), 2000 mm (H/D_v =2.2), and 3000 mm (H/D_v =3.3) for round and horizontally elliptical culverts; and 450 mm (H/D_v =0.3), 900 mm (H/D_v =0.6), 1500 mm (H/D_v =1), 2000 mm (H/D_v =1.3), and 3000 mm (H/D_v =2) for vertically elliptical culvert (Corrugated Steel Pipe Institute, 2010).

3.5 Results and discussion

Results from the FEM were analysed with respect to the deflection, strain, bending moment, and culvert thrust response across the parameter range examined in this study. The numerical sensitivity analysis evaluated the culvert mechanical response on a comparative basis and evaluated the numerical predictions with current engineering practice (e.g., CHBDC).

3.5.1 Section deformation

For a buried culvert subject to a single wheel pair service load, the normalized maximum vertical and horizontal displacement for the parameter range investigated, are presented in Figure 3.11a &b for different normalized cover depths (i.e., H/D_h, H/D_v) for specific modelling approaches (i.e., 2D & 3D equivalent section, 3D annular corrugated profile). The vertical diameter change is normalized with the vertical diameter ($\delta D/D_v$) and the horizontal diameter changes are normalized with horizontal diameter ($\delta D/D_h$). A negative value indicates a decrease (i.e., local contraction) in the culvert diameter and a positive value indicates an increase (i.e., local dilation) in the culvert diameter.

For all models, the maximum normalized vertical deflections were negative (i.e., radially inward) and the maximum normalized horizontal deflections were positive (i.e.,

radially outward). As shown in Figure 3.11, across the parameters investigated, a nonlinear relationship of increasing diameter change with decreasing cover depth was observed. The gradient of horizontal diameter change with respect to cover depth was relatively uniform across the parameter range studies for the 2D and 3D models investigated (Figure 3.11a). The gradient of vertical diameter changes with respect to cover depth exhibited greater sensitivity with aspect ratio (D_h/D_v).

The horizontal elliptical culvert (D_h/D_v = 1.44) aspect ratio exhibited a larger amplitude diameter change along the vertical direction in comparison with horizontal axis, whereas the opposite response was observed for the vertical elliptical culvert (D_h/D_v = 0.6). The round culvert (D_h/D_v = 1) 2D equivalent section model exhibited a symmetric deformation response (i.e., the ratio of the maximum vertical to maximum horizontal diameter change was equal to 1). This behaviour was related to the culvert geometry and orientation of the major elliptical axis (i.e., stiffness) relative to the loading direction.

The lowest magnitude of normalized horizontal and vertical diameter change was predicted by the 2D vertical elliptical culvert (D_h/D_v = 0.6). The largest magnitude of normalized horizontal diameter change was predicted by the 2D equivalent section model for the horizontal elliptical culvert (D_h/D_v = 1.44) and the 2D equivalent section model for the round culvert (D_h/D_v = 1) section. These observations are attributed to the relatively greater geometric stiffness of the 2D vertical elliptical culvert and increased burial depth to the springline, in comparison with circular and horizontal elliptical shapes.

Across the parameter range studied, the 3D equivalent section and 3D annular corrugated profile models are in close agreement with respect to the predicted maximum

horizontal and maximum vertical deflections on the plane of symmetry for the round culvert (Figure 3.11).

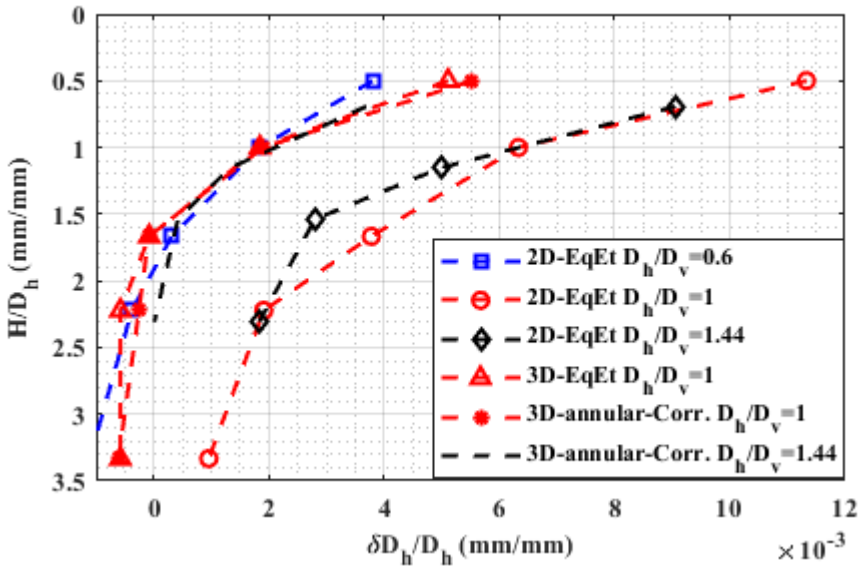

(a)

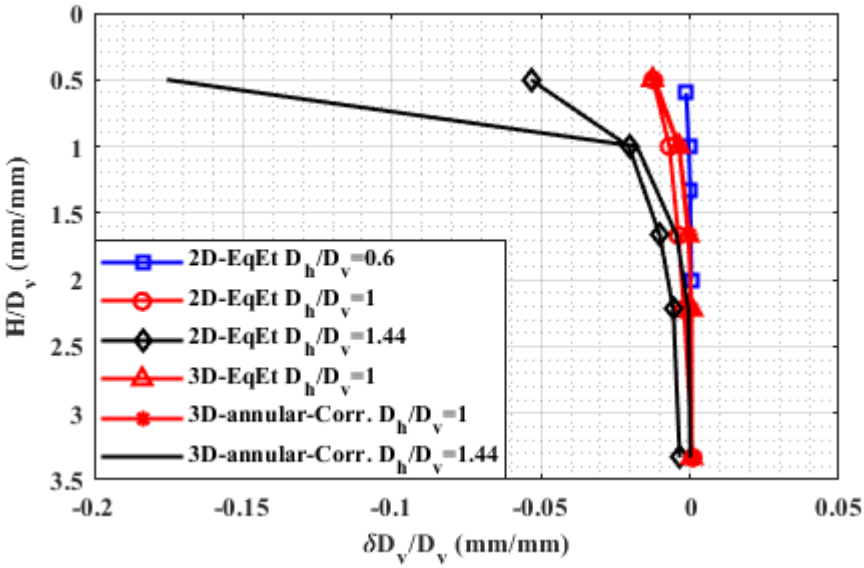

(b)

Figure 3.11. Maximum normalized a) horizontal ($\delta D_h/D_h$) and b) vertical ($\delta D_v/D_v$) diameter change at the plane of symmetry for the single wheel pair loading at 78 kN

The predicted culvert displacement response for the 3D modelling approaches used in this study is shown in Figure 3.12 using an isometric and profile view for the vertical (U3) and horizontal (U1) displacement response, respectively. As shown in Figure 3.12, consistent with the verification study (Figure 3.8 and Figure 3.9), the 3D modelling approaches predicted similar displacement amplitude at the plane of symmetry (i.e., culvert mid-length). However, the modelling approach influences the spatial distribution of the predicted deflection sense and amplitude along the culvert perimeter and length (e.g. compare Figure 3.12a &c with Figure 3.12b), which is also consistent with the verification study observations (Figure 3.8 and Figure 3.9). The 3D smooth cylinder section model (Figure 3.12b) had a relatively constant magnitude of culvert deflection (i.e., iso-contour band strip) along any line segment on the culvert longitudinal axis. In contrast, the 3D annular and spiral corrugated profile models exhibited a localization of the deformation pattern with the maximum vertical deflection and maximum horizontal deflection occurring at the culvert crown (12:00 clock position) and shoulder (10:30 and 1:30 clock positions), respectively. The vertical culvert deflection was an order of magnitude greater than the horizontal deflection at the pipe springline with a saddle type deformation mode. The maximum vertical and horizontal culvert deflection magnitudes occur on the plane of symmetry (i.e., vertical plane at the culvert mid-length) that decreases in amplitude away from the plane of symmetry along the culvert length towards the end boundaries (Figure 3.12a &c).

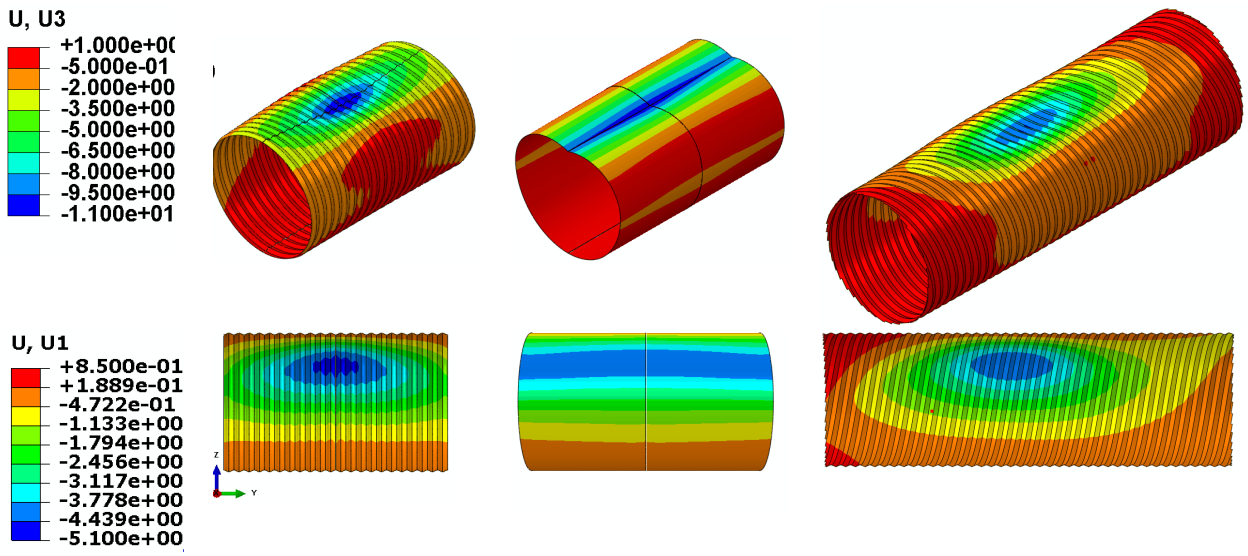

(a) (b) (c)

Figure 3.12. Contours of vertical (U3) and horizontal (U1) displacement (mm) for the a) 3D annular corrugated profile, b) 3D equivalent smooth cylinder profile, c) 3D spiral corrugated profile, FE models (×10 magnification factor; $H/D_v = 0.5$; $D_h/D_v = 1$)

Relative to the 3D annular corrugated profile model (Figure 3.2b), the 3D spiral corrugated culvert model (Figure 3.2c) incorporated a larger soil domain and increased length to diameter (L/D = 4.9), which was 1.7 for the 3D annular corrugated profile model (Figure 3.2b). As shown in Figure 3.12, further mitigation of boundary condition effects (i.e., increasing soil domain and L/D) and modifying the culvert corrugation pattern (i.e., spiral versus annular) did not have any significant influence on the magnitude or location of the maximum vertical (U3) and horizontal (U1) culvert displacement. Furthermore, the deformation gradient (i.e., distance between contour intervals along a defined path) within the central region of the model (i.e., ±0.85D) was not influenced by these modelling changes. In comparison with the 3D spiral response, although the shorter culvert length for the 3D annular and equivalent smooth cylinder end exhibit end boundary effects the models adequately captures the horizontal and vertical diameter change at the culvert mid-length,

which is the primary focus of this study. The 3D annular and spiral corrugated profiles (Figure 3.12a and Figure 3.12c) exhibited localized deformation patterns with the maximum vertical deflection and maximum horizontal deflection occurring at the culvert crown and shoulder, respectively. In contrast to the centrally localized response observed for the 3D corrugated culvert models, the 3D smooth cylinder profile exhibited patterns of uniform displacement amplitudes distributed along the culvert length.

3.5.2 Strain distribution

The modeling approach (i.e., 3D smooth cylinder, 3D annular and 3D spiral corrugated model) effects on predictions of culvert membrane strain and mechanical behaviour (i.e., section thrust, section moment) were also investigated. The 3D models predicted vertical deflections consistent with the verification study observation, but the magnitude and distribution of local strain (LE11, local strain in the direction of local axis 1, circumferential axis perpendicular to the cross-section) predictions were influenced by the modelling approach (Figure 3.13). This is due to the underlying mechanics that influence the global and local section response with respect to deformation mechanisms and strain response, and the load transfer mechanisms near the culvert crown.

The 3D smooth cylinder model (i.e., equivalent section model) considers a linear variation of strain through thickness with ring stiffness governing the sectional response and the transverse longitudinal stiffness providing flexural constraint. The 3D spiral and annular corrugated models account for a linear variation of strain through thickness but also consider membrane action and local flexure across the crest and through the depth. In addition, the 3D corrugated models can address local stress concentration effects or development of local plastic behaviour, within the ridged profile, that influence the

deformation mechanisms and the local magnitude and distribution of the thrust and bending moment response. The equivalent section modelling approach cannot properly account for local plastic behaviour due to the underlying basis of the section transformation, and the corresponding influence on the stress state distribution through thickness and evolution of localized deformation mechanisms.

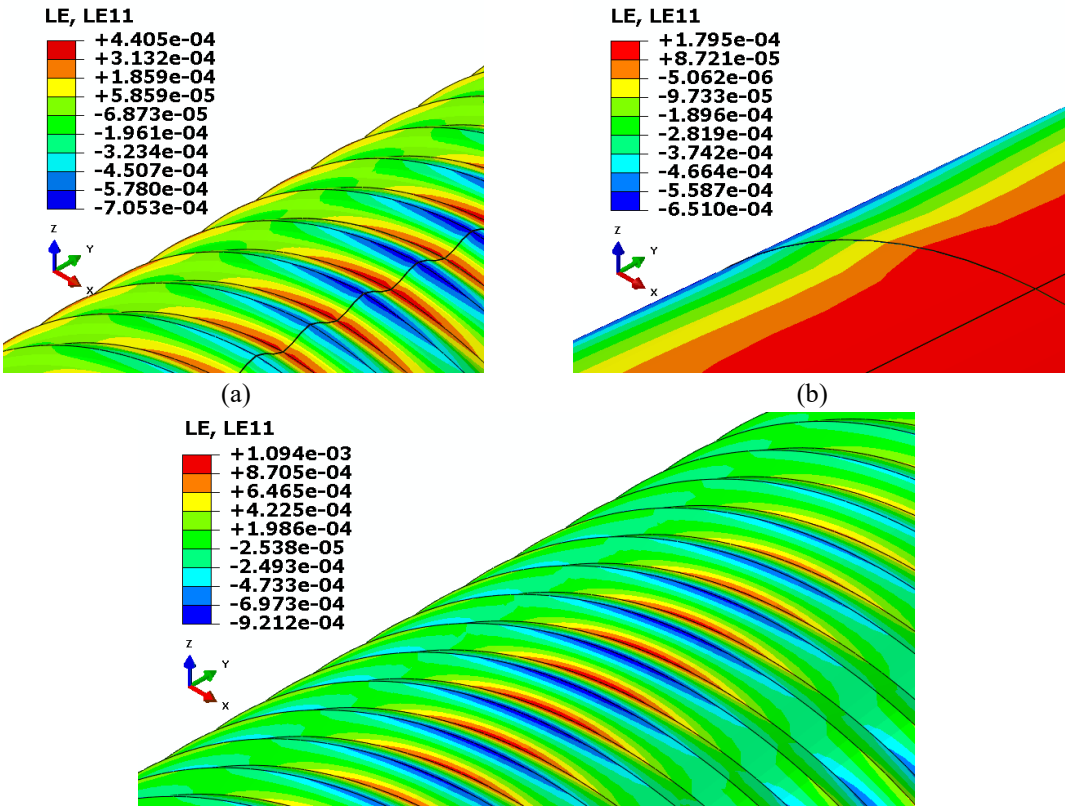

Figure 3.13. Strain contour for (a) 3D annular corrugated profile and (b) 3D smooth cylinder profile, and c) 3D spiral corrugated profile FE models (H/D_v = 0.5; D_h/D_v = 1) with 50kN single wheel pair loading

3.5.3 Procedures of calculating internal forces in the laboratory tests and FEM

In the laboratory tests, the thrust and bending moment of culverts due to the applied loads are calculated using the measured strains and theoretical considerations through

closed-form equations. Distributed fiber optic strain sensors and strain gauges are used to measure the responses of the buried culverts due to the applied loads. In the experimental program, the culvert strains were measured at the trough (ε_1) and crest (ε_2) locations on the outside culvert surface (at the culvert/soil interface) of the corrugated profile. The strain gauge measurements are used to estimate (extrapolate) the extreme fiber strain (ε_{EF}) at the trough location on the inside surface of the culvert corrugated profile (Equation 3.5)

Equation 3.5. $$\boldsymbol{\varepsilon_{EF} = \frac{(\varepsilon_1 - \varepsilon_2)}{h} t + \varepsilon_1}$$

where ε_1 and ε_2 are the surface membrane strains at the trough and crest locations, respectively, on the outside culvert surface (at the culvert/soil interface) of the corrugated profile, ε_{EF} is the estimated extreme fiber strain at the trough location on the inside surface of the culvert corrugated profile, h is radial distance between the strain gauges (mm) ε_1 and ε_2, and t is intact wall thickness (mm) of the corrugated pipe.

The average strain (ε_{avg}) and average thrust force can be estimated using Equation 3.6 and Equation 3.7, respectively. The local curvature (Equation 3.8) can provide estimates of the section bending moment (Equation 3.9) that was experienced during the physical modelling studies (Simpson et al., 2015, Simpson et al., 2016, Regier, 2015).

Equation 3.6. $$\boldsymbol{\varepsilon_{avg} = \frac{\varepsilon_2 + \varepsilon_{EF}}{2}}$$

Equation 3.7. $$\boldsymbol{N = \varepsilon_{avg} EA}$$

Equation 3.8. $$\boldsymbol{\kappa = \frac{\varepsilon_2 - \varepsilon_1}{h}}$$

Equation 3.9. $$\boldsymbol{M = EI.\kappa}$$

where N is thrust per unit length (N/mm), E is young's modulus (N/mm^2), A is cross section area per unit length (mm^2/mm), I is second moment of area per unit length

(mm^4/mm), κ is curvature (1/mm), and M is the section bending moment per unit length (N.mm/mm).

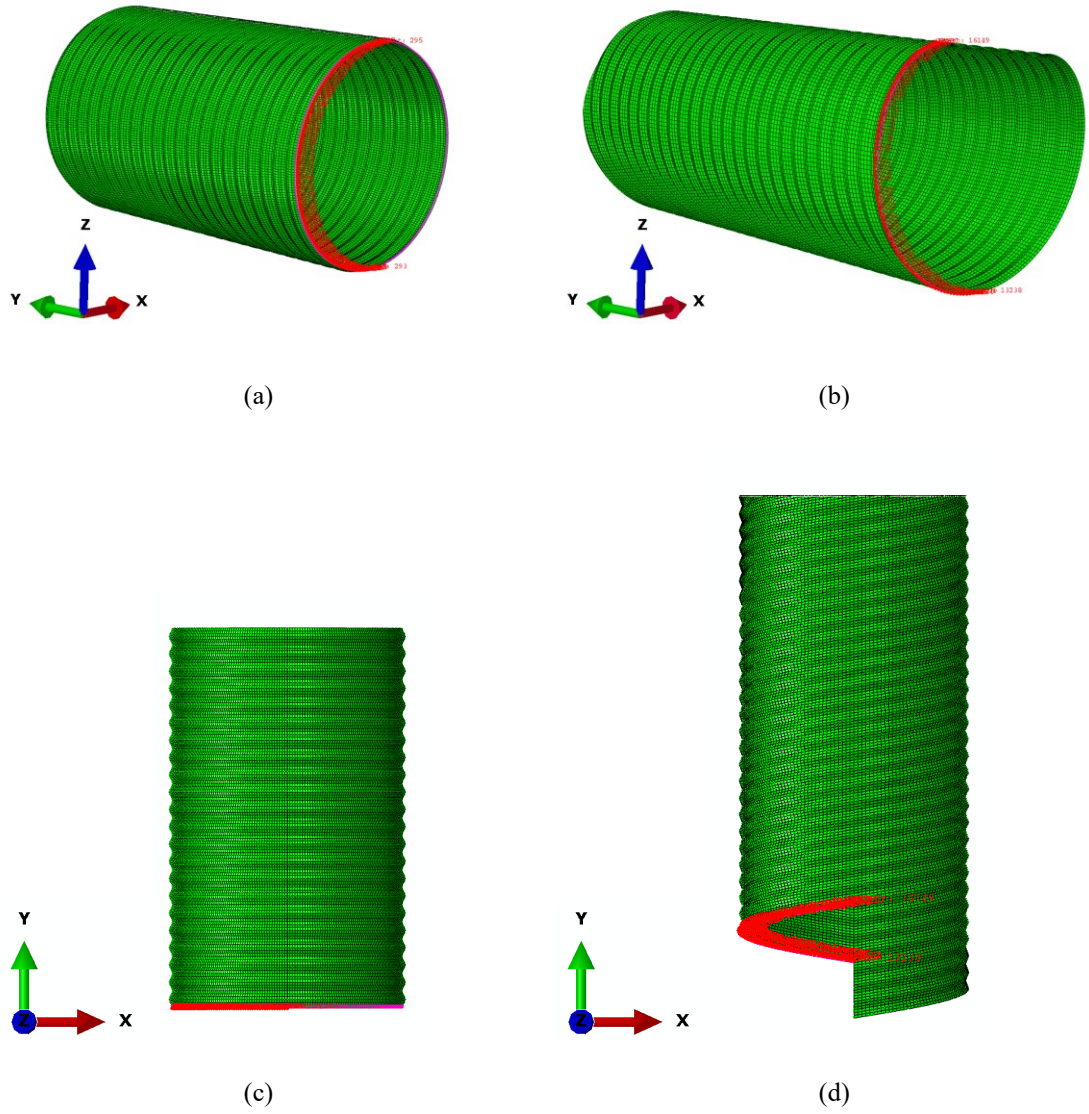

(a) (b)

(c) (d)

Figure 3.14. Defined paths to calculate the culvert membrane strain, section thrust and section moment for the 3D (a) annular and (b) spiral corrugated culvert profile models, and the plan view for the 3D (c) annular and (d) spiral corrugated culvert profile models to illustrate the relationship between the two approaches

Finite element simulation enables a detailed assessment of the magnitude and distribution (i.e., intensity or gradient) of mechanical response parameters (e.g., deflections, strain, stress) throughout the modelling domain. Figure 3.14 presents the defined path for sampling culvert membrane strain, thrust and bending moment for the 3D annular and spiral corrugated culvert profile modelling approaches used in this study.

Analysis of the culvert mechanical response along the spiral path (i.e., elliptical cross-section) in Figure 3.14b is consistent with the experimental study by Regier (2015), whereas the circular path (i.e., circular cross-section), Figure 3.14a, is offset by the spiral forming angle (Figure 3.14c &d). Based on these defined paths, Figure 3.15, Figure 3.16, and Figure 3.17 present the amplitude and perimeter distribution of membrane strain, section local and net force (thrust), and section bending moment for the finite element simulations and experimental observations. The analysis considered a single wheel pair load level of 50 kN with a culvert cover depth of H/Dv = 0.5. This load case was selected as the culvert material response was observed to be in the elastic range.

3.5.4 Circumferential strain

Based on results only from continuum FEM, the predicted perimeter distribution of membrane strain is shown in Figure 3.15. Culvert membrane strains were not reported by Regier (2015) and thus cannot be compared with the numerical simulations. The estimated membrane strain at the crest and trough of the corrugated culvert profile (Figure 3.15a), using different FE modelling procedures (i.e., model bias associated with annular versus spiral corrugated profile as shown in Figure 3.6 and Figure 3.8), was compared with the differences between these strain estimates with respect to the modelling approaches (Figure 3.15c). The results (Figure 3.15c) demonstrate that there are differences in the membrane

strain estimates with respect to the FE modelling approaches used in this study (i.e., FE model bias). The minimum deviation (0% strain) is located at the culvert invert and maximum deviation (±0.06% strain) at the culvert crown for both the crest and trough extreme fibers of the corrugated profile.

For perimeter locations extending below the culvert shoulder (at approximately the 2:00 clock position) towards the invert (6:00 clock position), the data illustrate nominally equivalent culvert deformation patterns that are primarily governed by the soil bearing and lateral earth pressures with limited influence from model bias. Conversely, for perimeter locations extending from the culvert shoulder towards the crown, the membrane strain exhibited greater sensitivity to model bias with the greatest influence on the culvert response at the crown and shoulder locations (Figure 3.15c). The differences in strain amplitude and gradient (i.e., rate of change along the culvert circumference) suggest that the modelling approaches influenced the culvert modal response, which is supported by predictions of culvert deformations (Figure 3.8, Figure 3.9, and Figure 3.12), membrane strain (Figure 3.13) and average strain (Figure 3.15b). The out-of-phase crest and trough response (i.e., corresponding negative and positive values at the extreme fiber locations), above the culvert springline, indicates local flexural response, which is illustrated in Figure 3.9. This membrane strain response (i.e., magnitude and strain gradient) was attributed to nonlinear soil behaviour and interaction effects (i.e., load transfer mechanisms, soil deformation patterns) with the maximum amplitude occurring at the culvert crown.

In comparison with the extreme fiber strain response (Figure 3.15a), the estimated average membrane strain (Figure 3.15b) has lower magnitude (i.e., maximum -0.03% strain) with model bias limited to culvert locations below the culvert shoulder that is

consistent with the extreme fiber strain response (Figure 3.15c). The average strain response cannot account for the local peak strain response as predicted by FEM at the culvert shoulder and crown locations (Figure 3.15a &b).

The differences in the estimated average membrane strain (Figure 3.15d), exhibits lower amplitude variation (i.e., maximum difference of 0.03%). Averaging two strains with different signs at crow and trough cancels the local effect of these stains and the calculated averaged strain is difference from the local strains. As shown in Figure 3.15a &c), from the culvert springline to invert, the culvert mechanical response is not significantly influenced by the modelling approach (i.e., annular or spiral corrugated profile) and is primarily governed by soil bearing and lateral earth pressure response.

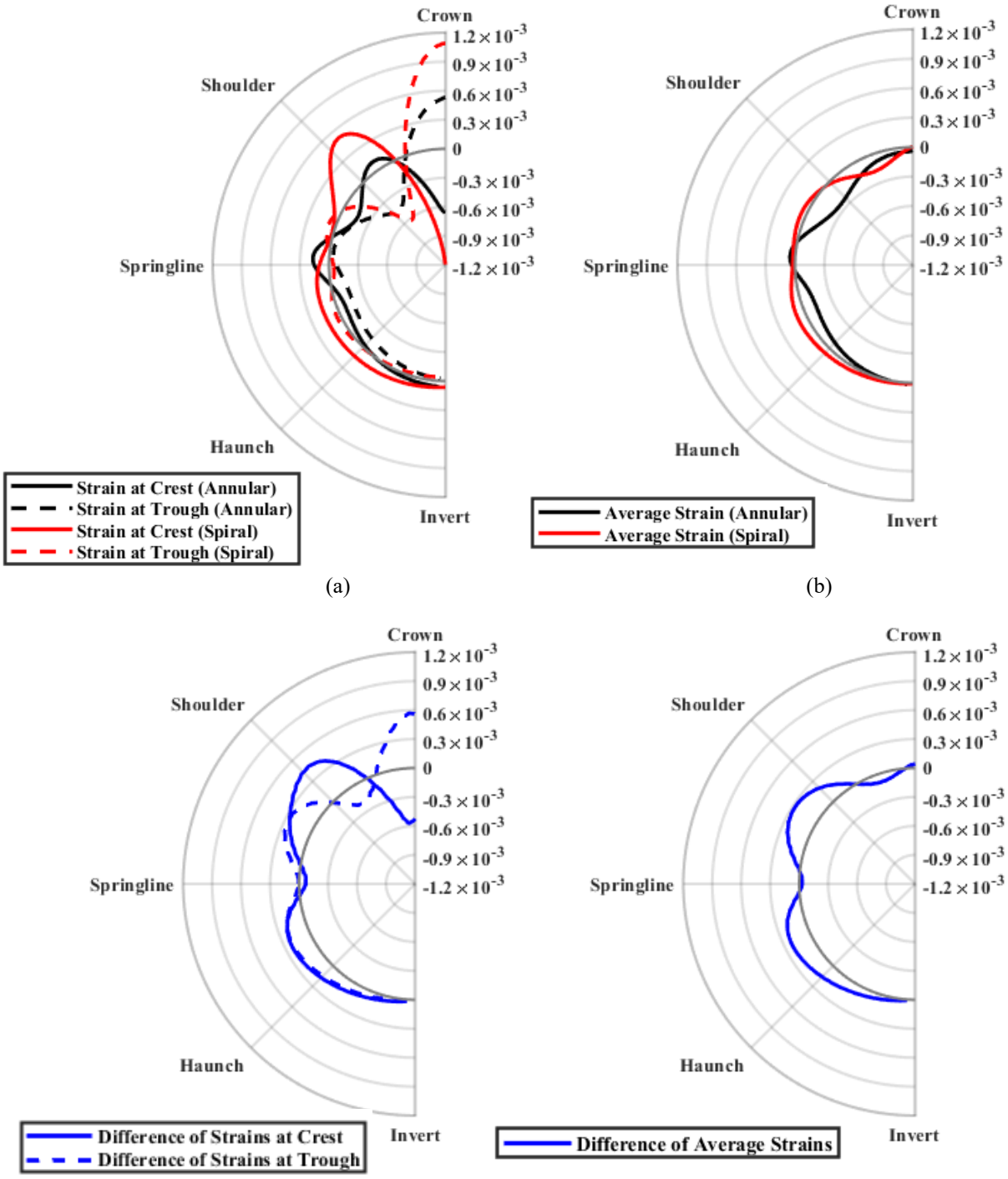

Figure 3.15. Perimeter distribution of membrane strain, at the plane of symmetry with the 50 kN single wheel pair loading for the a) local strain, b) average strain [Equation 3.6], c) the relative difference, between the FE modelling approaches in the predicted strain, and d) average strain

3.5.5 Circumferential section load and bending moment

Consistent with the analysis and discussion on the culvert perimeter membrane strain response, the same key observations and outcomes can also be used to interpret the thrust (Figure 3.16) and section bending moment (Figure 3.17) response.

As shown in Figure 3.16b, the FE predictions of average section thrust (net force in the section) are consistent with the closed-form estimates of the thrust load (Equation 3.7) as reported by Regier (2015) for the experimental test program. The net thrust (i.e., average strain) does not account for local variations in the culvert response (compare Figure 3.15a and Figure 3.16a with Figure 3.15b and Figure 3.16b), and, consequently, can underestimate the peak thrust response in the section.

Figure 3.17 presents the culvert section bending moments obtained through numerical simulation, for 3D annular and spiral corrugated profile models, and the experimental full-scale test (Regier, 2015). . The numerical simulations and physical test results are generally consistent along culvert perimeter locations below the springline. Similar to the observations on FE predictions for culvert section local force, the modelling approach can influence the estimated section moment response for perimeter location from the culvert shoulder to crown (Figure 3.17a and Figure 3.17c).

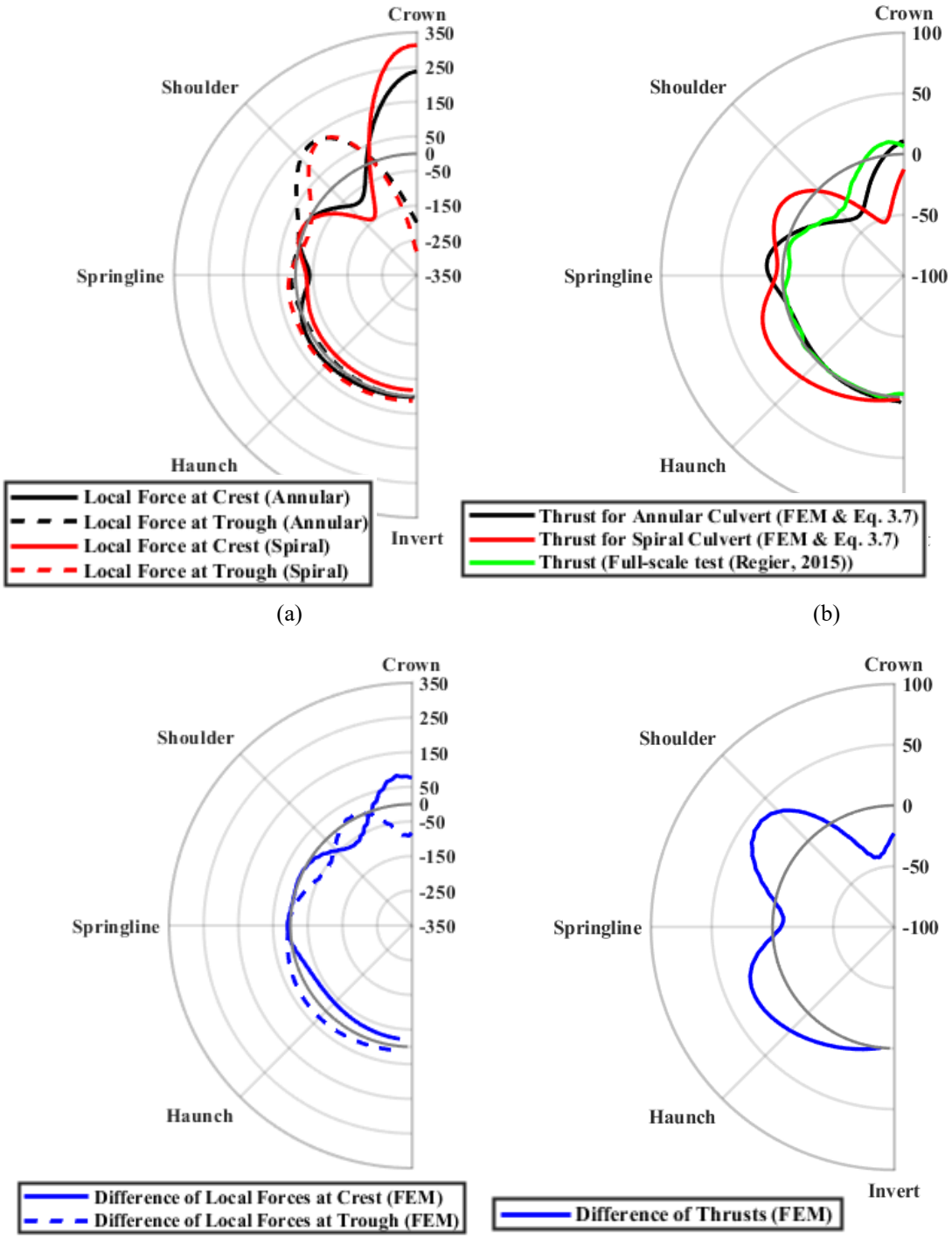

Figure 3.16. Perimeter distribution of section force per unit CSC length (N/mm), at the plane of symmetry with the 50 kN single wheel pair loading for the a) local force, b) thrust [Equation 3.7], c) the relative difference, between the FE modelling approaches for the predicted local forces, and d) difference of thrusts (FEM)

The numerical simulations and experimental observation deviate from the springline to shoulder locations with the spiral corrugated profile model providing better correspondence with the measured data. This discrepancy was attributed to both numerical and physical modelling considerations. The finite element simulations did not account for the effects of trench backfilling and compaction activities on the culvert deflection response and initial culvert imperfection due to ovalization (e.g., Mai, 2013; Regier, 2015). In addition, the numerical simulations did not account for the variation in soil strength properties (e.g., density, interface friction angle) with depth or spatially within the compacted trench backfill. The physical modelling tests exhibited variability in the test conditions where "…the variability in secant stiffness between each specimen is likely caused by differences in surrounding soil densities…" (Regier et al., 2018). Finally, a local moment was observed in the experimental test at the culvert invert location (Figure 3.17b) that may be associated with some differences in the measured response or bedding interaction response.

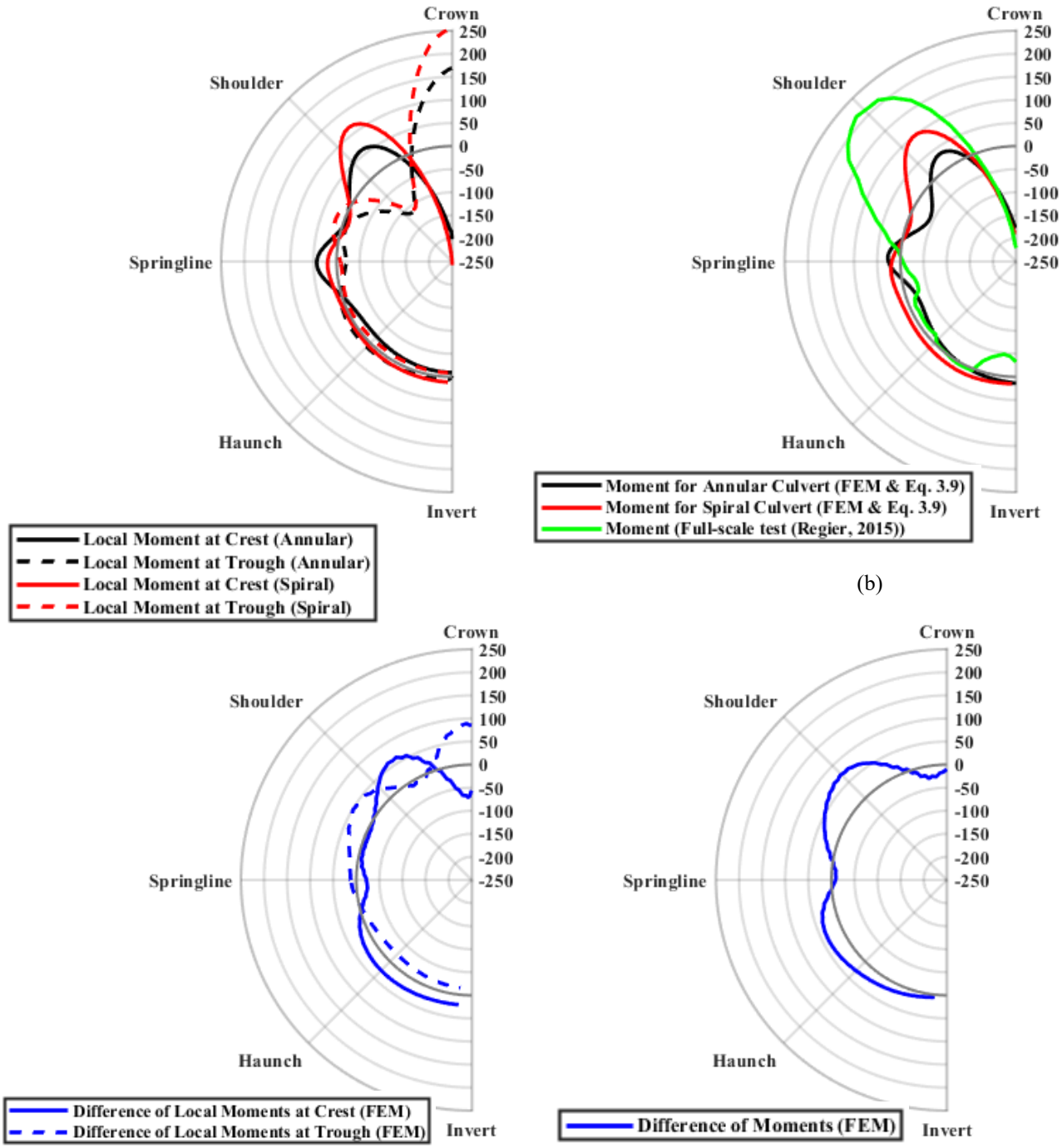

Figure 3.17. Perimeter distribution of bending moment per unit CSC length (N.mm/mm), at the plane of symmetry with the 50 kN single wheel pair loading for the a) local moment, b) average moment [Equation 3.9], c) the relative difference between the FE modelling approaches in the predicted local moment, and d) difference of moments (FEM)

Numerical simulations, using the 3D spiral corrugated profile model, were used to conduct a parameter study examining the influence of cover depth (H) and single wheel pair loading (LL) on the culvert section local force and moment response. As shown in Figure 3.18, decreasing the cover depth from 3 m to 0.45 m and increasing the applied surface load to maximum service load, influenced the magnitude and spatial distribution of the culvert mechanical response. Local section thrust responses focused on the culvert crown with a reduction at the shoulder and springline locations. In response to the local section thrusts, the culvert section moment developed a local peak moment response at the crown, shoulder and springline locations. As the cover depth decreases, the local section loads can exceed the material yield strength. The response at the culvert haunch and invert are not influenced across the range of parameters investigated. The numerical simulations suggest a transition in the culvert mechanical response related to the cover depth, which is consistent with current practice, analysis and research studies on the behaviour of buried structures (Pike and Kenny, 2016, Regier, 2015, Roy et al., 2015, Roy et al., 2018).

This response is linked with changes in the culvert failure mechanism from culvert section ovalization (see Figure 3.9 and Figure 3.12) to a double curvature saddle type mechanism for the deep and shallow burial cases, respectively. These results agree with previous studies that investigated the cross-sectional bending moment along the longitudinal axis (Nakhostin et al., 2017, Nakhostin et al., 2019), which evaluated the effects of local defects due to wall loss through corrosion and soil voids due at the soil/culvert interface to erosion.

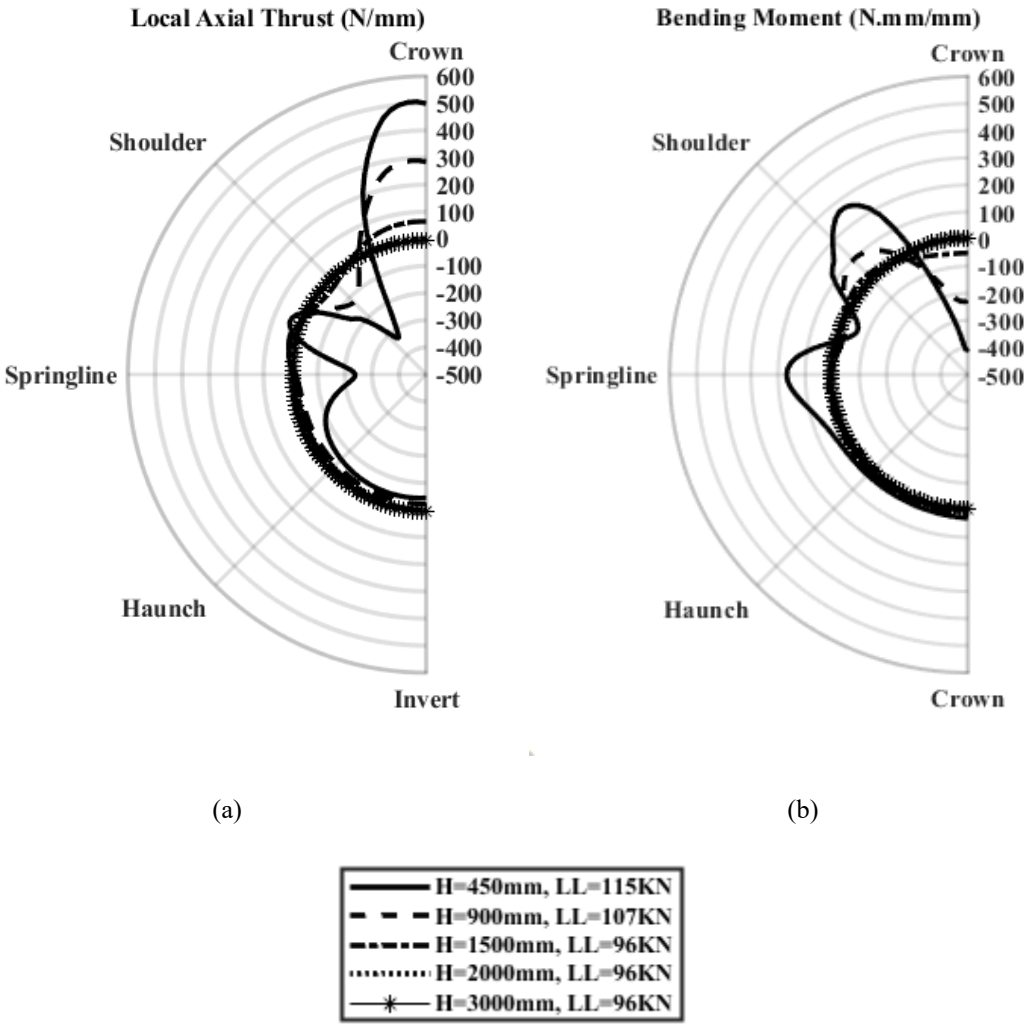

Figure 3.18. Perimeter distribution of section a) local circumferential force per unit CSC length axial thrust (N/mm), and b) local bending moment per unit CSC length (N.mm/mm) at crest for the 3D spiral corrugated profile with variation in the cover depth (H) and single wheel pair loading (LL) magnitude

3.5.6 Discussion on the numerical results and closed-form equations

This section provides an overview of the results and discussion addressing the relationship among theoretical models, numerical predictions and recommended practice (i.e., CSA S6-14, 2014) to assess the effect of the service loads on buried culverts. The parameter range included the culvert normalized cover depth ($\frac{H}{D_v}$), dimensional space (2D and 3D modeling), and modelling approach (equivalent section, spiral corrugated profile) subject to the single wheel pair loading. The analysis compares the numerical prediction of local and net forces at the springline and bending moment at culvert crown locations with a variation in the normalized cover depth ($\frac{H}{D_v}$). These locations are specified by current engineering practice (i.e., CSA S6-14, 2014). The analysis also compares the CHBDC (2014) guideline with local peak magnitudes of predicted section thrust load at the culvert crown, which are observed in Figure 3.16 and Figure 3.18.

A comparison of the predicted section force based on semi-empirical expression (i.e., Marston theory (Marston and Anderson, 1913; Spangler and Shafer, 1938)), current practice (i.e., CSA S6-14, 2014), and numerical simulation (i.e., FEA in this study) is presented in Figure 3.19. In the FEA of corrugated models, the onset of plastic behaviour was observed at the culvert crown and shoulder locations at a single wheel pair load of 78 kN with a cover depth of 450 mm ($\frac{H}{D_v} = 0.5$). Current engineering practice (i.e., CSA S6-14, 2014) assumes linear elastic response where, as highlighted in Table 5, the CHBDC (2014) unfactored design load is 87.5 kN.

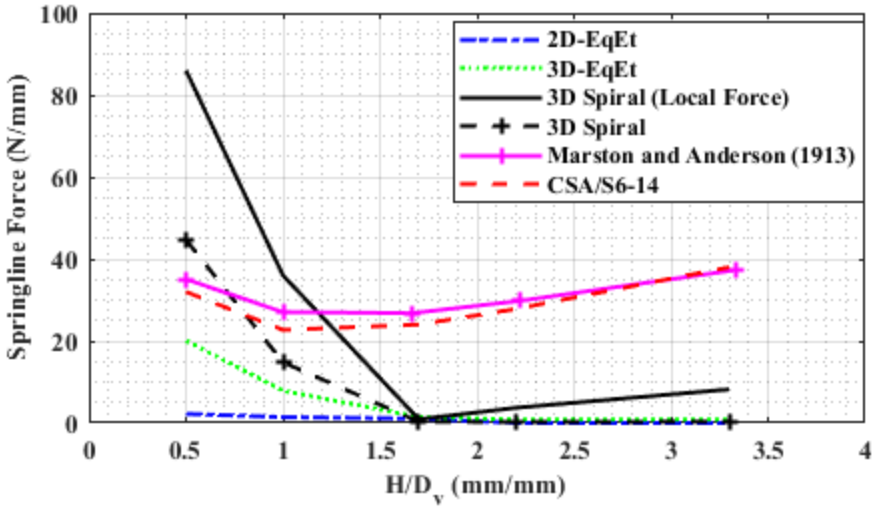

(a)

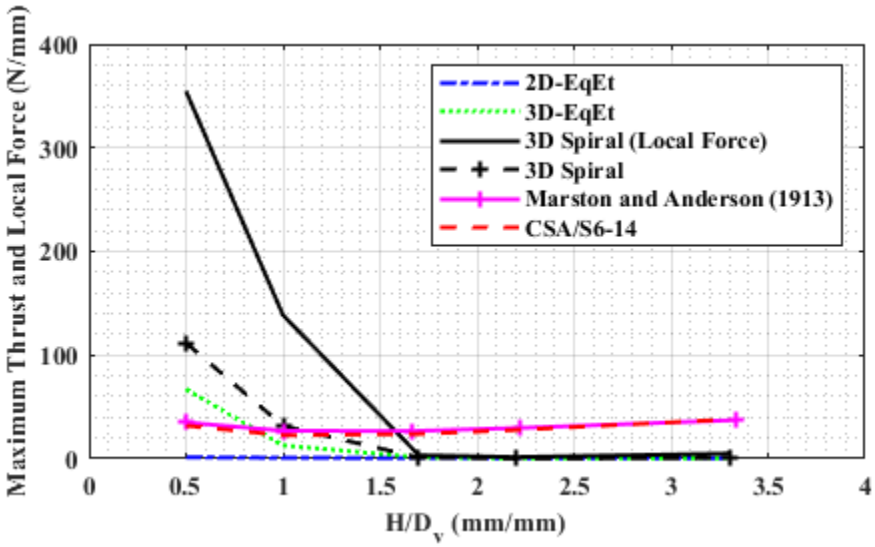

(b)

Figure 3.19. Variation in the culvert section force with normalized cover depth and single wheel pair loading at 78 KN a) at the springline and b) at crown based on FE simulation

As shown in Figure 3.19a, across the range of normalized cover depth (H/D_v) investigated, the equivalent thickness models underpredict the thrust relative to current engineering practice (i.e., Marston and Anderson, 1913, CSA S6-14, 2014). As expected,

the semi-empirical approach (i.e., Marston and Anderson, 1913) and current practice (CSA S6-14, 2014) are in close agreement. The 3D Spiral FEM predicts greater springline thrust for the model with shallowest cover depth ($\frac{H}{D_v} = 0.5$), up to a factor of 1.3 and 2.4 for thrust and local force respectively, in comparison with current engineering practice (Marston and Anderson, 1913; CSA S6-14, 2014), and suggests a transition in the load transfer and culvert deformation mechanisms occurs. By increasing the cover depth, the applied wheel load effects on internal forces decrease and the effects of fill load increase. This effect is noticeable in the predicted thrust using the current engineering practices (i.e., Marston and Anderson, 1913; CSA S6-14, 2014) and local force of FE simulation for 3D spiral corrugated model in Figure 3.19 a. The current engineering practice overestimates the fill load, and the FEM and current practices does not converge for deep normalized cover depths ($\frac{H}{D_v} > 1.7$).

Figure 3.19b compares the estimated springline thrust (Marston and Anderson, 1913; CSA S6-14, 2014) with the predicted local maximum circumferential force, at the CSC crown, using current engineering practice and FEA. The onset of plastic behaviour, at the culvert crown and shoulder locations, for the single wheel pair load, was predicted by FEA for a shallow normalized cover depth of 450 mm ($\frac{H}{D_v} = 0.5$). Current engineering practice assumes the maximum thrust occurs at the springline and does not account for the localization of circumferential forces at the CSC crown. This may lead to local deformations with section yield and local instability mechanisms, which has been reported in full-scale experimental observations (Regier, 2015) and the FEA presented in this study. Across the range of shallow cover depths ($\frac{H}{D_v} < 1.7$), the 3D spiral CSC FE simulations

predict a local circumferential force up to a factor of 10 times greater than the springline thrust estimated using current engineering practice.

Over the parameter range investigated, the 3D equivalent wall thickness FE models predicted conservative estimates of the maximum bending moment per unit CSC length, which was located at the CSC crown. In contrast with the circumferential force response (Figure 3.19), current engineering practice (i.e., CSA S6-14, 2014) provides conservative estimates of crown section bending moment response relative to the 3D spiral and 2D equivalent wall thickness FE model predictions (Figure 3.20). In comparison with current engineering practice, the 2D and 3D equivalent section models provide unconservative and conservative estimates of crown section bending moment, respectively. As previously discussed in Section 3.5.2, due to bias the equivalent section models cannot adequately predict the variation in curvature along the corrugated profile (Figure 3.13).

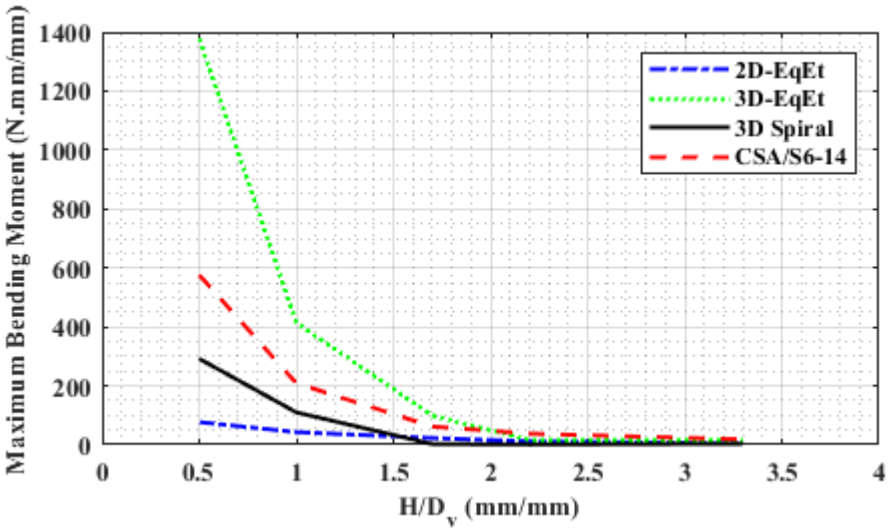

Figure 3.20. Variation in the maximum bending moment, at the culvert crown, with normalized cover depth and the single wheel pair loading at 78 KN

The 2D and 3D FEM with equivalent thickness are not able to capture the culvert's behaviour in the nonlinear phase. The results of 3D corrugated culvert are reported at this stage of loading and the results are compared with the CHBDC and presented in Figure 3.21a &b. As the applied single wheel pair loading increases to the final stage of loading, the 3D spiral corrugated profile model predicts the development of plastic deformation and strain at the culvert crown and shoulder locations for the shallowest cover depth case ($\frac{H}{D_v} = 0.5$). The local section thrust estimates are 5 to 10 times greater than current practice (i.e., CSA S6-14, 2014) load estimates for the shallowest cover depth and this value reduces to 1.8 to 3.6 times for calculated thrust. The CHBDC results are conservative for normalized cover depth greater than $1.7D_v$ (Figure 3.21a) in comparison with the 3D corrugated model results for both local and net forces (thrust). Although the transition cover depth ($\frac{H}{D_v} = 1.7$) is not influenced by the increased load level, there appear to be a second inflection point in the section thrust load response developing at deeper cover depth ($\frac{H}{D_v} = 2.1$). These results indicate that the load distribution of finite element model is different with the CHBDC, which uses linear pattern for surface and fill loads distribution in depth for thrust force calculations. Consequently, the calculated thrust at the springlines using the Canadian code is considerably different for those two mentioned methods, local force and net force (thrust) for buried cases in shallow cover depth and this discrepancy is greater for the local force responses. Contrary to the CHBDC hypothesis, it is worth mentioning that the maximum thrust load in the numerical modeling procedure happens at the crown and it is not located at the springline (Figure 3.21b).

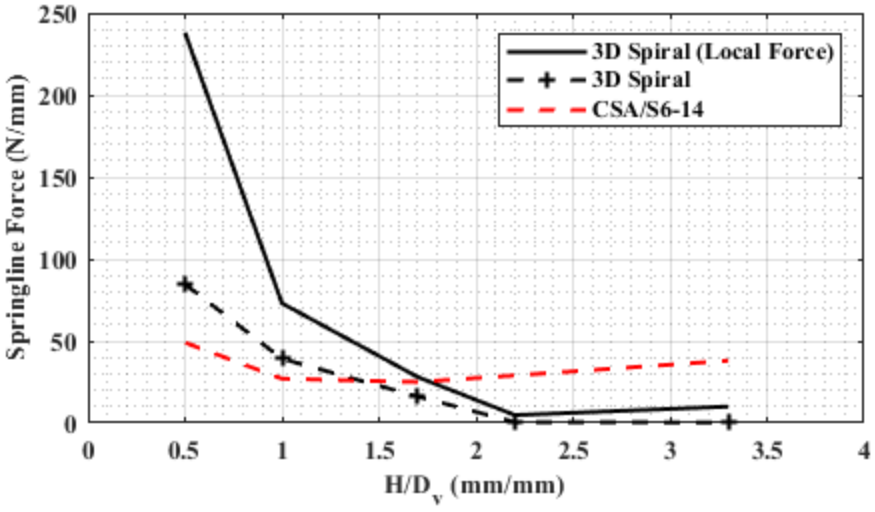

(a)

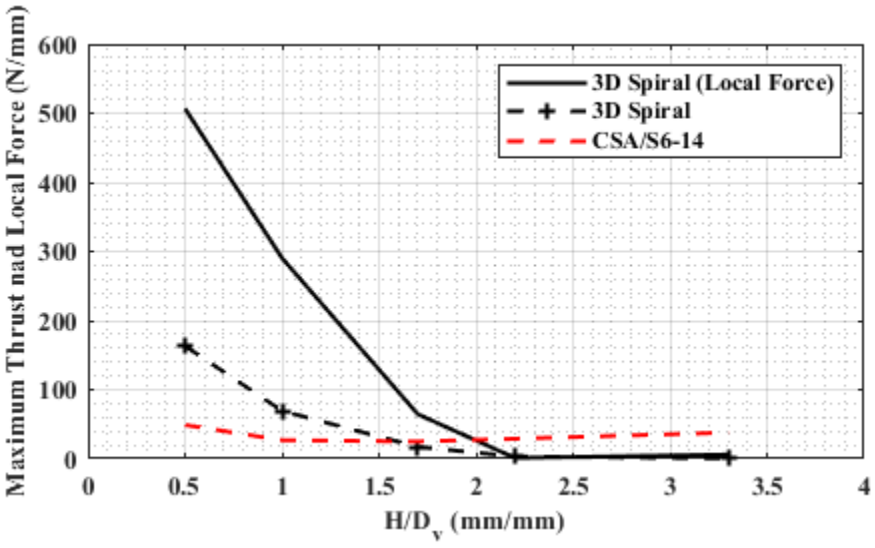

(b)

Figure 3.21. Variation in the culvert section force with normalized cover depth and single wheel pair loading at the final stage of loading a) at the springline and b) at crown based on FE simulation

The maximum bending moments for different normalized cover depths at the final stage of loading are presented in Figure 3.22. For normalized cover depths greater than 0.5 ($\frac{H}{D_v} > 0.5$), the 3D spiral corrugated profile model and current practice (CSA S6-14, 2014)

are in close agreement with respect to the predicted maximum bending moment at the culvert crown. The analysis suggests current practice based on CHBDC (2014) provides conservative estimates in the culvert section moment response. The FEA indicates a change in the load transfer and culvert/soil interaction mechanisms that influence the culvert section response of internal forces and deformational behaviour. The nonlinear behaviour at shallow cover depths is influenced by soil behaviour and the culvert sectional properties (i.e., geometry, stiffness) that affects the culvert deformation mechanisms.

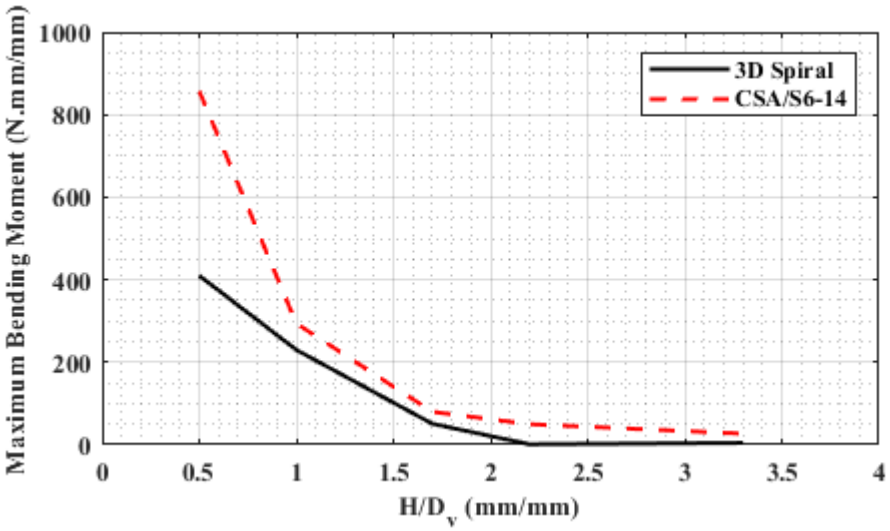

Figure 3.22. Variation in the maximum bending moment, at the crown, with normalized burial depth for the single wheel pair loading at the final stage of loading

This study demonstrates the importance of explicitly modelling the corrugated culvert profile (i.e., depth, pitch and wall thickness) to improve confidence in reliable estimates of the culvert mechanical response, particularly for shallow cover depths.

3.6 Conclusion

The influence of the culvert section profile on soil/structure interaction mechanisms and the culvert mechanical response (i.e., deformations, membrane strain, section thrust and section moment) was examined using continuum finite element methods in this study. The culvert was modelled, in two- and three-dimensional space, using an equivalent section (i.e., smooth cylinder), annular corrugated profile and spiral corrugate profile. Numerical performance of the corrugated culvert profile model was improved by increasing the mesh density characterizing the corrugation waveform and the use of surface smoothing algorithm to enhance contact interactions between the culvert and soil elements.

The simplified equivalent section models and the more complex corrugated profile models predicted a similar (~5% relative difference) maximum vertical diameter change on the plane of symmetry. However, the modelling approaches (i.e., equivalent smooth cylinder section versus corrugated profile) predicted very different patterns of diameter change (i.e., magnitude and spatial distribution) and deformation mechanisms. As the cover depth decreases, the equivalent smooth cylinder section models do not adequately account for the nonlinear load transfer mechanisms, soil/structure interaction processes and plastic material behaviour. The idealized, equivalent section model cannot capture the local strain response, thrust and section bending moments that develop during the interaction events. The need to incorporate the corrugated section profile in the numerical modelling procedures, particularly for shallow cover depth conditions, has been addressed in this study.

For round, shallow buried culverts ($\frac{D_h}{D_v} = 1$; $\frac{H}{D_v} = 0.5$), the numerical and experimental predictions, using closed form equations, of the magnitude and perimeter distribution of section thrust and bending moment were in good agreement for locations below the springline. The FE simulations predicted a local variation in the strain magnitude at the crest and trough locations of the corrugation profile, particularly along the culvert perimeter between the shoulder and crown, that significantly deviates from the average conditions. Closed-form equations and current practice do not reflect this localized section behaviour, which can exceed the material yield strength, and not adequately account for the mechanical response and deformation mechanisms at shallower cover depths. Consequently, the calculated thrusts by closed-form equations are an order lower than the predicted values using continuum FEM, in this study for net and local forces.

A sensitivity study was conducted to assess the effects of cover depth on the predicted section local force and bending moment for the 3D corrugated section profile model. The numerical simulations indicate a transformation in the load distribution and culvert/soil interaction mechanisms with decreasing cover depth that results in a higher order waveform response, in the distribution and magnitude of local force and section moment, above the culvert springline. Based on the parameter range investigated in this study, a transition in the load transfer and culvert response for deep to shallow burial interaction occurs at a shallow cover depth ($\frac{H}{D_v} \cong 1.7$). In comparison with the continuum FEM using the corrugated profile model, current practice (CSA S6-14, 2014) is conservative on thrust estimates for deeper cover depths (i.e., $\frac{H}{D_v} > 1.7$) as it overestimates the fill load, and it underestimates the maximum section thrust load at shallow cover depths (i.e., $\frac{H}{D_v} < 1.7$ for

local force and thrusts) and provides conservative estimates on the crown moment across all burial depths considered. Based on this numerical study, the thrust response has a greater proportion approaching the culvert yield strength than the section moment response across the parameter range studied.

References

Armendariz, R., and Bowman, M. (2018). Bridge load rating. In. Joint Transportation Research Program Publication No. FHWA/IN/JTRP-2018/07. Purdue University, West Lafayette, Ind. doi:10.5703/1288284316650.

ASTM. (2011). D 2487. Standard practice for classification of soils for engineering purposes (Unified Soil Classification System). Book of Standards, West Conshohocken, Pa. doi:10.1520/D2487-11.

Bakht, B. (1981). "Soil-steel structure response to live loads." *Journal of the Geotechnical Engineering Division*, 107(6), 779–798.

Bayoglu Flener, E. (2010). "Testing the response of box-type soil-steel structures under static service loads." *Journal of Bridge Engineering*, 15(1), 90–97.

Beaton, J. and Stratfull, R. (1962). "Field test for estimating service life of corrugated metal pipe culverts." *Highway Research Board Proceedings*, Vol. 41.

Billing, J. and Green, R. (1984). "Design provisions for dynamic loading of highway bridges." *Transportation research record*, (950), 94–103.

Brachman, R., Elshimi, T., Mak, A., and Moore, I. (2012). "Testing and analysis of a deep corrugated large-span box culvert prior to burial." *Journal of Bridge Engineering*, 17(1), 81–88.

Bradford, S. A. (2000). "The practical handbook of corrosion control in soils.

Choi, D.-H., Kim, G.-N., and Byrne, P. M. (2004). "Evaluation of moment equation in the 2000 canadian highway bridge design code for soil–metal arch structures." *Canadian journal of civil engineering*, 31(2), 281–291.

Corrugated Steel Pipe Institute. (2010). Handbook of steel drainage and highway construction products. In Handbook of steel drainage and highway construction products. Corrugated Steel Pipe Institute, Cambridge, ON, Canada.

CSA/S6-14. 2014. "Canadian Highway Bridge Design Code S6-14 CSA". Canadian Standards Association, Canada.

Deng, L., Cai, C., and Barbato, M. (2011). "Reliability-based dynamic load allowance for capacity rating of prestressed concrete girder bridges." *Journal of Bridge Engineering*, 16(6), 872–880.

Duncan, J. (1978). "Soil-culvert interaction method for design of metal culverts." *Transportation research record*, (678).

El-Taher,M. andMoore, I. D. (2008). “Finite element study of stability of corroded metal culverts.” *Transportation Research Record*, 2050(1), 157–166.

Elshimi, T., Mak, A., Brachman, R., and Moore, I. (2011). “Behaviour of a deep-corrugated largespan box culvert during backfilling.” *Pan-American Conference on Teaching and Learning of Geotechnical Engineering*, Toronto, Canada.

Elshimi, T. M. (2011). “Three-dimensional nonlinear analysis of deep-corrugated steel culverts.” Ph.D. thesis, Queen’s University.

Elshimi, T. M., Brachman, R. W., and Moore, I. D. (2014). “Effect of truck position and multiple truck loading on response of long-span metal culverts.” *Canadian Geotechnical Journal*, 51(2), 196–207.

Elshimi, T. M. and Moore, I. D. (2013). “Modeling the effects of backfilling and soil compaction beside shallow buried pipes.” *Journal of Pipeline Systems Engineering and Practice*, 4(4), 04013004.

Hibbitt, H., Karlsson, B., and Sorensen, P. (2013). Abaqus analysis user’s manual, version 6.13. Dassault Systèmes Simulia Corp., Providence, R.I., USA.

Lougheed, A. C. (2008). *Limit states testing of a buried deep-corrugated large-span box culvert*. Queen’s University Kingston, Ontario, Canada.

Maher, M., Hebeler, G., and Fuggle, A. (2015). “Service life of culverts–a synthesis of highway practice, synthesis 474.” *Transportation Research Board, National Cooperative Highway Research Program, Washington, DC*.

Mai, V. T. (2013). “Assessment of deteriorated corrugated steel culverts.” Ph.D. thesis, Queen’s University, 233p.

Mai, V. T., Hoult, N., and Moore, I. (2018). “Numerical evaluation of a deeply buried pipe testing facility.” *Advances in structural engineering*, 21(16), 2571–2588.

Marston, A. and Anderson, A. (1913). *The theory of loads on pipe in ditches and tests of cement and clay drain tile and sewer pipe*, Vol. 31. Iowa Eng. Experiment Station.

McGrath, T. J., Selig, E. T., Webb, M. C., Zoladz, G. V., et al. (1999). “Pipe interaction with the backfill envelope.” *Report no.*, University of Massachusetts at Amherst. Transportation Center.

Menetrey, P. andWillam, K. (1995). “Triaxial failure criterion for concrete and its generalization.” *Structural Journal*, 92(3), 311–318.

Moore, I. D., Hoult, N. A., et al. (2014). “Performance of two-dimensional analysis: Deteriorated metal culverts under surface live load.” *Tunnelling and underground space technology*, 42, 152–160.

Moore, I. D., Regier, C., and Hoult, N. A. (2017). “Surface load testing of new circular and ellipticalmetal culverts at shallow cover.” *Archiwum Instytutu Inżynierii Lądowej*.

Nakhostin, E., Kenny, S., and Sivathayalan, S. (2017). “Examination of buried corrugated metal culvert failure mechanisms using finite elements methods.” *GeoOttawa*.

Nakhostin, E., Kenny, S., and Sivathayalan, S. (2019). “Buried corrugated steel culvert failure mechanisms due to environmental deteriorations.” *International Conference on Sustainable Infrastructure 2019: Leading ResilientCommunities through the 21stCentury*,American Society of Civil Engineers Reston, VA, 29–40.

Pike, K. and Kenny, S. (2016). “Offshore pipelines and ice gouge geohazards: comparative performance assessment of decoupled structural and coupled continuum models.” *Canadian Geotechnical Journal*, 53(11), 1866–1881.

Ramberg, W. and Osgood, W. R. (1943). *Description of stress-strain curves by three parameters*. National Advisory Committee for Aeronautics, Washington, D.C.

Regier, C. (2015). “Investigation of the failure mechanisms of intact and deteriorated culverts.” Ph.D. thesis, Queen’s University. 147p.

Regier, C., Moore, I. D., and Hoult, N. A. (2018). “Remaining strength of deteriorated corrugated steel culverts.” *Journal of Pipeline Systems Engineering and Practice*, 9(2), 04018002.

Roy, K., Hawlader, B., Kenny, S., and Moore, I. (2015). “Finite element modeling of lateral pipeline–soil interactions in dense sand.” *Canadian Geotechnical Journal*, 53(3), 490–504.

Scarino, J. H. (2003). “Reappraisal of marston’s formula.” *Journal of transportation engineering*, 129(6), 703–712.

Simpson, B., Hoult, N. A., and Moore, I. D. (2015). “Distributed sensing of circumferential strain using fiber optics during full-scale buried pipe experiments.” *Journal of Pipeline Systems Engineering and Practice*, 6(4), 04015002.

Simpson, B., Moore, I. D., and Hoult, N. A. (2016). “Experimental investigation of rehabilitated steel culvert performance under static surface loading.” *Journal of Geotechnical and Geoenvironmental Engineering*, 142(2), 04015076.

Simulia, D.S. (2013). ABAQUS 6.13 User’s manual. Dassault Systems, Providence, R.I.

Spangler, M., Hennessy, R., and Barber, E. (1947). “A method of computing live loads transmitted to underground conduits.” *Highway Research Board Proceedings*, Vol. 26.

Spangler, M. G. (1964). “Pipeline crossings under railroads and highways.” *Journal-American Water Works Association*, 56(8), 1029–1046.

Spangler, M. G. and Shafer, G. (1938). “The structural design of flexible pipe culverts.” *Highway Research Board Proceedings*, Vol. 17.

Timoshenko, S. and Gere, J. (1961). *Theory of Elastic Stability*, Vol. 20. McGraw-Hill, New York.

Walker, A. and Williams, K. A. (1995). “Strain based design of pipelines.” *Report no.*, American Society of Mechanical Engineers, New York, NY (United States).

Warman, D. J., Hart, J. D., and Francini, R. B. (2009). “Development of a pipeline surface loading screening process & assessment of surface load dispersing methods.” *Canadian Energy Pipeline Association, Worthington, OH, Report No*.

Wriggers, P. (1995). “Finite element algorithms for contact problems.” *Archives of computational methods in engineering*, 2(4), 1–49.

Chapter 4: Internal thrust modification factors for corrugated steel culvert buried in shallow cover depth

4.1 Methodology

This chapter presents the numerical studies on shallow corrugated culverts buried in shallow cover depth. The main goal is to predict the internal forces (e.g., thrust, local force, bending moment) for shallow buried culverts with consideration of the corrugated geometry and soil/culvert interactions.

Three-dimensional continuum finite element modeling procedures, using Abaqus/Standard 6.13 finite element software, were developed to examine the mechanical response (i.e., membrane strain, thrust, local force, and bending moment) of a buried steel culvert. Confidence in the numerical modeling procedures was established through verification of the predicted bending moment response with data from third-party physical modeling studies (Regier, 2015).

The influential variables and their interactions were evaluated using the variance-based method (i.e., Sobol method) in a global sensitivity analysis (Saltelli et al., 2004; Saltelli et al., 2010). The first-order index, which represents the contribution of each input factor to the variance of the model response output (Iman and Hora, 1990, Saltelli et al., 1993, Homma and Saltelli, 1996), was evaluated. Interactions represent information about the combinations of model inputs, which is not described by the first-order effects. Total-order indices were evaluated to obtain information on the nonadditive features such as interactions among variables of the model (Homma and Saltelli, 1996; Saltelli, 2002; Sobol, 2005).

The elementary effects (EE) method was the second approach which is used to identify the influential variables. Morris (1991) introduced the concept of elementary effects which determines effective input factors in interaction with other factors for linear, additive, and nonlinear models using two sensitivity measure, the mean and the standard deviation of the distribution. The absolute values of the mean of the distribution was used in this study proposed by Campolongo et al. (2007) to solve the problem of type II errors (false negative) in the elementary effect analysis (Saltelli et al., 2008).

Finite element simulations and global sensitivity analysis (GSA) results were used to propose a modifying factor for the recommended closed-form equations, used in current engineering practices (i.e., CSA/S6-14), to estimate local force values in the corrugated cross section for culverts buried in shallow cover depths ($H/D < 2$).

4.2 Finite Element Modeling

4.2.1 Overview

Continuum finite element methods were used to examine the mechanical response of a buried steel culvert subject to service loads. In this study, the primary objective was to gain an improved understanding of the surface load transfer mechanisms and culvert mechanical response for shallow buried culverts.

Nakhostin et al. (2021) indicate the FE predictions of average section thrust are consistent with thrust estimates based on closed-form estimates (CSA/S6-14) and experimental observations (Regier (2015)). More details are presented in Chapter 3. The average thrust (i.e., average strain), however, does not account for local variations in the culvert response at corrugation trough and crest that may result in unconservative estimates

of the section peak local force (Nakhostin et al., 2019, Nakhostin et al., 2021). See Chapter 3 for more details. Consequently, a secondary objective of this study, was to develop a modification factor on the thrust to estimate local force in the corrugated culverts buried with shallow cover depth using current recommended practice (CSA/S6-14).

4.2.2 Numerical simulation procedures

Modeling the corrugated culvert profile explicitly is required for shallow burial depth conditions. The corrugated culvert section geometry used in this study is shown in Figure 4.1.

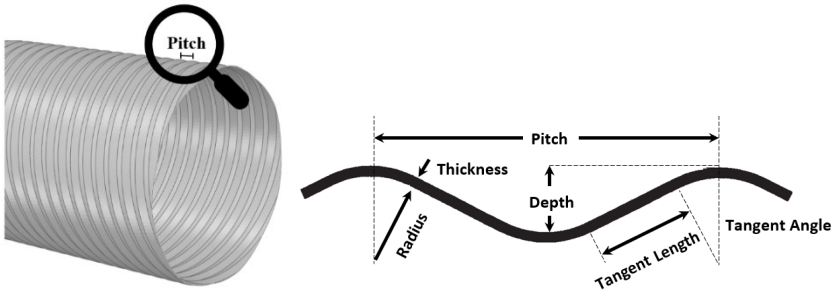

Figure 4.1. The variables of the corrugated steel culvert profile

The corrugated culvert profile had a nominal wall thickness (1.60 mm), depth (12.7 mm) and pitch (67.7 mm) with a 1.51 mm^2 cross-sectional area, 28.4 mm^4 moment of inertia (i.e., second moment of area), and 4.02 mm^3 section modulus per unit length of culvert (Corrugated Steel Plate Institute, 2010). This culvert profile was used in physical modelling studies to investigate the section local force and bending moment response of a 1500 mm long, 900 mm diameter culvert subjected to a single wheel pair load (71 kN) at a cover depth of 900 mm (Regier, 2015). This intact (i.e., no damage or deterioration) culvert was defined as the Control Pipe (CP) where additional tests examined the corrosion effects (i.e., damage due to loss of wall thickness loss) on culvert mechanical response. These experimental investigations were used to develop the finite element modeling

procedures, used in this study, and the circumferential section bending moment was used to verify the numerical predictions.

The culvert material was conventional steel grade with an elastic modulus of 200 GPa, yield strength of 230 MPa and ultimate strength of 310 MPa. The bedding and the backfill soil were compacted to 95% and 90% standard proctor respectively and were classified as a poorly graded sandy gravel soil, "GP-SP", using the unified soil classification system. The simulated standard wheel pair was imposed on the ground surface and positioned over the culvert crown and was applied using the wheel pad (250 mm x 600 mm in plan) based on CSA/S6-14 for the service load conditions. Further details on the verification procedures are presented in (Nakhostin et al., 2021) and chapter 3 of this thesis.

In the finite element simulation, the soil mechanical behaviour was defined using the modified Mohr-Coulomb model in Abaqus which simulates material hardening and softening behaviour in soils due to applied stresses and strains (Menetrey and Willam, 1995, Simulia, 2013). The soil parameters were based on experimental studies (McGrath et al., 1999, Elshimi et al., 2011, Elshimi and Moore, 2013), which were used to calibrate the numerical modeling procedures. For the experimental studies, the backfill could be characterized as poorly graded granular soil (GP-SP) using the unified classification system (ASTM, 2011).

The soil domain of FEM was consistent with the full-scale experiments (Regier, 2015), as shown in Figure 4.2, that was 8000 mm wide, 4400 mm long, and 2400 mm depth (with 900 mm cover). Figure 4.3 presents the defined spiral path at the mid-length

of the culvert where the wheel-load is applied on the surface. This path is used to sample data collected from the finite element analysis.

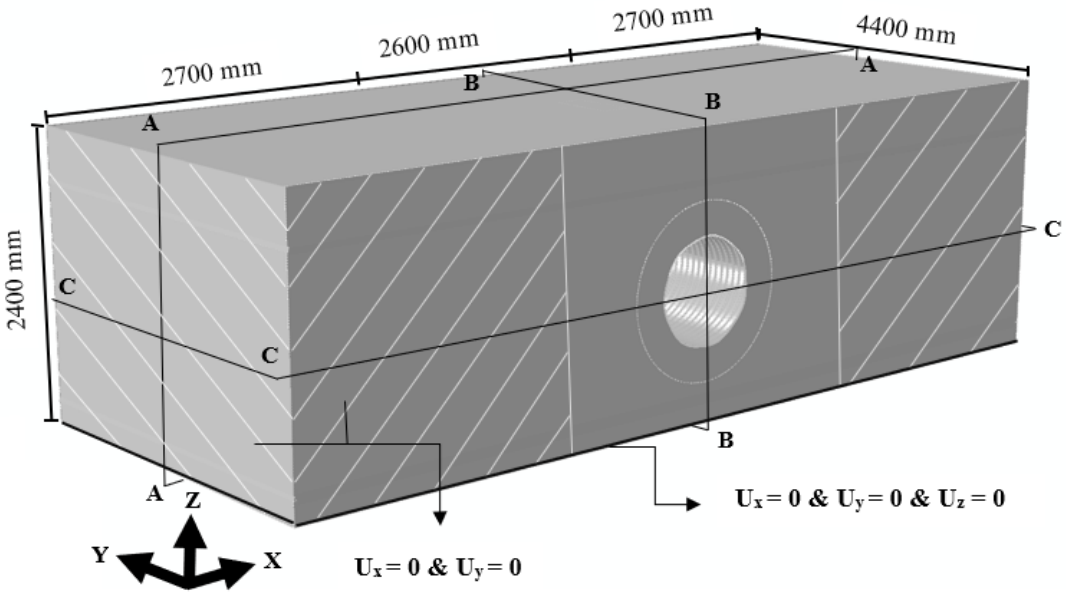

Figure 4.2. The model geometry for the Finite Element Analysis presenting soil backfill domain and kinematic (natural) boundary conditions

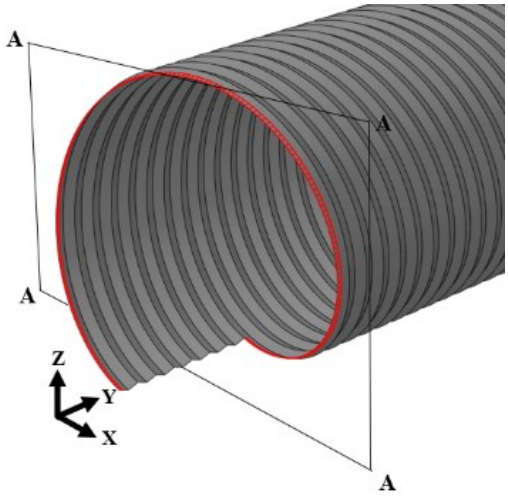

Figure 4.3. Defined spiral trough path at the culvert mid-length for sampling the FEM data

Table 4.1 presents the used value for different parameters in the numerical simulation using Abaqus software for the baseline finite element model.

Table 4.1. the parameters for the baseline finite element model

Description	Unit	Values
cover depth (H)	mm	900
culvert diameter (D)	mm	900
elastic modulus of culvert (E)	MPa	2e5
elastic modulus of soil (E_s)	MPa	63
unit weight of soil (γ)	kN/m^3	21
yield tensile stress (F_y)	MPa	230
number of lane load (NL)	-	1
culvert wall thickness (t)	mm	1.6
depth of culvert profile (De)	mm	12.7
pitch of culvert profile (Pi)	mm	67.7
tangent length of culvert profile (TL)	mm	19.58
radius of culvert profile (Ra)	mm	17.46
load pad dimensions	mm × mm	250 × 600
Soil box dimensions	m × m × m	8 × 4.4 × 2.4
nominal single wheel pair load	kN	71
maximum single wheel pair load	kN	107

4.2.3 Verified results, section bending moments

Figure 4.4a presents the culvert section bending moments obtained through numerical simulation and the experimental full-scale test (Regier, 2015).

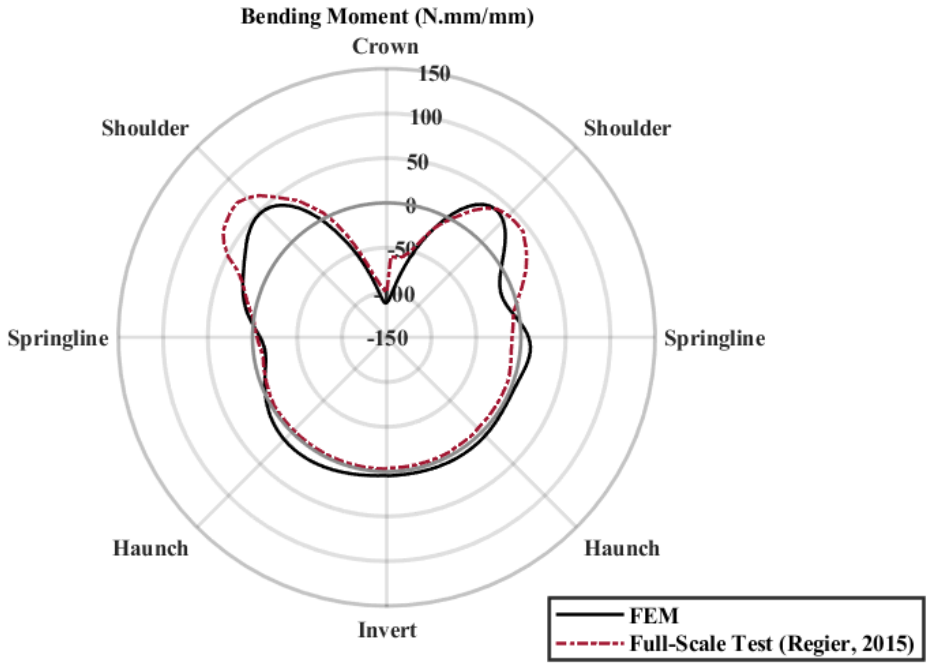

(a)

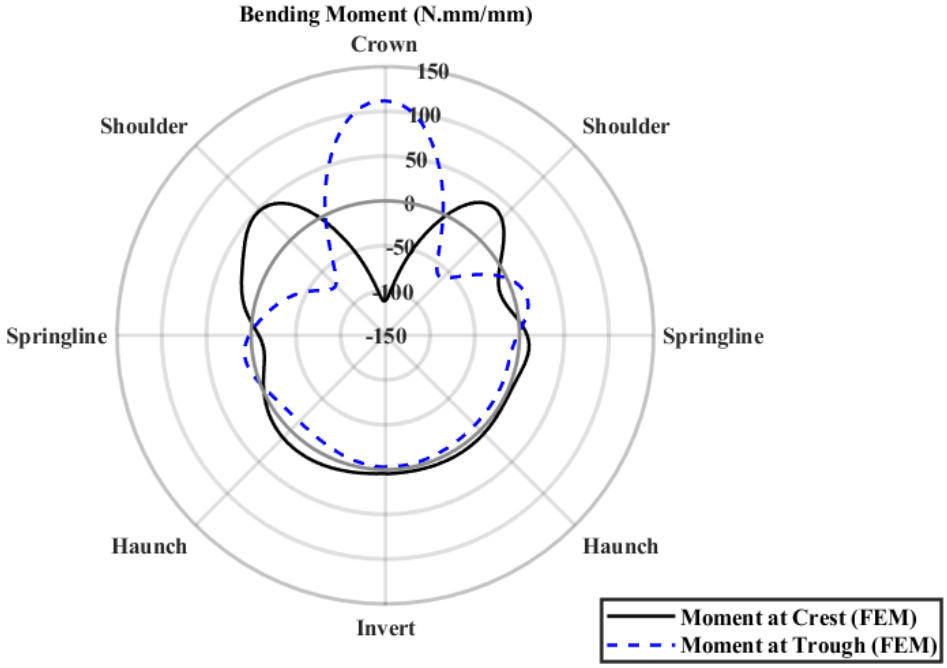

(b)

Figure 4.4. Spiral distribution of section bending moment (N.mm/mm) with 71 kN single wheel pair loading

The numerical simulations (FEM) and physical test results (Full-Scale Test) are generally consistent along culvert perimeter locations. The discrepancy between the predicted section moment at the culvert invert and the full-scale test (Regier, 2015) was attributed to variability in the CSC/soil interface conditions due to trench backfilling and compaction activities, which were not accounted for during the finite element simulations (Mai, 2013, Regier, 2015). Figure 4.4b presents the culvert local bending moments at crest and trough using FEM. This figure shows there is a sign change in moment from crest to trough while the culvert experiences very close magnitude for moments at crest and trough. This sign change is also reported in the strain and local force responses in the finite element simulations.

4.3 Corrugated culvert mechanical responses

4.3.1 Background

The study conducted by Nakhostin et al. (2021) indicates that the modeling approach (i.e., 3D spiral corrugated culvert model in comparison with an isotropic shell theory for a smooth cylinder with effective thickness) affects predictions of culvert membrane strain, as well as the magnitude and distribution of local strain. These results indicate modeling corrugated steel culvert explicitly is required for buried culverts in a shallow cover depth.

4.3.2 Corrugated culvert strain, thrust, and local force responses

Finite element simulations enable a detailed assessment of the magnitude and distribution (i.e., intensity or gradient) of mechanical response parameters (e.g., deflections, strain, stress) throughout the modelling domain. Based on the defined path in Figure 4.3, the estimated membrane strain at the crest and trough of the corrugated culvert

profile determined using explicit FE modelling procedures is presented in Figure 4.5. The circumferential strain do not exhibit a perfectly symmetric distribution due to data sampling along the spiral path (Figure 4.3). The results demonstrate that the membrane strain is greater for the perimeter locations extending from the culvert shoulder towards the crown. The corrugated culvert experiences the maximum strains at crown and shoulders with nearly equal magnitudes but opposite signs at crest and trough of corrugated profile.

Figure 4.5 presents the calculated average strain ($\varepsilon_{\mathrm{avg}}$) using the FEM strains. The FEM strains at trough (ε_1) and crest (ε_2) locations on the outside culvert surface (at the culvert/soil interface) of the corrugated profile were used to estimate (extrapolate) the extreme fiber strain (ε_{EF}) at the trough location on the inside surface of the culvert corrugated profile (Equation 4.1),

Equation 4.1 $$\boldsymbol{\varepsilon_{EF} = \frac{(\varepsilon_1 - \varepsilon_2)}{h} t + \varepsilon_1}$$

where h is radial distance between the strain gauges (mm) ε_1 and ε_2 are, and t is intact wall thickness (mm) of the corrugated pipe.

The average strain ($\varepsilon_{\mathrm{avg}}$) can be estimated using Equation 4.2 (Simpson et al., 2015, Simpson et al., 2016, Regier, 2015).

Equation 4.2 $$\boldsymbol{\varepsilon_{avg} = \frac{\varepsilon_2 + \varepsilon_{EF}}{2}}$$

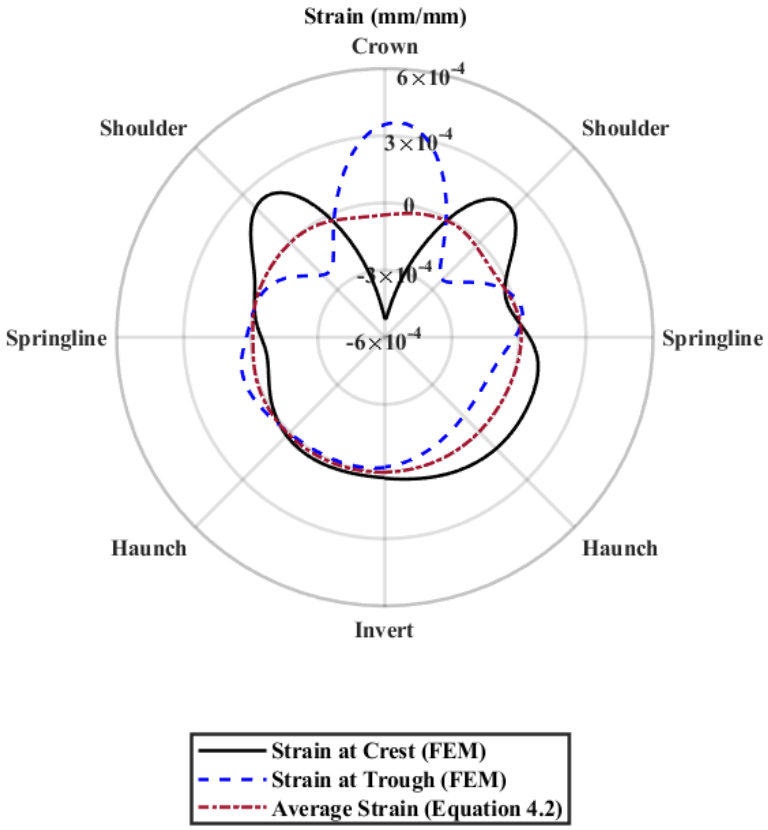

Figure 4.5. Perimeter distribution of membrane strain, with the 71 kN single wheel pair loading for the FE modelling approaches for the local strain at the crest, trough locations, and the average strain

The results presented in Figure 4.5 indicates that the average strain response cannot account for the local peak strain response as predicted by FEM at the culvert shoulder and crown locations.

Based on these defined paths (Figure 4.3), Figure 4.6 presents the amplitude and perimeter distribution of section local force for the finite element simulations and thrust for the reported lab test data. Consistent with the analysis and discussion on the culvert perimeter membrane strain response, calculating thrust (N) using the average strain (ε_{avg}) would cause the same key outcomes discussed for strains.

Equation 4.3 $\mathbf{N = \varepsilon_{avg} EA}$

where N is thrust per unit length (N/mm), E is young's modulus (N/mm^2), and A is cross section area per unit length (mm^2/mm).

As shown in Figure 4.6, the FE predictions of average section thrust are consistent with the closed-form estimates of the thrust (Equation 4.3) as reported by Regier (2015) for the experimental test program. The average thrust does not account for local variations in the culvert response (Figure 4.6), and, consequently, can underestimate the peak local force in the section.

The discussed results in the previous section (i.e., section 3.5.6) indicate that the full-scale test procedures and measuring strains in laboratories and calculating internal bending moments are compatible with the closed-form equations in CSA/S6-14 and Finite element model results.

The averaging method using closed-form equations for calculating strain and thrust in laboratories does not reflect the maximum local force in the corrugated culvert; and this effect is also not considered in the recommended equations for the thrust calculation. This study proposes a modification factor for recommended closed-form equations (i.e., CSA/S6-14) for calculating the local force of a corrugated culvert buried in a shallow cover depth using Finite Element simulations and Global Sensitivity Analysis.

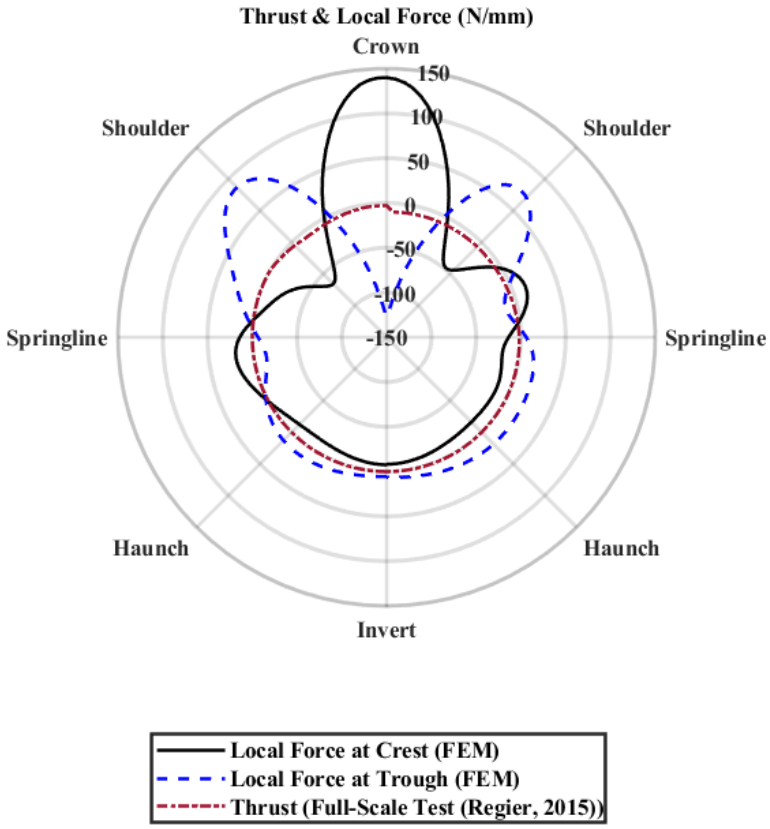

Figure 4.6. Perimeter distribution of section force (N/mm) with the 71 kN single wheel pair loading for the FE modelling for the local force at the crest and trough locations and the reported thrust form the lab test

4.4 Global Sensitivity Analysis Methods

4.4.1 Background

To identify influential variables in the thrust and bending moment calculations for the buried corrugated steel culvert shown in Figure 4.1 and Figure 4.2, variance-based sensitivity analysis and Elementary Effect screening method conducted. The culvert is subjected to the external fill load and traffic loads. The internal applied forces in the culvert is considered due to the external loads and the Canadian code (CSA/S6-14, 2014) is used to calculate the applied thrust and bending moments.

The thrust, T_f, in the conduit wall due to live loads and dead loads are defined as:

Equation 4.4 $$\boldsymbol{T_f = T_D + T_L(1 + DLA)}$$

where T_D and T_L are dead load and live load thrusts and the dynamic load allowance (DLA) are calculated based on the Canadian Highway Bridge Design Code.

The maximum moment in the culvert due to applied fill and truck loads per unit length (M_f) is estimated by:

Equation 4.5 $$\boldsymbol{M_f = |M_1 + M_D| + M_L(1 + DLA)}$$

where M_1 is moment in a soil-metal structure resulting from fill to the crown level, M_D is the moment in the wall of a soil-metal structure due to a dead load, and M_L is the moment in the wall of a soil-metal structure due to live load.

The recommended equations in the Canadian code for deep corrugated culverts calculates the maximum values of the bending moment and thrust in the culvert. The recommended equation for shallow corrugated culverts is considering thrust for internal forces. Both thrust and bending moment are considered for shallow corrugated culvert in this research study. The Canadian code provides detailed equations and calculations of thrust and bending moments and for additional discussions about the internal forces of the buried corrugated steel culvert see (CSA/S6-14, 2014, Nakhostin et al., 2021).

For completed soil-steel structures, the combined effects of the bending moment and axial thrust are considered in this study and calculated as:

Equation 4.6 $$\boldsymbol{\left[\frac{T_f}{P_{pf}}\right]^2 + \left|\frac{M_f}{M_{pf}}\right| \leq 1}$$

where P_{pf} is compressive strength of a corrugated metal section and M_{pf} is moment capacity of a corrugated metal section.

The ultimate limit state for combined effect of bending and thrust available in the Canadian code (CSA/S6-14, 2014) for buried culverts is used to define the failure region. This study considers thrust, bending moment and combined effect of these two internal forces. The failure condition is defined by development of the function where all applied loads and resistance of the culvert material are considered. The function is defined as $Y = \left[\frac{T_f}{P_{pf}}\right]^2 + \left|\frac{M_f}{M_{pf}}\right|$ which defines a safe region when $Y < 1$ and a failure region when $Y > 1$. The equation is a function of several random variables given in Table 4.2.

4.4.2 Input variables and estimating distributions

Based on defined limit state function, the independent input variables are presented in Table 4.2, are normally distributed with presented mean value and coefficient of variations (CV) which defines as a ratio of the standard deviation (σ) to the mean (μ). The values are based on recommended practices, literature or selected with engineering judgements (Ahammed and Melchers, 1997, Corrugated Steel Plate Institute, 2010, CSA/S6-14, 2014, CAN/CSA-G401-14, 2014, Regier, 2015, AASHTO, 2020).

The sensitivity analysis conducted in this study assumes the variables to have a normal distribution which is defined across range from -∞ to +∞. For many engineering applications, such as buried culverts, negative values for key variables (e.g., burial depth, diameter, or elastic modulus) do not have a physical meaning. The probability of obtaining a negative property value is very small, but the elementary effect method collects start and end points of the sample from standard continuous domain [0 1] as two levels of exploration of the space of the input factors. For nonnegative variables we cut 1% of the

distribution in each tail of the standard domain to get a reasonable domain for each input factor after transferring them to the input variable domain as shown in Figure 4.7.

Table 4.2. random variables of the input parameters

Variable Indices	Variable	Description	Mean	CV	References
1	LL	wheel load (N)	87500	0.10	(CSA/S6-14, 2014; Ahammed and Melchers, 1997)
2	H	cover depth (mm)	900	0.10	(Melchers and Beck, 2018)
3	D	culvert diameter (mm)	900	0.014	(ASTM A760/A760M-15, 2020)
4	E	elastic modulus of culvert (MPa)	2e5	0.033	(Ahammed and Melchers, 1997)
5	E_s	elastic modulus of soil (Mpa)	63	0.27	(Melchers and Beck, 2018; Regier, 2015)
6	γ	unit weight of soil (N/mm^3)	2.1e-5	0.10	(Ahammed and Melchers, 1997)
7	F_y	yield tensile stress (MPa)	230	0.05	(Ahammed and Melchers, 1997)
8	m_{NL}	lane loading modification factor	0.90	0.028	(CSA/S6-14, 2014)
9	t	culvert wall thickness (mm)	1.6	0.056	(CSA G401-14, 2014; Corrugated Steel Plate Institute, 2010)
10	De	depth of culvert profile (mm)	12.7	0.025	(ASTM A760/A760M-15, 2020; CSA G401-14, 2014)
11	Pi	pitch of culvert profile (mm)	67.7	0.026	(ASTM A760/A760M-15, 2020; CSA G401-14, 2014)
12	TL	tangent length of culvert profile (mm)	19.58	0.02	(ASTM A760/A760M-15, 2020; CSA G401-14, 2014)
13	Ra	radius of culvert profile (mm)	17.46	0.026	(ASTM A760/A760M-15, 2020; CSA G401-14, 2014)

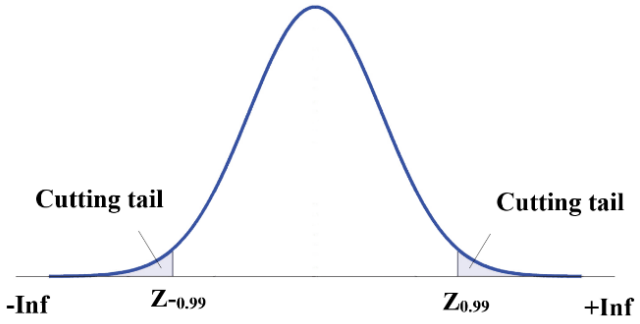

Figure 4.7. Normally distributed input variables with 1% tail cut

4.4.3 Elementary effects screening method, Morris method

Elementary effects (EE) method is a sensitivity analysis to identify noninfluential input variables. The original concept of EE method is derived from the One at a Time (OAT) screening method and introduced by Morris (1991). This method provides sensitivity measures for each input factor to identify the influential factors and Campolongo et al. (2007) proposed a revised version of the EE method that solved the problem of the nonmonotonic model with the effect of responses having opposite signs. EE is a screening method to determine which variables are negligible or influential. This method has the quantitative values to find out if the variables are involved in interaction with other factors and determine which model is linear and additive or nonlinear (Saltelli et al., 2008).

The EE sampling method, used in this study, introduces wider ranges for input variations and removes the dependence on a single sample point. In the EE sampling method, k independent variables vary in the k-dimensional unit cube across p selected level with the step of variation equal to Δ. Table 4.2 represents 13 independent variables considered in this study. The four-level p is selected to reflect the variation of input parameters inside the domain. The p is even and the Δ for all variables is chosen to be equal

to $p/(2(p-1))$ (Saltelli et al., 2008, Morris, 1991). The start point matrix, ${x^*}_{1\times k\times M}$, is a random selection of the start point for all input variables and is used to generate the trajectory points. Using this start point will generate a randomized version of the sampling matrix. For detailed procedure, see Saltelli et al. (2008).

To maximize the spread of the selected points in the variable domain a method is proposed by Campolongo et al. (2007). The method is selecting the best r trajectories out of M trajectories with scanning the input domain to achieve the highest spread. The design starts by generating $M = 30$ trajectories and selects the subset of $r = 10$ with the highest spread to optimize the scanning of the input space (Saltelli et al., 2008). The best r combinations of M with the highest value of the sum of the squared distances between all possible pairs of trajectories are chosen. Developing r trajectories.

The input points are not sampled directly for normally distributed variables. In a k - dimensional hypercube, each set of values varies in [0 1]. The actual input values are derived using the inverse of the normal cumulative distribution function (CDF). Figure 4.8 shows the sampling procedure for one of the input variables. The matrix of variables contains $(k+1)$ rows, and k columns for each trajectory.

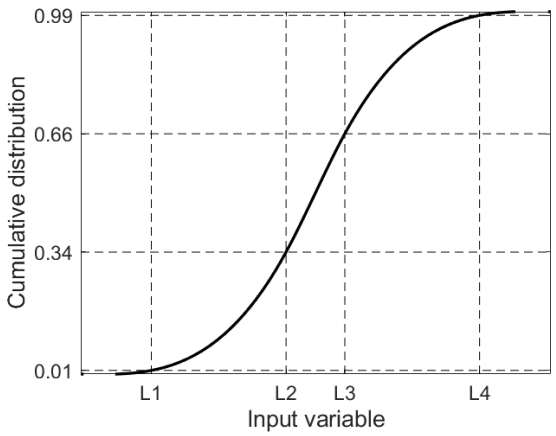

Figure 4.8. Indirect sampling procedure for normally distributed variables

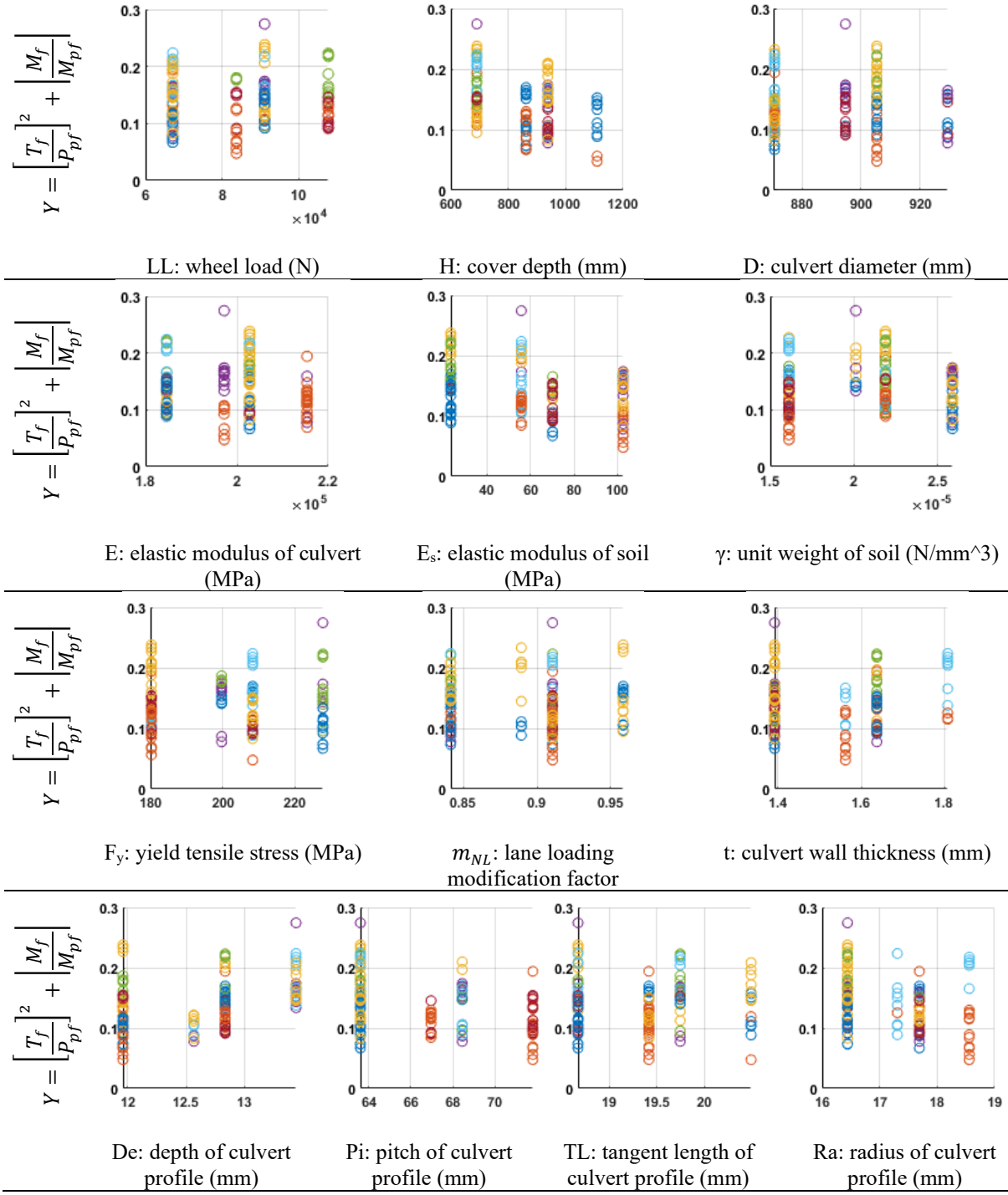

Figure 4.9. Scatterplots of $Y = \left[\frac{T_f}{P_{pf}}\right]^2 + \left|\frac{M_f}{M_{pf}}\right|$ as a function of input variables for intact culvert

The computation cost for elementary effect method is $r \times (k+1)$ runs to get $Y = \left[\frac{T_f}{P_{pf}}\right]^2 + \left|\frac{M_f}{M_{pf}}\right|$ vector for each set of variables. Figure 4.9 presents the scatter plot of system response due to the applied loads and deteriorations ($Y = \left[\frac{T_f}{P_{pf}}\right]^2 + \left|\frac{M_f}{M_{pf}}\right|$) versus the lower to upper bound of k independent input variables for p selected levels of sampling with 1% cutting tail and r trajectories.

The Elementary Effect of each variable can be calculated by the magnitude of variation of that specific variable in the model output. The elementary effect associated with factor i is:

Equation 4.7 $$EE_i^j(x^{(l)}) = \frac{[y(x^{(l+1)}) - y(x^{(l)})]}{\Delta}$$

if the ith component of $x^{(l)}$ is increased by Δ, and

Equation 4.8 $$EE_i^j(x^{(l+1)}) = \frac{[y(x^{(l)}) - y(x^{(l+1)})]}{\Delta}$$

if the ith component of $x^{(l)}$ is decreased by Δ (Saltelli et al., 2008).

While one trajectory allows the evaluation of one elementary effect for each parameter i, a set of *r* trajectories enables statistical evaluation of the finite distribution of the elementary effects. Once r elementary effects per input are available, the statistical measures for evaluation of the EE, the absolute mean (μ_i^*), and the standard deviation (σ_i), relative to the distributions can be computed for each input factor.

Equation 4.9 $$\mu_i^* = \frac{1}{r}\sum_{j=1}^{r}\left|EE_i^j\right|$$

Equation 4.10 $$\sigma_i = \sqrt{\frac{1}{r-1}\sum_{j=1}^{r}\left(EE_i^j - \mu\right)^2}$$

Figure 4.10 and Figure 4.11 present the performance of elementary effects method with 10 trajectories for pure thrust, pure bending, and combined thrust and bending.

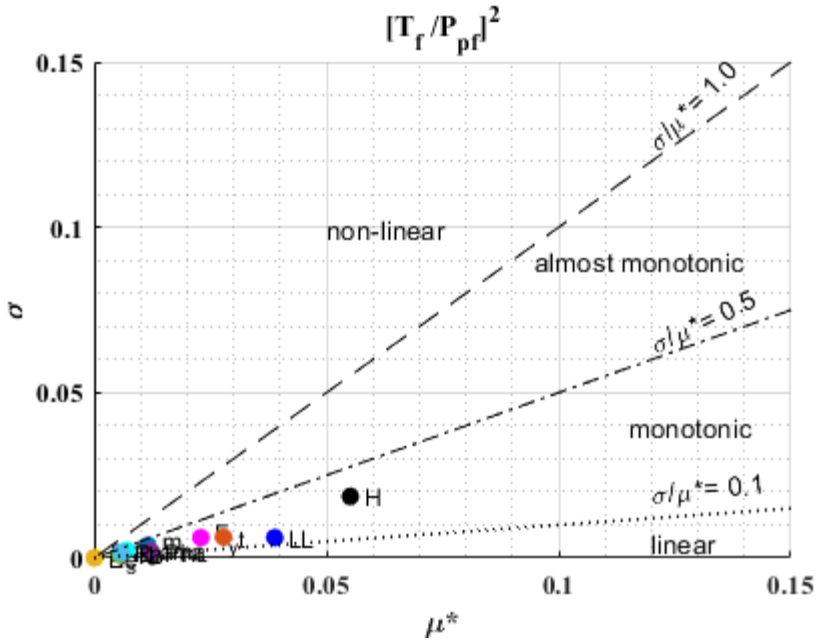

(a)

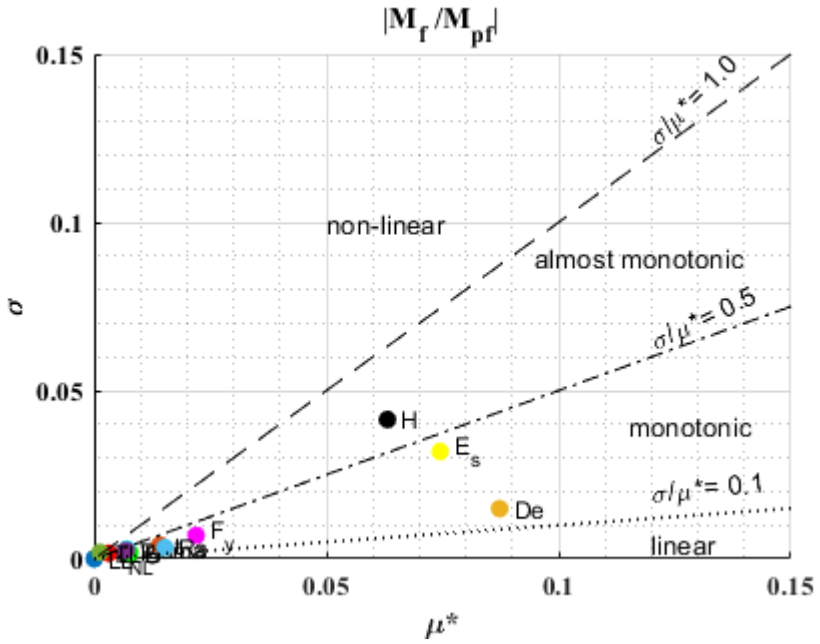

(b)

Figure 4.10. Estimated absolute average (μ_i^*) and standard deviation (σ_i) of the first-order EE for a) thrust, b) bending moment

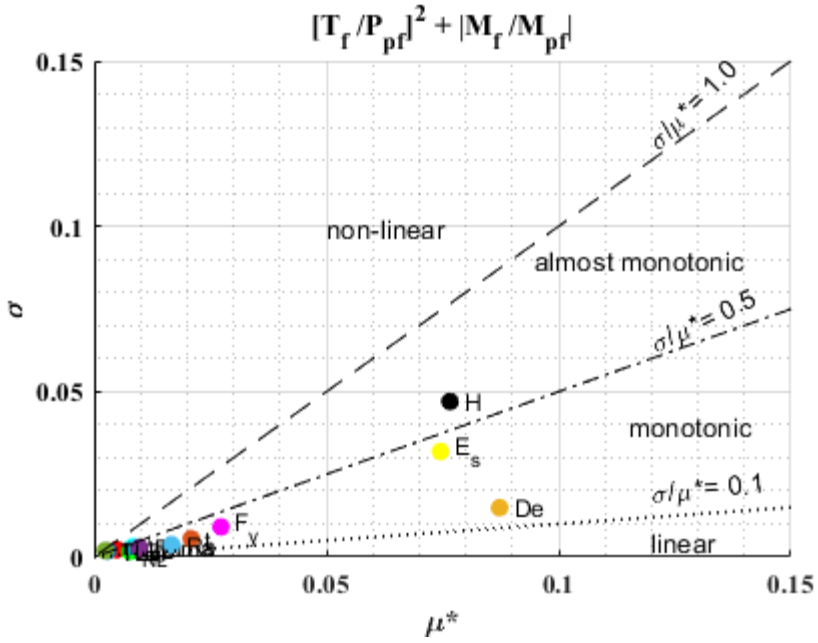

Figure 4.11. Estimated absolute average (μ_i^*) and standard deviation (σ_i) of the first-order EE for combined effect of thrust and bending moment

Each point in these figures represent the estimated absolute average (μ^*) versus standard deviation (σ) of the first-order EE screening method for each variable. Three straight lines of slope, $\frac{\sigma}{\mu^*} = 0.1, 0.5, and\ 1$, are plotted for identifying linear variables which are located below the line $\frac{\sigma}{\mu^*} = 0.1$, monotonic variables which are located between two lines $\frac{\sigma}{\mu^*} = 0.1\ and\ 0.5$, almost monotonic variables which are located between two lines $\frac{\sigma}{\mu^*} = 0.5\ and\ 1$, and non-linear or non-monotonic variables which are located above the line $\frac{\sigma}{\mu^*} = 1$ (Sanchez et al., 2014, Menberg et al., 2016). The absolute average (μ^*) versus standard deviation (σ) of the first-order EE for pure thrust of culvert in Figure 4.10a indicates that two variables, the cover depth of the buried culvert (H), and the truck wheel

load (LL) are influential variables and located between the lines $\frac{\sigma}{\mu^*} = 0.1$ and 0.5 with monotonic behaviour.

The small value of μ^* for pure thrust relative to the pure bending and combined bending and thrust, as shown in Figure 4.10b and Figure 4.11, indicates the bending moment is the significant internal force in shallow buried corrugated steel culvert based on the defined limit state function. It is noted that this result is in a disagreement with the finite element results that show the local force is the effective internal force in performance of the corrugated culvert where the local forces at crest and trough of crown are very close to the compressive strength (P_{pf}) of the corrugated metal culvert (Nakhostin et al., 2019, Nakhostin et al., 2021). The results for pure bending moment and combined thrust and bending effects are very similar with three influential variables, cover depth of the buried culvert from ground level (H), elastic modulus of the backfill soil (E_s), and corrugated culvert depth (D_e) where cover depth presents an almost monotonic behaviour and other two influential variables show a monotonic behaviour. The other variables are identified as noninfluential variables.

4.4.4 Variance based sensitivity analysis, Sobol method

Sensitivity analysis method is an effective method for identifying the important factors in a model. The Sobol Method has been used for computing the first- and total-order indices for the buried corrugated steel culvert with k ($k = 13$) independent variables introduced in Table 4.2.

One at a time (OAT) is a Fractional factorial sampling with two-level factorial design which considers low level and high level (two levels) for each variable. For this sampling

approach, k parameters would require 2^k simulation to cover all combinations for a factorial design. Latin Hypercube (LH) sapling is a full factorial design methos that has s levels greater than 2 and the number of simulations for the full factorial method with s levels and k variables would be s^k (Saltelli et al., 2008). LH sampling method is capable of determining the behaviour of system due to samples located inside the sampling space, but it does not have control on creation of clusters and gaps in the sampling space.

A fully random sequence of generated points has a high discrepancy with cluster and gaps in the domain. To avoid this problem, Quasi-random sampling technique which is a low discrepancy sequence is used in this study. This sampling technique is not completely random and unpredictable, but it biases the selection of points to maintain a uniformly distribution of points across the sampling domain. The Halton sequence is a well-known low-discrepancy sequence that is used in this study. This sequence is used to generate points in space. The bases of this sampling method is constructed according to a deterministic method but it has a control on creation of clusters and gaps in the sampling and is classified as a quasi-random sampling method (Homma and Saltelli, 1996; Saltelli, 2002; Saltelli et al., 2008). The base sample (N) is equal to 10000 in order to have an evident low discrepancy considering 13 independent variables in this study. Figure 4.12 shows the examples of generated 10000 samples and marginal probability density function (PDF) for two variables using Holton sequence.

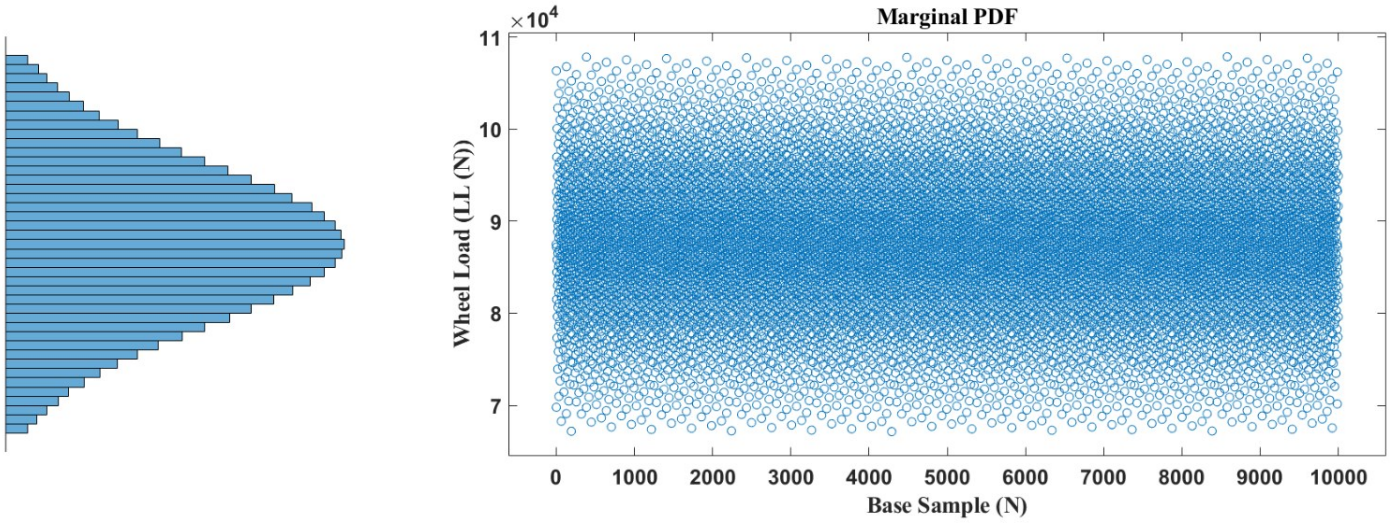

(a)

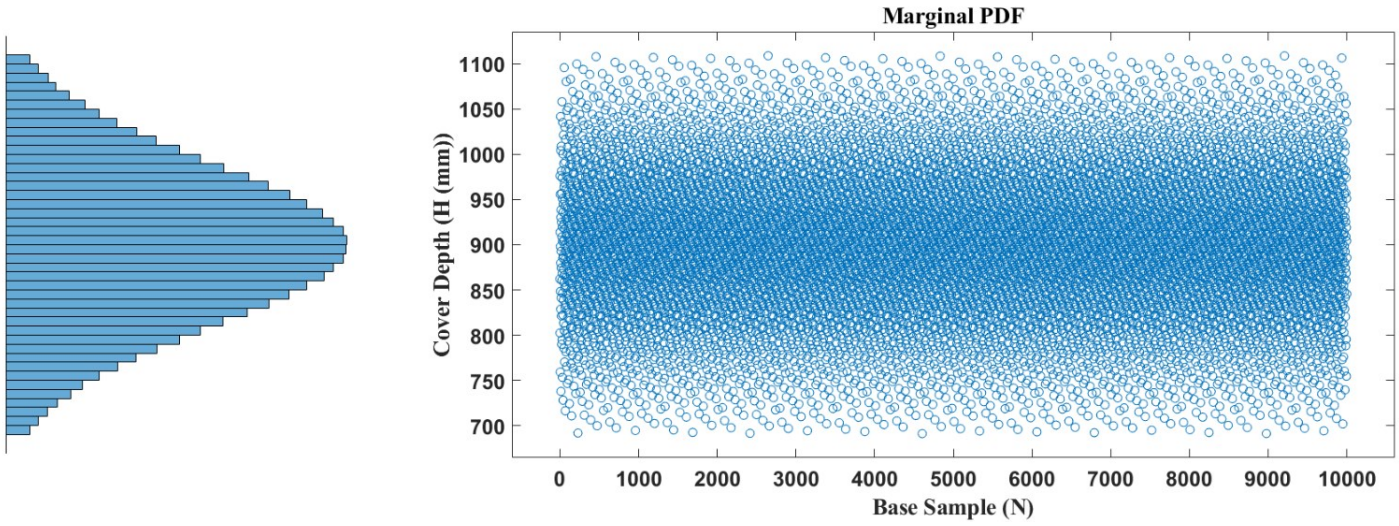

(b)

Figure 4.12. Marginal PDF of Holton sequence samples for 2 variables, a) wheel local, LL and b) cover depth, H

Monte Carlo-based implementation for computing sensitivity measures is provided by Sobol (2005). In this method, S_i is the first-order sensitivity index represents the main

effect contribution of each input factor to the variance of the output (Iman and Hora, 1990, Saltelli et al., 1993, Homma and Saltelli, 1996, Fenton and Griffiths, 2008).

Equation 4.11 $$S_i = \frac{V[E(Y|X_i)]}{V(Y)}$$

where X refers to the variables, Y is the output vector, $E(Y)$ is mean or expected value of Y, and $V(Y)$ is variance of Y.

First-order effect plus all higher-order effects of factor X_i is total effect index of factor X_i that is useful to investigate the all interactions involving the parameter X_i. Homma and Saltelli (1996) proposed a technique to calculate total effect indices at the same cost of first-order indices that is used in this study.

Equation 4.12 $$S_{Ti} = 1 - \frac{V[E(Y|X_{\sim i})]}{V(Y)} = S_i + S_{ij} + \cdots + S_{ij\ldots k}$$

where $X_{\sim i}$ is the vector of all factors but X_i.

The first-and total-effect indices are calculated in this study. Two matrices ($N \times k$) are generated called matrix A and B. N is the base sample which is equal to 10000 in this study to cover the entire parameter space. These matrices are generated by applying quasi-random Holton sequence. Matrix C_i formed by all columns of matrix B except the ith column which is taken from matrix A. The model output for all input values in the matrices A, B, and C are calculated, $y_A = f(A)$, $y_B = f(B)$ and $y_{Ci} = f(C_i)$. The computation cost for this method is $N \times (k + 2) = 150{,}000$ runs. The first-order and total-effect indices are estimated based on the following equations (Saltelli et al., 2008).

Equation 4.13 $$S_i = \frac{V[E(Y|X_i)]}{V(Y)} = \frac{y_A \times y_{Ci} - f_0^2}{y_A \times y_A - f_0^2}$$

Equation 4.14 $$S_{Ti} = 1 - \frac{V[E(Y|X_{\sim i})]}{V(Y)} = 1 - \frac{y_B \times y_{Ci} - f_0^2}{y_A \times y_A - f_0^2}$$

Equation 4.15 $$f_0^2 = \left(\frac{1}{N}\sum_{j=1}^{N} y_A^{(j)}\right)^2$$

The results of the variance-based sensitivity analysis are presented in Figure 4.13, Figure 4.14, and Figure 4.15 for intact buried culvert. These figures present the first-order and total effect indices (S_i and S_{Ti}) for 13 independent variables presented in Table 4.2 considering separate and combined effects of thrust and bending moment for the service load conditions. The results of total-effects for pure bending moment and combined thrust and bending effects are very similar as shown in Figure 4.14 and Figure 4.15 that shows the bending moment is more effective internal force in comparison with pure thrust (Figure 4.13) in shallow buried corrugated steel culvert based on defined limit state function. It is noteworthy that this result is in a disagreement with the finite element results that show the trust is the effective internal force in performance of the corrugated culvert, and the Canadian code recommends considering pure thrust in design of shallow corrugated culverts investigated in this study.

The influential parameters for the thrust output are the truck wheel load (LL) and the cover depth of the buried culvert (H). Three influential parameters with impact on the bending moment output responses are cover depth of the buried culvert from ground level (H), elastic modulus of the backfill soil (E_s), and corrugated culvert depth (De). All results of Variance based sensitivity analysis are consistent with first-order Elementary Effect analysis results.

The interaction between two variables can be defined as an effect of one variable on an output that depends on the state of a second variable. First-order sensitivity results are very similar to the total-effect results with $\sum_{i=1}^{k} S_i$ equal to 0.93, 0.94, and 0.95 for pure thrust, pure bending, and combined thrust bending, respectively. These values are almost

equal to 1 and this indicates that intact culvert system is an additive and linear model and there is not an important interaction among the variables.

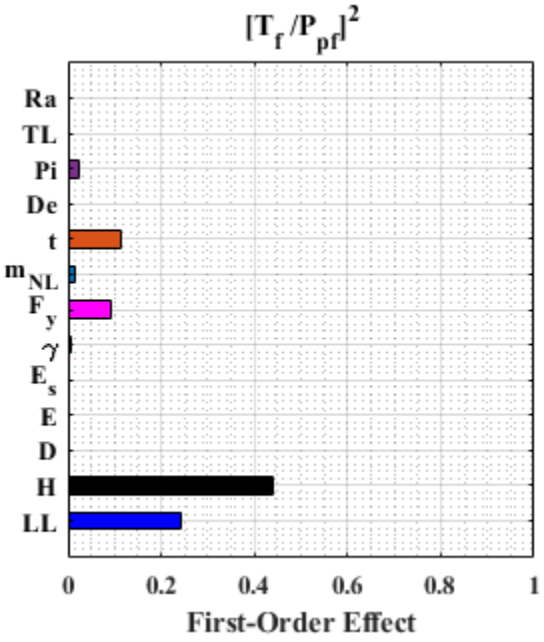

(a)

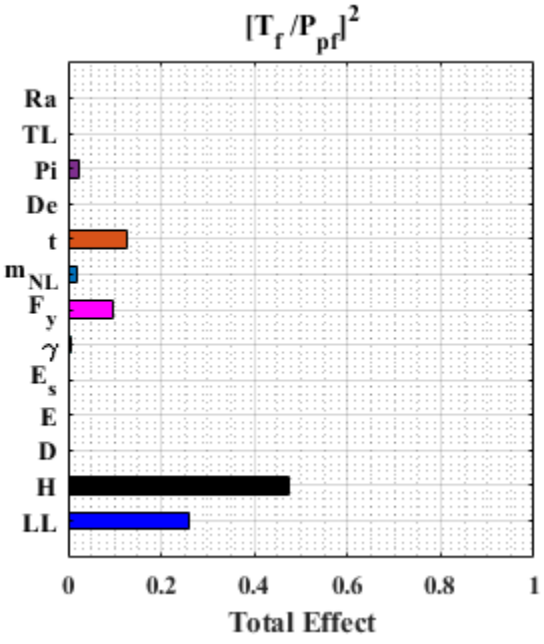

(b)

Figure 4.13. Results of Sobol method for intact buried corrugated culvert thrust

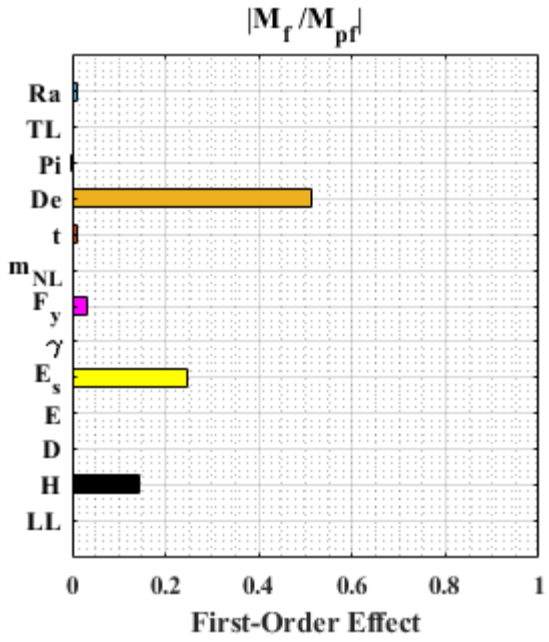

(a)

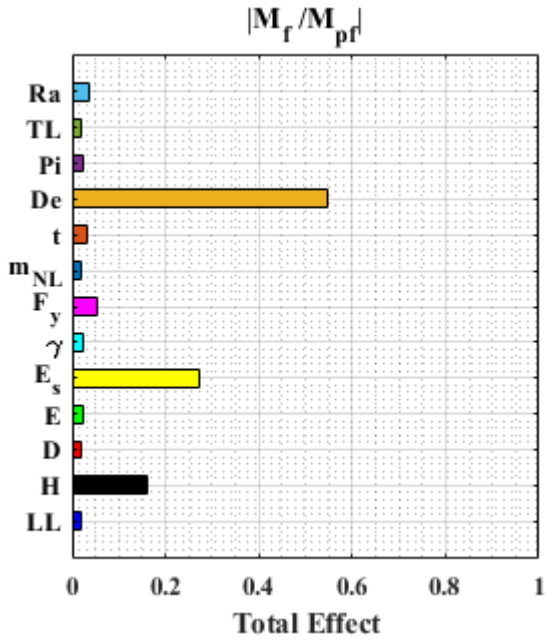

(b)

Figure 4.14. Results of Sobol method for bending moment of intact buried corrugated culvert

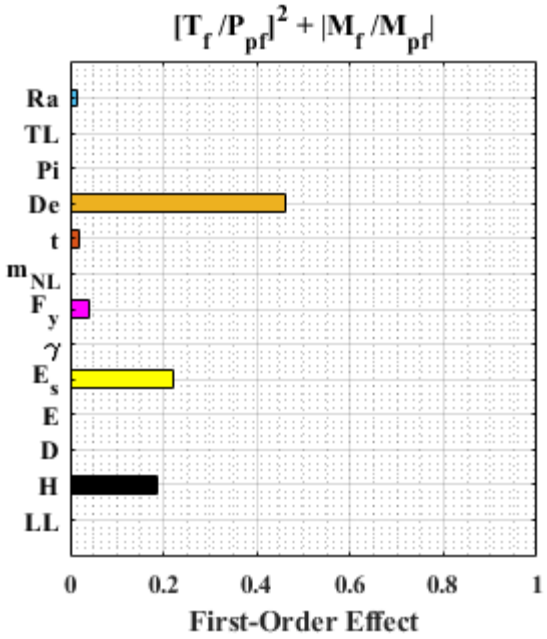

(a)

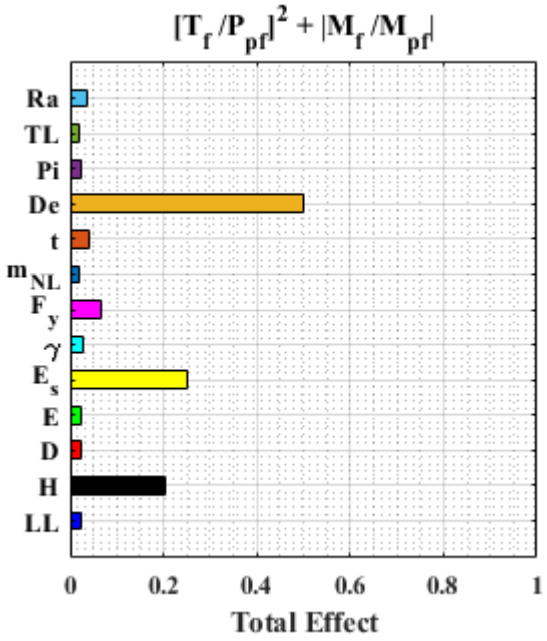

(b)

Figure 4.15. Results for Sobol method for combined effect of thrust and bending moment of intact buried corrugated culvert

4.5 Thrust coefficient of corrugated culvert buried in a shallow cover depth

Based on the global sensitivity analysis results, the behavioural character of variables with noninteraction features among them allow us to consider the effect of each influential variable (i.e., LL, H) individually on local force output using finite element simulation by keeping other variables constant. Based on the Canadian code (CSA/S6-14, 2014) and culvert diameter in this study, the maximum applied live load on buried culvert is axle no. 4 of CL-625 Truck wheel loads. Consequently, the truck wheel load (LL) remains constant for all FE analysis and effects of one variable (i.e., H) are investigated in FE analysis to define a modification coefficient for thrust to calculate local forces in the same cross section.

4.5.1 The cover depth of the buried culvert (H)

In this study, the shallow cover depth is defined as $\frac{H}{\mathrm{D}} \leq 2$ (Nakhostin et al., 2021). The minimum cover depth for culvert with 900 mm diameter is 600 mm (CSA/S6-14, 2014). Table 4.3 presents 6 different cover depths for buried corrugated culvert. The applied wheel load acting on the ground surface is based on the Canadian code (CSA/S6-14, 2014). The cover depth is the only variable parameter, and all other variables remain constant in the finite element analysis.

Figure 4.16 and Figure 4.17 present the maximum (local magnitude) moment , local force and thrust for the corrugated culvert using FEM and the closed-form equations (i.e., Equation 4.4 and Equation 4.5) for different cover depth normalized with the vertical diameter of culvert. As the applied single wheel pair loading increases to the final stage of service load, the corrugated culvert modeled with finite element method predicts the

internal local forces and moments. The maximum values of these internal forces are presented for every cover depth in these figures. The maximum bending and local force for cover 600 mm, 900 mm, and 1200 mm are located at crown of the culverts, but the location of maximum internal forces is moving from crown toward the shoulders and then springlines as cover depth increases.

The development of plastic strain at the culvert crown for the shallowest cover depth ($\frac{H}{\mathrm{D}} = \frac{6}{9}$) is observed in the numerical simulation. Finite element results indicate this yield appear at the crown because the internal local force reaches to its yield point. The culvert remains in the linear elastic phase of its material for all other models with cover depth greater than 600 mm.

Table 4.3. CSA/S6-14 (2014) single wheel pair loading for different cover depth (H)

Cover Depth (mm)	Unfactored Design Vehicle Load (kN)	Multiple Lane Loading Factor	Dynamic Load Allowance	Maximum Service Load (kN)
600	87.5	1	0.28	112
900	87.5	1	0.22	107
1200	87.5	1	0.16	102
1500	87.5	1	0.10	96
1800	87.5	1	0.10	96
2000	87.5	1	0.10	96

Over the parameter range investigated (i.e., H), Equation 4.5 provides conservative estimates of maximum bending moment response relative to the FE model predictions (Figure 4.16). The maximum local force load in the numerical modeling procedure (i.e., FEM) happens at the crown and shoulders of the culvert buried in a shallow cover depth and calculated thrust at the springlines using CSA/S6-14 is considerably different relative to the FEM predictions. The local force estimates using FEM are greater than current

practice thrust, Equation 4.4 (i.e., CSA/S6-14, 2014), for the shallow cover depths and the CSA/S6-14 results are conservative for normalized cover depth greater than 2 (Figure 4.17).

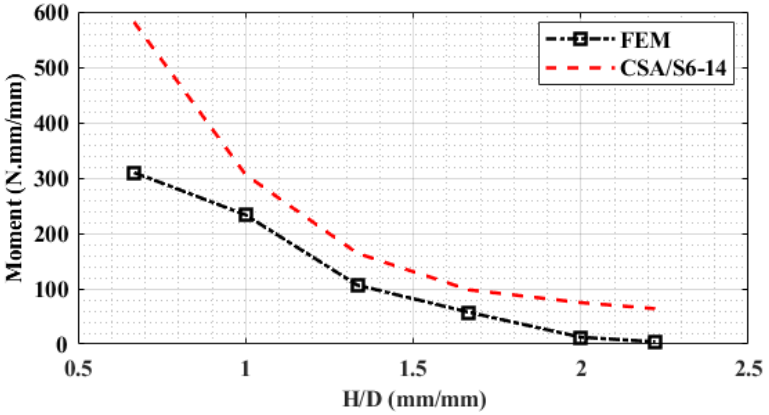

Figure 4.16. Variation in the maximum bending moment for different cover depth

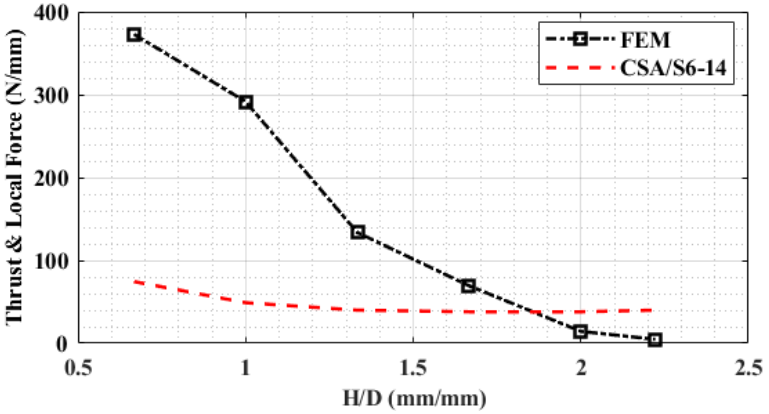

Figure 4.17. Variation in the maximum local force and thrust for different cover depth

These results indicate that the load distribution is different from the recommended approach in the Canadian code for buried corrugated culverts in a shallow cover depth and based on the investigated influential variables, cover depth (H) plays an important role in these circumstances. Consequently, the modification factor for thrust (α) is recommended based on the normalized cover depth $\left(\frac{H}{\mathrm{D}}\right)$, thrust multiplying coefficient (C_1), and thrust

power coefficient (C_2) presented in Equation 4.16 to calculate local force in the cross-section of corrugated culvert using the thrust equations presented in the Canadian code.

Equation 4.16 $$\alpha = C_1 \left(\frac{H}{D}\right)^{-C_2}$$

The shallow cover depth local force, F, due to live loads and dead loads is recommended to be calculated as follows:

Equation 4.17 $$F = \alpha T_f = \alpha \left(T_D + T_L(1 + DLA)\right)$$

To meet the CSA/S6-14 requirements, the value of C_1 and C_2 are set to 7 and 1.2, respectively. Calculated local force using the modified factor is compared with FEM results in Figure 4.18 for $1 \leq \frac{H}{D} \leq 2$. The shallowest cover depth (H/D= 600/900) experiences the development of plastic strain at the culvert crown in the numerical simulation but closed-form equations calculate responses in the linear elastic phase of material. Finite element results indicate this yield appear at the crown because the internal local force reaches to its linear elastic capacity. The culvert material remains in the linear elastic phase for models with greater cover depths. The multiplied thrust for calculating local force is presented for $H/D \geq 1$ since all responses remain in the linear elastic phase and are compatible with the used equations.

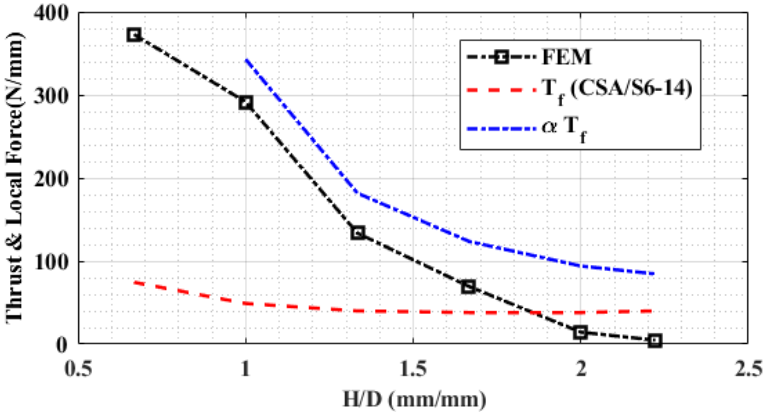

Figure 4.18. Modified force values for different cover depths

4.6 Sensitivity and Probabilistic Analysis considering the recommended thrust coefficients

Global Sensitivity Analysis is conducted for identifying the important factors in the proposed equation. Sobol and Morris methods are used for computing the quantitative indices for the proposed equation ($Y = \left[\frac{\alpha T_f}{P_{pf}}\right]^2 + \left|\frac{M_f}{M_{pf}}\right|$) with $k = 15$ independent variables introduced in Table 4.2 and local force coefficients, C_1, and C_2. These coefficients, C_1 and C_2, are normally distributed with mean equal to 7 and 1.2 respectively and coefficient of variation equal to 0.1. The results of the global sensitivity analysis for pure local force perpendicular to the cross-section, pure bending moment, and combined force and bending are presented in Figure 4.19 and Figure 4.20 for Morris method and Figure 4.21, Figure 4.22, and Figure 4.23 for Sobol method.

As shown in Figure 4.20 and Figure 4.23, there are limited influential variables for combined effects of local force and moment, with almost monotonic behaviour which are located below the line $\frac{\sigma}{\mu^*} = 1$.

The figures for Sobol method, Figure 4.21, Figure 4.22, and Figure 4.23, show the first-order and total effect indices are similar, and the results indicate the influential variables have additive or linear features with no or very limit interaction.

The effects of introduced coefficients are considered in these results which indicate the local force is the more significant internal force in shallow buried corrugated steel culvert (compare Figure 4.21a and Figure 4.22 for Morris and compare Figure 4.21 and Figure 4.23 for Sobol).

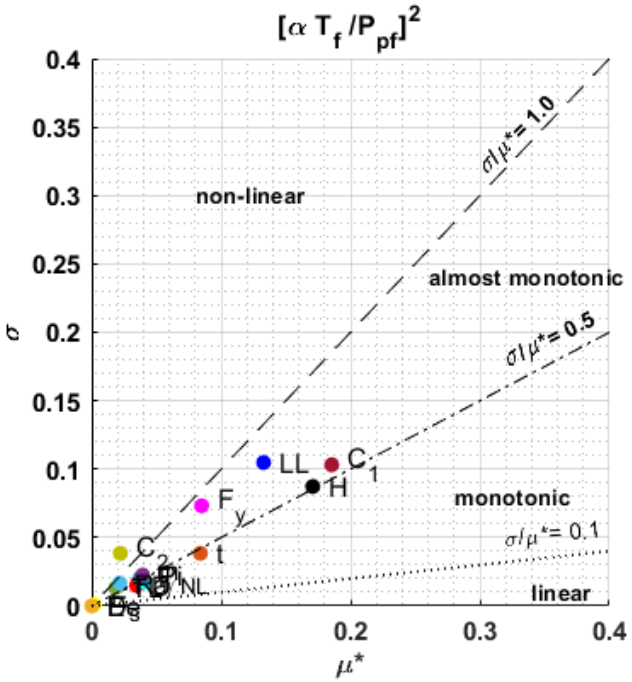

(a)

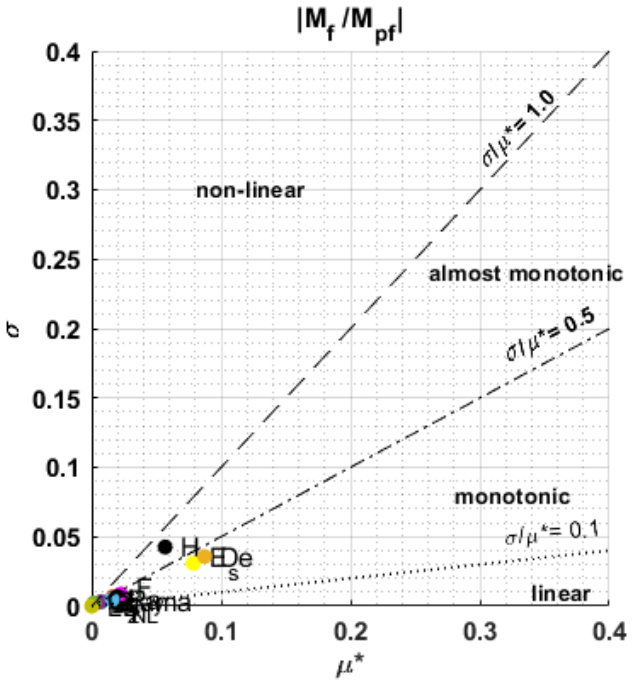

(b)

Figure 4.19. Estimated absolute average (μ_i^*) and standard deviation (σ_i) of the first-order EE for a) modified thrust (local force), b) bending moment

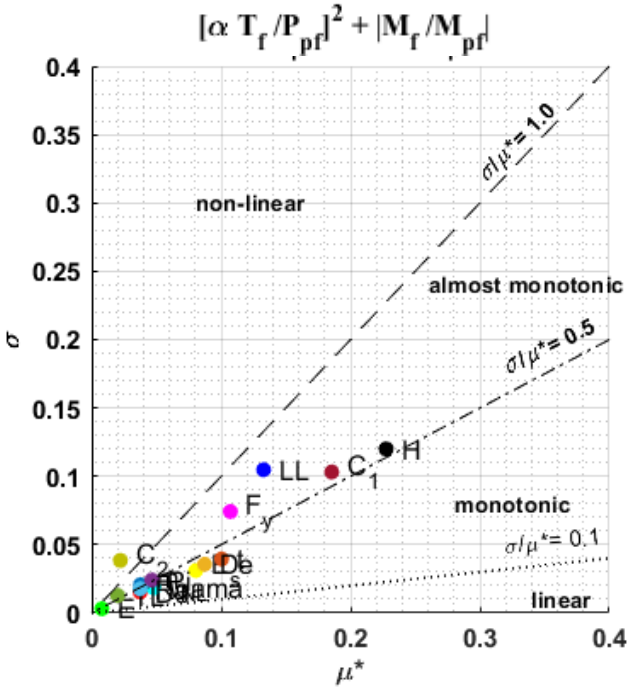

Figure 4.20. Estimated absolute average (μ_i^*) and standard deviation (σ_i) of the first-order EE for combined modified thrust (local force) and bending moment

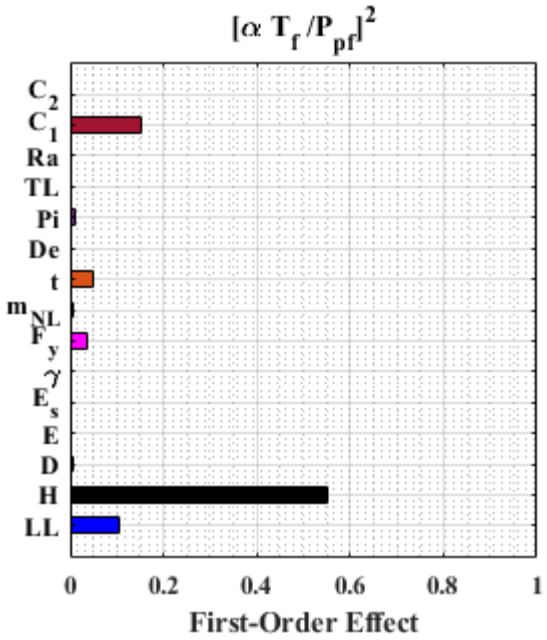

(a)

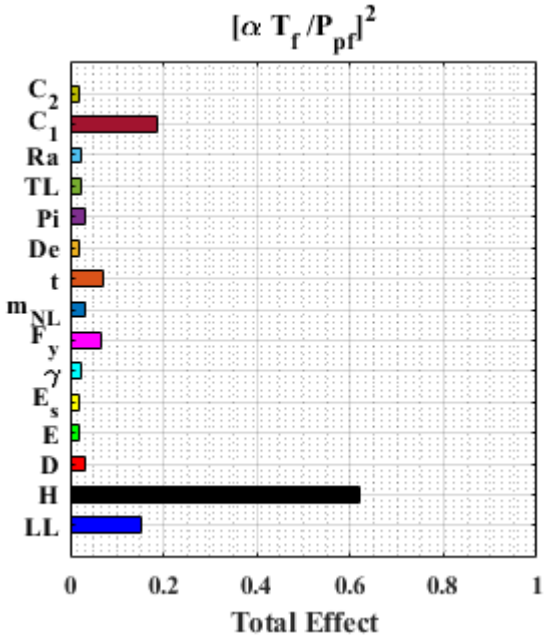

(b)

Figure 4.21. Results for S_i and S_{Ti} with Sobol method for pure local force $Y = \left[\frac{\alpha T_f}{P_{pf}}\right]^2$

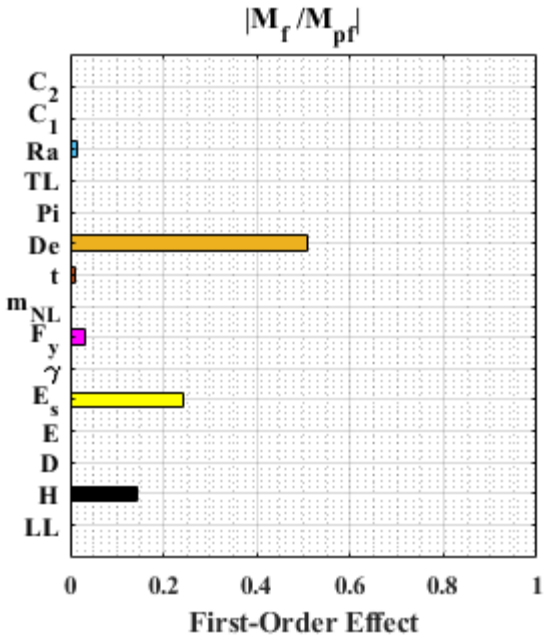

(a)

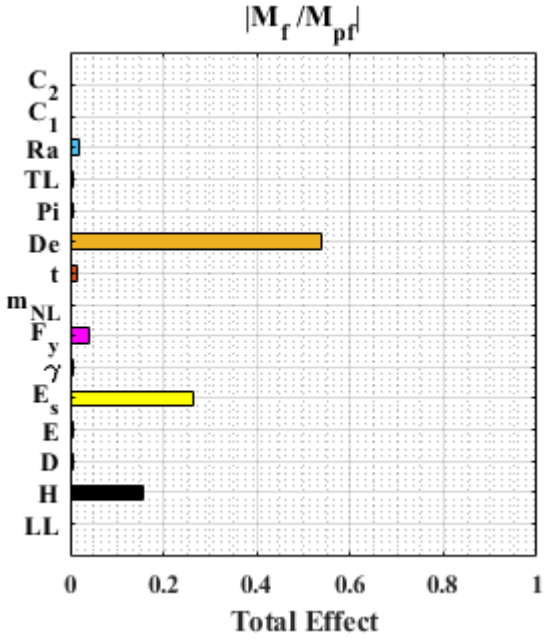

(b)

Figure 4.22. Results for S_i and S_{Ti} with Sobol method for pure bending moment $Y = \left|\frac{M_f}{M_{pf}}\right|$

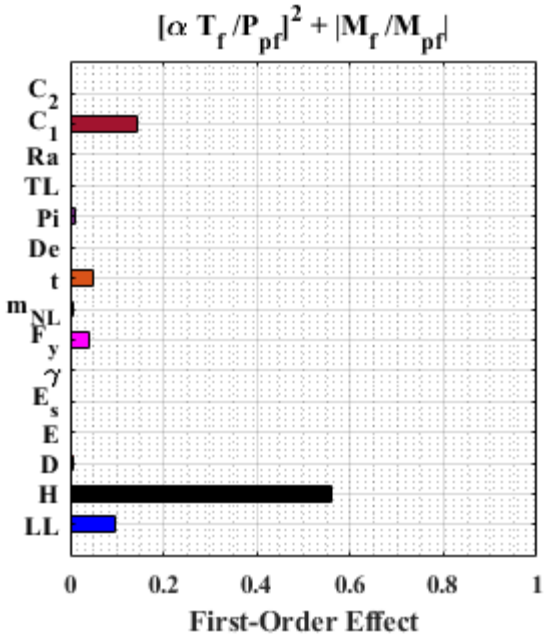

(a)

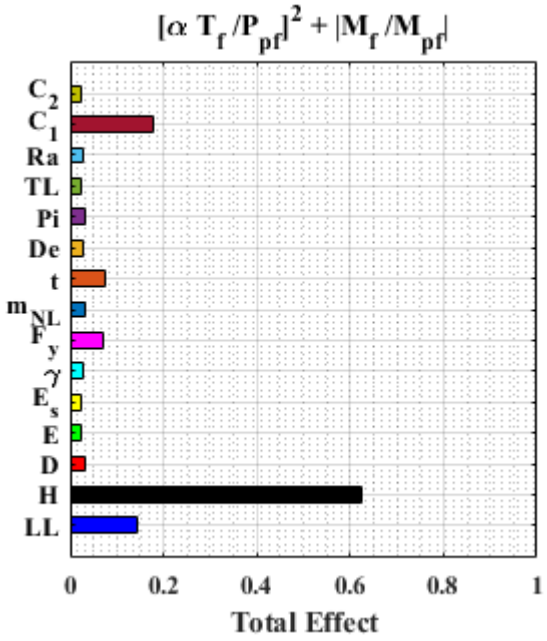

(b)

Figure 4.23. Results for S_i and S_{Ti} with Sobol method for combined section force and bending moment $Y = \left[\frac{\alpha\, T_f}{P_{pf}}\right]^2 + \left|\frac{M_f}{M_{pf}}\right|$

The Probabilistic analysis using the first-order second moment reliability method is conducted to investigate the effect of the introduced coefficients on the reliability index. For the probability analysis, the limit state function is defined as $Z = 1 - \left(\left[\frac{\alpha\, T_f}{P_{pf}}\right]^2 + \left|\frac{M_f}{M_{pf}}\right|\right)$ which defines a safe region when Z > 0 and a failure region when Z < 0. The limit state function variables defined including the wheel load, cover depth, two thrust coefficients, steel yield tensile stress, and culvert wall thickness (i.e., LL, H, F_{y}, t, C_1, and C_2). These influential variables take the values of mean and CV given in Table 4.2. The non-influential parameters are constant in probability analysis take their mean values. The coefficient of variation for C_1, and C_2 are equal to 0.1 and in the probability sensitivity analysis their coefficient of variations is varied from 0.05 to 0.5 in step of 0.05.

The reliability index (β) is calculated using Equation 4.18.

Equation 4.18 $\boldsymbol{\beta = \bar{z}/\sigma_z}$

where $\bar{z}$ is the mean value and σ_z is the standard deviation of the limit state function (Z) (Rackwitz and Flessler, 1978, Wang and Grandhi, 1996, Grandhi and Wang, 1999).

Figure 4.24 shows the result for two variables, C_1 and C_2 with different CV. The results indicate that the reliability index shows high sensitivity to C_1 and this variable with high CV (i.e., CV=0.5) has a significant effect on the reliability index. The results in Figure 4.24 show the variable C_2 does not have much influence on the reliability index and the probability of failure which is almost constant, and the result is consistent with the global sensitivity analysis result.

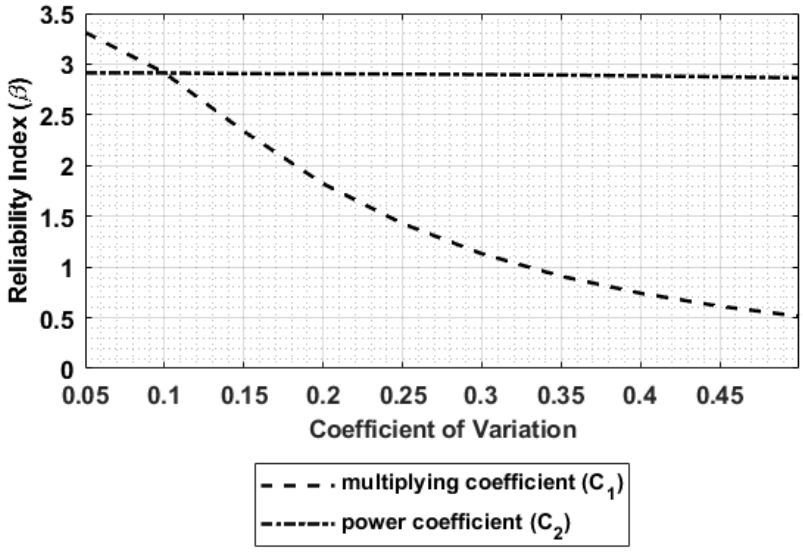

Figure 4.24. Reliability index vs coefficient of variation for C_1 and C_2

4.7 Summary and Conclusions

The continuum finite element method was used to examine the mechanical response of a buried corrugated steel culvert subject to service loads, and the results were verified with third-party full-scale tests. The finite element analysis indicate that the corrugated feature of culvert profile causes a specific distribution for strain and internal forces which they have a sign change in crest and trough of the corrugated profile. These results indicate that the average strain response cannot account for the local peak strain response. Consequently, the average thrust calculated using closed-form equations does not account for local variations in the culvert response and underestimates the peak local force in the section. The global sensitivity analyses have been conducted to identify influential variables in the thrust and bending moment calculations for the buried corrugated steel culvert. The results achieved by Sobol and Morris method considering the limit state function defined using the Canadian code indicates that there are two influential variables,

the truck load (LL), and the cover depth of the buried culvert (H), which are additive model with no interaction among the variables. The complementary finite element analysis was conducted to modify the thrust for calculating local force in the corrugated profile for buried culverts in a shallow cover depth. Consequently, the thrust modification factor proposed for buried corrugated culverts in shallow cover depths with two defined coefficients. The defined values are for the specific case studied in this analysis, and these values could be different for other backfills. Probabilistic analysis results indicate the variability of thrust multiplying coefficient (C_1) affects the reliability index significantly and it needs to be defined for every backfill condition. The thrust power coefficient (C_2) can be fixed in a constant value which is a non-influential variable.

References

AASHTO, M. (2020). Standard Specification for Corrugated Steel Pipe, Metallic-Coated for Sewers and Drains. American Association of State and Highway Transportation Officials.

Ahammed, M. and Melchers, R. (1997). "Probabilistic analysis of underground pipelines subject to combined stresses and corrosion." Engineering structures, 19(12), 988–994.

ASTM A760/A760M-15, (2020). Standard Specification for Corrugated Steel Pipe, Metallic-Coated for Sewers and Drains.

ASTM, D. (2011). 2487, 2006. Standard practice for classification of soils for engineering purposes (Unified Soil Classification System). Book of Standards, 4.

Bakht, B. (1981). "Soil-steel structure response to live loads." *Journal of the Geotechnical Engineering Division*, 107(6), 779–798.

Campolongo, F., Cariboni, J., and Saltelli, A. (2007). "An effective screening design for sensitivity analysis of large models." *Environmental modelling & software*, 22(10), 1509–1518.

CAN/CSA-G401-14 (2014). Corrugated steel pipe products Canadian Standard Association. Mississauga, ON, Canada: Canadian Standard Association.

Choi, D.-H., Kim, G.-N., and Byrne, P. M. (2004). "Evaluation of moment equation in the 2000 canadian highway bridge design code for soil–metal arch structures." *Canadian journal of civil engineering*, 31(2), 281–291.

Corrugated Steel Plate Institute (2010). Handbook of steel drainage and highway construction products. Handbook of steel drainage and highway construction products. Cambridge, Ontario, Canada: Corrugated Steel Pipe Institute.

CSA G401-14, (2014). National Standard of Canada, Corrugated Steel Pipe Products.

CSA/S6-14, (2014). Canadian Highway Bridge Design (CAN/CSA S6-14)(pp. 875). Ontario, Canada: Canadian Standard Association Group.

Duncan, J. 24 (1978). "Soil-culvert interaction method for design of metal culverts." *Transportation research record*, (678).

Elshimi, T., Mak, A., Brachman, R., and Moore, I. (2011). "Behaviour of a deep-corrugated largespan box culvert during backfilling." *Pan-American Conference on Teaching and Learning of Geotechnical Engineering*, Toronto, Canada.

Elshimi, T. M., Brachman, R. W., and Moore, I. D. (2014). "Effect of truck position and multiple truck loading on response of long-span metal culverts." *Canadian Geotechnical Journal*, 51(2), 196–207.

Elshimi, T. M. and Moore, I. D. (2013). "Modeling the effects of backfilling and soil compaction beside shallow buried pipes." *Journal of Pipeline Systems Engineering and Practice*, 4(4), 04013004.

Fenton, G. A., Griffiths, D. V., et al. (2008). *Risk assessment in geotechnical engineering*, Vol. 1. John Wiley & Sons New York.

Grandhi, R. V. and Wang, L. (1999). "Structural reliability analysis and optimization: Use of approximations." *Wright State University, Dayton*.

Homma, T. and Saltelli, A. (1996). "Importance measures in global sensitivity analysis of nonlinear models." *Reliability Engineering & System Safety*, 52(1), 1–17.

Iman, R. L. and Hora, S. C. (1990). "A robust measure of uncertainty importance for use in fault tree system analysis." *Risk analysis*, 10(3), 401–406.

Mai, V. T. (2013). "Assessment of deteriorated corrugated steel culverts." Ph.D. thesis, Queen's University, 233p.

Marston, A. and Anderson, A. (1913). *The theory of loads on pipe in ditches and tests of cement and clay drain tile and sewer pipe*, Vol. 31. Iowa Eng. Experiment Station.

McGrath, T. J., Selig, E. T., Webb, M. C., Zoladz, G. V., et al. (1999). "Pipe interaction with the backfill envelope." *Report no.*, University of Massachusetts at Amherst. Transportation Center.

Melchers, R. E. and Beck, A. T. (2018). *Structural reliability analysis and prediction*. John wiley & sons.

Menberg, K., Heo, Y., and Choudhary, R. (2016). “Sensitivity analysis methods for building energy models: Comparing computational costs and extractable information.” *Energy and Buildings*, 133, 433–445.

Menetrey, P. andWillam, K. (1995). “Triaxial failure criterion for concrete and its generalization.” *Structural Journal*, 92(3), 311–318.

Moore, I. D., Hoult, N. A., et al. (2014). “Performance of two-dimensional analysis: Deteriorated metal culverts under surface live load.” *Tunnelling and underground space technology*, 42, 152–160.

Morris, M. D. (1991). “Factorial sampling plans for preliminary computational experiments.” *Technometrics*, 33(2), 161–174.

Nakhostin, E., Kenny, S., and Sivathayalan, S. (2019). “Buried corrugated steel culvert failure mechanisms due to environmental deteriorations.” *International Conference on Sustainable Infrastructure 2019: Leading ResilientCommunities through the 21stCentury*,American Society of Civil Engineers Reston, VA, 29–40.

Nakhostin, E., Kenny, S., and Sivathayalan, S. (2021). “Numerical performance assessment of buried corrugated metal culvert subject to service load conditions.” *Canadian Journal of Civil Engineering*, 48(2), 99–114.

Rackwitz, R. and Flessler, B. (1978). “Structural reliability under combined random load sequences.” *Computers & Structures*, 9(5), 489–494.

Regier, C. (2015). “Investigation of the failure mechanisms of intact and deteriorated culverts.” Ph.D. thesis, Queen’s University. 147p.

Saltelli,A. (2002). “Making best use ofmodel evaluations to compute sensitivity indices. ”*Computerphysics communications*, 145(2), 280–297.

Saltelli, A., Andres, T., and Homma, T. (1993). “Sensitivity analysis of model output: an investigation of new techniques.” *Computational statistics & data analysis*, 15(2), 211–238.

Saltelli, A., Annoni, P., Azzini, I., Campolongo, F., Ratto, M., and Tarantola, S. (2010). “Variance based sensitivity analysis of model output. design and estimator for the total sensitivity index.”*Computer physics communications*, 181(2), 259–270.

Saltelli, A., Ratto, M., Andres, T., Campolongo, F., Cariboni, J., Gatelli, D., Saisana, M., and Tarantola, S. (2008). *Global sensitivity analysis: the primer*. John Wiley & Sons.

Saltelli, A., Tarantola, S., Campolongo, F., and Ratto, M. (2004). *Sensitivity analysis in practice: a guide to assessing scientific models*, Vol. 1. Wiley Online Library.

Sanchez, D. G., Lacarrière, B., Musy, M., and Bourges, B. (2014). “Application of sensitivity analysis in building energy simulations: Combining first-and second-order elementary effects methods.” *Energy and Buildings*, 68, 741–750.

Scarino, J. H. (2003). “Reappraisal of marston’s formula.” *Journal of transportation engineering*, 129(6), 703–712.

Simpson, B., Hoult, N. A., and Moore, I. D. (2015). “Distributed sensing of circumferential strain using fiber optics during full-scale buried pipe experiments.” *Journal of Pipeline Systems Engineering and Practice*, 6(4), 04015002.

Simpson, B., Moore, I. D., and Hoult, N. A. (2016). “Experimental investigation of rehabilitated steel culvert performance under static surface loading.” *Journal of Geotechnical and Geoenvironmental Engineering*, 142(2), 04015076.

Simulia, D. (2013). ABAQUS 6.13 User’s manual. Dassault Systems, Providence, RI.

Sobol’, I. M. (2005). “Global sensitivity indices for the investigation of nonlinear mathematical models.” *Matematicheskoe modelirovanie*, 17(9), 43–52.

Spangler, M., Hennessy, R., and Barber, E. (1947). “A method of computing live loads transmitted to underground conduits.” *Highway Research Board Proceedings*, Vol. 26.

Spangler, M. G. (1964). “Pipeline crossings under railroads and highways.” *Journal-American Water Works Association*, 56(8), 1029–1046.

Spangler, M. G. and Shafer, G. (1938). “The structural design of flexible pipe culverts.” *Highway Research Board Proceedings*, Vol. 17.

Wang, L. and Grandhi, R. V. (1996). “Safety index calculation using intervening variables for structural reliability analysis.” *Computers & structures*, 59(6), 1139–1148.

Warman, D. J., Hart, J. D., and Francini, R. B. (2009). “Development of a pipeline surface loading screening process & assessment of surface load dispersing methods.” *Canadian Energy Pipeline Association, Worthington, OH, Report No*.

Chapter 5: The Effects of Wall-Thickness Loss due to Corrosion and Influential Aspect of This Deterioration on Shallow Corrugated Steel Culverts Responses

The loss of structural strength of the CSC buried with a shallow cover depth with depth of cover less than 2 m is investigated in this chapter. Shallow cover influences transfer in the load distribution and magnitude of culvert internal responses. The CSC is also influenced by general or uniform corrosion through reduction of the CSC wall thickness. The effect of wall loss on the CSC mechanical behaviour is investigated using finite element simulations, and numerical sensitivity and probability analysis. The finite element simulation was verified using the circumferential bending moment in the full-scale test conducted by Regier (2015). The applied backfill soil and truck loads are based on the Canadian Highway Bridge Design Code (CSA/S6-14, 2014). A nonlinear corrosion model as a function of time is used to present the loss of steel wall thickness. The internal forces of culvert due to the applied loads proposed in the Canadian code and closed-form equations are modified to apply corrosion deterioration effects and a limit state function developed for the culvert/soil system. The Finite Element analysis conducted to study the effect of corrosion variables (i.e., corrosion angle and location) that are not considered in the closed-form equations. The Global Sensitivity Analysis, (e.g., Sobol and Morris methods), is used for performing the quantitative sensitivity analysis to identify the influential variables for the corroded culverts up to 100 years exposure time. The identified

influential variables are used in First-Order Second-Moment probability analysis to predict probability of failure for damaged culverts in their service lives.

5.1 FEM modeling and verification procedures of intact buried culvert

Continuum finite element methods are used to examine the mechanical response of a buried metal culvert subject to service loads, and this numerical simulation is verified using full-scale physical modeling data conducted by Regier (2015). As shown in Figure 3.1, the CSC-soil model explicitly simulated the nominal wall thickness (1.60 mm), depth (12.7 mm) and pitch (67.7 mm) of the corrugated culvert. These selected parameters, based on physical modelling studies for a culvert with a cross-sectional area of 1.51 mm^2, a moment of inertia of 28.4 mm^4, and section modulus 4.02 mm^3 per unit length (Corrugated Steel Pipe Institute, 2010), are used to verify the finite element modeling results. The selected analysis parameters are based on an assessment of the knowledge gap in current practice and the expected nonlinear behaviour across the parameter range. The CSC constitutive behaviour was defined using J_2 plasticity theory with the von Mises yield criterion and combined hardening model (Hibbitt et al., 2013).

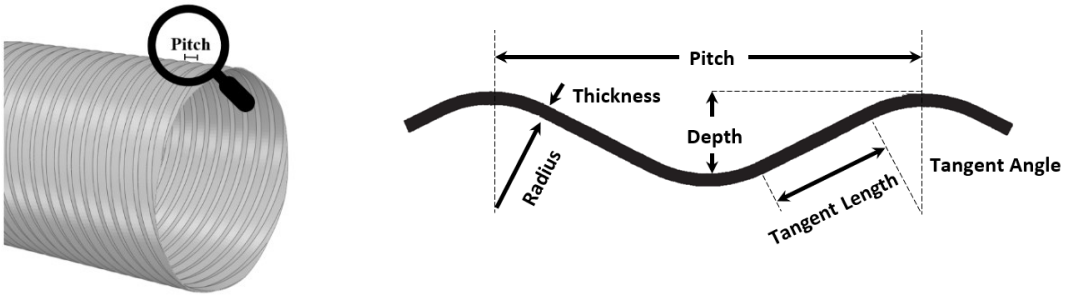

Figure 5.1. The variables of the corrugated steel culvert profile

In the finite element simulation, the soil mechanical behaviour is defined as elastic-plastic with the Mohr-Coulomb yield criterion (Menetrey and Willam, 1995, Simulia,

2013). The soil parameters are based on experimental studies (McGrath et al., 1999, Elshimi et al., 2011, Elshimi and Moore, 2013), which are used to calibrate the numerical modeling procedures. For the experimental studies, the backfill could be characterized as poorly graded granular soil (GP-SP) using the unified classification system and the bedding and the backfill soil were compacted to 95% and 90% standard proctor respectively (ASTM, 2011). The soil type and its domain in FEM is consistent with the full-scale lab test conducted at Queen's University, Kingston. The simulated standard wheel pair was imposed on the ground surface and positioned over the culvert crown and was applied using the wheel pad (250 mm x 600 mm in plan) based on CSA/S6-14 for the service load conditions. Figure 5.2 shows the soil domain for the verified model that was extended to 8000 mm wide, 4400 mm long, and 2400 mm depth (with 900 mm cover).

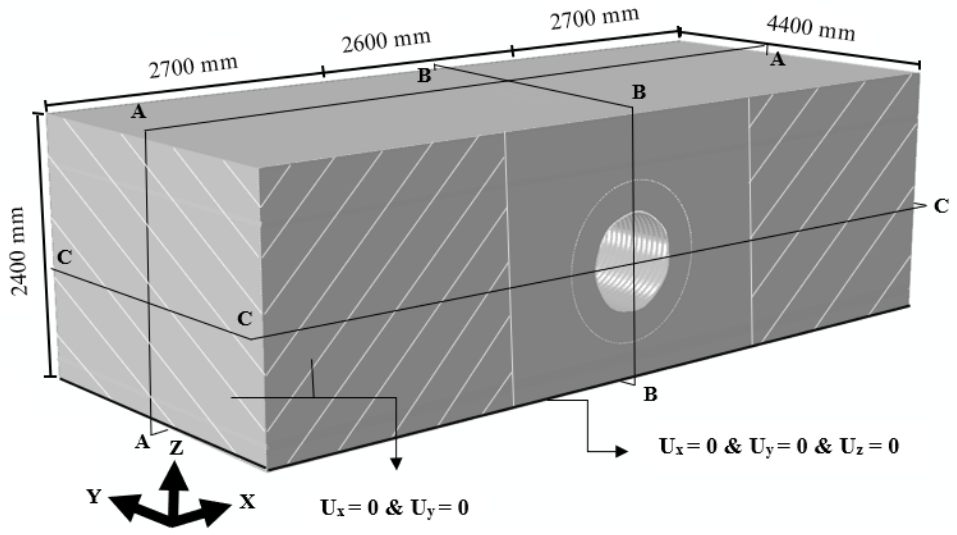

Figure 5.2. The model geometry for the Finite Element Analysis presenting soil backfill domain and kinematic (natural) boundary conditions

Based on the experimental test data, the intact (non-deteriorated) corrugated culvert was subjected to the single wheel pair at 900 mm of cover depth and he internal force

results (i.e., bending moment) were presented at 71 kN under the single wheel pair (Regier, 2015). The defined spiral path as shown in Figure 5.3 is located at the mid-length of the culvert and is consistent with the laboratory test that is used to verify FEM accuracy. Figure 5.4 shows the bending moments for the finite element simulation and full-scale test. The small discrepancy between the numerical simulation and laboratory test results is due to trench backfilling and compaction activities. These processes are not applied in the numerical simulation. Further details on the verification procedures are presented in chapter 4.

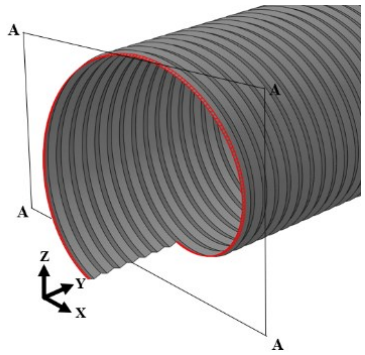

Figure 5.3. Defined spiral trough path, at the culvert mid-length, for sampling the FEM data

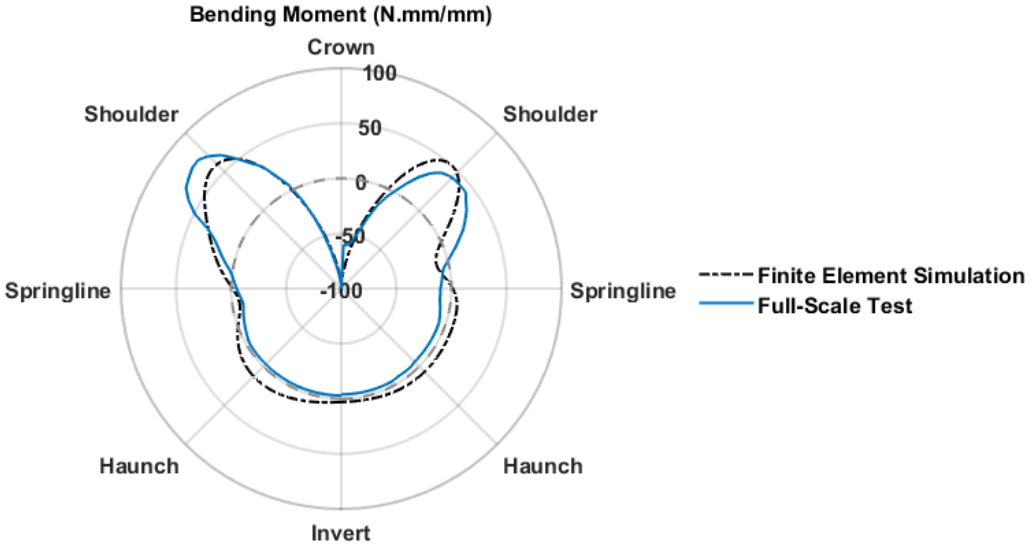

Figure 5.4. spiral distribution of section bending moment (N.mm/mm) with 71 kN single wheel pair loading

5.2 Closed-form equations

This section is presented in two parts to discuss the internal forces of intact corrugated culvert, and the time dependent corrosion model. The closed-form equations based on the Canadian code (CSA/S6-14, 2014) are used as primary equations, and the thrust equation is modified to calculate local forces for corrugated culverts buried in shallow cover depth as detailed in chapter 4. The original thickness of the culvert is modified using the closed-form equation as time dependent corrosion model to apply corrosion deterioration to the intact culvert/soil formula.

5.2.1 Corrugated culvert internal forces

The buried corrugated steel culvert subjected to the external fill load and traffic loads is investigated using the recommended closed-form equations. The internal applied forces in the culvert is considered due to the external loads and the Canadian code (CSA/S6-14, 2014) is used to calculate the applied thrust and bending moments. The Canadian code recommends using thrust equation as internal force in the shallow corrugated profiles and does not consider bending moment effects in the internal forces. This research study considers the effect of bending moment and thrust for this case in both analytical and numerical simulation responses.

The maximum culvert section moment, due to applied fill and truck loads per unit length (M_f), is calculated as follows:

Equation 5.1. $$\boldsymbol{M_f = |M_1 + M_D| + M_L(1 + DLA)}$$

where M_1 is moment in a soil-metal structure resulting from backfill load to the crown level, M_D is the moment in the wall of a soil-metal structure due to a dead load, and

M_L is the moment in the wall of a soil-metal structure due to live load and the dynamic load allowance (DLA) are calculated based on the Canadian Highway Bridge Design Code.

The recommended equations in the Canadian code calculate the maximum values of the bending moment and thrust in the culvert. Chapter 3 of this manuscript, the code and published paper provide further details and more discussion about the buried corrugated steel culvert (CSA/S6-14, 2014, Nakhostin et al., 2021).

The proposed modification factor for calculating CSC local force buried at a shallow cover depth is used in this study. The modification factor for thrust (α) is recommended based on the normalized cover depth $\left(\frac{H}{D}\right)$, thrust multiplying coefficient (C_1), and thrust power coefficient (C_2) presented in Equation 5.2.

Equation 5.2. $$\boldsymbol{\alpha = C_1 \left(\frac{H}{D_v}\right)^{-C_2}}$$

The shallow cover depth local force, F, due to live loads and dead loads is calculated as:

Equation 5.3 $$\boldsymbol{F = \alpha\,(T_D + T_L(1 + DLA))}$$

where T_D and T_L are dead load and live load thrusts. To meet the CSA/S6-14 requirements, the value of C_1 and C_2 are set to 7 and 1.2 respectively. For more discussion about the internal forces of the buried corrugated steel culvert see chapter 4.

For culvert-soil structures, the combined effects of the bending moment and local force are considered in this study and calculated as follows:

Equation 5.4 $$\boldsymbol{\left[\frac{\alpha T_f}{P_{pf}}\right]^2 + \left|\frac{M_f}{M_{pf}}\right| \leq 1}$$

where P_{pf} is compressive strength of a corrugated metal section and M_{pf} is moment capacity of a corrugated metal section (CSA/S6-14, 2014).

5.2.2 Culvert corrosion

Corrosion in buried culverts is defined as a deterioration and loss of steel material and its critical properties due to chemical, electrochemical and other reactions. The evidence proves that the corrosion rate in steel is high and nonlinear. It decreases with time and gradually becomes constant eventually. The loss of wall thickness due to corrosion is modeled empirically by a power law (Kucera and Mattsson, 1987) in the form of

Equation 5.5 $$P = k\,T^n$$

where P is loss of wall thickness, k is a multiplying constant, T is the exposure time, and n is an exponential constant. The recommended values for two constants, k and n, in the wall thickness loss equation are based on analytical and experimental investigations. These two parameters are determined for different underground corrosion cases and the regression analysis method was used to determine these constant values (Schwerdtfeger, 1969, Ahammed and Melchers, 1997, De la Fuente et al., 2011). Figure 5.5 shows the corrosion model used in this study with mean value for k and n equal to 0.066 and 0.53, respectively.

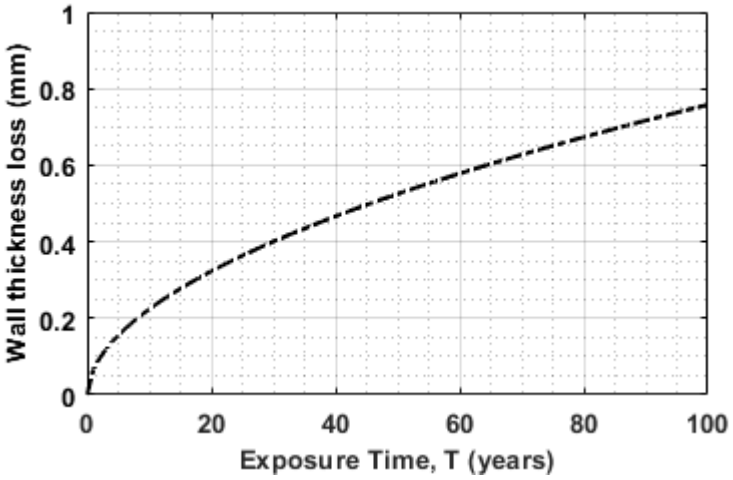

Figure 5.5. wall thickness loss versus exposure time for k = 0.066 and n = 0.53 (Equation 5.5**)**

5.3 Sensitivity analysis

Sensitivity analysis orders the importance of the input factors in determining the variation in the output. Two types of local and global sensitivity analysis are conducted in this study. For local sensitivity analysis, the finite element model of buried corrugated culvert is simulated, and corrosion deteriorations is applied in the model. This study investigates two individual variables of corrosion (i.e., corrosion angle and location) which is not considered in closed-form equations and their effect on the responses. Closed-form equations are used to conduct global sensitivity analysis and this method provides sensitivity measures for each input factor to identify the influential variables.

5.3.1 Finite Element simulation and analyses

The introduced closed-form equations calculate the maximum internal forces in culverts, and primary experimental and numerical simulations indicate that it happens at the crown for buried culverts in shallow cover depth (Nakhostin et al., 2021). Corrosion deterioration can happen in any location of culverts with different corrosion angles. 3D continuum finite element modeling procedures are developed to examine the mechanical response of a CSC, with deterioration associated with the thickness loss because of corrosion considering two variables (i.e., location and angle of corrosion). The effect of corrosion is simulated as a uniform wall thickness reduction at five locations (i.e., invert, haunch, springline, shoulder, and crown) on the CSC perimeter and imposed as a symmetric distribution. The effect of this deterioration is idealized as a uniform wall thickness loss along an arc length with 52% remaining wall thickness of culvert, subtended by the angle, θ, equal to 90 deg. in each arc as shown in Figure 5.6.

For buried CSC in a shallow cover depth with cover less than 1200 mm, maximum local force and moment are located in the crown and for deeper cases this location is changing from crown to shoulder and springline because of the changes in the cover and surrounding soil supports. In this study, the cover depth is 900 mm, and this is considered as a shallow cover depth ($H/D = 1$), and the corrosion location is fixed at crown and its angle, θ, is changed to different values (i.e., 15, 30, 60, 90, and 120 degrees) to study the effect of corrosion angle as second corrosion variable in FE analysis. The remaining wall thickness of culvert in the corroded models remains constant equal to 52% of intact wall thickness which is equal to 100-year exposure time based on the defined values in Table 5.1.

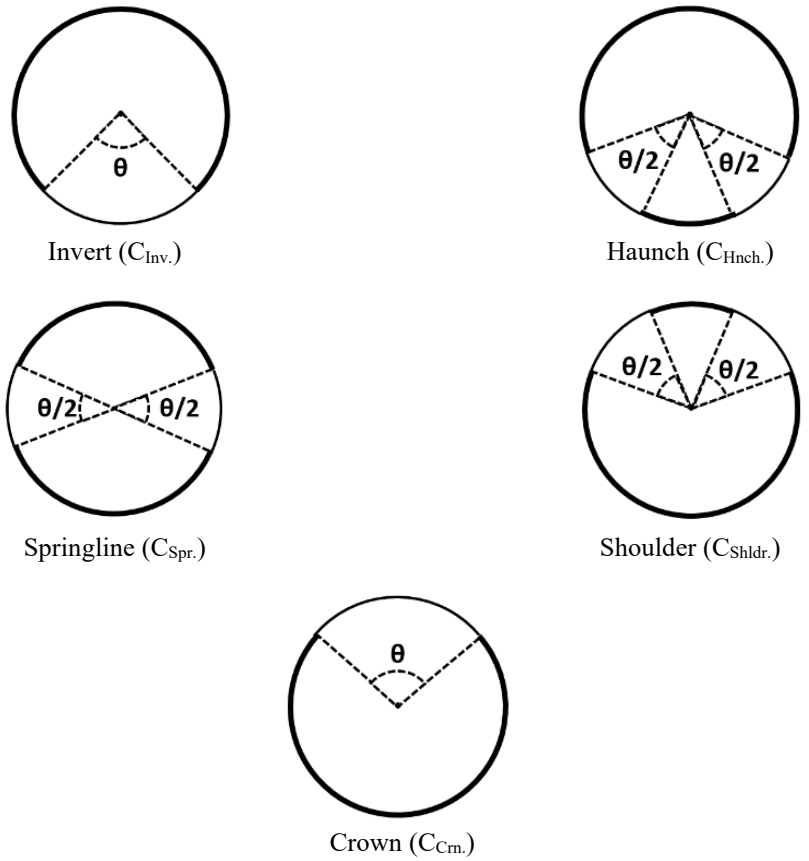

Invert ($C_{Inv.}$) Haunch ($C_{Hnch.}$)

Springline ($C_{Spr.}$) Shoulder ($C_{Shldr.}$)

Crown ($C_{Crn.}$)

Figure 5.6. Schematic illustration of wall thickness corrosion at different location with $\theta = 90°$

Table 5.1 Random variables of the input parameters for GSA

Variable Indices	Variable	Description	Mean	CV	References
1	LL	wheel load (N)	87500	0.10	(CSA/S6-14, 2014; Ahammed and Melchers, 1997)
2	H	cover depth (mm)	900	0.10	(Melchers and Beck, 2018)
3	D	culvert diameter (mm)	900	0.014	(ASTM A760/A760M-15, 2020)
4	E	elastic modulus of culvert (MPa)	2e5	0.033	(Ahammed and Melchers, 1997)
5	E_s	elastic modulus of soil (Mpa)	63	0.27	(Melchers and Beck, 2018; Regier, 2015)
6	γ	unit weight of soil (N/mm^3)	2.1e-5	0.10	(Ahammed and Melchers, 1997)
7	Fy	yield tensile stress (Mpa)	230	0.05	(Ahammed and Melchers, 1997)
8	n	exponential constant for corrosion model	0.53	0.26	(Schwerdtfeger, 1969, Ahammed and Melchers, 1997, De la Fuente et al., 2011
9	k	multiplying constant for corrosion model	0.066	0.36	(Schwerdtfeger, 1969, Ahammed and Melchers, 1997, De la Fuente et al., 2011)
10	m_{NL}	modification factor for multi lane loading	0.9	0.028	(CSA/S6-14, 2014)
11	t	design thickness of culvert wall (mm)	1.6	0.056	(CSA G401-14, 2014; Corrugated Steel Plate Institute, 2010)
12	De	depth of corrugation (mm)	12.7	0.025	(ASTM A760/A760M-15, 2020; CSA G401-14, 2014)
13	Pi	pitch of corrugation (mm)	67.7	0.026	(ASTM A760/A760M-15, 2020; CSA G401-14, 2014)
14	TL	tangent length of culvert profile (mm)	19.58	0.02	(ASTM A760/A760M-15, 2020; CSA G401-14, 2014)
15	Ra	radius of culvert profile (mm)	17.46	0.026	(ASTM A760/A760M-15, 2020; CSA G401-14, 2014)
16	C_1	thrust multiplying coefficient	7	0.1	(Ahammed and Melchers, 1997)
17	C_2	thrust power coefficient	1.2	0.1	(Ahammed and Melchers, 1997)

5.3.2 Global sensitivity analysis, variance-based sensitivity analysis

Table 5.1 represents input variables and their mean value and coefficient of variation (CV) for each variable with a normal distribution. The CV is the ratio of the standard deviation to the mean value. These values are obtained from the literature or selected based on practice with engineering judgements (Ahammed and Melchers, 1997, Corrugated Steel Pipe Institute, 2010, CSA/S6-14, 2014, CAN/CSA-G401-14, 2014, Regier, 2015, Melchers and Beck, 2018, AASHTO, 2020, ASTM A760/A760M-15, 2020). The normal distribution range is from -∞ to +∞ and for buried culverts negative values for most variables like burial depth, pipe diameter, or elastic modulus do not have a physical meaning. 1% of the distribution in each tail of the standard domain has been cut to get a reasonable domain for each input factor after transferring them to the input variable domain.

Sensitivity analysis method is an effective method for identifying the influential factors in the model. The Morris and Sobol Methods have been used for computing the indices for the buried corrugated steel culvert with k ($k = 17$) independent variables introduced in Table 5.1.

The EE sampling method is used in Morris method where k, independent variables vary in the k-dimensional unit cube across p selected level with the step of variation equal to Δ. The four-level p is selected to reflect the variation of input parameters inside the domain. The Δ is chosen to be equal to $p/(2(p-1))$ (Saltelli et al., 2008, Morris, 1991). The start point matrix, $x^*_{1\times k\times M}$, is a random selection of the start point for all input variables and is used to generate the trajectory points. Using this start point will generate a randomized version of the sampling matrix. The best r trajectories out of M trajectories are

selected with scanning the input domain to achieve the highest spread. For detailed procedure, see Saltelli et al. (2008).

The computation cost for elementary effect method is $r \times (k+1) = 15 \times (17+1) = 270$ runs to get $Y = \left[\frac{\alpha T_f}{P_{pf}}\right]^2 + \left|\frac{M_f}{M_{pf}}\right|$ vector for each set of variables.

The Elementary Effect of each variable can be calculated by the magnitude of variation of that specific variable in the model output. The elementary effect associated with factor i is:

Equation 5.6 $$EE_i^j(x^{(l)}) = \frac{[y(x^{(l+1)}) - y(x^{(l)})]}{\Delta}$$

if the i[th] component of $x^{(l)}$ is increased by Δ, and

Equation 5.7 $$EE_i^j(x^{(l+1)}) = \frac{[y(x^{(l)}) - y(x^{(l+1)})]}{\Delta}$$

if the ith component of $x^{(l)}$ is decreased by Δ (Saltelli et al., 2008).

While one trajectory allows the evaluation of one elementary effect for each parameter i, a set of r trajectories enable statistical evaluation of the finite distribution of the elementary effects. Once r elementary effects per input are available, the statistical measures for evaluation of the EE, the absolute mean (μ_i^*), and the standard deviation (σ_i), relative to the distributions can be computed for each input factor.

Equation 5.8 $$\mu_i^* = \frac{1}{r}\sum_{j=1}^{r}\left|EE_i^j\right|$$

Equation 5.9 $$\sigma_i = \sqrt{\frac{1}{r-1}\sum_{j=1}^{r}\left(EE_i^j - \mu\right)^2}$$

This procedure is repeated 10 times to present error bars for each set of results.

Fully random sequence of generated points has a potential for discrepancy with cluster and gaps in the domain. To avoid this problem, Quasi-random sampling technique,

which is a low discrepancy sequence, is used in Sobol method. These sampling techniques are not unpredictable, and it biases the selection of points to maintain a uniform distribution of points across the sampling domain. The Halton sequence is a well-known low-discrepancy sequence that is used in this study (Homma and Saltelli, 1996, Saltelli, 2002, Saltelli et al., 2008). The base sample (N) for each variable is equal to 10000 in order to have an evident low discrepancy considering 17 independent variables in this study.

Monte Carlo-based implementation for computing sensitivity measures are provided by Sobol (2005). In this method, S_i is the first-order sensitivity index and it represents the contribution of each input factor to the variance of the output (Iman and Hora, 1990, Saltelli et al., 1993, Homma and Saltelli, 1996, Fenton and Griffiths, 2008).

Equation 5.10 $$\boldsymbol{S_i = \frac{V[E(Y|X_i)]}{V(Y)}}$$

where X refers to the variables, Y is the output vector, $E(Y)$ is mean or expected value of Y, and $V(Y)$ is variance of Y.

First-order effect plus all higher-order effects of factor X_i is total effect index of factor X_i and is useful to investigate the all interactions involving the parameter X_i. Homma and Saltelli (1996) proposed a technique to calculate total effect indices at the same cost of first-order indices that is used in this study.

Equation 5.11 $$\boldsymbol{S_{Ti} = 1 - \frac{V[E(Y|X_{\sim i})]}{V(Y)} = S_i + S_{ij} + \cdots + S_{ij\ldots k}}$$

where $X_{\sim i}$ is the vector of all factors but X_i.

The first-order effect and total-effect indices are calculated in this study. Two matrices ($N \times k$) called matrix A and B are generated. These matrices are generated by applying quasi-random Holton sequence. Matrix C_i formed by all columns of matrix B

except the ith column which is taken from matrix A. The model output for all input values in the matrices A, B, and C are calculated, $y_A = f(A)$, $y_B = f(B)$, and $y_{Ci} = f(C_i)$. The computation cost for this method is $N \times (k+2) = 190{,}000$ runs. The first-order and total-effect indices are estimated based on the following equations (Saltelli et al., 2008).

Equation 5.12 $$S_i = \frac{V[E(\boldsymbol{Y}|\boldsymbol{X_i})]}{V(Y)} = \frac{y_A \times y_{Ci} - f_0^2}{y_A \times y_A - f_0^2}$$

Equation 5.13 $$S_{Ti} = 1 - \frac{V[E(\boldsymbol{Y}|\boldsymbol{X}_{\sim i})]}{V(Y)} = 1 - \frac{y_B \times y_{Ci} - f_0^2}{y_A \times y_A - f_0^2}$$

Equation 5.14 $$f_0^2 = \left(\frac{1}{N}\sum_{j=1}^{N} y_A^{(j)}\right)^2$$

For sensitivity analysis, the failure region is defined based on Equation 5.4 ($Y = \left[\frac{\alpha T_f}{P_{pf}}\right]^2 + \left|\frac{M_f}{M_{pf}}\right| \leq 1$) which defines a safe region when $Y \leq 1$ and a failure region when $Y > 1$. This equation is a function of several random variables is given in Table 5.1. These variables are independent, and all variables are normally distributed with presented mean value and coefficient of variations.

5.4 Probability analysis

The probabilistic approach used to assess the reliability of CSC deteriorated by corrosion. The influential variables mentioned in the global sensitivity analysis result section with an estimated mean and coefficient of variation given in Table 5.1 is used to conduct the probabilistic analysis using first-order second moment method. The limit state function for the probability analyses is defined as:

Equation 5.15 $$Z = 1 - \left(\left[\frac{\alpha T_f}{P_{pf}}\right]^2 + \left|\frac{M_f}{M_{pf}}\right|\right)$$

where the safe region is defined when $Z > 0$ and the failure region when $Z < 0$.

The first two moments of non-linear limit state function cannot be obtained exactly. Consequently, two-point Adaptive Nonlinear Approximation (TANA) method is used to find the most probable point in the solution space to estimate the safety index (β).

The reliability index (β) is calculated as:

Equation 5.16 $\boldsymbol{\beta = \bar{z}/\sigma_z}$

where $\bar{z}$ is the mean value and σ_z is the standard deviation of the limit state function (Z).

The allowable error between the exact and approximate function is chosen to be less than 0.001 in this study. Detailed discussion of this method can be found in literature (Rackwitz and Flessler, 1978, Wang and Grandhi, 1996, Grandhi and Wang, 1999, Melchers and Beck, 2018). Based on this analysis, the failure probability is calculated for the corroded culvert buried in a shallow cover depth condition. The safety index is calculated for influential coefficients to investigate the effect of the coefficient of variation (CV) on the safety index (β).

5.5 Results and discussion

This section provides the results of numerical analysis for local sensitivity using finite element simulations, global sensitivity, and probability studies. The corrugated steel culvert is buried in a shallow cover depth and live load and backfill load effects are considered in culverts evaluation during their service lives.

5.5.1 Finite element simulation results

Finite element simulation enables a detailed assessment of the magnitude and distribution (i.e., intensity or gradient) of mechanical response parameters (e.g., deflections, local forces, bending moments) throughout the modeling domain.

The maximum deflection occurs at the culvert crown in a location under the applied wheel load, mid length of the culvert which is the intersection between sections A-A and B-B in Figure 5.2, for the Abaqus simulation modeled based on the provided mean value of variables in Table 5.1. Deformed shape of culverts affected by corrosion deteriorations at different locations and corrosion angles has a heart shape which is presented in Figure 5.7. The deflection shape is similar to the deflection of corroded culvert at lower half (i.e., haunch and invert) and intact culvert. This figure shows culvert deflections shape depends on surrounding soil support and interaction between soil and culvert (see Figure 6.26) and corrosion deteriorations only change the magnitude of deflections.

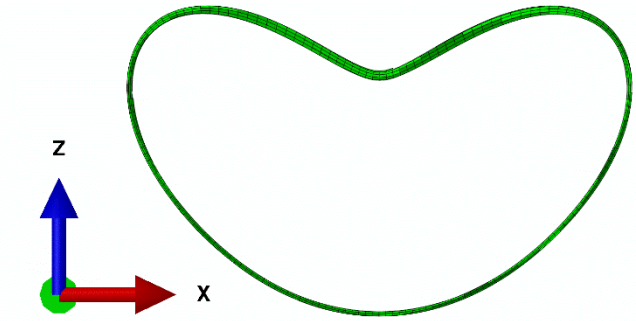

Figure 5.7. Deformed shape of CSC affected by corrosion at section A-A (× 50 magnification factor)

The magnitudes of these deflections are presented in Figure 5.8 for different location and angle of corrosion. These results indicate that the corrosion location on culvert can be influential if it happens in upper half of the culvert and can cause 10% to 14% greater deflection at crown for corroded sections in shoulder and crown respectively in comparison

with the intact culvert (Figure 5.8a). As shown in Figure 5.8b, the subtended angle of corrosion has an almost linear relation with the vertical deflection at crown.

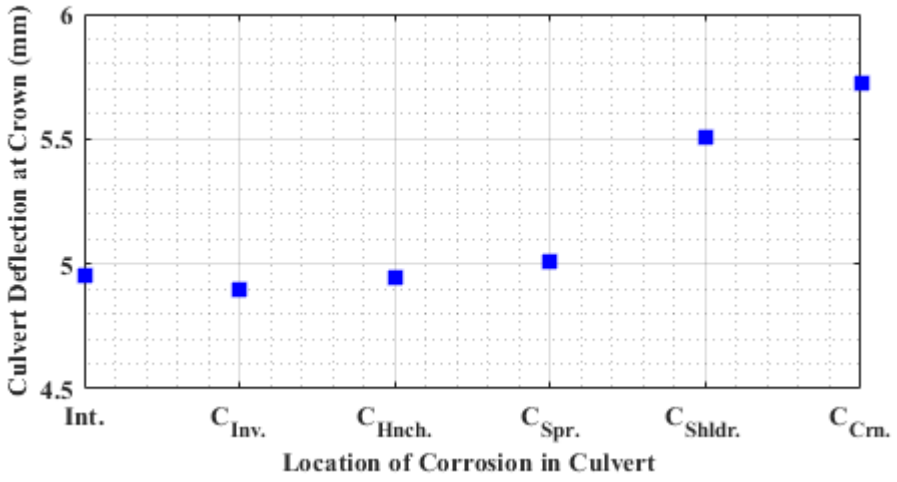

(a)

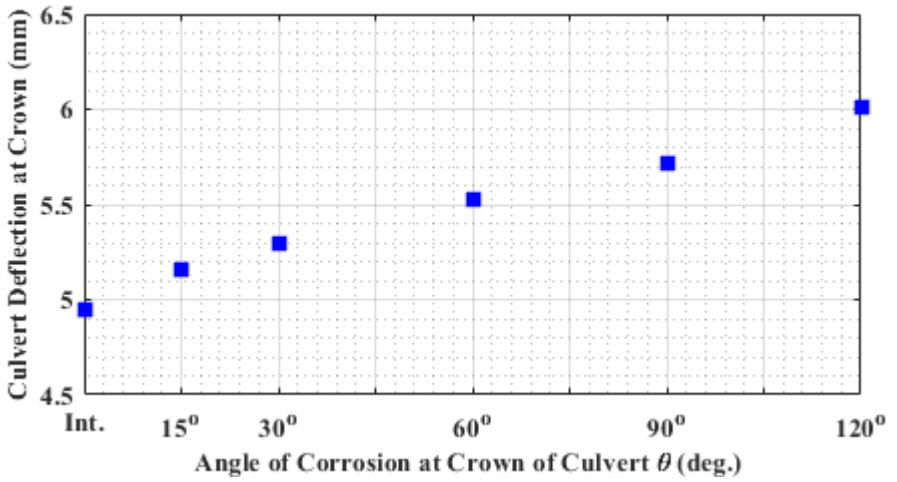

(b)

Figure 5.8. CSC deflection at crown for applied corrosion a) at different location with $\theta = 90°$, and b) at crown with different values for θ

The finite element analysis results for internal forces are presented in Figure 5.9 for the defined path in Figure 5.3. The Y value, $Y = \left[\frac{T}{P_{pf}}\right]^2 + \left|\frac{M}{M_{pf}}\right|$ is calculated for each

corroded FE model for the defined spiral path. The values of local force (T) and bending moment (M) are obtained directly from the finite element analysis, and the combined local force and moment capacity values are calculated for the spiral path in the models. These results indicate the culvert experiences high value of Y in shoulders and crown in all intact and deteriorated models. Figure 5.9a presents circumferential values of Y for corrugated models with deterioration in different locations, but with constant corrosion angle and corroded wall thickness ($\theta = 90°, t' = 0.52\ t$). The model with deterioration at the crown, $C_{Crn.}$, experiences $Y > 1$ at crown that is a failure region based on the function definitions and the Y value approaches 1 at the shoulders. For the applied corrosion in shoulders ($C_{Shldr.}$), the Y value approaches 1 along the CSC shoulder and crown. The Y value from the shoulder to invert shows very small value of internal forces for these cases.

Figure 5.9b presents the Y value for corroded cases at crown with different angles. All corroded cases experience $Y > 1$ values at crown (Figure 5.9b). The models with corrosion angle equal/greater than 60 degrees (i.e., θ equal to 60, 90, and 120 degrees) experience greater values of Y more generalized in upper half of the culvert especially at shoulders and crown. The corroded cases at crown with limited angles (i.e., θ equal to 15 and 30 degrees) experience concentrated and more severe local responses at crown where Y value is almost equal to 1.5 in this location. This result indicates that the small corrosion with limited angle located in a critical location can cause stress concentrations and yield can occur at this location of the CSC.

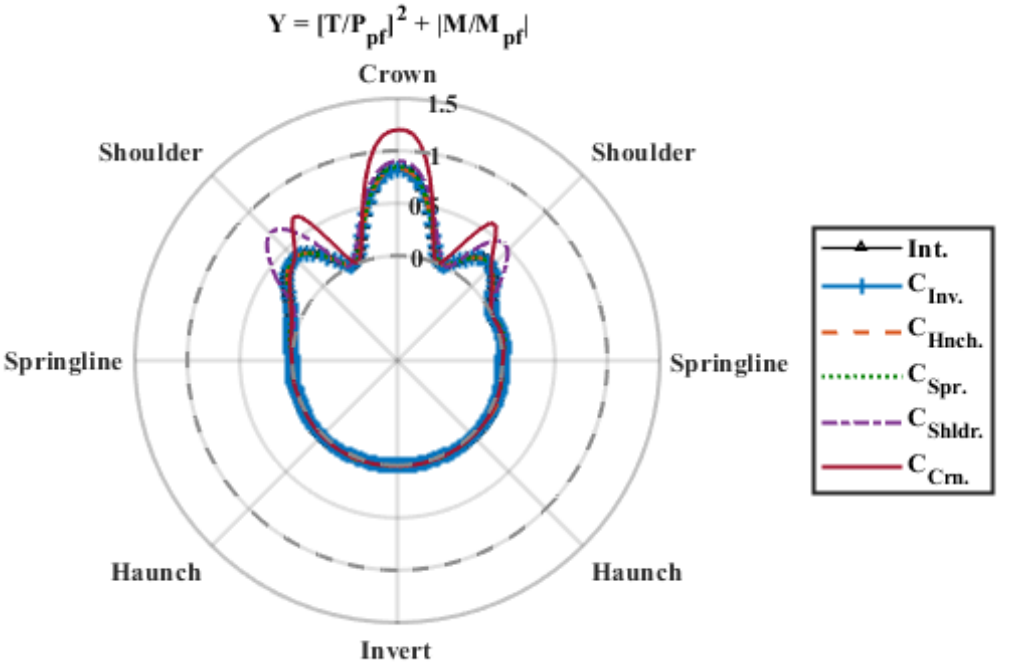

(a)

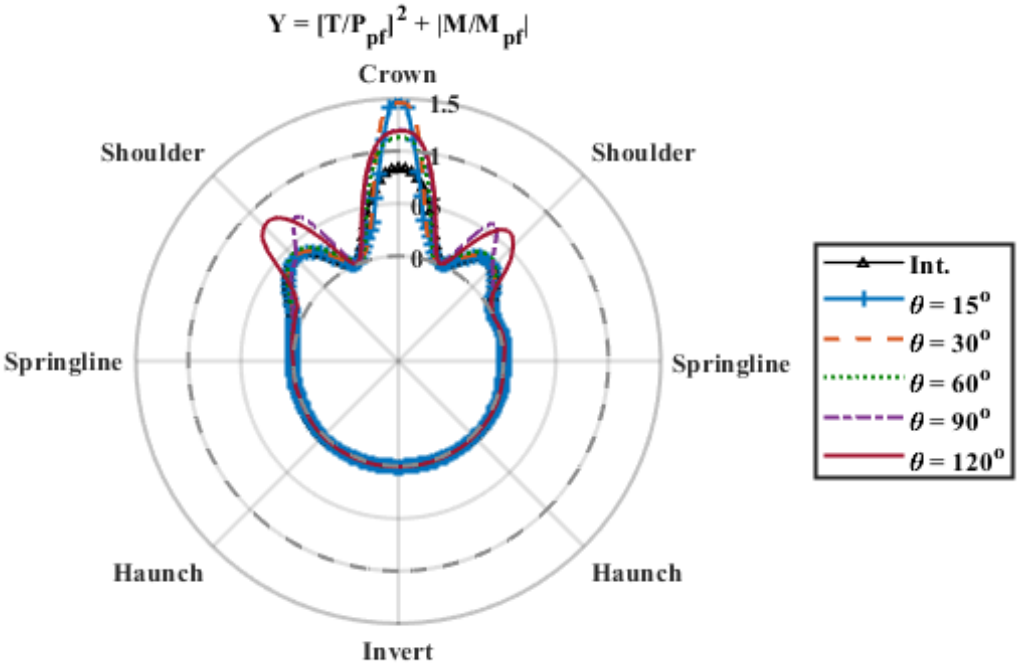

(b)

Figure 5.9. Magnitude of $Y = \left[\frac{T}{P_{pf}}\right]^2 + \left|\frac{M}{M_{pf}}\right|$ for CSC for the defined spiral path, at the culvert mid-length for applied corrosion a) at different location with $\theta = 90°$, and b) at crown with different values for θ

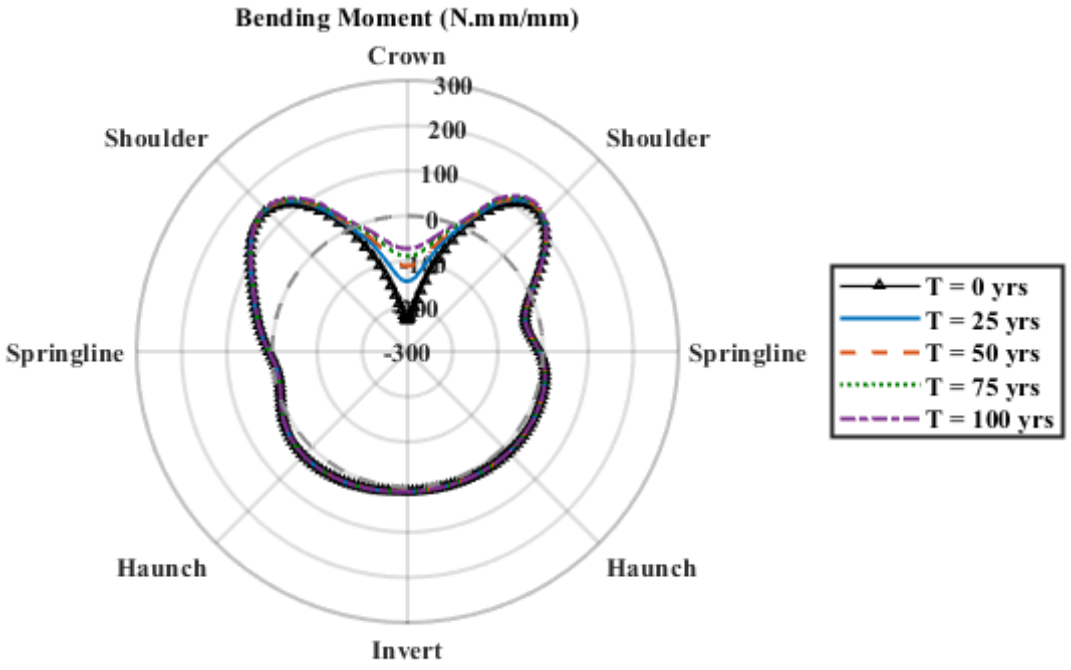

(a)

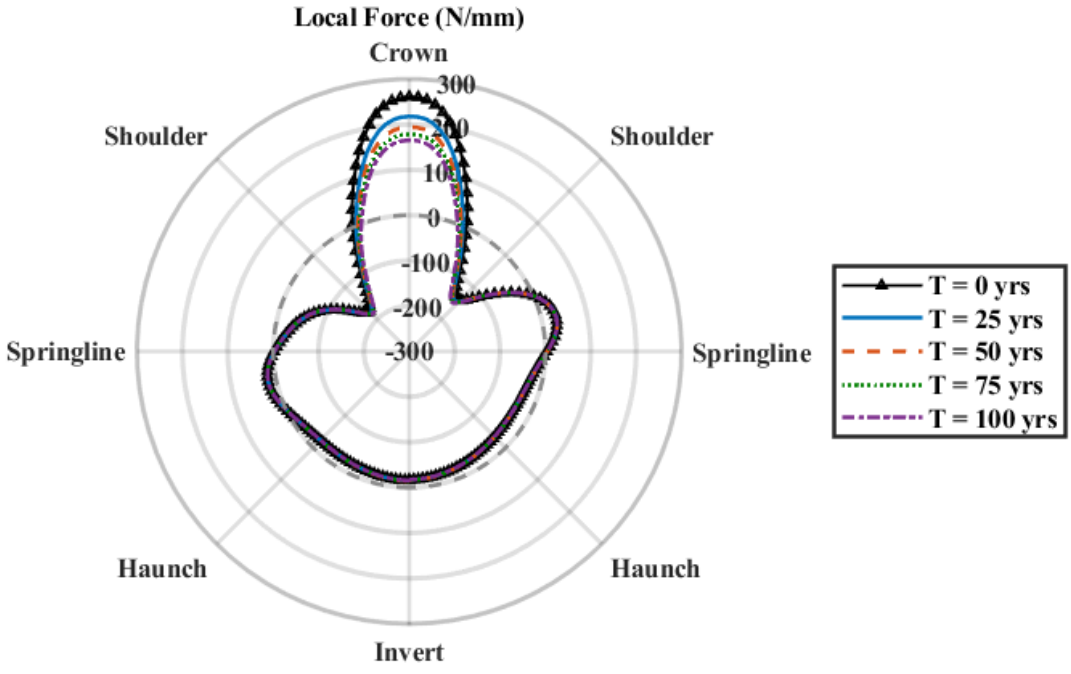

(b)

Figure 5.10. Circumferential a) bending moment and b) local force using FEM for introduced corrosion at crown with $\theta = 60°$ for T = 0- to 100-year exposure time

Figure 5.10 presents the circumferential bending moment and local force of deteriorated culvert in the defined spiral path. The exposure life is changing from 0 to 100 years and the thickness of deteriorated section of culverts are defined in FE simulations based on the exposure time. Corroded sections are defined at the crown of the culvert with $\theta = 60^{\circ}$. Bending moment and local force responses are presented in Figure 5.10a and b respectively. These results indicate that in comparison with the intact culvert, the internal forces are reduced at the corroded section because of thinner thickness of culvert, but the strength of this section is reduced as well and the culvert experiences $Y > 1$ at crown for exposure time equal to and greater than 75 years (Figure 5.11).

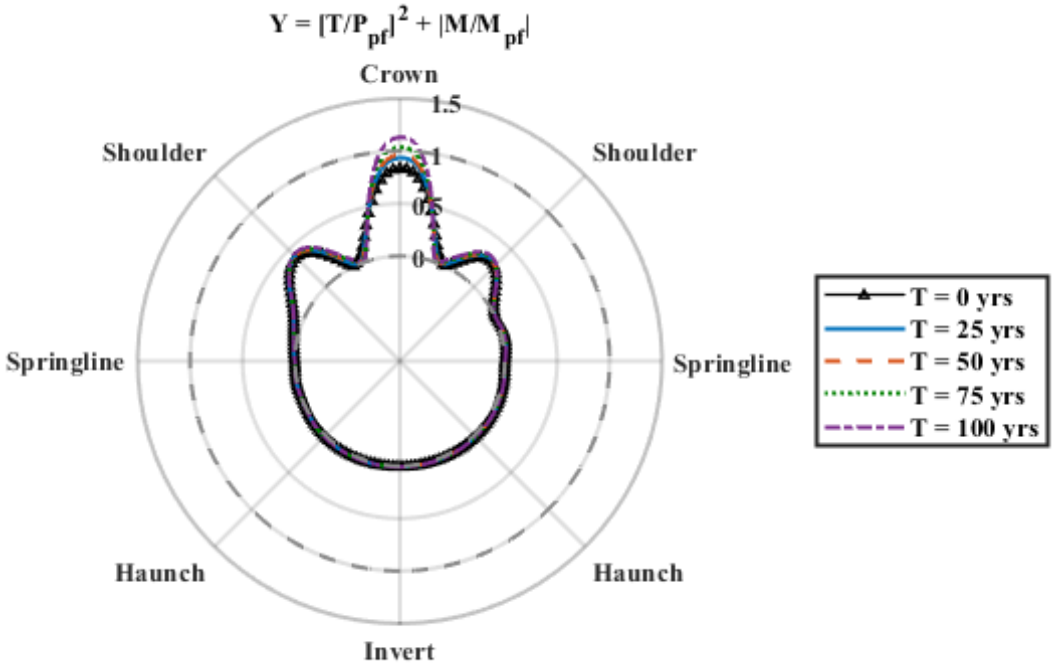

Figure 5.11. Magnitude of $Y = \left[\frac{T}{P_{pf}}\right]^2 + \left|\frac{M}{M_{pf}}\right|$ for CSC corroded at crown with $\theta = 60°$ for T = 0- to 100-year exposure time

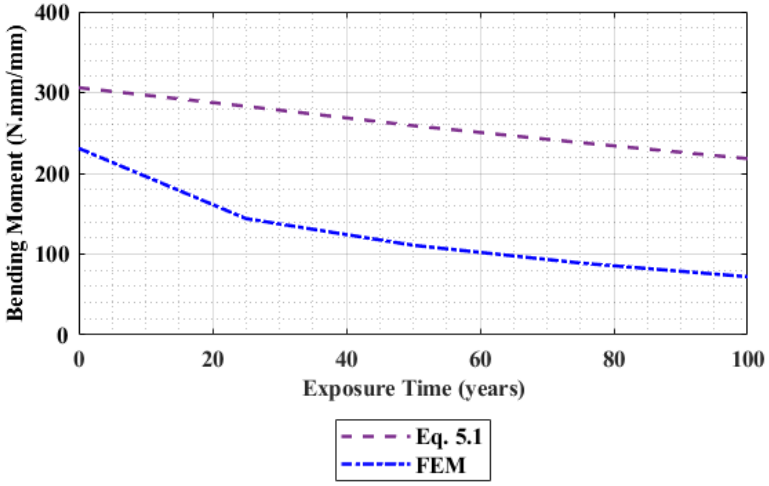

(a)

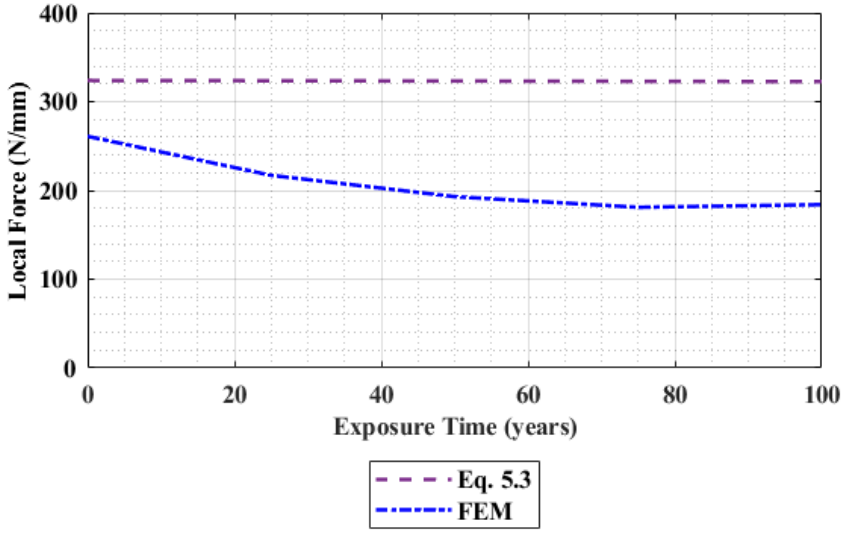

(b)

Figure 5.12. Comparing finite element analysis results and closed-form equations for a) bending moment, and b) local force for T = 0- to 100-year exposure time

The bending moment and thrust are calculated using closed-form equations, Equation 5.1 and Equation 5.3. These equations calculates the maximum internal force in the section and does not reflect the internal force changes at different location of culvert. These

calculations are conducted for 100-year exposure time. The results of analytical solutions are compared with internal forces obtained from the finite element simulations. The exposure time is applied in models and equations by using the reduced culvert wall thickness due to the corrosion (Equation 5.5). In finite element models, the corrosion deterioration is located at crown with 60 degrees angle for all exposure times. Figure 5.12a presents bending moment values for finite element model and closed-form equation. This figure shows that analytical solution using Equation 5.1 can capture moment changes due to corrosion deteriorations. These moments calculated by closed-form equations are conservative in comparison with FEM, and it reflects the effects of the exposure time and reduction in the culvert wall thickness in the responses. Both FEM and closed-form equation moments are decreasing by time, while the section capacity is decreasing as well because of the culvert wall-thickness loss and these results are consistent. The local force values are presented in Figure 5.12b and the closed-form equation responses are conservative in comparison with the finite element models. The calculated local force value is expected to be reduced through the aging mechanism, but the local force values calculated using Equation 5.3 do not reflect the deterioration effects in the responses and it remains constant for 100 years of exposure time.

5.5.2 Morris method sensitivity analysis results

Figure 5.13 presents the performance of elementary effects method with 17 variables. Each point in this figure represents the estimated absolute average (μ^*) versus standard deviation (σ) of the first-order EE screening method (Morris method) for each variable. The error bars present the results of 10 independent evaluations of elementary effects. These results are reported for corroded culverts with different exposure time and indices

are reported for exposure time greater than zero in a time frame of 10 years for a 100-year service life. Three straight lines of slope, $\frac{\sigma}{\mu^*} = 0.1, 0.5, and\ 1$, are plotted for identifying linear variables which are located below the line , $\frac{\sigma}{\mu^*} = 0.1$, monotonic variables which are located between two lines , $\frac{\sigma}{\mu^*} = 0.1\ and\ 0.5$, almost monotonic variables which are located between two lines , $\frac{\sigma}{\mu^*} = 0.5\ and\ 1$, and non-linear variables which are located above the line , $\frac{\sigma}{\mu^*} = 1$ (Menberg, Heo, & Choudhary, 2016; Sanchez, Lacarrière, Musy, & Bourges, 2014).

The absolute average (μ^*) versus standard deviation (σ) of the first-order EE presented in Figure 5.13. The figure for 10 years exposure (T=10) indicates that all variables are in linear, monotonic or almost monotonic region with very low μ^* values. The values of μ^* for variables number 2, 8, 9 and 11 (i.e., cover depth (H), exponential constant for corrosion model (n), multiplying constant for corrosion model (k), and culvert wall thickness (t)) are growing and moving to nonlinear region with increasing the exposure time.

The rate of growing of μ^* and σ values for variable number 1, 16, and 7 (i.e., wheel load (LL), thrust multiplying coefficient (C_1), and yield tensile stress (F_y)), are increasing and are greater than other variables which are considered as non-influential variables. The variable 3 (i.e., culvert diameter (D)) is influential for T=100 year of exposure time. The results indicate the mentioned parameters are influential variables and they exhibit non-linear behaviour where they are located above the line $\frac{\sigma}{\mu^*} = 1$ for $T \geq 20$ years.

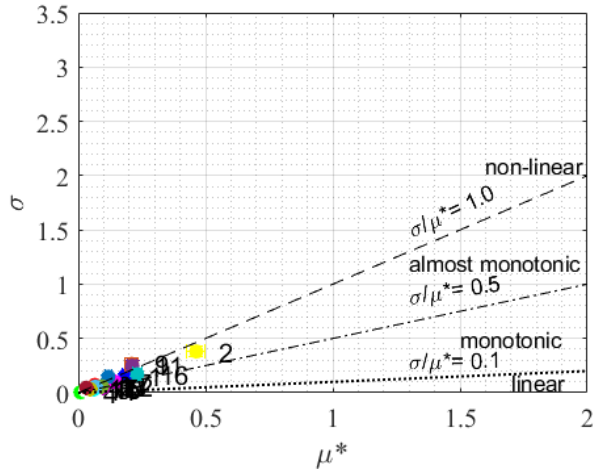

T = 10 yrs

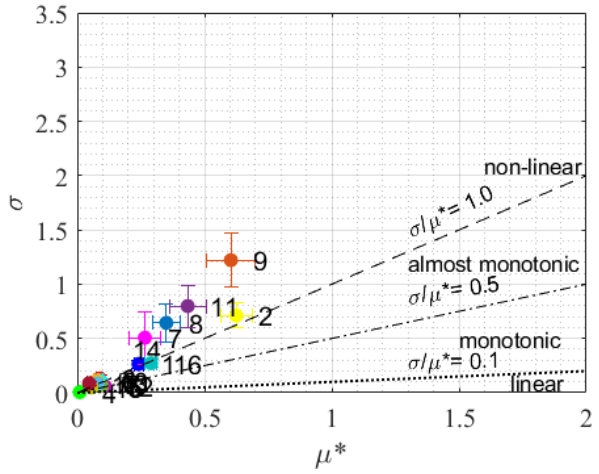

T = 20 yrs

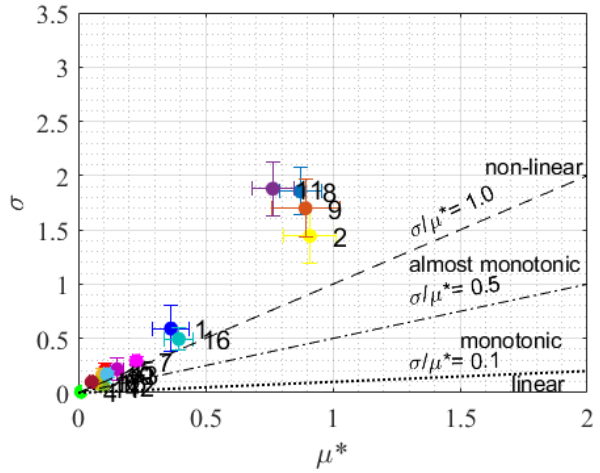

T = 30 yrs

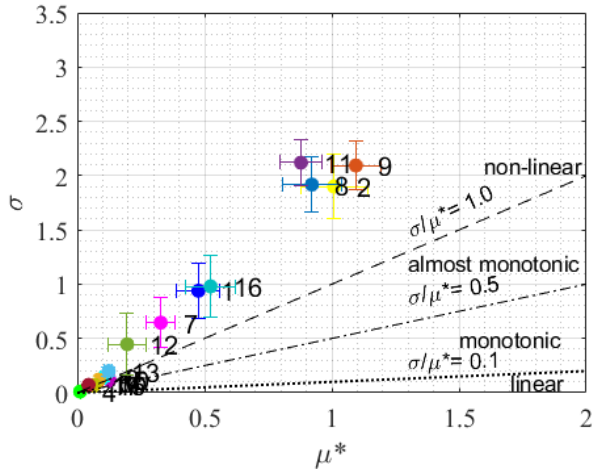

T = 40 yrs

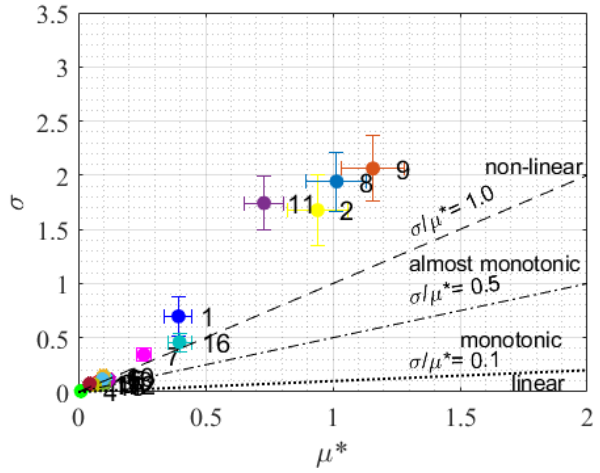

T = 50 yrs

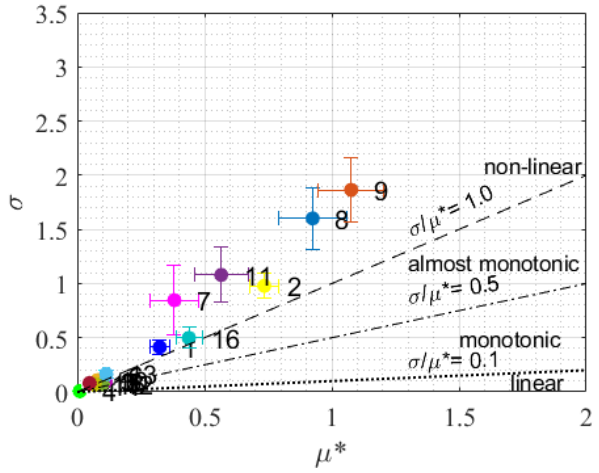

T = 60 yrs

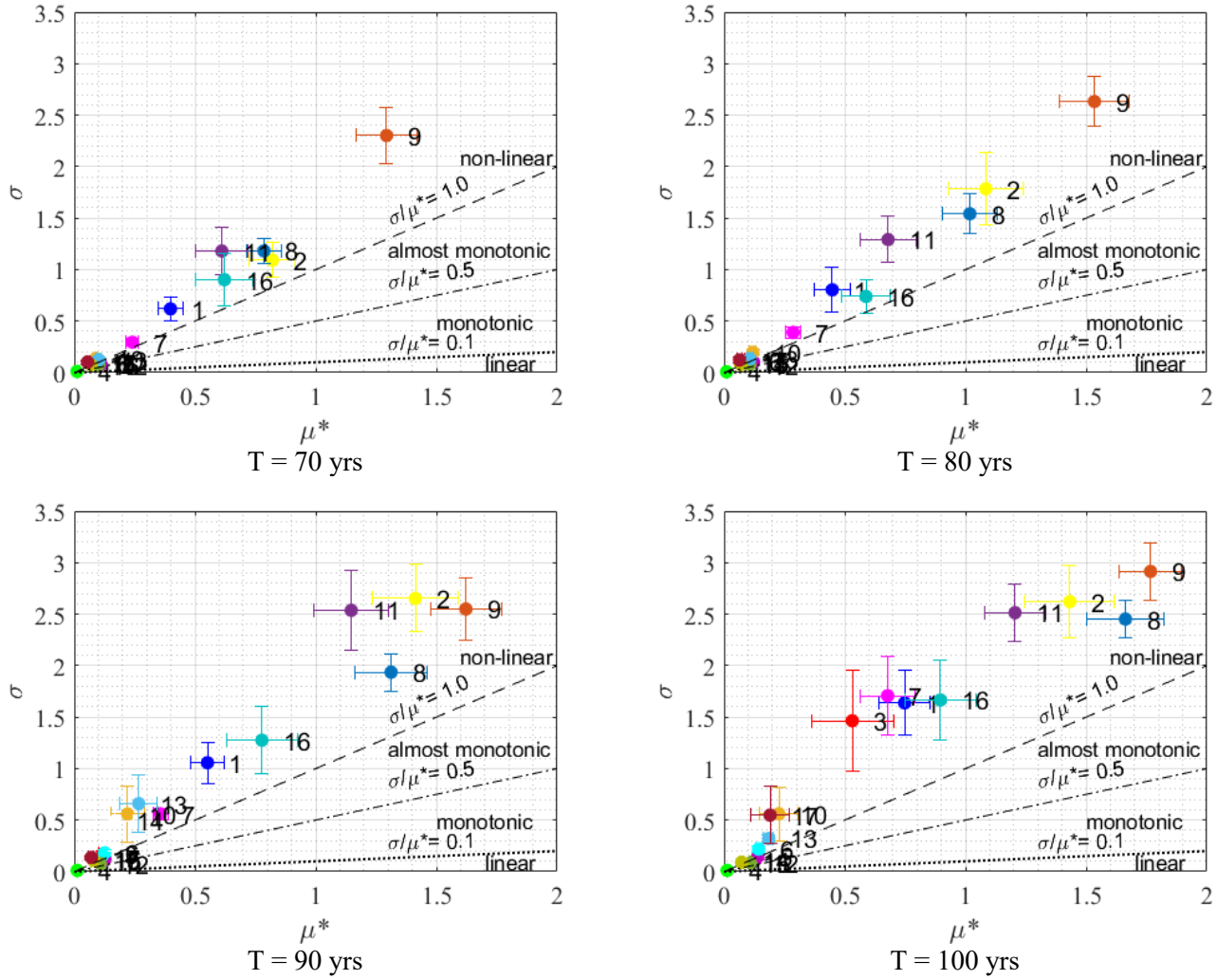

Figure 5.13. Estimated absolute average (μ_i^*) and standard deviation (σ_i) of the first-order EE (the numbers on the plot are the variable indices)

5.5.3 Sobol method sensitivity analyses results

The results of the variance-based sensitivity analysis are presented in Figure 5.14 and Figure 5.15 for intact and corroded buried CSC. Figure 5.14 presents $\sum_{i=1}^{k} S_i$ for exposure time from zero to 100 years. For intact culvert T = 0 and corroded culvert with 10-year exposure time, $\sum_{i=1}^{k} S_i$ is almost equal to 1 and this indicates that this system is an additive and linear model. The results in Figure 5.14 shows by increasing the exposure time (T) the value of $\sum_{i=1}^{k} S_i$ is decreasing that indicates there is an interaction among variables and the

first-order index results, S_i, is not valid for exposure time greater than 10 years and the value of total indices (S_{Ti}) needs to be considered in this evaluation.

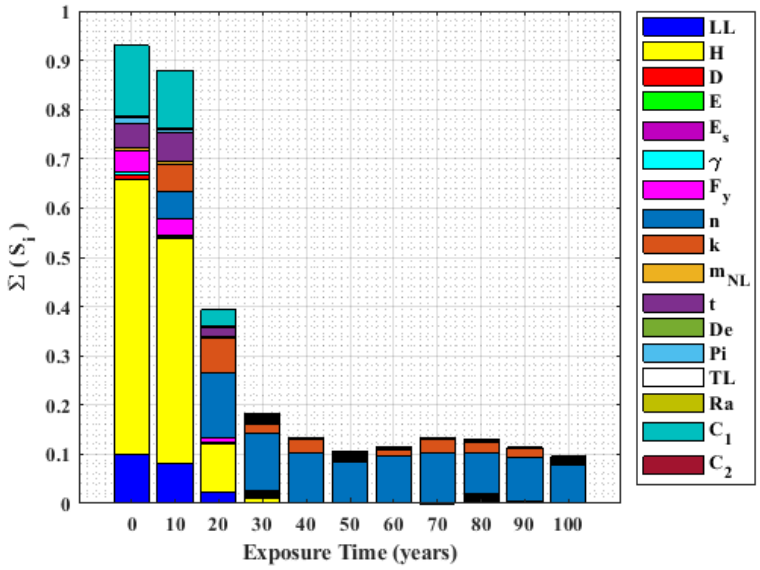

Figure 5.14. Global sensitivity analysis results for $\sum_{i=1}^{k} S_i$ with Sobol method for T = 0- to 100-year exposure time

Figure 5.15 presents the total effect indices (S_{Ti}) for 17 independent variables presented in Table 5.1 considering combined effect of local force and bending moment for the service load conditions. For intact culvert, three variables are influential including the truck wheel load (LL), the cover depth of the buried culvert (H), and the thrust multiplying coefficient (C_1) in an additive system (Figure 5.15, T = 0 yr). The index values for the exponential and multiplying constants for corrosion model is growing by increasing the exposure time (Figure 5.15). The number of influential variables for exposure time greater than 30 years remain constant. This result indicates the non-linear behaviour and strong interaction among the variables for deteriorated culvert with exposure time greater than 50 years. The total effect results of the Sobol method are strongly consistent with first-order EE method (Morris method).

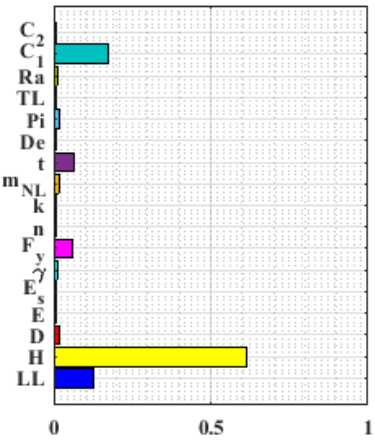

a) Intact culvert

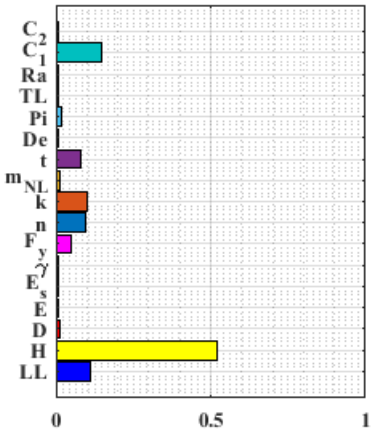

T = 10 yrs

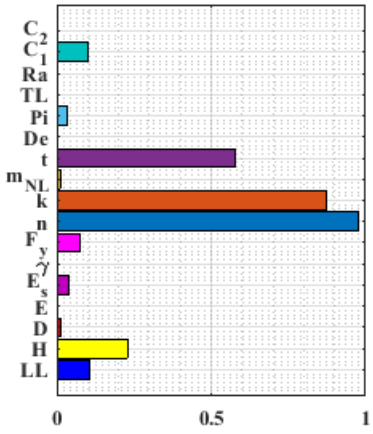

T = 40 yrs

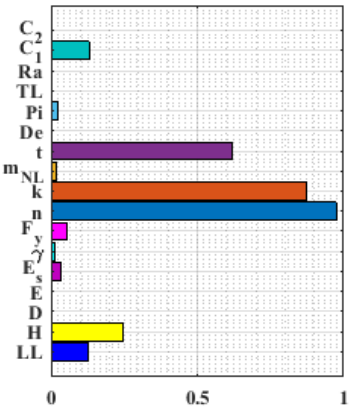

T = 70 yrs

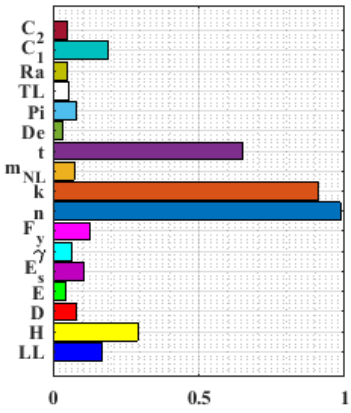

T = 100 yrs

b) T = exposure time

Figure 5.15. Global sensitivity analysis results, total effect index (S_{Ti}) with Sobol method for a) intact and b) corroded culverts with T exposure time

The influential parameters with total order index equal or greater than 0.1 are used as a variable in the probabilistic analysis. For probability analysis the influential parameters are the main variables using the values presented in Table 5.1 and the non-influential parameters remain constant with their mean value in Table 5.1 for the first-order second-moment probability analysis. Probability analysis results are presented in next section for exposure time from 10 to 100 years. The thrust multiplying coefficient (C_1), exponential constant for corrosion model (n), and multiplying constant for corrosion model (k) are variables that can be different for every environmental condition or different type of backfill soil. Probabilistic sensitivity analyses are conducted for these 3 coefficients to investigate their effects on the reliability index of the level of variability. The coefficient of variation for the thrust multiplying coefficient (C_1) is varied from 0 to 0.4, and it is varied from 0 to 0.5 for the exponential constant (n) and multiplying constant (k) for corrosion model. The coefficient of variation for other variables are equal to presented value in Table 5.1 while doing probabilistic sensitivity analysis for the specific coefficient (i.e., C_1, n, or k).

5.5.4 Probabilistic analysis results

The effect of variation of exposure time T and probability of failure is presented in Figure 5.16. The exposure time is changing from 10 to 100 years and the value of influential variables are picked based on the given values in Table 5.1 and other noninfluential variables are kept constant at the given values. The result shows the probability of failure, based on the defined limit state function, increases with exposure time. The rate of change is increasing from T = 10 to T = 40 and remain almost constant form T = 40 to T = 70

while there is a small reduction in failure rate from T = 70 to T = 100. This figure gives a clear picture of failure risk of CSC deteriorated by corrosion in its service life.

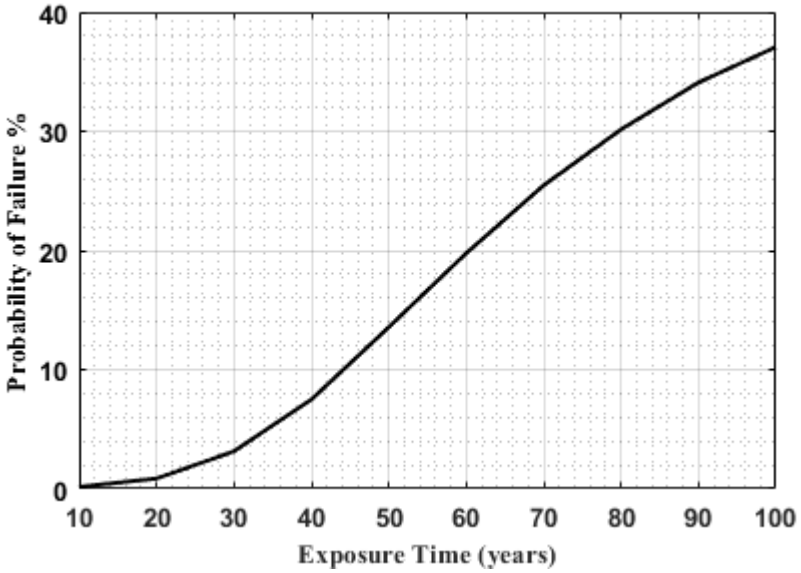

Figure 5.16. Probability of failure versus CSC exposure time in years

The sensitivity study is conducted to investigate the effect of the degree of variation (i.e., coefficient of variation CV) of the influential coefficients on safety index (β). The variables chosen for this study are thrust multiplying coefficient (C_1), exponential constant for corrosion model (n), and multiplying constant for corrosion model (k). The coefficient of variations for the chosen variable is varied from 0.1 to 0.4 for C_1 and 0.1 to 0.5 for n and k and the coefficient of variations for all the other variables remain constant at the value given in Table 5.1. This procedure is repeated for three chosen variables. The value of n and k are functions of buried culvert localized conditions (i.e., availability of oxygen and moisture, chemical substance in backfill soil or drainage water). The coefficient of variation for n and k varies from 0 to 0.5 to cover wide range of environmental conditions with the defined engineering model.

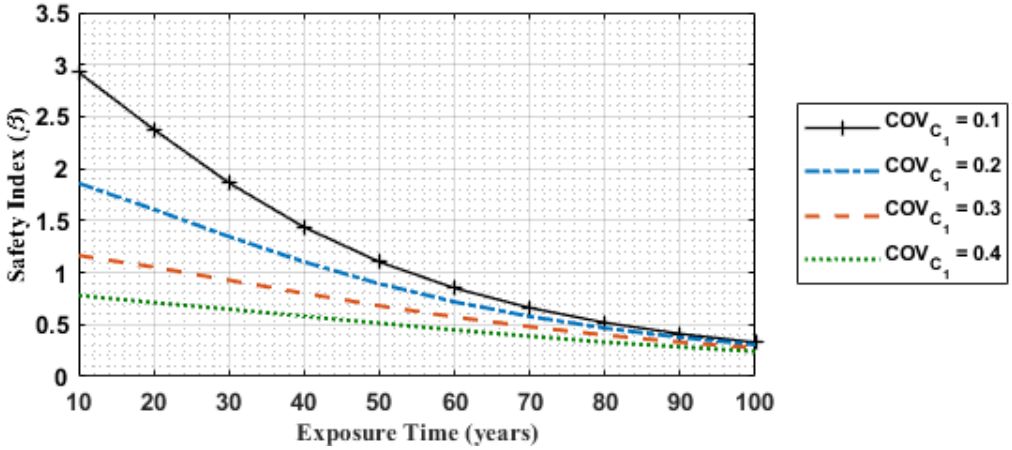

(a)

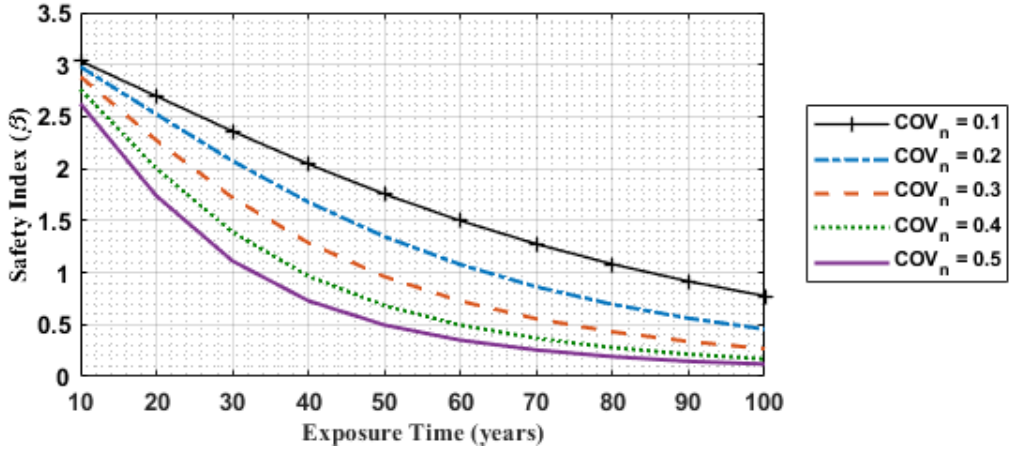

(b)

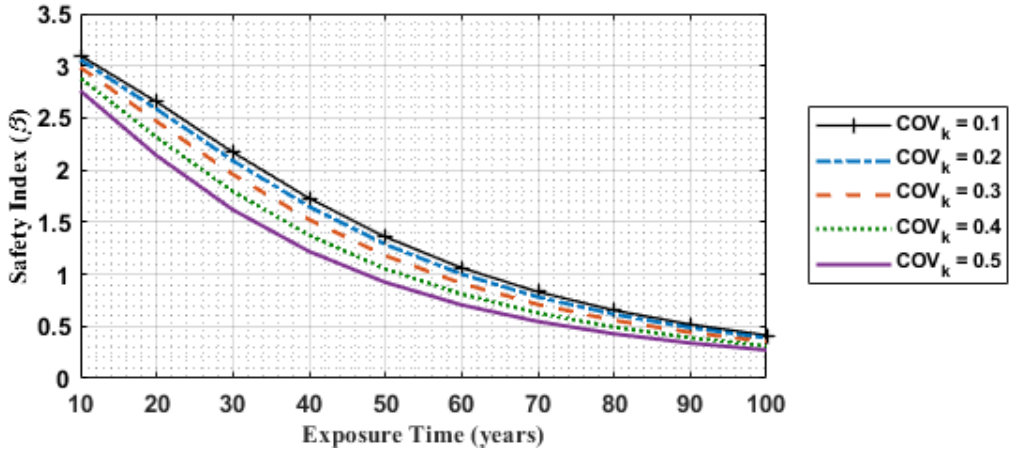

(c)

Figure 5.17. Safety index (β) versus CSC exposure time for various values of coefficient of variation for a) thrust multiplying coefficient (C_1), b) exponential constant for corrosion model (n) , and c) multiplying constant for corrosion model (k)

Figure 5.17 presents the results of safety index versus exposure time for different coefficient of variations for C_1, n, and k. The safety index decreases as the exposure time and the coefficient of variations of C_1, n, and k increase. As Figure 5.17a presents, the sensitivity of variable C_1 is dependent on the deterioration degrees or the exposure time. Although the safety index shows high sensitivity for intact and lightly corroded CSC, this sensitivity decreases for deeply corroded culverts. This indicates that the uncertain character of this variable does not affect safety index of structures with deep corrosions. The results of analysis for variable n presented in Figure 5.17b, indicate the safety index shows high sensitivity for changing in the coefficient of variation values and exposure time. This variable has a strong influence on the probability of failure of deteriorated culverts. For variable k, the results indicate that the variability of this parameter have fewer effects on the safety index in comparison with variable n (Figure 5.17c).

5.6 Summary and conclusion

Three different numerical approaches (i.e., finite element simulation, global sensitivity analysis, and probabilistic analysis) have been used to study the reliability of Corrugated Steel Culvert (CSC) buried in a shallow cover depth and crossed by a roadway. The CSC is subjected to corrosion deterioration and its sensitivity on the service life has been investigated. It is observed from the local sensitivity using finite element analysis that the culvert is vulnerable to corrosion deterioration. The occurrence of plastic strain at the crown has been observed in the analysis considering corrosion location, angle, and wall thickness loss. The internal forces and stresses are distributed more uniformly in corroded culverts with a wide angle of corrosion. The corroded cases with limited angles, smaller

than 30 degrees, experience concentrated and more severe internal responses at the deteriorated locations that can cause stress concentrations and yield can occur at this location of the CSC.

The intact and lightly corroded culvert systems are additive and linear models. But increasing exposure time and deterioration degrees, the number of influential variables increase with highly nonlinear features. The probability analyses results show the probability of failure increases with exposure time and life-span of buried culvert in a shallow cover depth can be predicted using the figure of probability of failure (based on the defined limit state function) versus culvert exposure time. The sensitivity of the variable, thrust multiplying coefficient (C_1), is dependent on the exposure time. Although the safety index shows high sensitivity for intact and lightly corroded CSC, this sensitivity decreases for deeply corroded culverts. The results of the analysis for the variable exponential constant for corrosion model (n) indicate that the safety index shows high sensitivity on the coefficient of variation values and exposure time. Consequently, for heavily corroded culvert this parameter of corrosion should be chosen with an accurate determination.

References

AASHTO, M. (2020). Standard Specification for Corrugated Steel Pipe, Metallic-Coated for Sewers and Drains. American Association of State and Highway Transportation Officials.

Ahammed, M. and Melchers, R. (1997). "Probabilistic analysis of underground pipelines subject to combined stresses and corrosion." *Engineering structures*, 19(12), 988–994.

ASTM A760/A760M-15, (2020). Standard Specification for Corrugated Steel Pipe, Metallic-Coated for Sewers and Drains.

ASTM, D. 2011. 2487 (2006) Standard practice for classification of soils for engineering purposes, Unified Soil Classification System. Book of Standards, 4.

Bakht, B. (1981). "Soil-steel structure response to live loads." *Journal of the Geotechnical Engineering Division*, 107(6), 779–798.

Beaton, J. and Stratfull, R. (1962). "Field test for estimating service life of corrugated metal pipe culverts." *Highway Research Board Proceedings*, Vol. 41.

Bradford, S. A. (2000). "The practical handbook of corrosion control in soils.

CAN/CSA-G401-14, (2014). Corrugated steel pipe products Canadian Standard Association. Mississauga, ON, Canada: Canadian Standard Association.

Cichocki, R., Moore, I., and Williams, K. (2021). "Steel buried structures: condition of Ontario structures and review of deterioration mechanisms and rehabilitation approaches." Canadian Journal of Civil Engineering, 48(2), 159–172.

Corrugated Steel Pipe Institute. (2010). Handbook of steel drainage and highway construction products. Handbook of steel drainage and highway construction products. Cambridge, Ontario, Canada: Corrugated Steel Pipe Institute.

CSA/S6-14, (2014). Canadian Highway Bridge Design (CAN/CSA S6-14)(pp. 875). Ontario, Canada: Canadian Standard Association Group.

De la Fuente, D., Díaz, I., Simancas, J., Chico, B., and Morcillo, M. (2011). "Long-term atmospheric corrosion of mild steel." *Corrosion Science*, 53(2), 604–617.

Elshimi, T., Mak, A., Brachman, R., and Moore, I. (2011). "Behaviour of a deep-corrugated largespan box culvert during backfilling." *Pan-American Conference on Teaching and Learning of Geotechnical Engineering*, Toronto, Canada.

Elshimi, T. M. and Moore, I. D. (2013). "Modeling the effects of backfilling and soil compaction beside shallow buried pipes." *Journal of Pipeline Systems Engineering and Practice*, 4(4), 04013004.

Feliu, S., Morcillo, M., and Feliu Jr, S. (1993). “The prediction of atmospheric corrosion from meteorological and pollution parameters—ii. long-term forecasts.” Corrosion Science, 34(3), 415–422.

Fenton, G. A., Griffiths, D. V., et al. (2008). *Risk assessment in geotechnical engineering*, Vol. 1. John Wiley & Sons New York.

Grandhi, R. V. and Wang, L. (1999). “Structural reliability analysis and optimization: Use of approximations.” *Wright State University, Dayton*.

Hepfner, J. J. et al. (2002). “Statewide corrosivity study on corrugated steel culvert pipe.” Report no., Montana. Department of Transportation. Research, Development and Technology.

Hibbitt, H., Karlsson, B. & Sorensen, P. (2013). Abaqus analysis user’s manual version 6.13. Dassault Systèmes Simulia Corp.: Providence, RI, USA.

Homma, T. and Saltelli, A. (1996). “Importance measures in global sensitivity analysis of nonlinear models.” *Reliability Engineering & System Safety*, 52(1), 1–17.

Iman, R. L. and Hora, S. C. (1990). “A robust measure of uncertainty importance for use in fault tree system analysis.” *Risk analysis*, 10(3), 401–406.

Kucera,V. and Mattsson, E. (1987). “Atmospheric corrosion.” *Corrosion mechanisms*, 28, 211 284.

Marston, A. and Anderson, A. (1913). *The theory of loads on pipe in ditches and tests of cement and clay drain tile and sewer pipe*, Vol. 31. Iowa Eng. Experiment Station.

McGrath, T. J., Selig, E. T., Webb, M. C., Zoladz, G. V., et al. (1999). “Pipe interaction with the backfill envelope.” *Report no.*, University of Massachusetts at Amherst. Transportation Center.

Meegoda, J. N., Juliano, T. M., and Tang, C. (2009). “Culvert information management system. ” Transportation research record, 2108(1), 3–12.

Melchers, R. E. and Beck, A. T. (2018). *Structural reliability analysis and prediction*. John wiley & sons.

Menetrey, P. andWillam, K. (1995). “Triaxial failure criterion for concrete and its generalization.” *Structural Journal*, 92(3), 311–318.

Mikhailov, A., Tidblad, J., and Kucera, V. (2004). “The classification system of iso 9223 standard and the dose–response functions assessing the corrosivity of outdoor atmospheres.” *Protection of metals*, 40(6), 541–550.

Moore, I. D., Hoult, N. A., et al. (2014). “Performance of two-dimensional analysis: Deteriorated metal culverts under surface live load.” *Tunnelling and underground space technology*, 42, 152–160.

Nakhostin, E., Kenny, S., and Sivathayalan, S. (2021). “Numerical performance assessment of buried corrugated metal culvert subject to service load conditions.” *Canadian Journal of Civil Engineering*, 48(2), 99–114.

Perrin Jr, J., Jhaveri, C. S., and Perrin Jr, J. (2004). “The economic costs of culvert failures.” Prepared for TRB 2004 Annual Meeting, Washington DC.

Rackwitz, R. and Flessler, B. (1978). “Structural reliability under combined random load sequences.” *Computers & Structures*, 9(5), 489–494.

Regier, C. (2015). “Investigation of the failure mechanisms of intact and deteriorated culverts.” Ph.D. thesis, Queen’s University. 147p.

Saltelli,A. (2002). “Making best use ofmodel evaluations to compute sensitivity indices. ”*Computerphysics communications*, 145(2), 280–297.

Saltelli, A., Andres, T., and Homma, T. (1993). “Sensitivity analysis of model output: an investigation of new techniques.” *Computational statistics & data analysis*, 15(2), 211–238.

Saltelli, A., Annoni, P., Azzini, I., Campolongo, F., Ratto, M., and Tarantola, S. (2010). “Variance based sensitivity analysis of model output. design and estimator for the total sensitivity index.”*Computer physics communications*, 181(2), 259–270.

Saltelli, A., Ratto, M., Andres, T., Campolongo, F., Cariboni, J., Gatelli, D., Saisana, M., and Tarantola, S. (2008). *Global sensitivity analysis: the primer*. John Wiley & Sons.

Saltelli, A., Tarantola, S., Campolongo, F., and Ratto, M. (2004). *Sensitivity analysis in practice: a guide to assessing scientific models*, Vol. 1. Wiley Online Library.

Scarino, J. H. (2003). “Reappraisal of marston’s formula.” *Journal of transportation engineering*, 129(6), 703–712.

Schwerdtfeger, W. (1969). “Polarization measurements as related to corrosion of underground steel piling.” *J. Res. Nat. Bur. Stand. (US) C*, 75, 107–121.

SIMULIA, D. (2013). ABAQUS 6.13 User’s manual. Dassault Systems, Providence, RI.

Sobol’, I. M. (2005). “Global sensitivity indices for the investigation of nonlinear mathematical models.” *Matematicheskoe modelirovanie*, 17(9), 43–52.

Spangler, M., Hennessy, R., and Barber, E. (1947). “A method of computing live loads transmitted to underground conduits.” *Highway Research Board Proceedings*, Vol. 26.

Spangler, M. G. (1964). “Pipeline crossings under railroads and highways.” *Journal-American Water Works Association*, 56(8), 1029–1046.

Spangler, M. G. and Shafer, G. (1938). “The structural design of flexible pipe culverts.” *Highway Research Board Proceedings*, Vol. 17.

Wang, L. and Grandhi, R. V. (1996). “Safety index calculation using intervening variables for structural reliability analysis.” *Computers & structures*, 59(6), 1139–1148.

Warman, D. J., Hart, J. D., and Francini, R. B. (2009). “Development of a pipeline surface loading screening process & assessment of surface load dispersing methods.” *Canadian Energy Pipeline Association, Worthington, OH, Report No*.

Chapter 6: Erosion void and corrosion effects on the performance of CSC

6.1 Methodology

Corrugated Steel Culverts (CSC) are core municipal infrastructure components used as part of a drainage system for watercourse and stormwater management. CSC products are thin-walled structures that have been used since the 1960's due to their beneficial economic and technical characteristics such as strength and ductility. CSC products have a wide range of service life, from 10 to 100 years, depending on a number of factors that include geographic location, climate and CSC coatings (Beaton and Stratfull 1962). Physical processes, related to environmental factors and ageing, can deteriorate the CSC/soil system and impair the mechanical performance and reduce the CSC service life.

Erosion voids can develop in the backfill due to environmental conditions. The deterioration mechanisms are influenced by the presence of moisture, and soil characteristics including type, homogeneity, density, clay content and mineralogy (Bradford 2000; Hepfner 2002). The deterioration of the culvert system can result in life-threatening and expensive damage to the culverts and its related system (Perrin Jr and Jhaveri 2004; Meegoda, et al. 2009).

The creation of voids within the backfill, particularly adjacent to the structure/soil interface, can influence the structure/soil interaction and load transfer processes (i.e., amplitude, distribution), and failure mechanisms that may affect the stability and integrity of buried structures. Operational experience with buried structures, such as pipelines and

tunnels, indicates the creation of local soil voids distributed around the structure, which can affect the structural load carrying capacity. The soil voids may be created due to water leakage through corrosion features at the base of the CSC. Hydraulic pressure and flow may washout and transport fines within the backfill that results in the creation of soil voids. Field observations have indicated that the concentration of solid particles transported with the sewage causes the formation of a groove around the pipe (Rubin, et al. 2013; Cichocki, et al. 2021).

The erosion void creates a separation or region of non-contact between the structure and surrounding soil backfill, which may result in undesirable deformation and stress being developed within the buried structure (Yasuda, et al. 2017). The simulation of erosion voids can be achieved through considerations of the contact region and interaction mechanics between the structure and surrounding soil (Xu and Cheng 2013; Giresini, et al. 2016). Local, discrete voids (i.e., separation between the structure and soil) may be introduced at different locations on the interface. Due to these changes in the contact interface, changes in the normal contact pressure were measured and the simulations indicated noticeable changes in the magnitude and distribution of earth pressure within the region experiencing loss of contact (Leung and Meguid 2011; Wang, et al. 2014). The presence of soil voids may reduce structural load carrying capacity, induce local soil deformation mechanisms, cause eccentric loading on the structure that can lead to unexpected stresses and may cause progressive structural deterioration and failure (Meguid and Dang 2009; Meguid and Kamel 2014).

In this chapter, results from a numerical study exploring the effects of local soil voids on the structure/soil interaction mechanisms, (i) with, and (ii) without corrosion

deteriorations in CSC are presented. The research investigates the effect of introduced deteriorations on mechanical responses at the present state and does not consider the process of a void creation and corrosion deterioration evolution. The mechanical response of a buried thin-walled CSC is presented for these deteriorations. Three-dimensional (3D) continuum finite element modeling procedures, using Abaqus/Standard software, were developed. Based on previous results (Nakhostin, et al. 2020), the culvert corrugated profile was modelled with nonlinear constitutive relationships defining the CSC and soil material behaviour and contact interactions at the CSC/soil interface. A single-wheel pair and single axle loads positioned over the culvert crown at the ground surface defined the surface loading condition. Confidence in the numerical modeling procedures was established through verification with data from third-party physical modeling studies (Peter, et al. 2019). The parameter study investigated the influence of soil erosion void volume (i.e., angle, depth, length) and relative position with the culvert (i.e., distance, location), on the CSC mechanical response. The effects of combined erosion and corrosion is studied in this chapter for two cases. The cover depth effects on deteriorated system are other variable that is investigated in this study for buried culverts with shallow cover. The analysis includes an assessment of the culvert serviceability with respect to the sectional local force, moment, thrust, strain, and displacement of CSC and the soil pressure in presence of soil voids and corroded culverts. The mechanical responses were examined with respect to a variation in the soil void factors with a constant CSC/soil material and geometric properties.

6.2 Numerical modeling of CSC/Soil and loading system

Continuum finite element modeling procedures were used to examine the mechanical response of a buried CSC subject to the applied surface loads with deteriorated backfill conditions due to soil voids at the CSC/soil interface. Based on previous studies (El-Taher and Moore 2008, Mai 2013; Nakhostin, et al. 2017; Mai, et al. 2018; Nakhostin, et al. 2019) the corrugated profile of the culvert must be explicitly incorporated within the model geometry in order to accurately predict (relative to physical modelling data used in the verification) the CSC section moment and local force, particularly for shallow burial conditions. The numerical modelling procedures used in this study are presented in Chapter 3 with supporting results presented in a previous investigation (Nakhostin, et al. 2020).

A 900 mm diameter CSC with a specific corrugated profile (depth and pitch), but of variable wall thickness was considered in the analysis (Figure 6.1). Table 6.1 presents the section properties for two CSC profile used in this study.

The culvert section was discretized using fully integrated linear 4-node (S4) shell elements for the model space with three elements from crest to trough to have optimum mesh density.

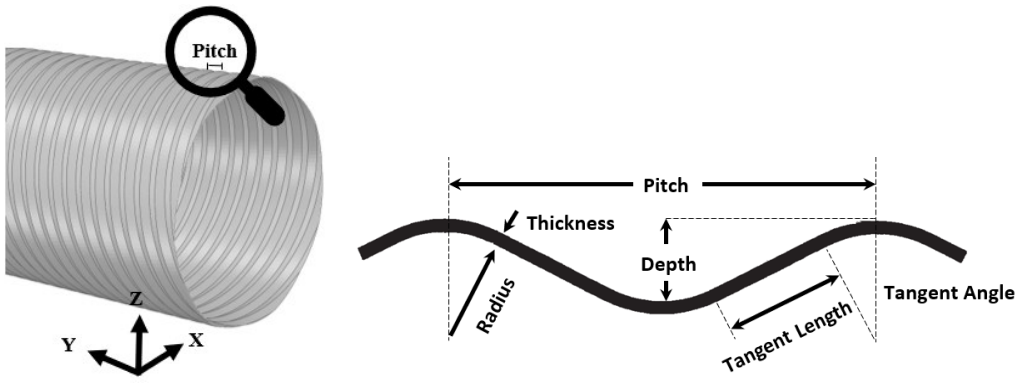

Figure 6.1. Corrugated culvert profile

Table 6.1. Section properties for CSC (Corrugated Steel Pipe Institute. 2010)

	Pitch (mm)	Depth (mm)	Radius (mm)	Thickness (mm)	TL	Angle	Area (mm^2/mm)	Moment of Inertia (mm^4/mm)	Section Modulus (mm^3/mm)
Profile I	67.7	12.7	17.46	3.5	18.269	27.381	3.621	70.16	8.74
Profile II	67.7	12.7	17.46	1.6	19.578	26.734	1.512	28.37	4.02

The culvert was buried at 900 mm cover depth (H/D = 1) within a soil domain representing backfill conditions as shown in Figure 6.2. The soil box dimensions were selected based on the numerical convergence sensitivity study and third-party experience (Regier, 2015; Mai et al., 2018; Peter et al., 2019), requirements for applying the surface load (CSA-S6 2014; Regier 2015; Mai, et al. 2018) effects on the CSC/soil response, and bedding (> 0.5 D) thickness (McGrath, et al. 1999; Elshimi, et al. 2011; Elshimi and Moore 2013). Eight node linear brick elements (C3D8) were used to discretize the soil domain with the boundary conditions, which replicate the experimental setup. The soil domain base was fixed from motion (i.e., $U_X = U_Y = U_Z = 0$), and the sidewall vertical faces were constrained from the transverse lateral motion (i.e., $U_X = U_Y = 0$).

In the full-scale tests, plastic deformations were observed in culvert at crown in buried case at shallow cover depth (Regier 2015, Nakhostin et al. 2020). Consequently, in this numerical study, the CSC and soil constitutive relationships accounted for nonlinear material behaviour. The culvert constitutive relationship was based on J_2 plasticity theory with the von Mises (equivalent stress) yield criterion and combined hardening rule (Hibbitt, et al. 2013). The stress-strain relationship was constructed using piecewise approximation based on Ramberg-Osgood expression assuming Grade A steel was representative of the

coupon test data with yield strength and ultimate strength of 230 MPa and 330 MPa, respectively (Ramberg and Osgood 1943, Walker and Williams 1995).

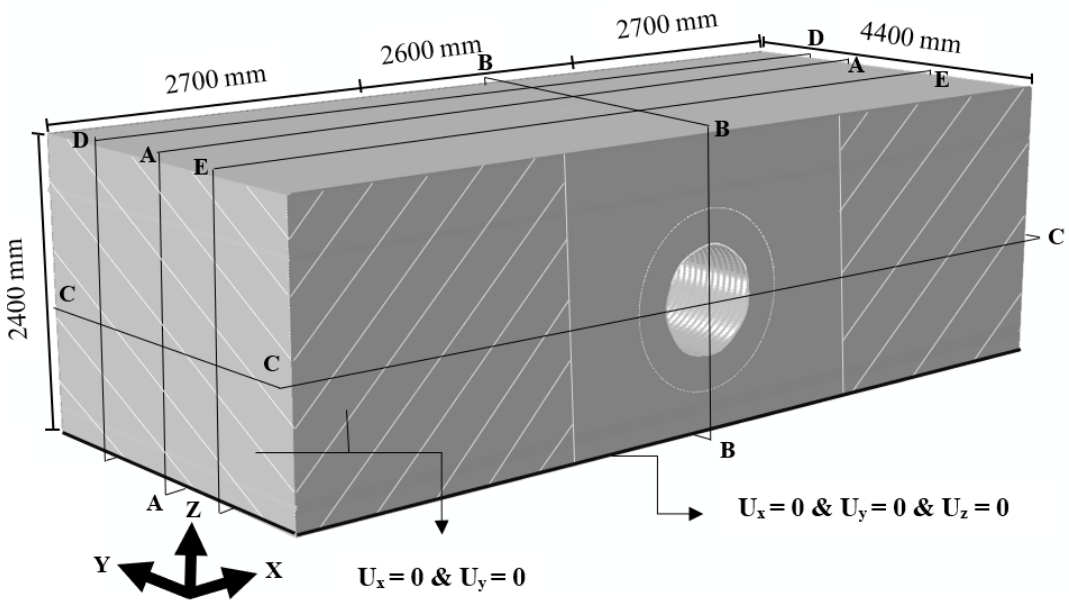

Figure 6.2. Continuum finite element model geometry for the soil backfill domain and kinematic (natural) boundary conditions

The backfill conditions were considered to be poorly graded granular soil (ASTM 2011) with a unit weight of 21 kN/m^3. Table 6.2 summarizes the mechanical properties of the two types of soils that were used in verification study. Soil I is the main soil used in the parametric study. In verification procedure, Soil II is used for soil from invert to crown in the numerical simulation. The defined magnitude for each parameter in **Table 6.2** were based on the conducted experimental full-scale tests and some sensitivity numerical studies (McGrath et al. 1999; Elshimi et al. 2011; Elshimi and Moore 2013).

The plastic response was governed by the Mohr-Coulomb failure criterion with the flow potential was defined as a hyperbolic function in the meridional stress plane and smooth elliptic function in the deviatoric stress plane. A non-associated flow rule was used

in the simulation (Menetrey and Willam 1995; Hibbitt, et al. 2013). The defined modified Mohr-Coulomb model is capable to simulate soil material hardening and softening behaviour due to applied stresses and strains (Atkinson et al. 1977; Wood 1990; Simulia, 2013). A cohesion value of 1 kPa was defined to mitigate issues with numerical convergence.

Table 6.2. Soil material properties

Soil parameters	Symbol	Magnitude, Soil I	Magnitude, Soil II	Units
Young's modulus	E	14.8	14.8	MPa
Poisson's ratio	ν	0.3	0.3	
Angle of friction	φ	43	30	deg.
Dilation angle	ψ	13	0	Deg.
Cohesion	c	1	1	kPa
Unit weight	γ	21	21	kN/m^3

The CSC/soil backfill contact interface was modelled as deformable surfaces with the culvert defined as the master surface for the contact pair. Tangential interface behaviour is used with finite sliding on the contact area is used to model CSC/soil interface (Wriggers 1995; Hibbitt, et al. 2013).

As shown in Figure 6.3, the single axle and wheel pair loadings based on CHBDC guidance is applied as a service load for the soil cover depths examined in this study (Billing and Green 1984; Deng, et al. 2011; CSA-S6 2014). Table 6.3 summarizes the unfactored design load and maximum service load for different cover depth with consideration of the dynamic load allowance for single wheel pair loading. To apply the truck load, the load pad was modeled based on the experimental program and measured 600 mm in length and 250 mm in width (CSA-S6 2014; Peter et al. 2019).

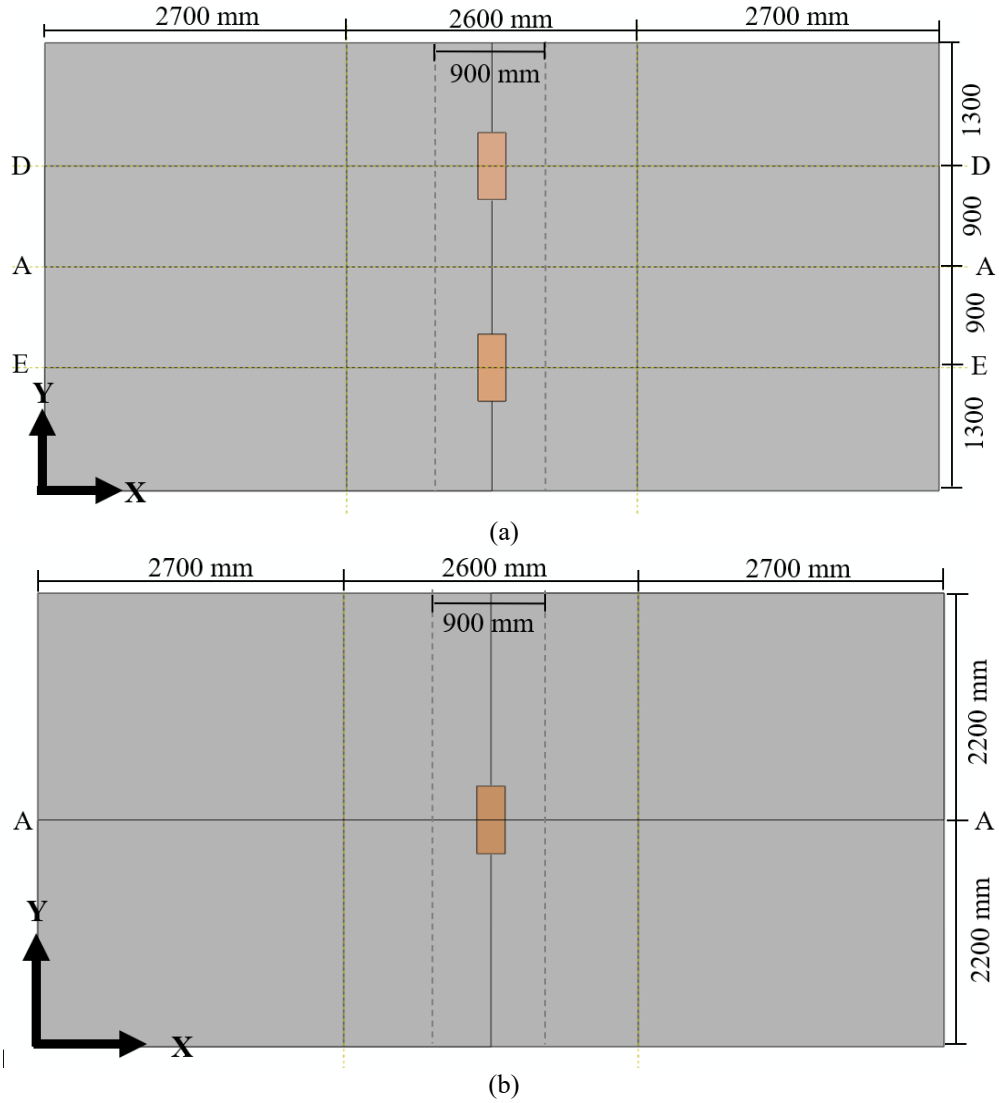

Figure 6.3. x-y plan view of a) single axle loading and b) single wheel pair loading

Table 6.3. Single wheel pair loadings based on CHBDC (CSA-S6, 2014)

Burial Depth (mm)	Unfactored Design Vehicle Load (kN)	Dynamic Load Allowance	Maximum Service Load (kN)
600	87.5	0.28	112
900	87.5	0.22	107
1200	87.5	0.16	102

The effects of soil erosion voids on the predicted CSC mechanical response (i.e., damaged CSC/soil system) and soil backfill stress response is compared with the baseline

simulation of an intact (i.e., non-deteriorated) CSC/soil system. The predicted CSC local force, section moment and displacement response, and the predicted soil pressure distributions were analyzed. Figure 6.4 illustrates the defined spiral path for sampling the CSC strain, local force, and bending moment response for the 3D corrugated culvert profile modelling approaches used in this study (Nakhostin, et al. 2020).

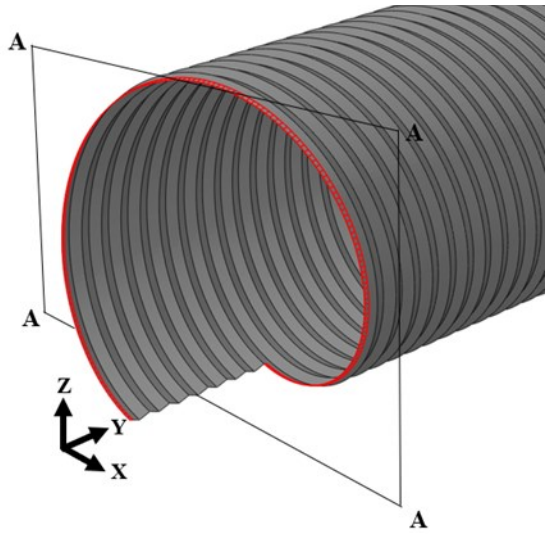

Figure 6.4. Defined spiral path at the mid-length of the pipe parallel to the corrugation of the culvert

Thrust is the dominant force in the soil-culvert structure with shallow corrugated steel plate based on the Canadian code. The code recommends considering flexural effects in deep corrugated plates. The corrugated plate used in culvert modeling in this study is classified as shallow corrugated plate (pitch < 380 mm, and depth < 140 mm), but to meet research objectives, the combined effects of the bending moment and local force are considered in this study and calculated as follows:

Equation 6.1 $$Y = \left[\frac{T}{P_{pf}}\right]^2 + \left|\frac{M}{M_{pf}}\right| \leq 1$$

where T and M are maximum local force and bending moment due to dead and live loads calculated using FE simulations, P_{pf} is compressive strength of a corrugated culvert section, and M_{pf} is moment capacity of a corrugated culvert section (CSA-S6 2014).

6.3 Verification study

The numerical modelling procedures were verified with respect to the horizontal and vertical diameter change response of the deteriorated soil/CSC system based on full-scale experimental tests (Peter et al. 2019). The diameter change of CSC is verified at 189 kN under the single axle load at 900 mm of cover depth. The control pipe test examined the response of the corroded culvert with a 900 mm diameter and 3140 mm length of a buried culvert subject to changes in the service load conditions. The corrugated spiral profile of the control pipe had a depth of 12.5 mm, pitch of 67.7 mm, and nominal wall thickness of 3.5 mm with no deterioration effects (*Profile I* in Table 6.1). The culvert material was conventional steel with an elastic modulus of 200 GPa, yield strength of 230 MPa and ultimate strength of 330 MPa. The soil of bedding, invert to crown, and cover were compacted to almost 88%, 87%, and 93% standard proctor respectively and were classified as a poorly graded sandy gravel soil, “GP-SP”, using the unified soil classification system. The simulated standard single axle was imposed on the ground surface and positioned over the culvert crown (Sections D-D and E-E in Figure 6.3a) and was applied using the wheel pad (250 mm x 600 mm in plan) based on CHBDC for the service load conditions.

Figure 6.5 presents 2D view of the verified model (control pipe) with full-scaled test results conducted at Queen’s university (Peter et al. 2019). The culvert is heavily corroded at the invert from haunch to haunch (with 15% remaining thickness in the numerical

models) and the void is located on one side of the culvert/soil system from the haunch to the springline. These deteriorations are applied along the full length of the culvert/soil system. For modeling erosion void, the void geometry is defined in the backfill soil part and the soil elements have been removed from the backfill soil part in finite element simulation mesh.

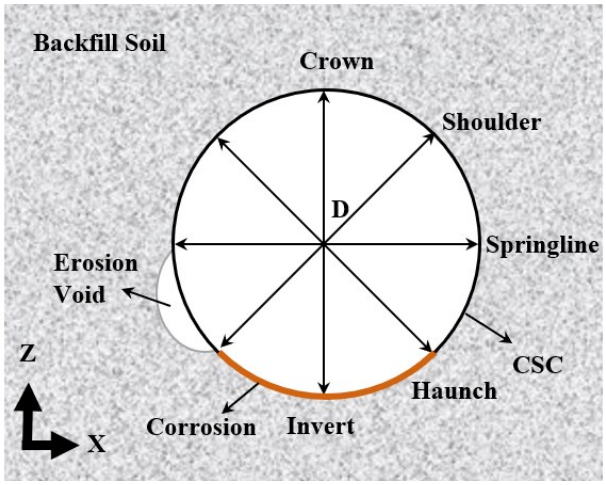

Figure 6.5. 2D representation of the soil erosion void and corroded culvert for Control Pipe verified with the laboratory test conducted by the third party

In the full-scale test, the surrounding soil has been compacted less than the backfill soil (87% versus 93%) to simulate the environment of eroded soil with creation of void. Two models (e.g., *Model 1* and *Model 2*) have been simulated using FEM to replicate the experimental test conditions.

The same parameters, as in verification, are used in the numerical simulations. The responses of two numerical models are compared with the results of full-scale test. In *Model 1*, the material of backfill soil is *Soil I*, and the bedding and circumferential soil material from invert to crown are *Soil II*. In *Model 2*, the soil material for backfill, bedding,

and circumferential soil are *Soil I* (**Table 6.2**). Figure 6.7 presents X-Z view of *Model 1* and *Model 2*.

The verification process in this study focused on numerical predictions of culvert vertical and horizontal diameter change at the end of loading 189 KN.

Figure 6.7 presents the culvert diameter change in vertical and horizontal directions for *Model 1* and *Model 2*, and *Lab Test* obtained through numerical simulations and the experimental full-scale test (Peter et al. 2019).

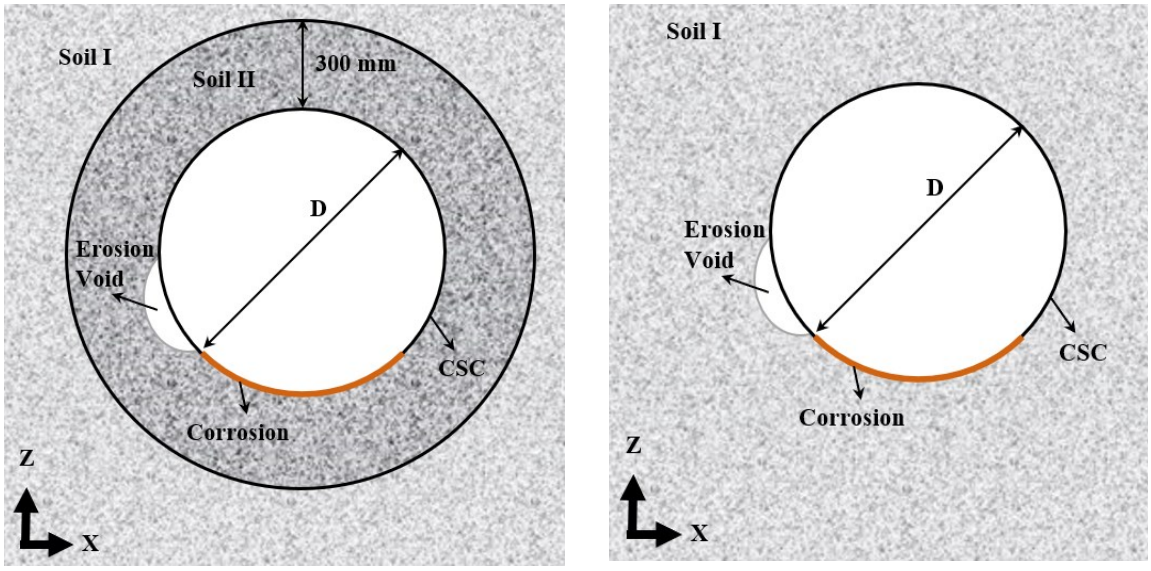

Model 1 *Model 2*

Figure 6.6. 2D representation of the soil erosion void and corroded culvert for Control Pipe verified with the laboratory test conducted by the third party

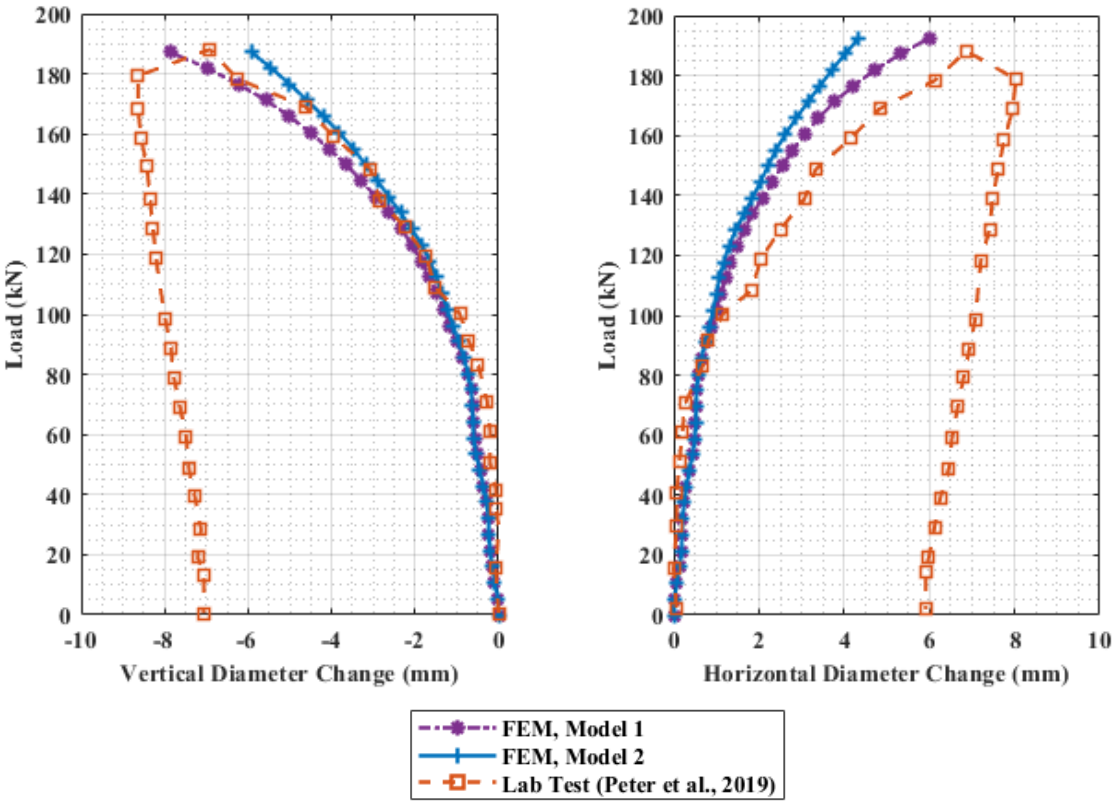

(a) (b)

Figure 6.7. a) vertical and b) horizontal diameter change of culvert under single axle loading

The numerical simulations (FEM) and physical test results (Full-Scale Test) are generally consistent. *Model 1* and *Model 2* predicted culvert vertical diameter change differences of -14% and 14% respectively, and these values were 13% and 36% for horizontal diameter changes, respectively at the end of loading 189 KN. There is a small discrepancy between the FEM results of this study and the Full-Scale Test results. This deviation was attributed to variability in the CSC/soil loading conditions due to unloading activities, which were not accounted for during the finite element simulations.

6.4 Soil erosion void simulations

Soil voids are associated with erosion mechanisms due to hydraulic gradients, pressure and water flow that tend to remove fines within the backfill. The void creation

process is not modelled in this study, and the analysis considers the effects of voids at the present state. The soil voids within the backfill domain are simulated as a discrete geometric feature on or near the CSC/soil interface and was modelled as a non-contact region (Figure 6.8). The soil material used in these simulations are Soil II (Table 6.2) for all sections of backfill soil and for the culvert, Profile II is used (Table 6.1).

The soil erosion void geometry (i.e., volume) is defined by the void depth (d_v) normal to the CSC surface in the radial direction, void angle (β) prescribing the circumferential arc length subtended from the CSC longitudinal axis, and void length (L_v) parallel to the CSC longitudinal axis). The soil void position was defined relative to the CSC perimeter by the location (i.e., crown, shoulder, springline, haunch, invert), and distance from the CSC wall edge (r_v). The soil void erosion features are illustrated in (see Figure 6.8, Figure 6.9, and Figure 6.10 as 3D and 2D graphical representations.

The soil void parameters were based on engineering judgement and consideration of field observations, experimental data, and numerical simulations (Balkaya, et al. 2011, Leung and Meguid 2011, Meguid and Kamel 2014, Wang, et al. 2014, Cichocki, et al. 2021). The soil void was asymmetrically modelled on one-side of the CSC/soil system.

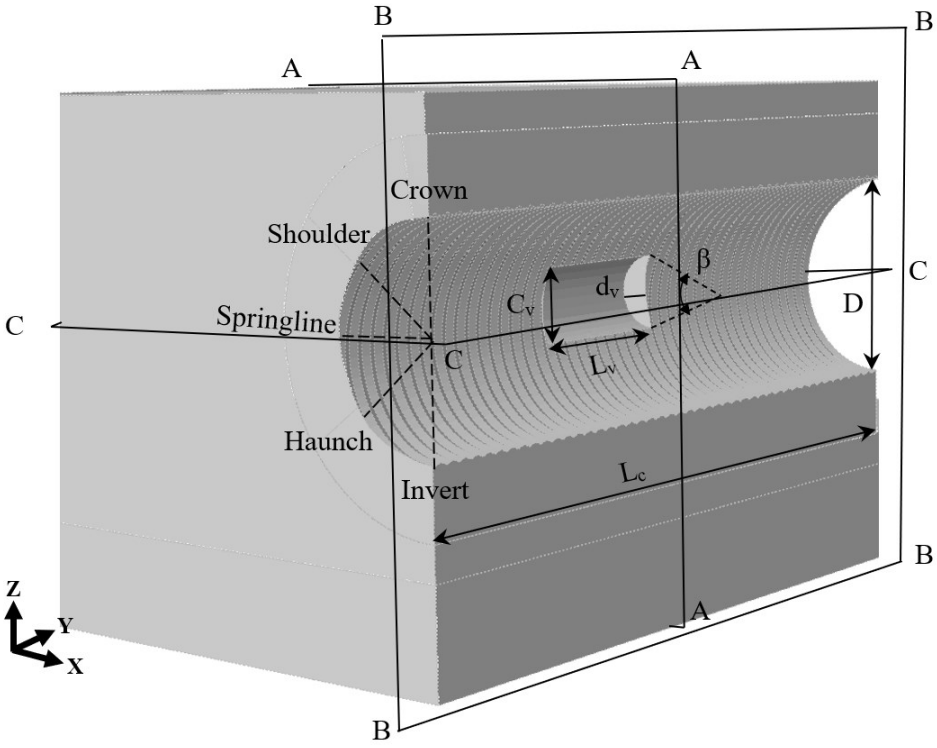

Figure 6.8. 3D view of soil void characterization, Section B-B

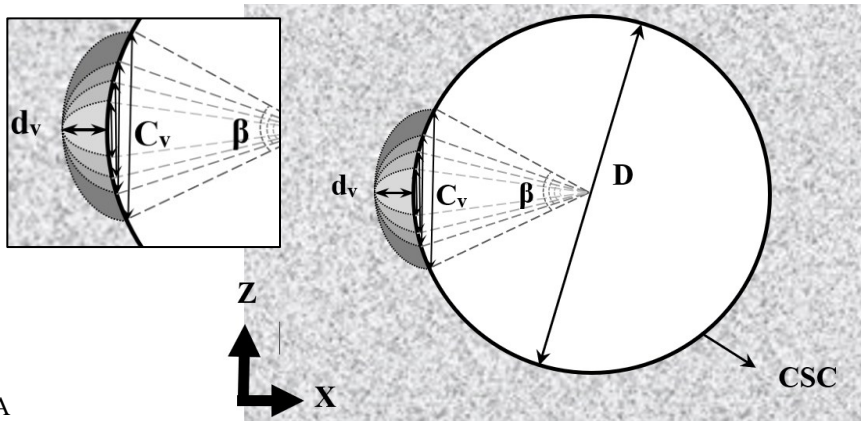

a)Section A-A

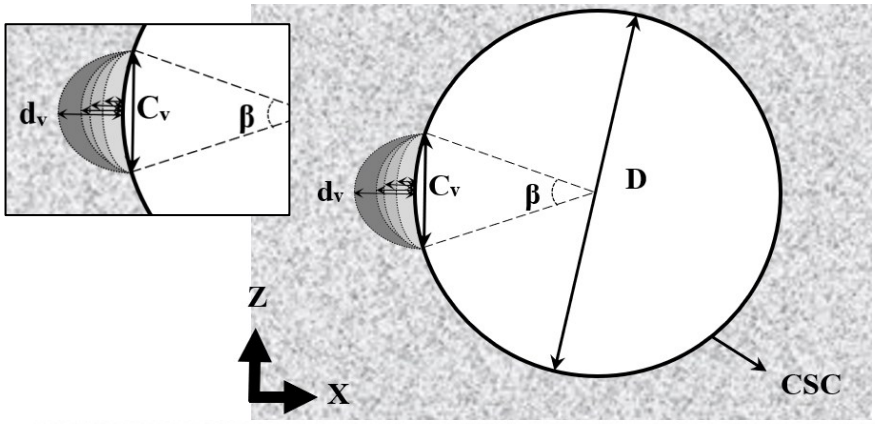

b)Section A-A

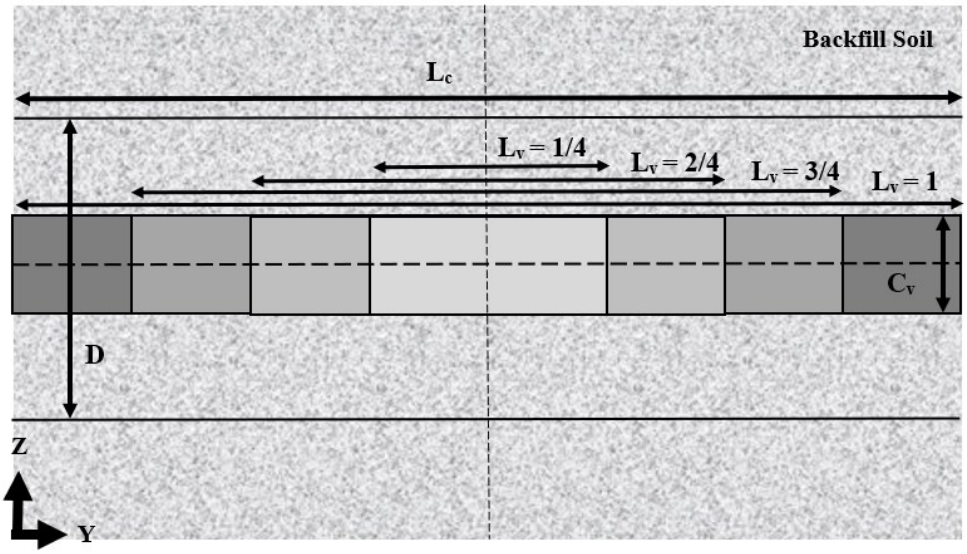

c) Section B-B

Figure 6.9. 2D representation of the soil erosion volume for a change in the void a) angle (β), b) depth (d_v), and c) length (L_v)

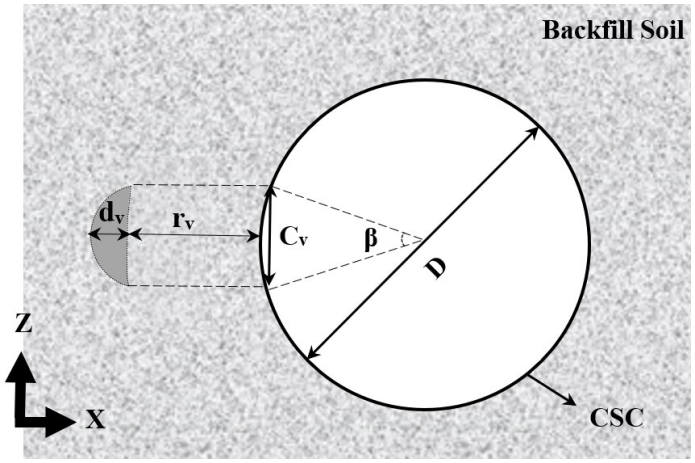

a) Section A-A

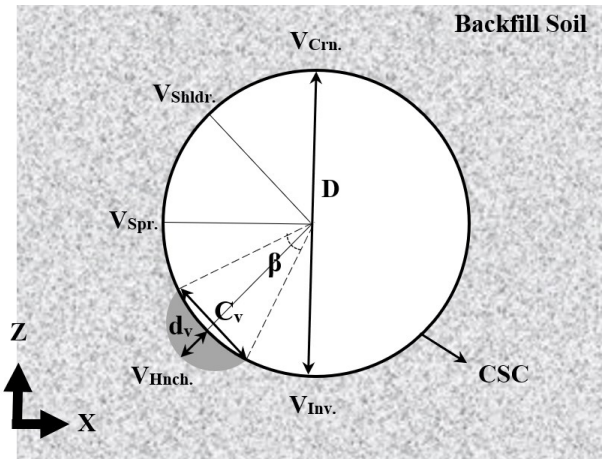

b) Section A-A

Figure 6.10. 2D representation of the soil erosion void position for a change in the void a) distance (r_v), and b) location

6.4.1 Parametric study of erosion void

The baseline parameters for FE models incorporating the soil erosion void are summarized in Table 6.4 that include the void angle (β) of π/4, void depth (d_v) normalized with void chord length (c_v) of 0.5, void length (L_v) normalized with culvert length (L_c) of 1, and void distance (r_v) normalized with culvert diameter (D) of 0 with introduced void at springline.

Table 6.4. Baseline eroded model for sensitivity analysis on soil void geometry and location

Soil Void Parameters	
Void Angle, β (rad.)	$\frac{\pi}{4}$
Normalized Void Depth, $\frac{d_v}{c_v}$	0.5
Normalized Void Length, $\frac{L_v}{L_c}$	1
Normalized Void Distance, $\frac{r_v}{D}$	0
Void Location, $V_{Loc.}$	Springline

A sensitivity study evaluated the influence of each parameter, while all other parameters were kept constant, on the CSC mechanical response (i.e., section force, section moment) for uniform soil conditions (Table 6.2) and specific operational parameters (Table 6.3). The sensitivity analysis (Table 6.5) extended the baseline parameters (Table 6.4) across a range defining the soil erosion void size or volume (i.e., angle, depth, length) and relative position (i.e., distance from the culvert, location on the culvert perimeter). Except for the studies exploring the effects of void length on the CSC mechanical response, the numerical simulations incorporated a soil void length equal to the culvert length (i.e., $\frac{L_v}{L_c} = 1$). A shaded greyscale legend was defined to map the soil erosion void parameter variation (Table 6.5) with the graphical representations (Figure 6.9). A schematic illustration of the soil erosion void position (i.e., distance, location) relative to the culvert is shown in Figure 6.10. The separation between culvert and surrounding soil might happen due to soil washout by flood or heave rainfall. Presence of corrosion deterioration at waterline can also cause this separation between soil and culvert at invert as well. Two auxiliary studies were also conducted to evaluate the effects of a distributed soil erosion void on the culvert

mechanical response (Figure 6.11), which included a distributed soil erosion void extending from the culvert crown to spring line, while the other case examined a distributed soil erosion void extending from the culvert haunch to haunch.

Table 6.5. Parameter range for sensitivity analysis on soil void geometry and location

Figure Legend Colour Key (**Figure 6.9**)					
Soil Erosion Void Parameters	Soil Erosion Void Parameter Range				
Void Angle, β (rad.)	$\frac{\pi}{12}$	$\frac{\pi}{6}$	$\frac{\pi}{4}$	$\frac{\pi}{3}$	
Normalized Void Depth, $\frac{d_v}{c_v}$	0.3	0.4	0.5	0.6	
Normalized Void Length, $\frac{L_v}{L_c}$	$\frac{1}{4}$	$\frac{2}{4}$	$\frac{3}{4}$	1	
Normalized Void Distance, $\frac{r_v}{D}$	1	$\frac{2}{3}$	$\frac{1}{3}$	0	
Void Location, $V_{Loc.}$	Invert	Haunch	Springline	Shoulder	Crown

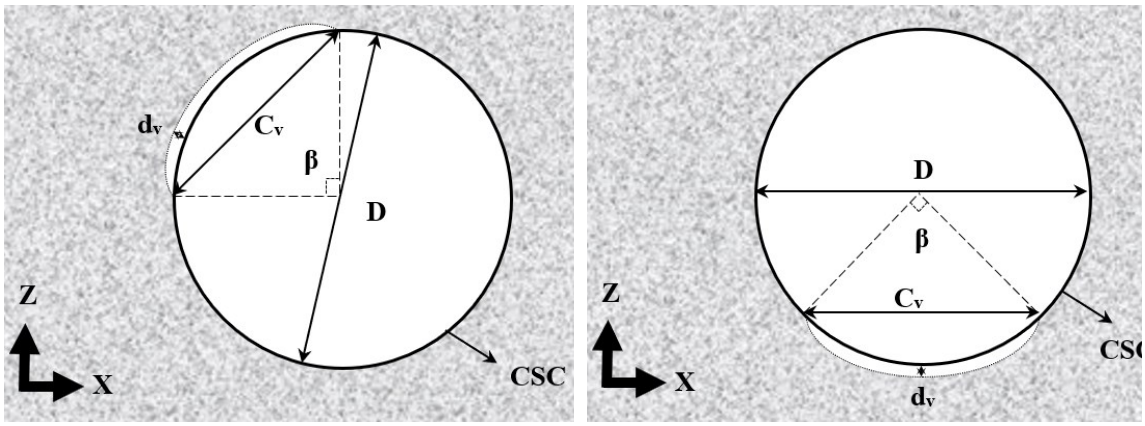

Case 1 Case 2

Figure 6.11. 2D representation of the distributed soil erosion void extending from the culvert crown to springline, and from the haunch to haunch

Figure 6.11 presents two models for evaluating the effect of extended soil voids. The distributed soil void examined the loss of contact due to soil void extending from the CSC

crown to springline (Case 1) and haunch to haunch (Case 2). The Void information for these two cases is presented in Table 6.6.

A total of 24 FE simulations were conducted for the erosion void section that includes 1 simulation to model intact system, 12 simulations to investigate the effect of void geometry (i.e., void angle, depth, and length), 9 FE simulations to assess the effects of void location and distance (Table 6.5), and 2 FE simulations evaluating the effects of an extended soil void (Table 6.6).

Table 6.6. Two particular cases of erosion voids

Soil Void Parameters	Case 1	Case 2
Void Angle, β (rad.)	$\frac{\pi}{2}$	$\frac{\pi}{2}$
Normalized Void Depth, $\frac{d_v}{c_v}$	0.04	0.04
Normalized Void Length, $\frac{L_v}{L_c}$	1	1
Normalized Void Distance, $\frac{r_v}{D}$	0	0
Void Location, $V_{Loc.}$	Crown-Springline	Haunch-Haunch

6.5 Simulation of combined erosion and corrosion deteriorations

Corrosion and erosion deterioration features occur in the culvert invert and surrounding soil simultaneously. The influence of combined deterioration features was examined in this study. The corrosion deteriorations are applied in internal surface of CSC located at invert with different corrosion angles (θ). The general corrosion defined at invert section with 34% remaining thickness. The corroded section length (L_{cr}) is equal to the culvert length (L_c). Two-dimensional *X*-*Z* view of culvert/soil section presented in **Figure**

6.12 for two studied cases and **Table 6.7** presents magnitudes of corrosion deterioration variables.

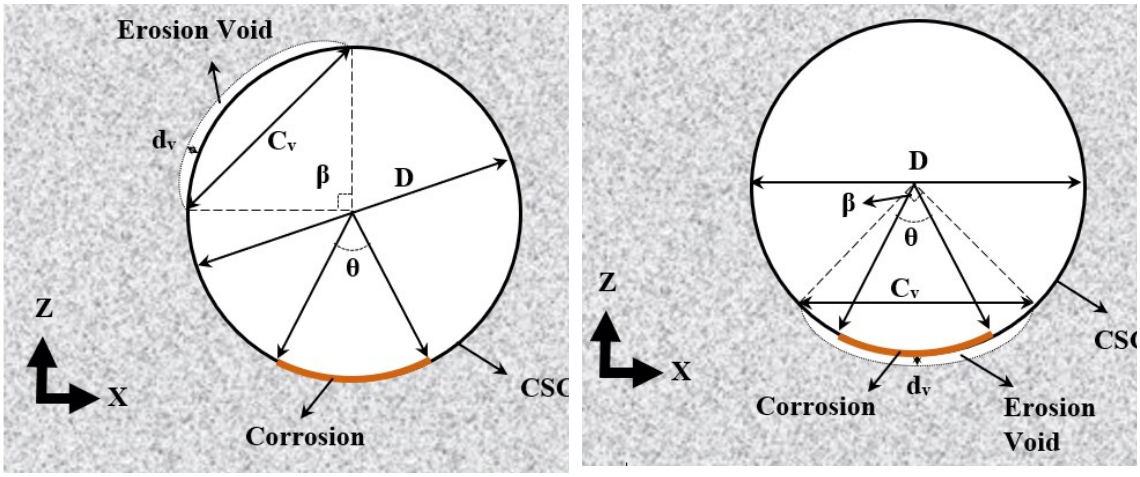

Case 1 & Corrosion Case 2 & Corrosion

Figure 6.12. 2D representation of the distributed soil erosion void and applied corrosion

Table 6.7. Two particular cases of combined erosion void & corrosion

Culvert Corrosion Parameters	Case 1&Corrosion	Case 2&Corrosion
Corrosion Angle, θ (deg.)	90^o *and* 180^o	$45^o, 90^o,$ *and* 135^o
Remaining Thickness (%)	34	34
Corrosion Length, $\frac{L_{cr}}{L_c}$	1	1
Corrosion Location	Invert	Invert

6.6 Results and discussion

Results are presented for each component variation of erosion void (i.e., 3 void geometries, 2 void locations, and 2 extended void profiles), combined erosion and corrosion, and effects of cover depth investigated in the parameter study. The CSC mechanical response with respect to the local force, section moment, combined force and moment, and soil backfill stress response is examined and compared with the intact CSC/soil system.

6.6.1 Soil erosion volume effects (angle, depth, and length)

As shown in Figure 6.13, Figure 6.14, and **Figure 6.15**, the section bending moment and force do not exhibit a perfectly symmetric distribution due to data sampling along the spiral path (Figure 6.4). Across the range of soil void erosion parameters (Table 6.4, Table 6.5) investigated, the culvert section moment and force response was effectively identical to the intact CSC/soil system response for the righthand side (i.e., crown to invert for the 12 to 6 clock positions). Due to the presence of the soil erosion voids, the predicted CSC section moment and force exhibited an asymmetric distribution that was biased on the left-hand side (i.e., clock positions 6 through 12).

Increasing the soil erosion void angle (β), depth (d_v), and length (L_v) increased the predicted section moment and force with the local maximum change positioned near the springline. The soil erosion voids influenced the magnitude and mode (i.e., sense, gradient, distribution) of the CSC section moment and force response. A local maximum change of response was developed that was focused on the culvert springline (i.e., 9 clock position) relative to the intact CSC/soil system predictions. As the soil erosion void parameters increased, and reached the study range limits, the magnitudes of local maximum force and section moment at the springline (i.e., 9 clock position) equaled the peak magnitudes for the CSC/soil system response. Across the range of parameters studied, there were observed differences between the intact and perturbed system for the section moment and force response between the culvert invert (i.e., 6 clock position) and crown (i.e., 12 clock position).

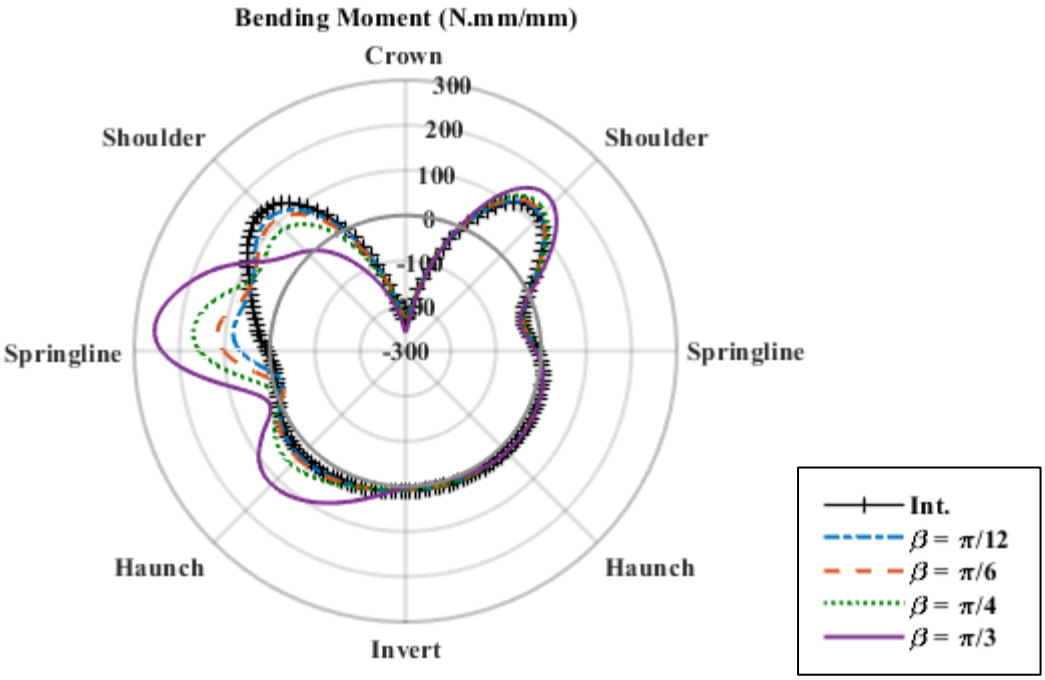

(a)

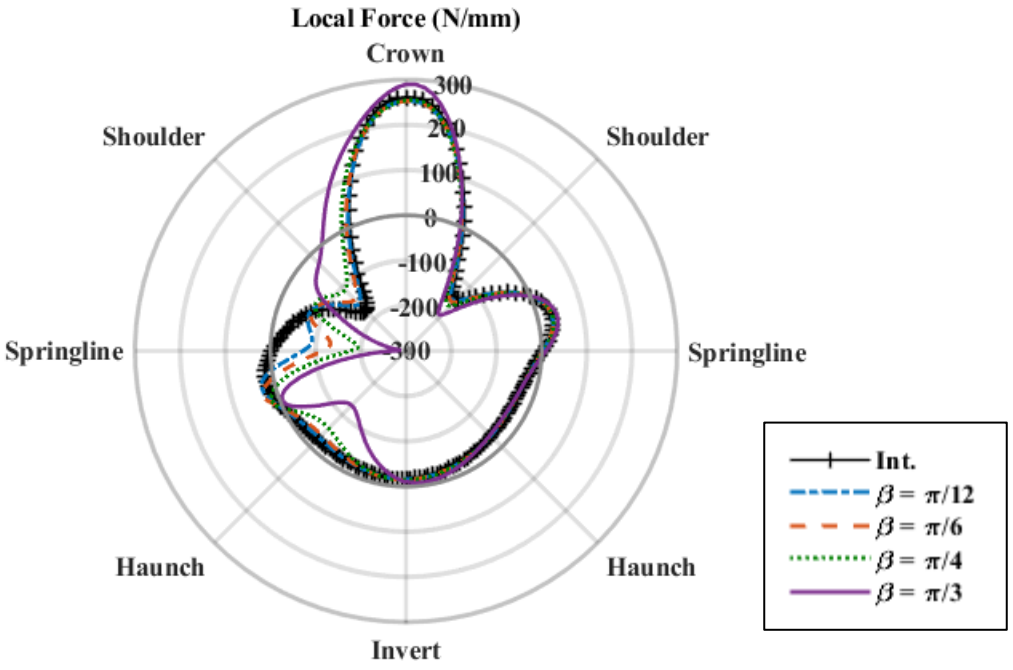

(b)

Figure 6.13. Spiral path distribution of culvert section a) bending moment and b) local force for the intact case and change in void angle (β)

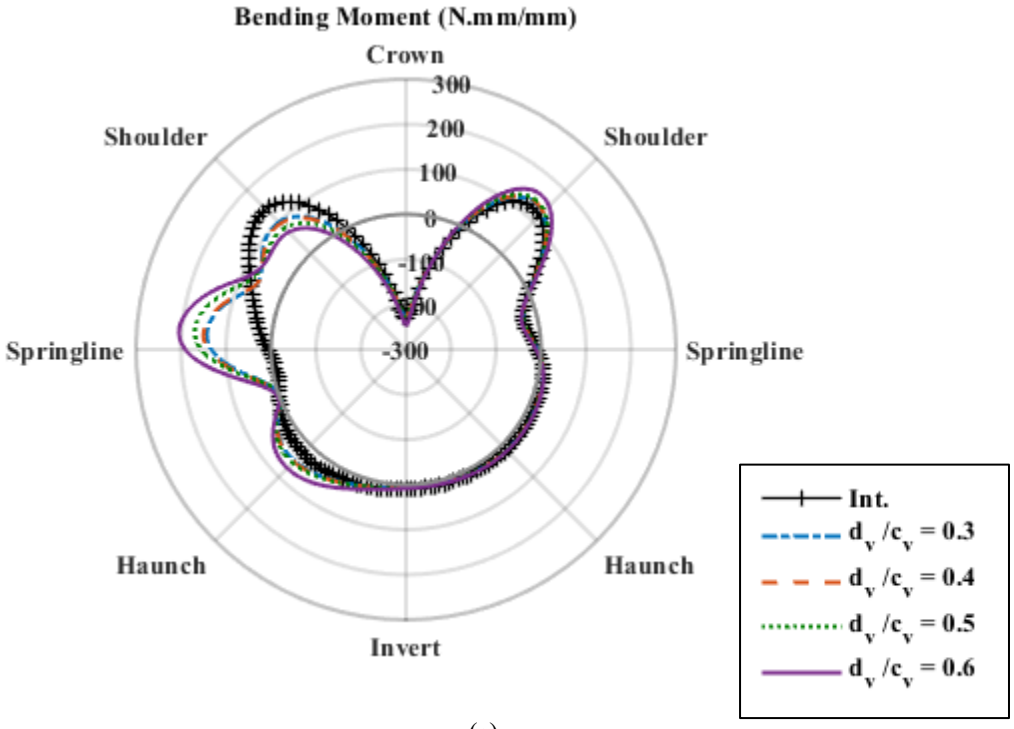

(a)

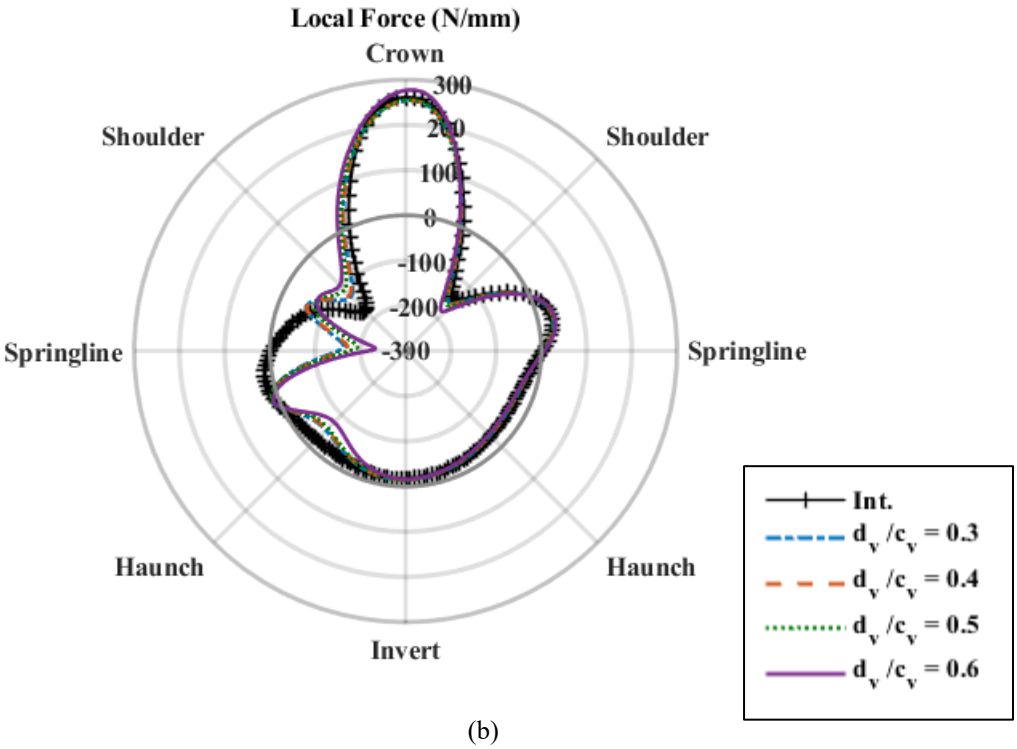

(b)

Figure 6.14. Spiral path distribution of culvert section a) bending moment and b) local force for the intact case and change in void depth (d_v)

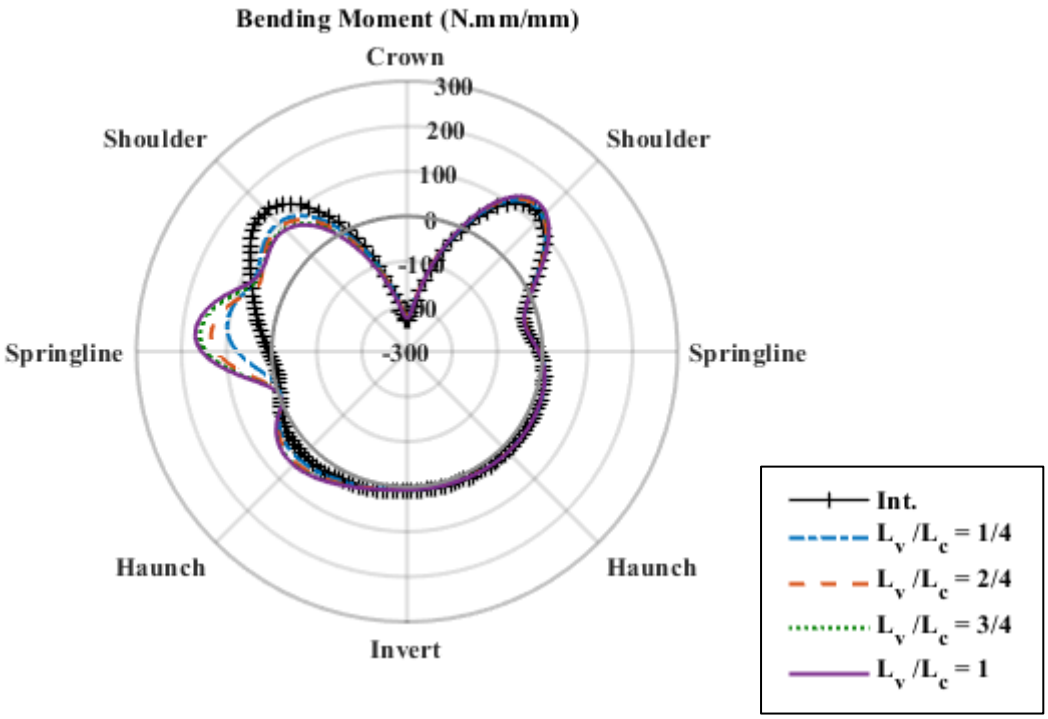

(a)

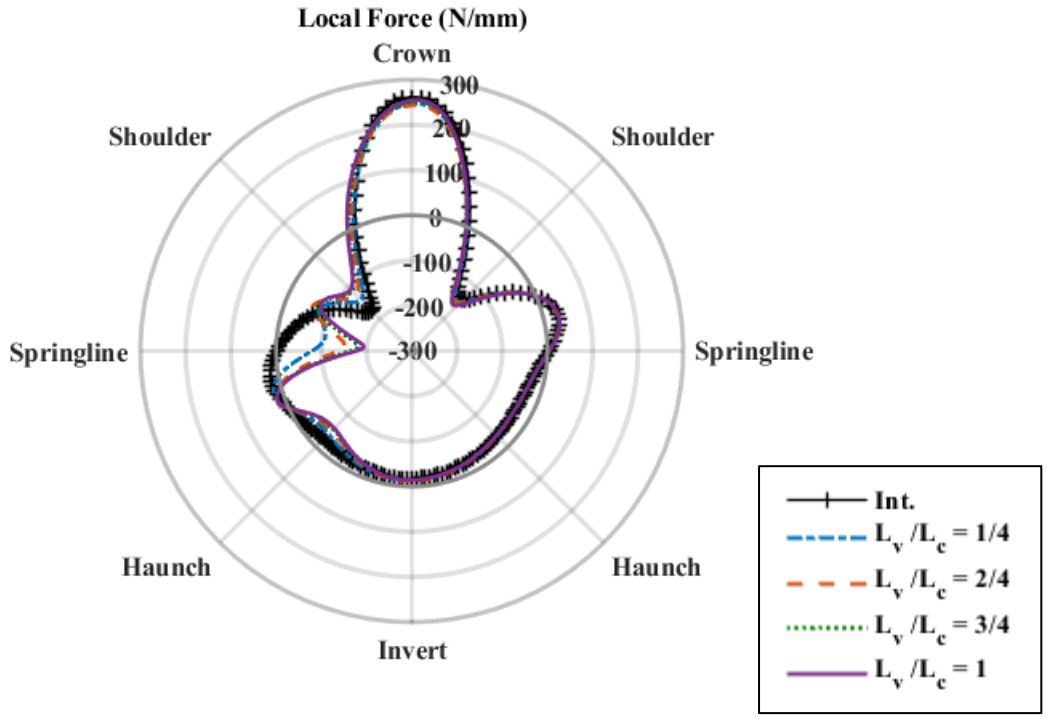

(b)

Figure 6.15. Spiral path distribution of culvert section a) bending moment and b) local force for the intact case and change in void length (L_v)

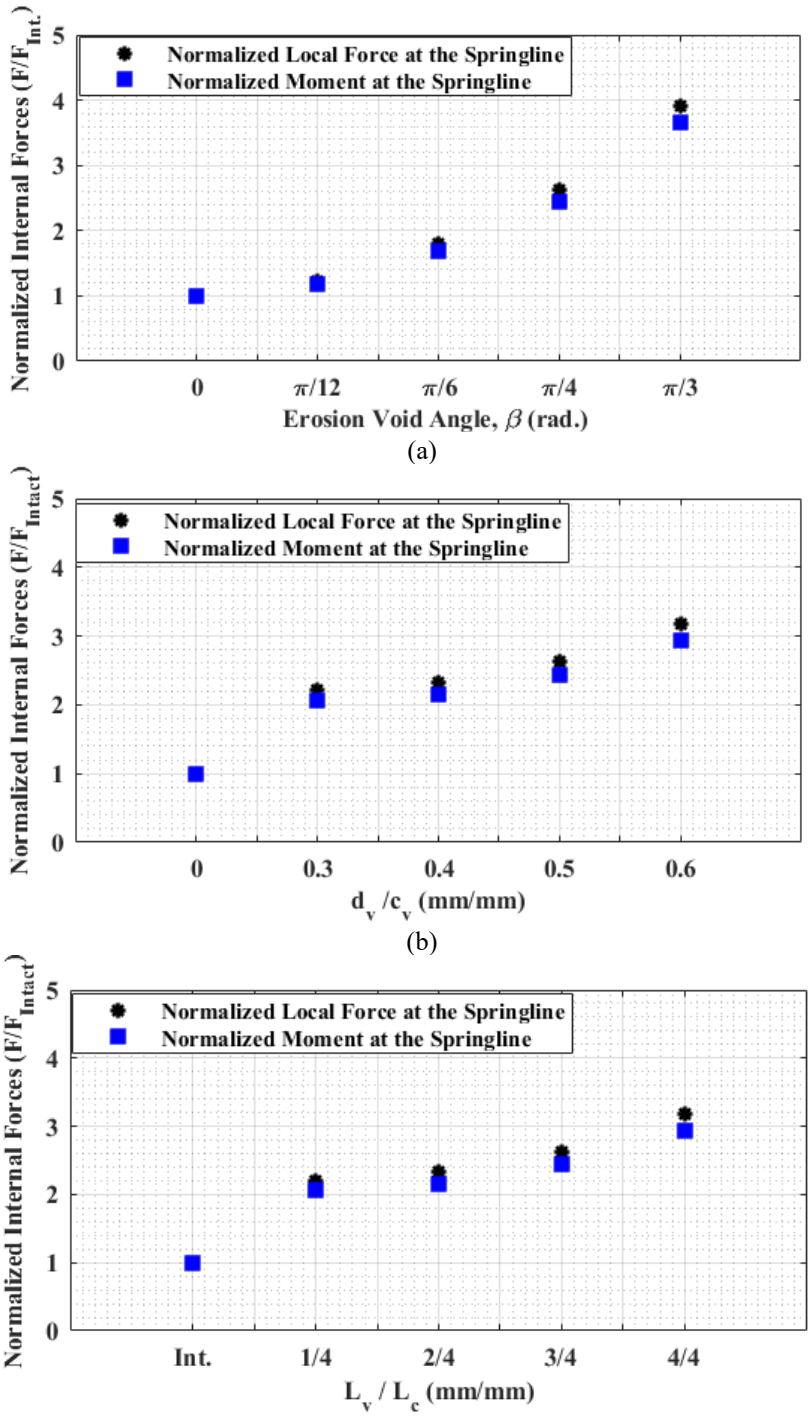

Figure 6.16. Effect of soil erosion void volume on the culvert internal forces, at the springline, normalized with the intact CSC/soil response for a change in the void a) angle (β), b) depth (d_v), c) length (L_v)

For increasing void angle (Figure 6.13), the CSC section behaviour exhibits a more generalized CSC response distributed between the invert and crown and tended to shift the peak magnitude response away from the CSC crown and localize at the springline with a positive section moment and negative force. In response to the culvert section forces and deformation mechanisms, a localized response develops at culvert haunch due to the coupled interaction effects among the soil erosion void, culvert invert and bedding conditions. The soil erosion void depth (Figure 6.14) and length (Figure 6.15) have a localized effect at the introduced void location and there are not noticeable changes in the responses at the crown, invert, and the non-defected half of the culvert.

The spiral path distribution of the culvert section moment and force response (Figure 6.13) indicates, across the range of parameters investigated, that the soil erosion void angle had the greatest influence on the culvert mechanical response. This observation is further explored in Figure 6.16 presenting the variation of normalized internal forces (i.e., normalized section moments and forces) as a function of the soil erosion void volume parameters (i.e., angle, depth and length). The culvert internal forces are normalized with the intact system response where the data is sampled at the culvert springline. Across the range of parameters investigated, a nonlinear response was observed and, for a specific sensitivity parameter, the relative change on section forces was the effectively the same magnitude. The soil void angle (β) exhibited a quadratic influence on the normalized section forces with a maximum multiplier value of (effectively) 4. This indicates the internal forces (bending moment and local force) at the springline are approximately 4 times greater than the intact CSC/soil system response. The soil erosion void depth (d_v)

and length (L_v) initially exhibited a step change in the normalized section forces (multiplier of 2) with a relatively lower gradient and maximum multiplier of 3.

Figure 6.17 presents the effect of void angle on the changes in the circumferential soil pressure. The maximum pressure in the reported section is located at the crown and it approaches zero at lower half following to the invert. The soil pressure is presented on the horizontal axis and the angle from the invert (θ) on the vertical axis is shown in Figure 6.17. The presence of soil voids in the backfill for these modeling sets results in a localized soil pressure response at the void location for models $\beta = \pi/12$, $\beta = \pi/6$, and $\beta = \pi/4$. Erosion void with angle equal to π/3 ($\beta = \pi/3$) has a noticeable impact on the surface load distribution and soil pressure. This model influences the magnitude and mode of the circumferential pressure for the backfill soil over the entire circumference. This result indicates the presence of voids can affect transferring surface load mechanism from ground level to CSC.

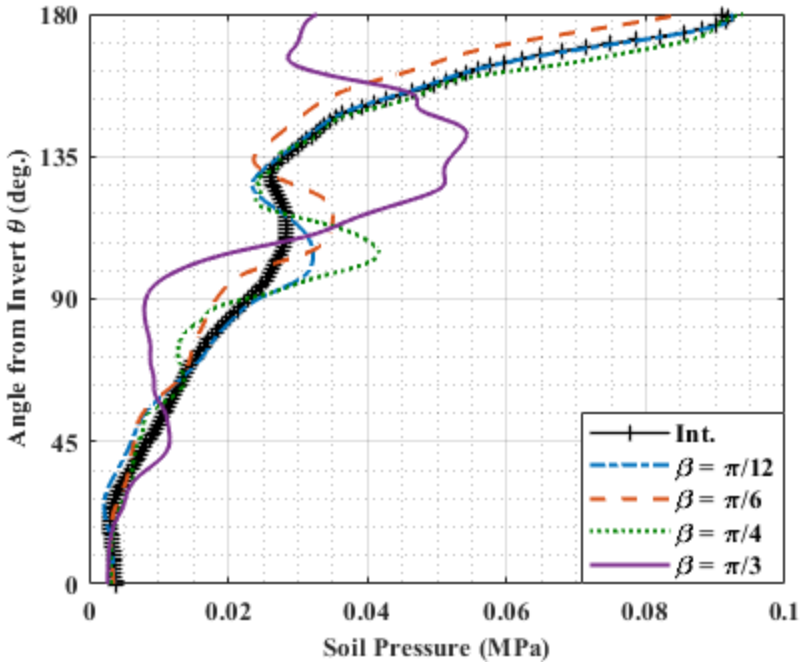

Figure 6.17. Effect of void angle on the changes in soil pressure

Figure 6.18 shows the culvert horizontal displacement at the circumferential spiral path (Figure 6.18a) and at the springline in longitudinal direction (Figure 6.18b) for soil voids with different lengths. The horizontal culvert displacement profile is consistent with the internal force response. The culvert with longest soil erosion void length (equal to the culvert length) experienced the greatest horizontal displacement at the void location and the intact CSC/soil model has the smallest horizontal displacement. All void length cases follow the similar pattern of displacement with maximum value at the mid-length and minimum values at the far ends of culvert length. The voids with finite length have localized effect on the CSC displacement in longitudinal direction and culvert section has a greater horizontal displacement at void location, while other lengths of the culvert that has soil support, approach the intact culvert horizontal displacement. The normalized length of soil erosion void equal to ¼ in Figure 6.18 is consistent with the observed step change in Figure 6.16 where the discontinuity enforces tighter curvature and increases section forces. Continued increasing void length results in greater flexibility and deflection with increased section forces. The reported displacement values are for three-meter length of the culvert and these values reach to zero at the two far ends of the boundary conditions.

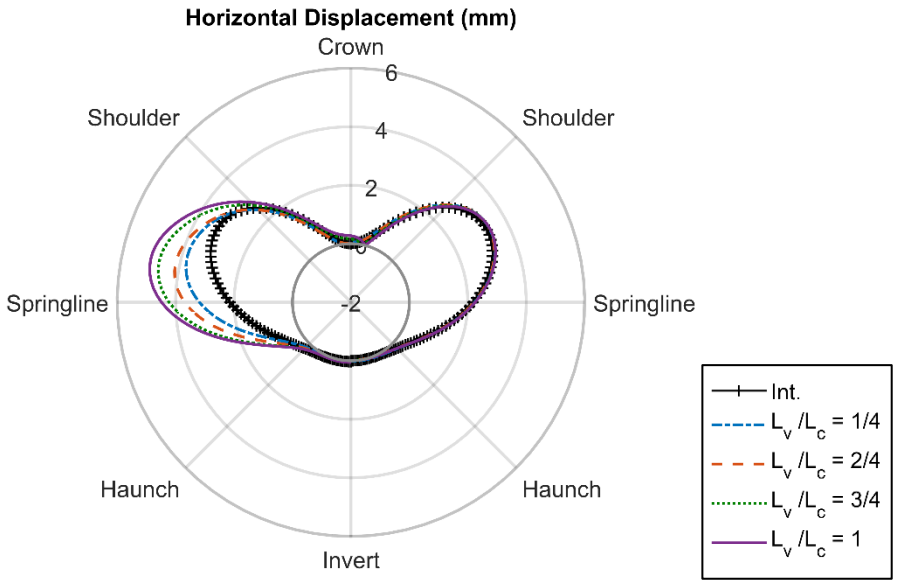

(a)

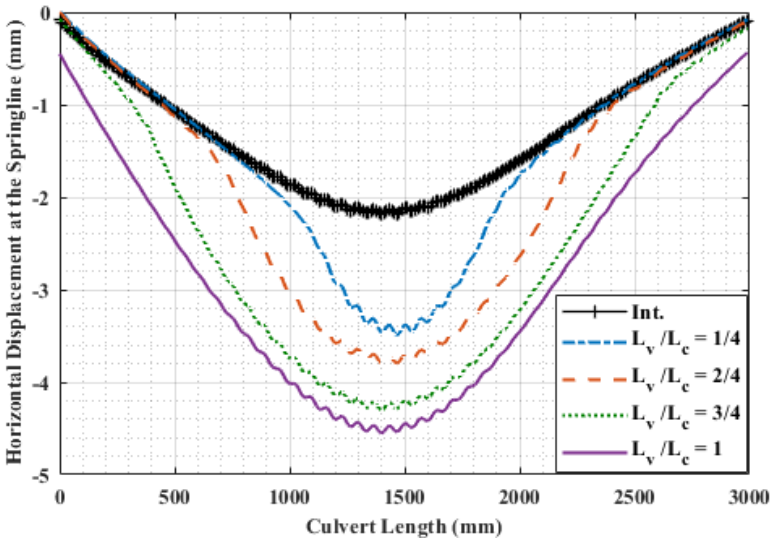

(b)

Figure 6.18. a) Circumferential distribution of culvert section horizontal displacement, and b) longitudinal distribution of the horizontal springline culvert displacement, section C-C

6.6.2 Effect of soil erosion void position (distance and location)

Two void position variables, void distance and circumferential location, are introduced as the independent parameters to study void location effects on the CSC/soil system responses. Figure 6.10a and Table 6.5 present two-dimensional view of the

introduced erosion void at the springline with nonzero distance from culvert wall edge and the assigned values for each parameter related to the void position. The normalized void distance from the CSC wall edge, is the only parameter that is changing for each model. The void distance is normalized with the culvert diameter ($\frac{r_v}{D}$) which is distance of void edge from CSC wall edge as shown in Figure 6.10a with assigned values equal to 1, 2/3, 1/3, and 0 mm distance. Based on the literatures and reports, circumferential location of void is an independent variable that its effect in the CSC/soil responses is investigated in this numerical study. Two-dimensional view of the located erosion void at the haunch as an example of void location and the assigned values for each parameter related to the void size and position are presented in Figure 6.10b and Table 6.5 respectively. Five different circumferential locations are assigned as the void location (i.e., Crown, Shoulder, Springline, Haunch, and Invert).

As shown in **Figure 6.19**, decreasing soil erosion distance (r_v) increased the predicted section moment and force with the local maximum change near the void location (springline) with greater impact for the model with zero distance (r_v / D = 0). The normalized void distance greater than 1/3 do not have a noticeable impact on the culvert mechanical response which is almost equal to the intact CSC/soil responses and the CSC section moment and force responses are effectively identical throughout the non-defected half of the circumference.

The circumferential internal forces of the CSC due to the applied voids in the backfill soil at different circumferential locations are presented in Figure 6.20. Erosion voids located at the invert and haunch have a small local impact on the culvert mechanical response ($V_{Inv.}$ and $V_{Hnch.}$). The presence of soil voids at springline ($V_{Spr.}$) has more

generalized impact on the responses. The presence of soil voids at the shoulder ($V_{shldr.}$) influence the magnitude of the section force and moment response for the CSC practically over the entire circumference. The maximum internal forces for the intact system happen at the crown and shoulder and a small change in the responses of these areas cause a noticeable change in CSC performance. Void located at the shoulder ($V_{shldr.}$) causes increasing internal forces at the crown and shoulder and the culvert experiences yield at the crown and shoulder for the applied service load recommended in the Canadian code. The local force reaches its maximum capacity in the linear elastic phase and has a greater portion in appearance of this plastic behaviour in comparison with the bending moment (Figure 6.20). Results indicate the location of erosion void relative to the culvert is destructive when it is in the upper half of the culvert, and this can cause undesirable deformation and stress concentration in the culvert at crest and trough. This changes the failure mechanism for shallow cover depth which is sensitive to the deterioration conditions. The presence of soil voids at crown ($V_{crn.}$) influence the mode (i.e., direction, distribution) of the section force and moment response for the CSC. The maximum local force and bending moment for the intact system are located at crown which is transferring the surface load to the culvert. Loss of contact between the backfill soil and culvert affects load transferring mechanisms and culvert experiences lower internal forces all over the CSC in comparison with the intact system (Figure 6.20). In contrast with the CSC, soil pressure increases on both side of the erosion void in upper half of the culvert for $V_{crn.}$ and the location of maximum soil pressure is transferred from crown to the shoulder. This change is observed in Figure 6.21 which shows soil pressure in defected half of the model

where the voids are applied. The soil experience maximum pressure somewhere between crown and shoulder for model with void at the crown of culvert/soil structure.

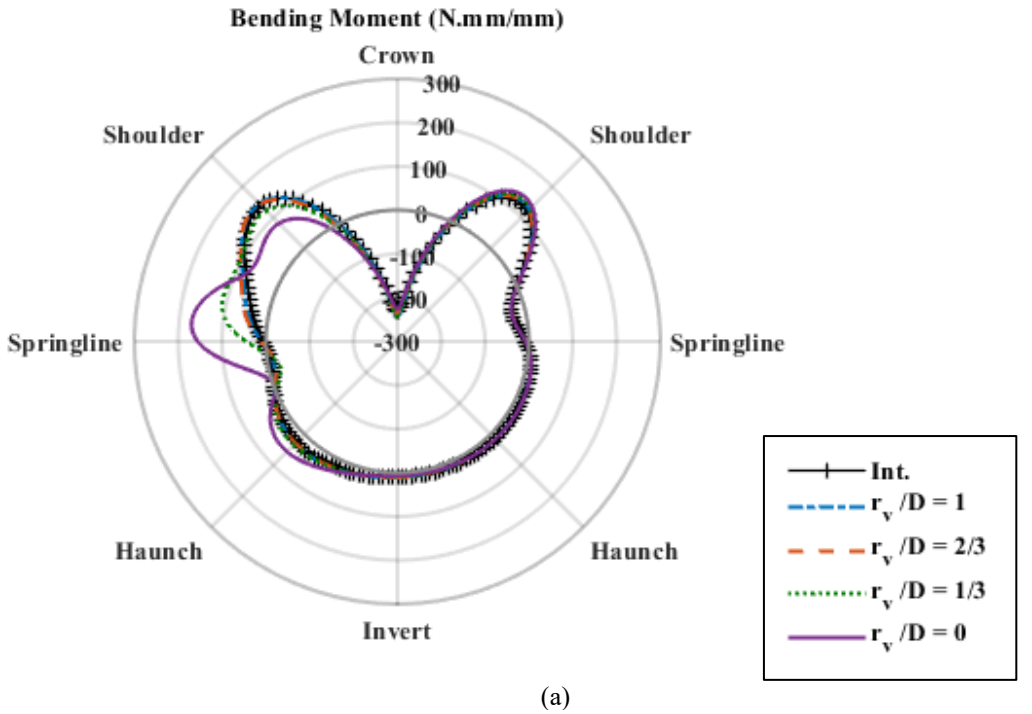

(a)

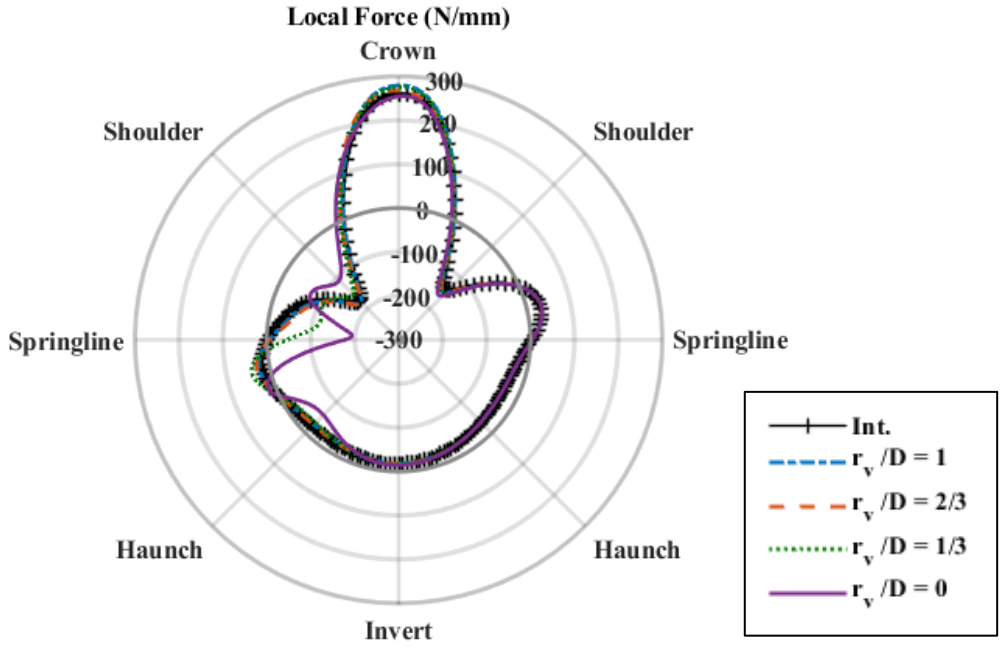

(b)

Figure 6.19. Spiral path distribution of CSC section a) bending moment and b) thrust for erosion voids introduced in the backfill soil with changing void distance (r_v) for each model

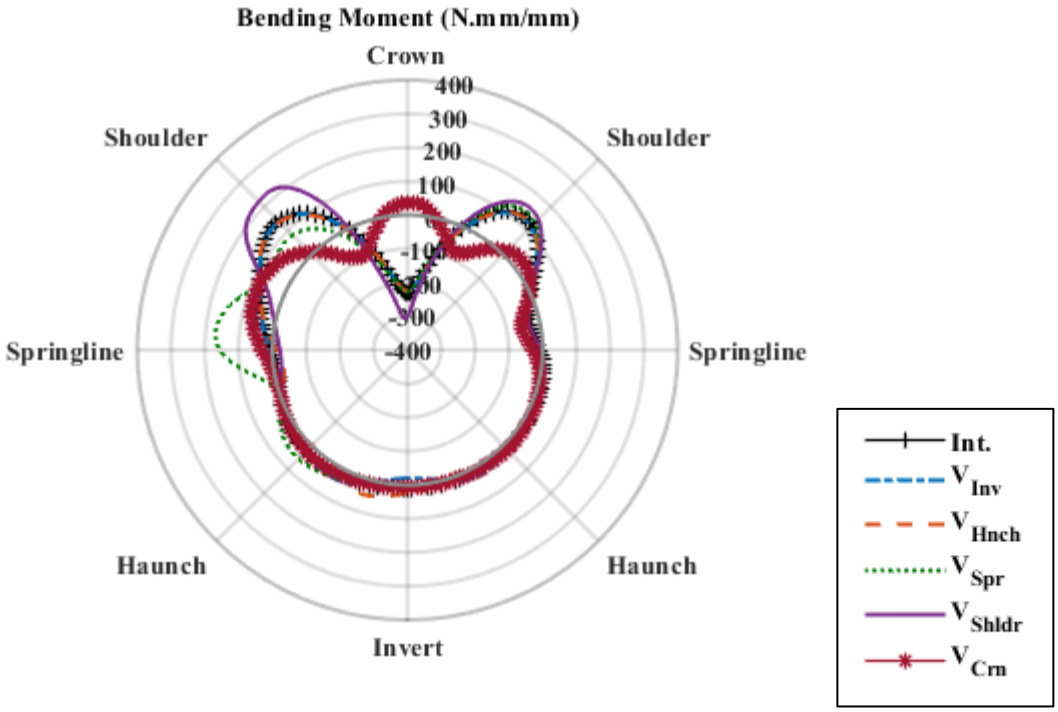

(a)

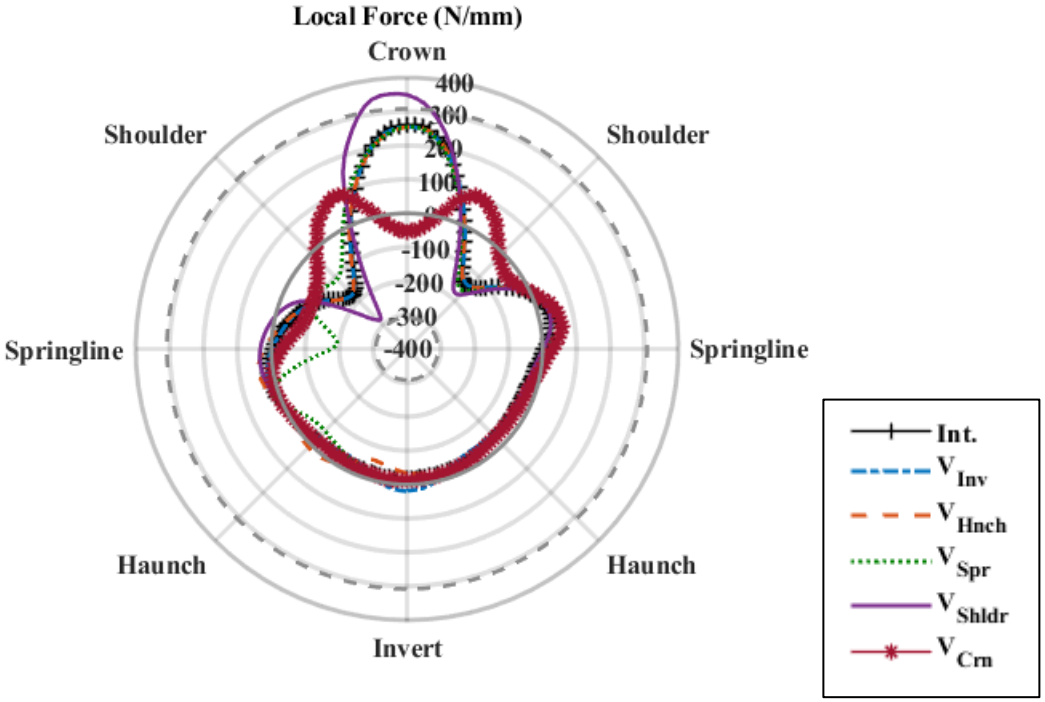

(b)

Figure 6.20. Spiral path distribution of CSC section a) bending moment and b) local force for erosion voids introduced in the backfill soil with changing void location ($V_{Loc.}$) for each model

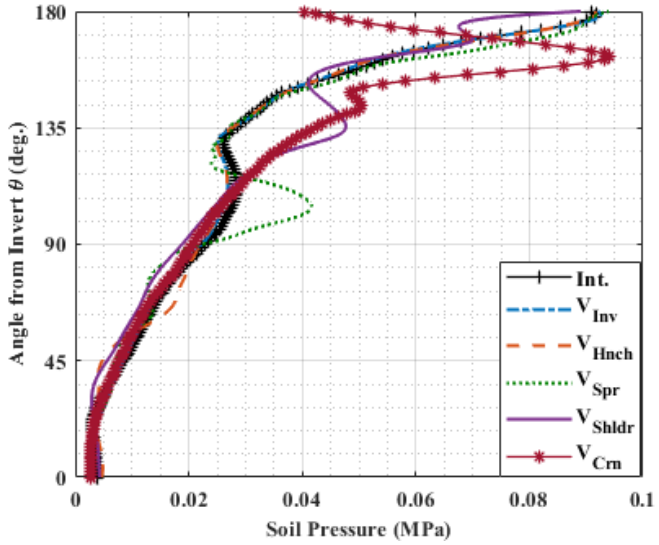

Figure 6.21. Effect of void location on the changes in soil pressure

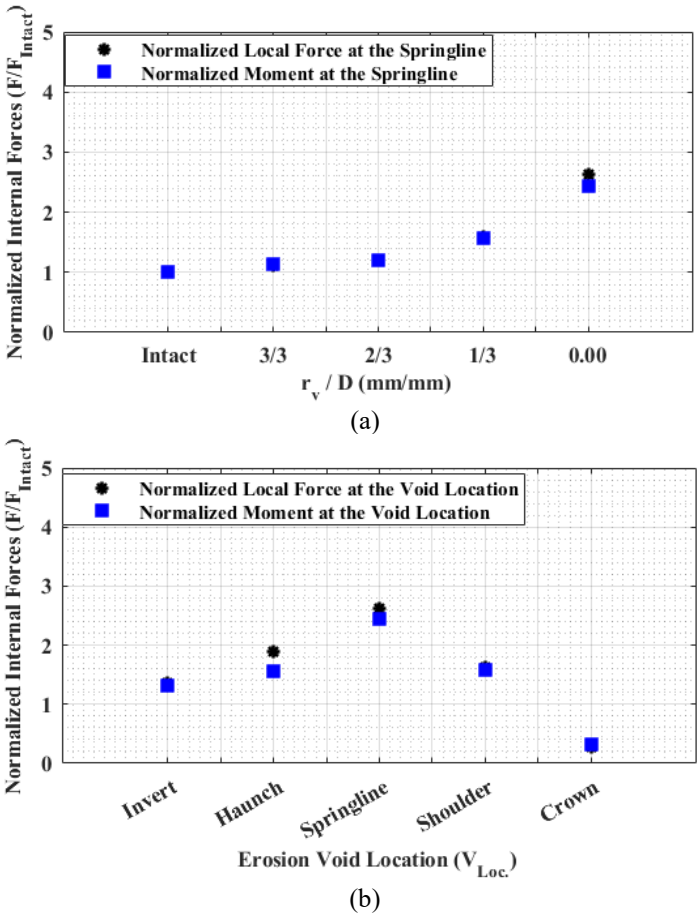

Figure 6.22. Effect of the soil erosion void relative position on the culvert internal forces, at the springline, normalized with the intact CSC/soil response for a change in a) distance (r_v), and b) location

Figure 6.22 presents the variation of normalized internal forces (i.e., normalized section moments and local forces) as a function of the soil erosion void position parameters (i.e., distance, and location). The normalized internal forces of CSC increase at the springline by decreasing the void distance from the CSC (Figure 6.22a). The soil void distance (r_v) exhibited a quadratic influence on the normalized section forces with a maximum multiplier value of 2.5. This indicates the internal forces (bending moment and local force) at the springline are approximately 2.5 times greater than the intact CSC/soil system response.

The significance of the location effect is illustrated in Figure 6.22b. The presence of soil voids at the CSC springline ($V_{Spr.}$) results in a localized increment of the CSC response at the springline (void location) with magnitude equal to 2.6 greater than the internal forces of intact system. Erosion void located at the shoulder increases internal responses at shoulder about 1.6 times in comparison with the intact system. Void located at the shoulder causes increasing internal forces at the crown. The maximum internal forces for the intact system happen at the crown and shoulder and a small change in the responses of this area causes a noticeable change in CSC performance and the culvert experiences plastic strain at the crown and shoulder for the applied service load recommended in the Canadian code (see Figure 6.25). The soil voids located on the CSC crown appears to have greater relative influence on the CSC mechanical response. The maximum local force and bending moment for the intact system are located at crown which is transferring the surface load to the culvert. Loss of contact between the backfill soil and culvert affects load transferring

mechanisms and culvert experiences lower internal forces all over the CSC, about 0.3 at crown, in comparison with the intact system.

6.6.3 Extended distribution of soil erosion voids

Two special cases have been studied in this numerical model, which place more emphasis on erosion void location with a noticeable non-contact region between soil and CSC. At these special cases, erosion void angle is equal to $\pi/2$ with a very limited normalized depth of 0.04, and full-length void as presented in Table 6.6. Based on the literature review and results from this research, the circumferential location of void is specified from crown to shoulder for *Case 1* to represent the contact loss condition in the upper half of the CSC/soil system. The second special case (i.e., *Case 2*) simulates the contact loss in the lower half of the CSC/soil system from haunch to haunch where has lower internal forces in the intact system (Figure 6.11).

The magnitude and distribution of the CSC section bending moment and local force, along the spiral path (Figure 6.4), is presented in Figure 6.23. In comparison with the intact CSC/soil system response, the soil void introduced in *Case 1* influenced the predicted section moment and force, particularly in the upper half of the CSC. The culvert experiences yield at the crown and shoulder for the applied service load and local force in comparison with the bending moment has a greater portion in appearance of yield stress and the local force in the culvert reaches its linear elastic capacity (Figure 6.23b). The results presented for *Case 1* indicates that losing the contact between CSC and soil can cause stress concentration which can lead to failure while the upper half of the CSC/soil system is very sensitive to the deterioration conditions. *Case 2* presents more localized effects in the internal responses of CSC. The culvert experiences small increase of local

forces and bending moments at invert and haunches. These results show that a noticeable contact loss in the lower half of the culvert does not have a significant effect on the general performance of the culvert/soil system.

The circumferential pressure of the backfill soil is presented in Figure 6.24 with increasing soil pressure at crown for *Case 1* and no change of circumferential soil pressure for *Case 2* in comparison with the intact system.

The results of the numerical study, and experimental tests show that the maximum internal force happens at crown and shoulders. The magnitude of the force is very close to the yield value and a small increase in these internal forces will lead to creation of plastic strains (see Figure 6.20b and Figure 6.23b). In this numerical study, two models experience the plastic strain at crown and shoulder that is presented in Figure 6.25. Both models, ($V_{Shldr.}$ and *Case 1*), experience creation of voids in shoulder and crown where is very sensitive location to put the whole system in a weak position. These results show the importance of having non-deteriorated system at upper half of the culvert.

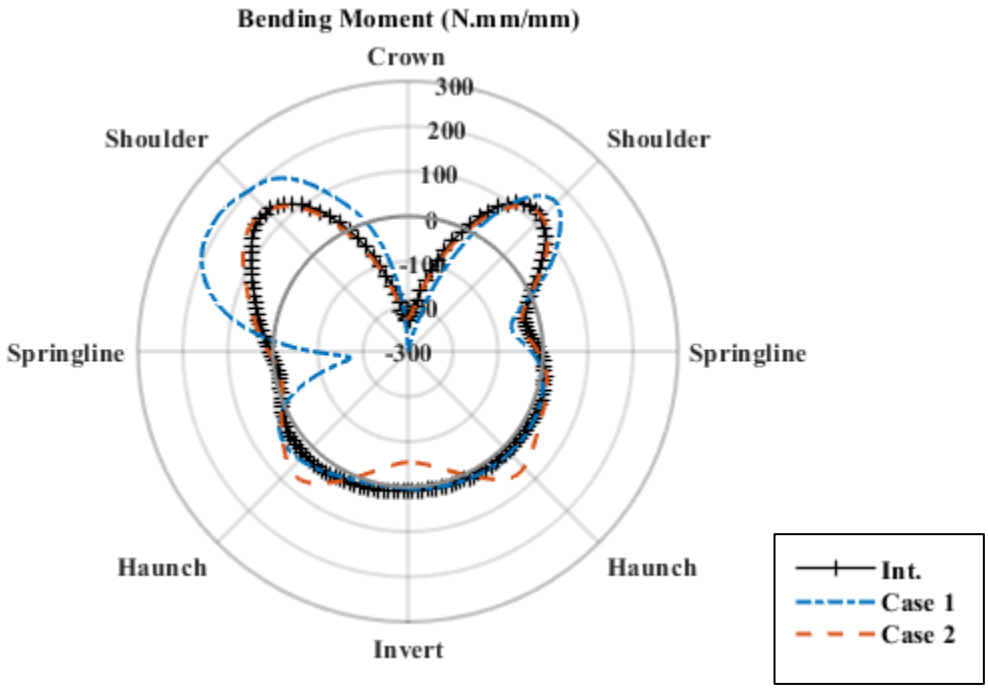

(a)

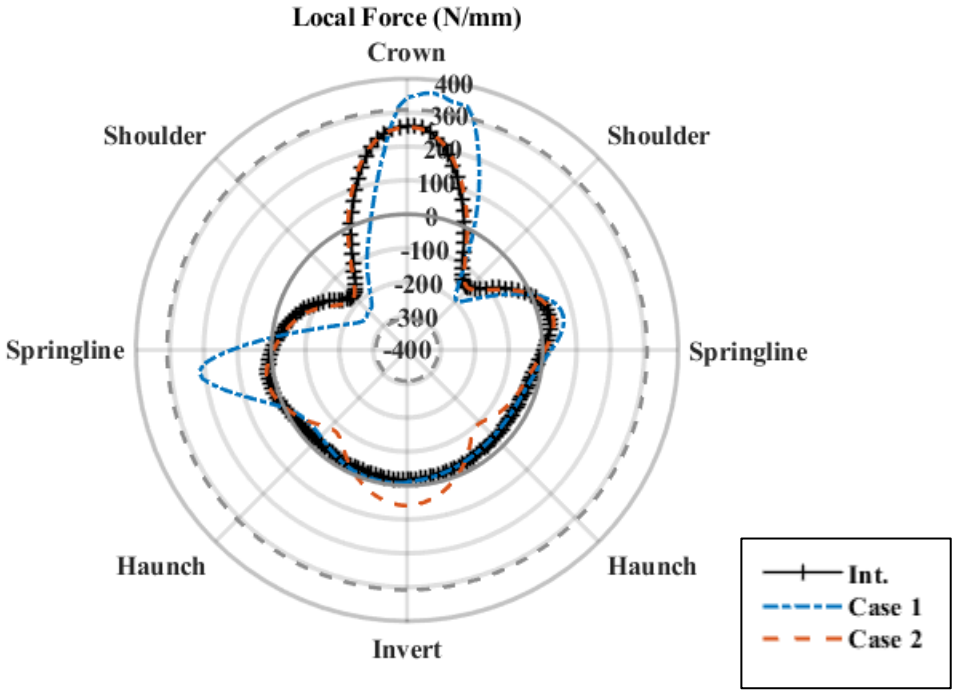

(b)

Figure 6.23. Spiral path distribution of the a) bending moment and b) local force due to an extended soil erosion void

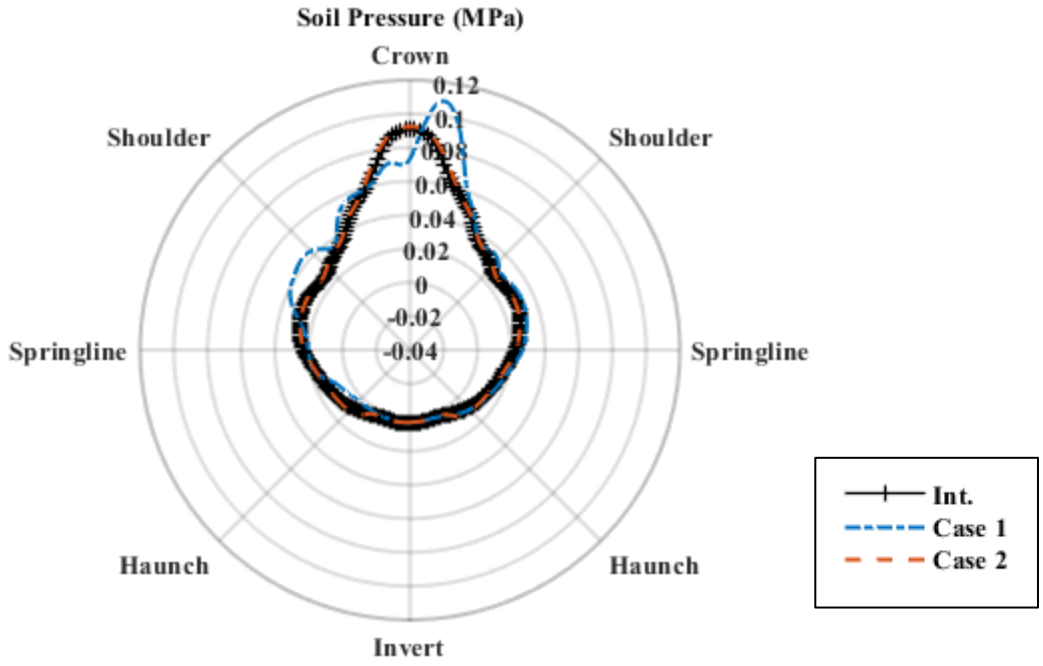

Figure 6.24. Effect of losing contact between soil and culvert due to erosion voids on the changes in soil pressure

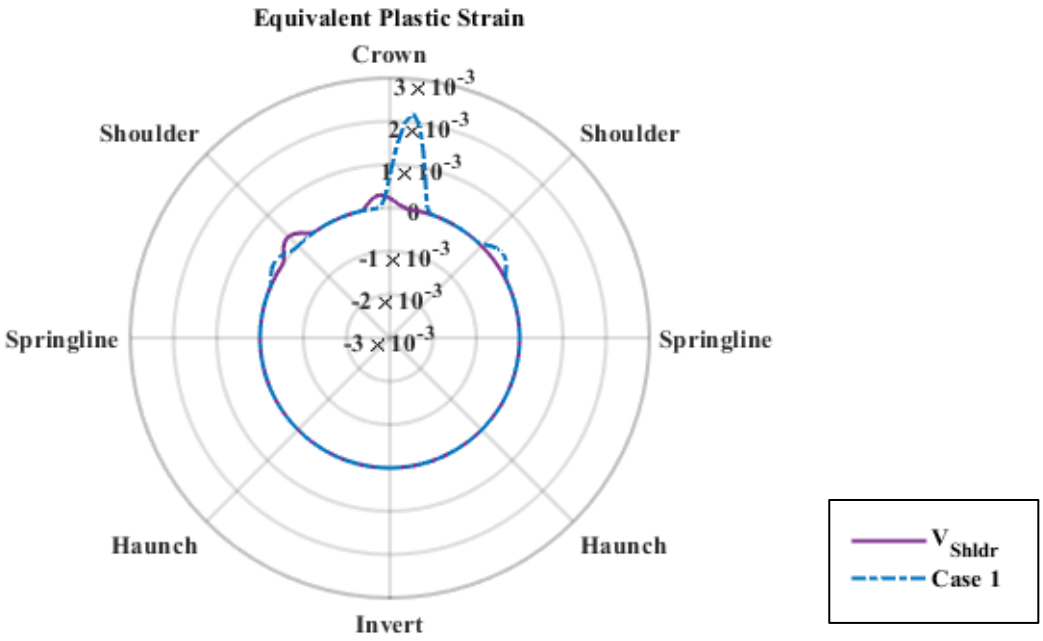

Figure 6.25. Equivalent plastic strain in the spiral path

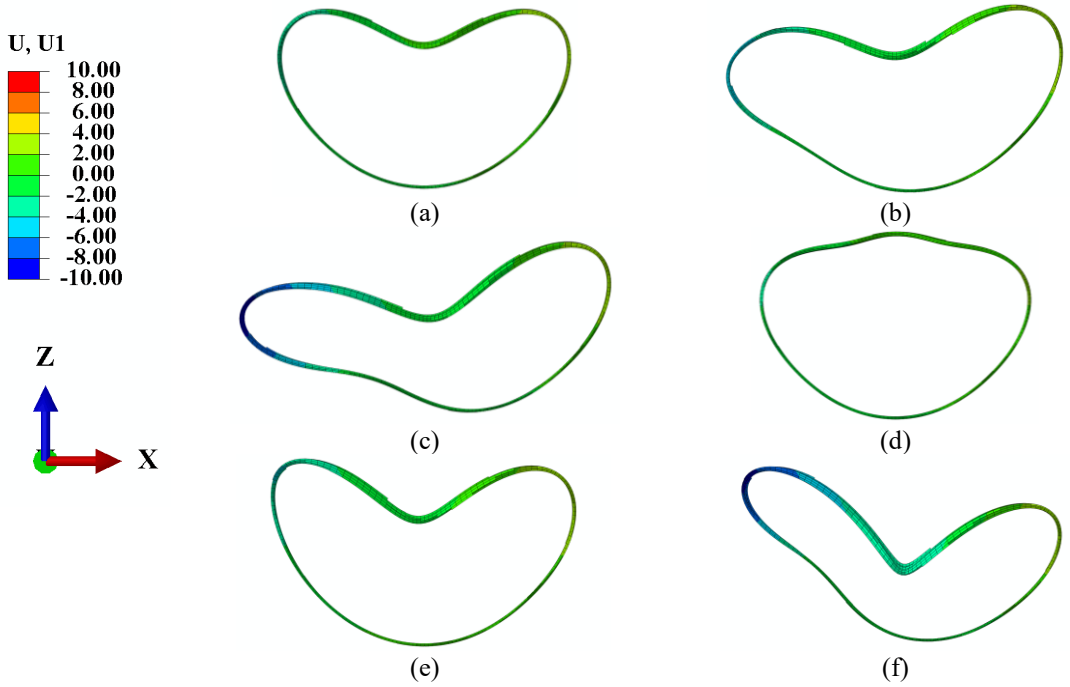

Figure 6.26. Culvert horizontal displacement (mm) for the spiral corrugated profile FE models (×50 magnification factor) for a) Intact culvert/soil system, b) baseline eroded FEM (Table 6.4), c) model with void Angle $\boldsymbol{\beta} = \frac{\pi}{3}$, d) void located at Crown ($V_{Crn.}$), e) void located at shoulder ($V_{Shldr.}$), and f) Case1

Figure 6.26 shows the horizontal displacement of CSC in the mid-length underneath the applied surface load for the selected models with a magnification factor of 50. Figure 6.26a&b shows the dominant mode of the horizontal displacement is heart shape for the intact CSC/soil system and there is an increment in the void location for the baseline eroded model. By introducing greater void angle at springline, the CSC experiences grater horizontal displacement in the void location Figure 6.26c. The presence of soil voids at crown influences the mode of the displacement response for the CSC. The surface load transferring mechanism from ground surface to the culvert is changed and culvert experiences lower displacement specially at crown of the CSC in comparison with the intact system (Figure 6.26d).

The presence of soil voids at shoulder ($V_{Shldr.}$) and special model for contact loss, *Case 1*, are two models that experience plastic strain at crown and shoulders. The horizontal displacements of these two models are presented in Figure 6.26e&f. Figure 6.26a&e indicates that the shoulder is very sensitive location to have a defect and the presence of soil voids at shoulder only influence the magnitude of the displacement which leads to creation of the plastic hinges at the shoulder and crown. Increasing length of contact loss between soil and culvert in *Case 1* leads to more severe displacement magnitude change (Figure 6.26f).

6.6.4 Combined erosion and corrosion deteriorations

The combined effect of erosion void and corrosion is considered for two models of eroded soil (*Case 1* and *Case 2*). The corrosion deteriorations for both cases are applied at the invert with 34% remaining culvert thickness. **Figure 6.27**a, presents the circumferential values of $Y = \left[\frac{\mathrm{T}}{P_{pf}}\right]^2 + \left|\frac{\mathrm{M}}{M_{pf}}\right|$ for spiral path under the wheel load section (**Figure 6.4**) for Intact model (non-deteriorated culvert-soil system), model *Case 1* deteriorated by erosion (erosion void from crown to springline at the left side), and model *Case 1* for erosion plus corrosion with angles equal to 90° and 180°. The results indicate that circumferential *Y* is approaching to the value equal to one at springline and shoulder in the left side deteriorated by erosion void and this value is greater than one at the crown. Applying corrosion deterioration at invert (e.g., *Case1 & θ=90º* and *Case1 & θ=180º*) does not have significant effect in the predicted response.

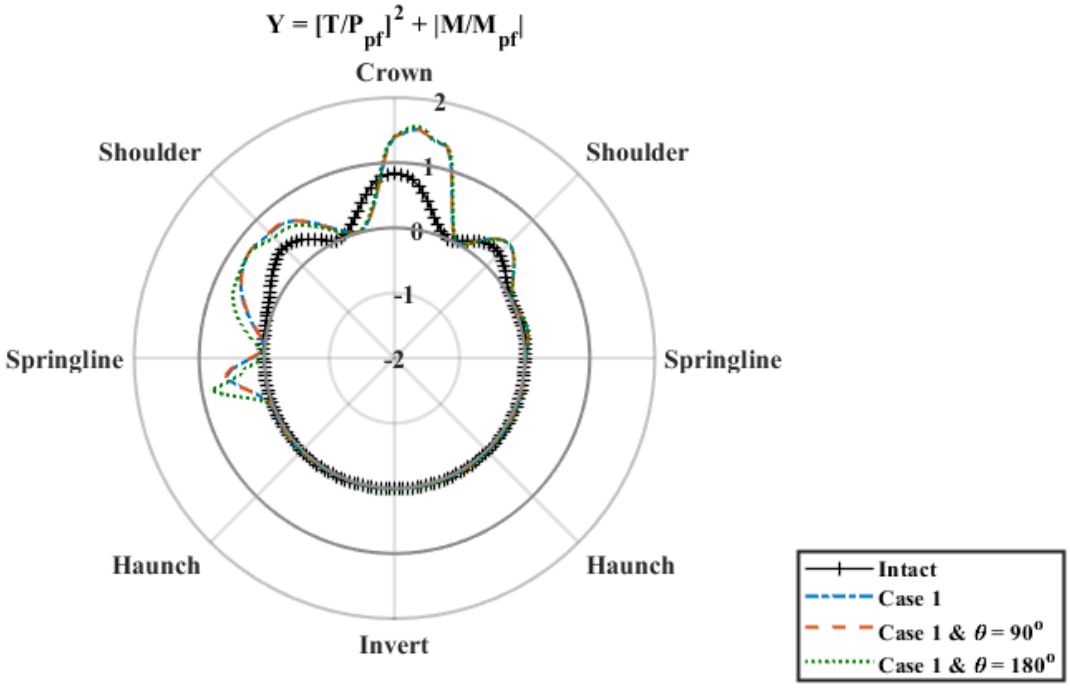

(a)

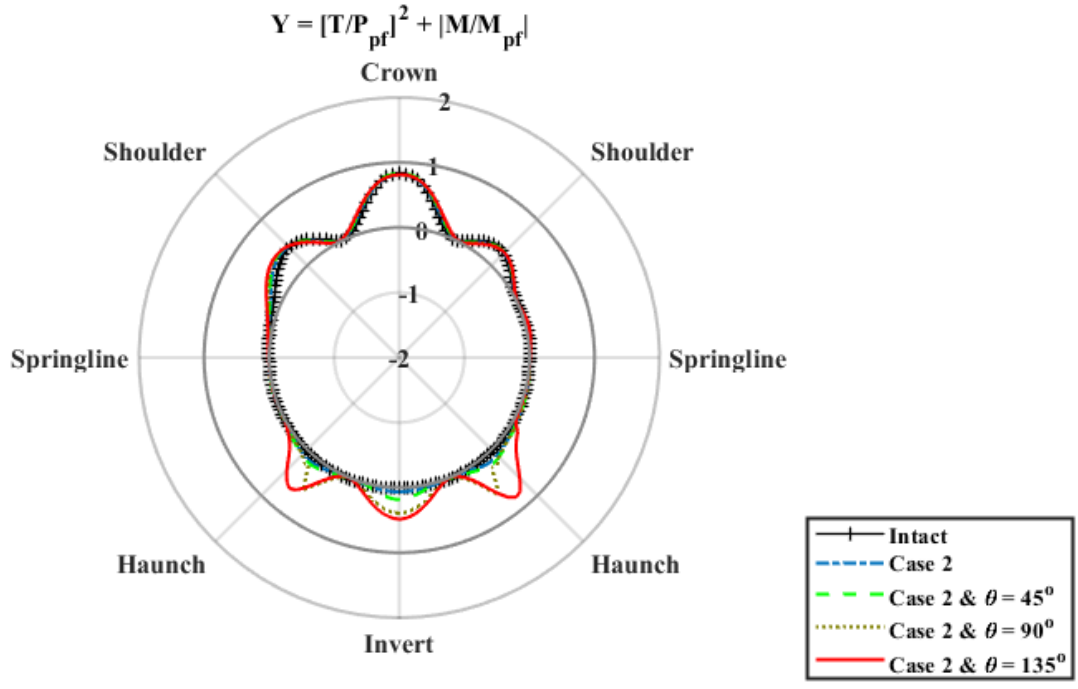

(b)

Figure 6.27. Magnitude of $Y = \left[\frac{T}{P_{pf}}\right]^2 + \left|\frac{M}{M_{pf}}\right|$ for CSC for the defined spiral path, at the culvert mid-length for applied erosion and corrosion deteriorations a) Case1 & Corrosion, and b) Case 2 & Corrosion

Figure 6.27b presents the circumferential values of Y for Intact model (non-deteriorated culvert-soil system), model *Case 2* deteriorated by erosion (erosion void from haunch to haunch), and model *Case 2* for erosion plus corrosion with angles equal to 45°, 90° and 135°. The results indicate that having only erosion voids at the lower half of the culvert does not have significant effect on responses and Y value remains close to zero. The results indicate that the concurrent presence of corrosion and erosion voids affects load and moment carrying capacity with respect to the reduction in the culvert thickness and this changes the load distribution. However, having only erosion void (e.g., *Case 2*) at lower half of the culvert which experiences lower internal forces in comparison with upper half, does not have a significant effect in the general behaviour of the buried culvert. The culvert experiences severe increase in Y responses for the cases that both erosion void and corrosion are applied at the same location. These results show that the appearance of both deteriorations in the lower half can increase the possibility of culvert failure in the lower half remarkably.

6.6.5 Cover depth effects

The burial cover depth is one of the influential variables that affects the CSC response. Two different cover depths have been studied in addition to the cover depth of the base model which is 900 mm. The numerical model for studying cover depth includes both erosion void and corrosion deteriorations in the numerical simulations. The introduced erosion void is model Case 2 with corrosion at invert with angle equal to 135 degrees ($Case\ 2\ \&\ \theta = 135°$), required information for these deteriorations are presented in Table 6.6 and Table 6.7. Three cover depth (e.g., 600, 900, and 1200 mm) with 900 mm culvert diameter considered in this study that all are in the shallow cover depth category and Table

6.3 presents applied single wheel pair for each cover depth considering dynamic load allowance.

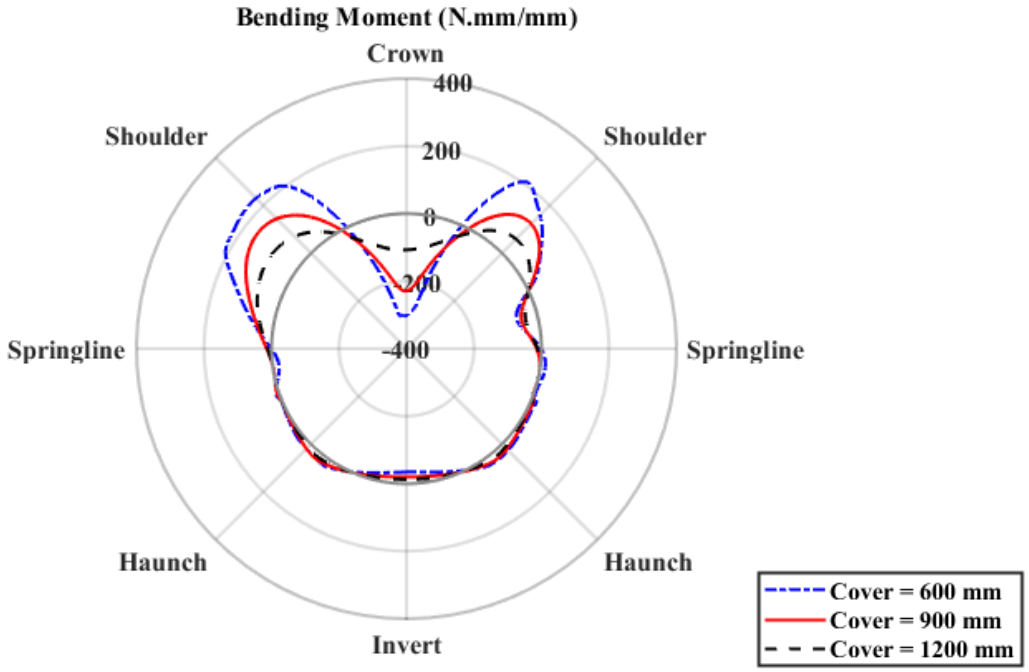

(a)

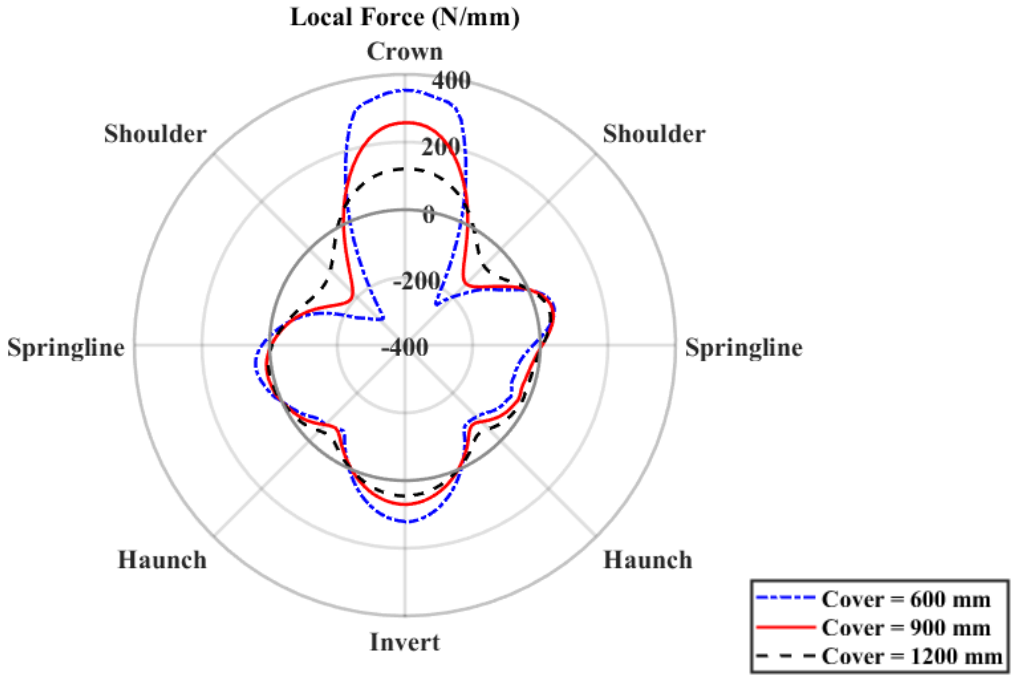

(b)

Figure 6.28. Variation in a) bending moment and b) local force for different cover depth

Figure 6.28 shows the circumferential bending moment and force for the defined spiral path (Figure 6.4). The general mode response is not affected by changing cover depth. The culvert experiences higher bending moment and force at crown and shoulders for buried culverts in shallower cover depths. The bending moment at lower half of the culvert shows very small increases of response for shallower cover depths (e.g., 600 mm and 900 mm). But this affects the culvert force more at invert and haunches. The bearing capacity of culvert is decreased because of the sectional thickness loss (remaining thickness is 34% in this study) due to corrosion and small increase of responses in this section causes the culvert to experience $Y = \left[\frac{T}{P_{pf}}\right]^2 + \left|\frac{M}{M_{pf}}\right|$ greater than one at invert and crown. This result is presented in Figure 6.29.

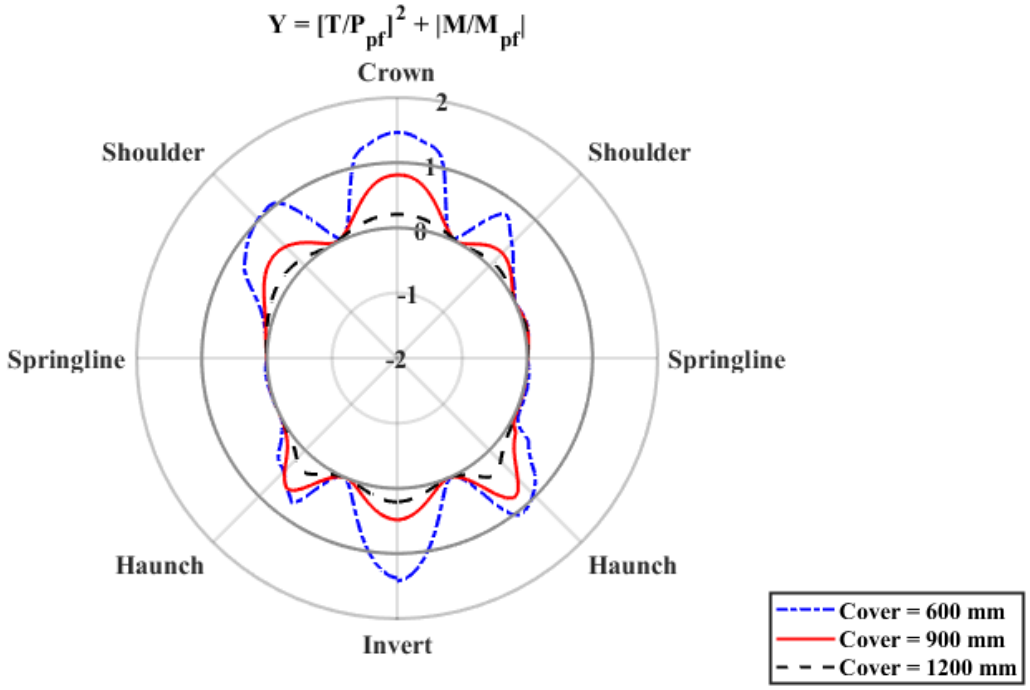

Figure 6.29. Variation in $Y = \left[\frac{T}{P_{pf}}\right]^2 + \left|\frac{M}{M_{pf}}\right|$ for different cover depth

The local sensitivity study shows that cover depth is an influential parameter that affects all responses of CSC. The responses are more severe for buried culverts in shallow cover depth and appearing environmental deteriorations in culvert/soil system increase the probability of experiencing yield or failure in this infrastructure.

6.7 Summary and conclusions

The effect of soil erosion voids on the soil pressure and the mechanical response of the CSC subject to overburden and surface loading was examined. Based on the conducted study for the void distance variable, these results indicate that applied void in the backfill soil with high soil pressure, where it transfers the truck load, affects the CSC results. The void if located out of this area has negligible effect in the CSC/soil system responses. The study of void angle and void depth indicates that the loss of surface contact and support between the culvert and surrounding soil in the upper half of the culvert/soil structure is the key contributing factor to load transfer and deformation mechanisms. The influential aspect in the void size is contact surface (void angle) and void depth does not play an important role because the culvert diameter change for this flexible case is in the order of 10 millimeter. The loss of surface contact is the key parameter that can affect culvert performance and integrity. These outcomes may support the development of mitigation strategies for maintaining the serviceability of culvert systems and support decision making for sustainability solutions.

For all analysis cases, the maximum local force and and bending moment occurred in the upper half of the culvert section between the springlines and responses are more severe in comparison with the lower half. The voids located in the upper half of the culvert

have more noticeable effects in the load transferring mechanism and internal force responses for systems deteriorated with erosion voids. In the model with introduced void in the shoulder, the culvert was experienced the plastic strains in the Crown and Shoulder due to the wheel and fill loads. This change in the performance affects the local force and bending moment distribution in the culvert.

The internal force responses do not change due to the introduced erosion voids in the lower half of culvert/soil system. But this system approaches yield point when erosion void is combined with corrosion deterioration at the invert and the culvert does not satisfy the combined bending moment and force and exceeds the capacity of the section for the case with shallowest cover depth with 600 mm cover.

The invert, haunch, shoulder, and crown of circumferential area approach the yield stress for cases with shallow cover depth and deteriorated by combined erosion void and corrosion in lower half due to section force and bending moment in this structural system, but the local force is the influential internal force in comparison with the bending moment. This can cause undesirable deformation, stress concentration and eventually failure of load-carrying system for the shallow cover depth cases.

References

ASTM, D. 2011. 2487. (2006). Standard practice for classification of soils for engineering purposes, Unified Soil Classification System. Book of Standards. 4.

Atkinson, J.H. and Bransby, P.L., (1977). The mechanics of soils, an introduction to critical state soil mechanics.

Balkaya, M., Moore, I. D., and Sağlamer, A. (2012). "Study of nonuniform bedding support because of erosion under cast iron water distribution pipes." *Journal of geotechnical and geoenvironmental engineering*, 138(10), 1247–1256. https://doi.org/10.1061/(ASCE)GT.1943-5606.0000689.

Beaton, J. and Stratfull, R. (1962). "Field test for estimating service life of corrugated metal pipe culverts." *Highway Research Board Proceedings*, Vol. 41: 255-272. http://onlinepubs.trb.org/Onlinepubs/hrbproceedings/41/41-017.pdf.

Billing, J. and Green, R. (1984). "Design provisions for dynamic loading of highway bridges." *Transportation research record*, (950), 94–103. http://onlinepubs.trb.org/Onlinepubs/trr/1984/950/950v1-015.pdf.

Bradford, S. A. (2000). "The practical handbook of corrosion control in soils". CASTI Publishing Inc. Edmonton, Alberta, Canada.

Cichocki, R., Moore, I., and Williams, K. (2021). "Steel buried structures: condition of Ontario structures and review of deterioration mechanisms and rehabilitation approaches." Canadian Journal of Civil Engineering, 48(2), 159–172. https://doi.org/10.1139/cjce-2019-0580.

Corrugated Steel Pipe Institute. (2010). Handbook of steel drainage and highway construction products. In Handbook of steel drainage and highway construction products. Corrugated Steel Pipe Institute, Cambridge, ON, Canada.

CSA-S6. (2014). Canadian Highway Bridge Design Code S6-14 CSA Canadian Standards Association, Canada.

Deng, L., Cai, C., and Barbato, M. (2011). "Reliability-based dynamic load allowance for capacity rating of prestressed concrete girder bridges." *Journal of Bridge Engineering*, 16(6), 872–880. https://doi.org/10.1061/(ASCE)BE.1943-5592.0000178.

El-Taher,M. andMoore, I. D. (2008). "Finite element study of stability of corroded metal culverts." *Transportation Research Record*, 2050(1), 157–166. https://doi.org/10.3141/2050-16.

Elshimi, T., Mak, A., Brachman, R., and Moore, I. (2011). "Behaviour of a deep-corrugated largespan box culvert during backfilling." *Pan-American Conference on Teaching and Learning of Geotechnical Engineering*, Toronto, Canada.

Elshimi, T. M. and Moore, I. D. (2013). "Modeling the effects of backfilling and soil compaction beside shallow buried pipes." *Journal of Pipeline Systems Engineering and Practice*, 4(4), 04013004. https://doi.org/10.1061/(ASCE)PS.1949-1204.0000136.

FHWA. (2007). Highway Statistics, 2005, Federal Highway Administration.

Giresini, L., Puppio,M. L., and Sassu,M. (2016). "Collapse of corrugatedmetal culvert in northern sardinia: analysis and numerical simulations." International Journal of Forensic Engineering, 3(1-2), 69–85. doi:10.1504/IJFE.2016.075991.

Hepfner, J. J. et al. (2002). "Statewide corrosivity study on corrugated steel culvert pipe." Report no., Montana. Department of Transportation. Research, Development and Technology. https://rosap.ntl.bts.gov/view/dot/24850.

Hibbitt, H., B. Karlsson and P. Sorensen. (2013). Abaqus analysis user's manual version 6.13. Dassault Systèmes Simulia Corp.: Providence, RI, USA.

Leung, C. and Meguid, M. (2011). "An experimental study of the effect of local contact loss on the earth pressure distribution on existing tunnel linings." T*unnelling and underground space technology*, 26(1), 139–145.https://doi.org/10.1016/j.tust.2010.08.003.

Mai, V. T. (2013). "Assessment of deteriorated corrugated steel culverts." Ph.D. thesis, Queen's University, 233p.

Mai, V. T., Hoult, N., and Moore, I. (2018). "Numerical evaluation of a deeply buried pipe testing facility." *Advances in structural engineering*, 21(16), 2571–2588. https://doi.org/10.1177/1369433218783769.

McGrath, T. J., Selig, E. T., Webb, M. C., Zoladz, G. V., et al. (1999). "Pipe interaction with the backfill envelope." *Report no.*, University of Massachusetts at Amherst. Transportation Center. https://rosap.ntl.bts.gov/view/dot/48814.

Meegoda, J. N., Juliano, T. M., and Tang, C. (2009). "Culvert information management system. " Transportation research record, 2108(1), 3–12. https://doi.org/10.3141/2108-01.

Meguid, M. A. and Dang, H. (2009). "The effect of erosion voids on existing tunnel linings." Tunnelling and Underground Space Technology, 24(3), 278–286. https://doi.org/10.1016/j.tust.2008.09.002.

Meguid, M. A. and Kamel, S. (2014). "A three-dimensional analysis of the effects of erosion voids on rigid pipes." Tunnelling and underground space technology, 43, 276–289. https://doi.org/10.1016/j.tust.2014.05.019.

Menetrey, P. andWillam, K. (1995). "Triaxial failure criterion for concrete and its generalization." *Structural Journal*, 92(3), 311–318.

Nakhostin, E., Kenny, S., and Sivathayalan, S. (2017). "Examination of buried corrugated metal culvert failure mechanisms using finite elements methods." *GeoOttawa*.

Nakhostin, E., Kenny, S., and Sivathayalan, S. (2019). "Buried corrugated steel culvert failure mechanisms due to environmental deteriorations." *International Conference on*

Sustainable Infrastructure 2019: Leading Resilient Communities through the 21stCentury, American Society of Civil Engineers Reston, VA, 29–40. doi:10.1061/9780784482650.004.

Nakhostin, E., Kenny, S., and Sivathayalan, S. (2021). "Numerical performance assessment of buried corrugated metal culvert subject to service load conditions." *Canadian Journal of Civil Engineering*, 48(2), 99–114. https://doi.org/10.1139/cjce-2019-0316.

Perrin Jr, J., Jhaveri, C. S., and Perrin Jr, J. (2004). "The economic costs of culvert failures." Prepared for TRB 2004 Annual Meeting, Washington DC.

Peter, J. M. and Moore, I. D. (2019). "Effects of erosion void on deteriorated metal culvert before and after repair with grouted slip liner." *Journal of Pipeline Systems Engineering and Practice*, 10(4), 04019031.

Ramberg, W. and Osgood, W. R. (1943). *Description of stress-strain curves by three parameters*. National Advisory Committee for Aeronautics, Washington, D.C.

Regier, C. (2015). "Investigation of the failure mechanisms of intact and deteriorated culverts." Ph.D. thesis, Queen's University. 147p.

Rubin, H., Tokarev, D., Rubin, E., and Schuttrumpf, H. (2013). "Bed load erosion patterns and their effect on the structural strength of rigid pipes made of homogeneous materials." The Open Civil Engineering Journal, 7(1), 32–49. doi: 10.2174/1874149520130417001.

Simulia, D. (2013). ABAQUS 6.13 User's manual. Dassault Systems, Providence, RI.

Walker, A. and Williams, K. A. (1995). "Strain based design of pipelines." *Report no.*, American Society of Mechanical Engineers, New York, NY (United States).

Wang, J., Huang, H., Xie, X., and Bobet, A. (2014). "Void-induced liner deformation and stress redistribution." Tunnelling and Underground Space Technology, 40, 263–276. https://doi.org/10.1016/j.tust.2013.10.008.

Wood, D.M., (1990). Soil behaviour and critical state soil mechanics. Cambridge university press.

Wriggers, P. (1995). "Finite element algorithms for contact problems." *Archives of computational methods in engineering*, 2(4), 1–49. doi:10.1007/BF02736195.

Xu, L. and Cheng, Y. (2013). "Development of a finite element model for simulation and prediction of mechanoelectrochemical effect of pipeline corrosion." Corrosion Science, 73, 150–160. https://doi.org/10.1016/j.corsci.2013.04.004.

Yasuda, N., Tsukada, K., and Asakura, T. (2017). "Elastic solutions for circular tunnel with void behind lining." Tunnelling and Underground Space Technology, 70, 274–285. https://doi.org/10.1016/j.tust.2017.08.032.

Chapter 7: Summary and Conclusions

7.1 Overview

The continuum finite element method was used to examine the influence of culvert profile section on the mechanical response of culverts (i.e., deformations, membrane strain, section force and section moment). This study considered soil/structure interaction mechanisms through numerical parametric study where the procedures were verified and compared with laboratory tests. The finite element models simulated, in two- and three-dimensional space, three different sections including an equivalent section (i.e., isotropic smooth cylinder), annular corrugated profile and spiral corrugate profile. An optimum FEM mesh density was established to achieve requisite numerical performance and optimize the running wall clock time. The surface smoothing algorithm was used to enhance contact interactions between the culvert and soil elements. The culvert corrugated profile was modelled with nonlinear constitutive relationships defining the CSC and soil material behaviour, and contact interactions at the CSC/soil interface. A single axle and wheel pair positioned over the culvert crown at the ground surface defined the surface loading condition.

The maximum vertical diameter changes predicted were similar using two modeling techniques, the simplified equivalent section models and the more complex corrugated profile models, in both two- and three-dimensional space. However, the modelling approaches (i.e., equivalent smooth cylinder section versus corrugated profile) predicted very different patterns of diameter change and deformation mechanisms. The smooth

cylinder section model cannot capture the detailed performances of corrugated section, especially for buried corrugated culverts in shallow cover depths where these differences in predicting the performance makes noticeable changes in the internal forces. As the cover depth decreases, the commonly used equivalent smooth cylinder section models do not adequately account for the nonlinear load transfer mechanisms, soil/structure interaction processes and plastic material behaviour. The idealized, equivalent section model cannot capture the local strain response, force, and section bending moments that develop during the interaction events. The need to incorporate the corrugated section profile in the numerical modelling procedures, particularly for shallow cover depth conditions, has been demonstrated in this study.

7.2 Thrust Modification for Intact CSC at Shallow Cover Depth

For round, shallow buried culverts ($D_h/D_v = 1$; $H/D_v = 0.5$), the numerical and experimental predictions, and closed form equations of the magnitude and perimeter distribution of section thrust and bending moment were in good agreement for locations below the springline which have very low (close to zero) internal forces. The value of internal forces above the springline is greater than lower half and influences the culvert-soil system performances. The reported bending moments based on the conducted tests in the laboratory and calculated moments using the closed-form equations suggested in the Canadian Highway Bridge Design Code were consistent with the predicted bending moment using FEM simulations of the corrugated culvert response.

There were noticeable differences among the reported thrusts and local forces in the upper half of the culvert estimated by FEM simulations, the lab tests results, and the

Canadian code calculations for the buried culverts in a shallow cover depth ($H/D < 2$). The FE simulations predicted a local variation in the strain magnitude at the crest and trough locations of the corrugation profile, particularly along the culvert perimeter between the shoulder and crown that significantly deviates from the average conditions. The local variation in the strain magnitude is reported in the laboratory test measurements. The common method for calculating internal bending moment and thrust force in the corrugated culverts in the experimental tests is using closed-form equations and measured strains. These closed-form equations and current practice do not reflect this localized section behaviour and the calculated thrusts by closed-form equations are an order lower than the predicted values using continuum FEM in this study.

A local sensitivity study was conducted using FE simulation to assess the effects of cover depth on the predicted section force and bending moment for the 3D corrugated section profile model. The numerical simulations indicate a transformation in the load distribution and culvert/soil interaction mechanisms with decreasing cover depth results in a higher order waveform response, in the distribution and magnitude of local force and section moment, above the culvert springline. Based on the parameter range investigated in this study, a transition in the load transfer and culvert response for deep to shallow burial interaction occurs at a shallow cover depth ($H/D \sim 2$). In comparison with the continuum FEA using the corrugated profile model, current practice, CSA-S6 2014, calculates net force as thrust and is conservative on the estimates for deeper cover depths (i.e., $H/D > 2$), and it underestimates the maximum section thrust at shallow cover depths (i.e., $H/D < 2$) in comparison with the local forces in the section. Furthermore, the current practice provides conservative estimates on the section moment across all burial depths

considered. Across the parameter range examined in this numerical study, the local force response has a greater proportion approaching the culvert yield strength than the section moment response.

Two types of analysis are conducted to provide a modification factor on the thrust load estimates to calculate local forces. First, the explicit model of corrugated culvert is simulated using Abaqus/Standard 6.13 finite element software developed to examine the mechanical response (i.e., local thrust, bending moment, and membrane strain) of a buried steel culvert. Confidence in the numerical modeling procedures was established through verification of the predicted bending moment response with data from third-party physical modeling studies. Second, the limit state function is defined based on closed-form equations using current practice, CSA-S6 2014, and the global sensitivity conducted on the defined equations. The global sensitivity assessed how uncertainty in the model input can affect the model output (i.e., predicted responses, thrust, moment and combined effects). The analysis identified the influential variables of Live Load (LL) and cover depth (H) that affect the prediction of thrust and bending moment for intact corrugated steel culverts particularly buried at shallow cover depths. The sensitivity analysis result indicates the intact model is an additive model with no interaction among its independent variables. The complementary finite element simulations used to conduct local sensitivity analyses to investigate the recognized influential variables individually. These results and their comparison with the Canadian code estimations indicate that the cover depth of the buried culvert (H) is the only variable that plays an important role in local force and thrust response differences between FEM and closed-form equations. Consequently, the thrust modification factor proposed for buried corrugated culverts in shallow cover depths with

two defined coefficients, thrust multiplying coefficient (C_1) and thrust power coefficient (C_2).

A probabilistic analysis was conducted to evaluate the sensitivity of two introduced thrust coefficients. The probabilistic analysis results indicate the variability of thrust multiplying coefficient (C_1) affects the reliability index which is changing from 3.3 to 0.5 for coefficient of variation from 0.05 to 0.5.

7.3 Effects of corrosion and erosion void on CSC mechanical response

The second part of this thesis studied the environmental deterioration effects (e.g., culvert corrosion and erosion voids in backfill) on the performance of the culvert/soil structure. Corrugated steel culvert (CSC) products have a wide range of service life, from 10 to 100 years, depending on a number of factors related to environmental factors and ageing. Physical processes, related to environmental factors and ageing can deteriorate the CSC/soil system that can impair the mechanical performance and reduce the CSC service life.

The corrosion deterioration is an environmental factor that affects the culvert performance during its service life. The loss of structural strength of the CSC buried in a shallow cover depth with depth of cover less than 2 m is investigated in this research study. The CSC was influenced by general or uniform corrosion through reduction of the CSC wall thickness and investigated using finite element simulations, global sensitivity, and probability analysis. Some variables of corrosion deterioration (e.g., corrosion angle and location) are not considered in the recommended equations, so the finite element simulations used to cover these aspects of corrosion variables through some local

sensitivity analysis. In the second part of corrosion study, a global sensitivity analysis is conducted to identify the influential variables and their interactions using defined closed-form equations and limit state functions.

The CSC is subjected to corrosion deterioration and its local sensitivity has been investigated in the service life using FEM. The internal forces at the lower half of the culvert are very close to zero and the appearance of corrosion deterioration at the lower half does not have significant effect in the responses (fewer than 1% change in culvert deflection, maximum internal force and bending moment) and this deterioration does not cause any changes in the backfill soil supports. It is observed from the local sensitivity using finite element analyses that the culvert is much more vulnerable to corrosion deterioration located at shoulders and crown, and the creation of plastic hinges at these locations have been observed in the analyses. The results of applied corrosion in the crown of culvert indicate that the internal forces and stresses are distributed more uniformly in corroded culverts with a wide angle of corrosion (angle greater than 30 degrees). The corroded cases at the same location but with limited angles, fewer than 30 degrees, experience concentrated and more severe internal responses at the deteriorated locations that can cause stress concentrations at the system. This finding indicates that corroded culvert with small corrosion angle which at locations with high internal forces such as crown can be more destructive than the general corrosion that appears at the same location.

The second part of corrosion study considered sensitivity and probability analyses. A nonlinear corrosion model as a function of time (presented in a form of closed-form equation) was used to present the loss of steel wall thickness. The internal forces of culvert due to the applied loads proposed in the Canadian code and closed-form equations is used

to develop limit state function. The Global Sensitivity Analysis using Sobol and Morris methods are used for performing the quantitative sensitivity analysis to identify the influential variables for the corroded culverts up to 100 years exposure time. The results show that the intact and lightly corroded culvert systems are additive and linear models with three influential variables. By increasing the exposure time and deterioration degrees, the number of influential variables increase with highly nonlinear features.

The identified influential variables in sensitivity analysis were used in First-Order Second-Moment probability analysis to predict probability of failure for damaged culverts in their service lives. The probability analyses results show the probability of failure increases with exposure time; the probability of failure for 10-year exposure is essentially 0%, but it is 37% for 100-year exposure time. The sensitivity of the variable, thrust multiplying coefficient (C_1), is dependent on the exposure time. For variable multiplying coefficient (C_1), although the safety index shows high sensitivity, ($\beta = 0.75 - 3$) for intact and lightly corroded CSC, this sensitivity decreases for deeply corroded culverts. The results of analysis for the variable exponential constant for corrosion model (n) indicate that the safety index shows high sensitivity for changing in the coefficient of variation values and exposure time.

Erosion voids is another deterioration that can develop in the backfill due to environmental conditions. The numerical study explored the effects of local soil voids on the structure/soil interaction mechanisms and CSC mechanical response. The parametric study investigated the influence of soil erosion void volume (i.e., angle, depth, length) and relative position with the culvert (i.e., distance, location) on the mechanical response of the CSC. The material and geometric properties for the CSC and soil backfill were held

constant for a shallow cover depth ($H/D < 2$) and the mechanical responses were examined with respect to a variation in the soil void factors. The analysis includes an assessment of the culvert serviceability with respect to the sectional moment, local force, strain, and displacement of CSC and the soil pressure in presence of soil voids.

The culvert response was sensitive to the loss of soil support in upper half of the culvert that influenced load transfer mechanisms and affected the internal force (i.e., local force, section moment) response. The introduced void at the invert, haunch, and springline results in noticeable increasing of internal forces more localized at the void location. In the models that introduced void in the shoulder and crown, the culvert experienced plastic strains in the crown and shoulder due to the wheel and fill loads. The increase of internal force responses due to the introduced erosion voids has a great influence in the performance as it leads to the culvert not satisfying the combined bending moment and force requirements, with a greater proportion of local force, that exceed the capacity of the section.

The results indicate that applied void in the backfill soil, with high soil pressure due to transferring wheel load, affects the CSC response and voids located outside of this area has little effect in the CSC/soil system responses. The results show that the appearance of the voids within the effective length can be of critical interest. The study of void angle and void depth indicates that the loss of surface contact and support between the culvert and surrounding soil in the upper half of the culvert is the key contributing factor to load transfer and deformation mechanisms. The loss of surface contact due to void creation is the parameter that can affect culvert performance and integrity, and this variable is the most influential among all.

The combined effect of erosion void and corrosion is considered in the numerical study. The numerical modelling procedures were verified with respect to the horizontal and vertical diameter change response of the deteriorated soil/CSC system (e.g., corroded culvert from haunch to haunch with backfill void from haunch to springline) based on full-scale experimental tests.

The results indicate that having only erosion void at lower half of the culvert, where the CSC experiences smaller internal forces in comparison with upper half, does not have a significant effect on the general behaviour of the buried culvert. The culvert experiences severe increase in the limit state function responses ($Y = \left[\frac{\mathrm{T}}{P_{pf}}\right]^2 + \left|\frac{\mathrm{M}}{M_{pf}}\right| < 1$) for the cases that both erosion void and corrosion are applied at the same location at the lower half. These results show that the appearance of both deteriorations in the lower half, can increase the possibility of $Y > 1$ in the lower half where Y value is increasing from almost 0 and approaches 1 value at this location.

7.4 Recommendations for future research

Based on the outcomes of the research reported, the following topics are suggested as potential areas for future research investigations to further improve the understanding of the failure mechanisms and interactions of soil and CSC.

1. Verify the thrust coefficient for shallow cover: Physical tests on CSC buried at shallow cover depths is needed to establish confidence in the proposed thrust coefficient (C_1) that accounts for a range of design parameters (e.g., elastic modulus, Proctor density, friction angle, dilation angles). In addition to the average strain, the experimental instrumentation should monitor the local strain

at the crest and trough along the CSC perimeter. It is recommended to verify measured values with explicit numerical models.

2. Improve knowledge on the soil erosion void mechanism: Study the processes for the creation and evolution of erosion voids around the pipes and their rising rate in different environmental conditions to formulate these deterioration effects in closed-form equations to be used in the service life performance studies
3. Study of local strain for other profiles: Study deep corrugated and spiral rib profiles of culvert and pipe using explicit numerical modeling to examine the mechanical responses at crest and trough (i.e., membrane strain, local force, and bending moment). It is recommended to conduct numerical simulations with explicit models of profiles and experimental tests to validate the results.
4. Corrosion deterioration in joints: Study the flexible corrugated culverts and pipes considering a variety of pipe joints used for connecting the lengths of corrugated steel pipe and corrosion deterioration in joints. It is recommended to consider the joints in upper half of the culvert which experience higher internal forces.
5. Dynamic load effects on buried culvert in shallow cover depth: Apply dynamic CL-W Truckload with all five axles on the roadway and study its effect on buried culverts in shallow cover depth. This study can investigate the load transferring mechanism and culvert-soil interaction effects on the responses.
6. Environmental deterioration effects on large span culverts: Study large span culverts ($S > 3m$) which are used as a bridge with different cross-sectional shapes (i.e., pipe arch, vertically and horizontally elliptical shapes). Buried cases at

shallow cover depth are recommended to study considering environmental deteriorations in the culvert and surrounding backfill soil.